USGS
science for a changing world

U.S. Department of the Interior
U.S. Geological Survey

Hydrothermal Mineralogy of Core from Geothermal Drill Holes at Newberry Volcano, Oregon

Professional Paper 1578

Hydrothermal Mineralogy of Core from Geothermal Drill Holes at Newberry Volcano, Oregon

KEITH E. BARGAR AND TERRY E. C. KEITH

U.S. GEOLOGICAL SURVEY PROFESSIONAL PAPER 1578

UNITED STATES GOVERNMENT PRINTING OFFICE, WASHINGTON : 1999

DEPARTMENT OF THE INTERIOR

BRUCE BABBITT, *Secretary*

U.S. GEOLOGICAL SURVEY

Charles G. Groat, *Director*

Manuscript approved for publication, April 20, 1997

Text and illustrations edited by Jeff Troll

Library of Congress Cataloging-in-Publication Data

Bargar, Keith E.
Hydrothermal minerology of core from geothermal drill holes at Newberry Volcano, Oregon / Keith E. Bargar and Terry E.C. Keith.
p. cm -- (U.S. Geological Survey professional paper ; 1578)
Includes bibliographical references.
Supt. of Docs. no.: I 19. 16: 1578
ISBN 0-607-91905-1
1. Hydrothermal alteration--Oregon--Newberry Volcano Region. 2. Minerals--Oregon--Newberry Volcano Region. 3. Geothermal resources--Oregon--Newberry Volcano region. I. Keith, Terry E.C. II. Title. III. Series.
QE390.5.B375 1999
551.2'3'09795--dc21 99-32015
CIP

For sale by
U.S. Geological Survey, Map Distribution
Box 25286, MS 306, Federal Center
Denver, CO 80225

CONTENTS

Abstract---------- 1
Introduction---------- 2
Analytical methods---------- 4
Acknowledgments---------- 6
Geologic setting---------- 6
Geothermal exploration---------- 7
Drill holes within the caldera---------- 7
USGS-N2---------- 7
Lithology---------- 8
Hydrothermal alteration---------- 8
Surface to 320-m depth---------- 8
320- to 697-m depth---------- 9
697-m to 932-m depth---------- 12
Fluid inclusions---------- 16
RDO-1---------- 22
Lithology---------- 22
Hydrothermal alteration---------- 23
Fluid inclusions---------- 23
Drill holes outside the caldera---------- 24
GEO-N1---------- 24
Lithology---------- 24
Hydrothermal alteration---------- 26
GEO-N2---------- 27
Lithology---------- 28
Hydrothermal alteration---------- 28
Fluid inclusions---------- 30
GEO-N3---------- 30
Lithology---------- 30
Hydrothermal alteration---------- 32
GEO-N4---------- 32
Lithology---------- 32
Hydrothermal alteration---------- 32
GEO-N5---------- 32
Lithology---------- 33
Hydrothermal alteration---------- 33
SF NC-01---------- 35
Lithology---------- 35
Hydrothermal alteration---------- 35
Fluid inclusions---------- 36
SF NC72-03---------- 38
Lithology---------- 38
Hydrothermal alteration---------- 38
Fluid inclusions---------- 39
Other drill holes---------- 40
Hydrothermal mineralogy of drill core specimens---------- 41
Drill holes within the caldera---------- 41
Drill holes outside the caldera---------- 41
Hydrothermal minerals---------- 42

Zeolite minerals---------- 42
Analcime---------- 42
Chabazite---------- 43
Clinoptilolite---------- 44
Dachiardite ---------- 44
Erionite---------- 45
Faujasite---------- 45
Heulandite---------- 45
Laumontite---------- 45
Mordenite---------- 46
Phillipsite---------- 46
Calcium silicate hydrate minerals---------- 47
Gyrolite---------- 47
Okenite---------- 47
Carbonate minerals---------- 48
Ankerite-dolomite---------- 49
Aragonite---------- 50
Calcite---------- 50
Kutnohorite---------- 51
Magnesite---------- 51
Rhodochrosite---------- 51
Siderite---------- 52
Clay minerals---------- 53
Kaolinite and halloysite---------- 53
Smectite---------- 54
Mixed-layer illite-smectite---------- 56
Illite---------- 56
Mixed-layer chlorite-smectite---------- 57
Chlorite---------- 58
Silica minerals---------- 59
Opal---------- 59
Cristobalite---------- 59
Quartz and chalcedony---------- 60
Sulfide minerals---------- 62
Pyrrhotite---------- 62
Pyrite---------- 63
Marcasite---------- 64
Sphalerite---------- 65
Sulfate minerals---------- 65
Anhydrite---------- 65
Barite---------- 66
Jarosite, natroalunite, and natrojarosite---------- 66
Gypsum---------- 67
Iron oxide and iron hydroxide minerals---------- 67
Hematite and lepidocrocite---------- 67
Goethite---------- 67
Magnetite---------- 68
Amorphous iron oxide---------- 68
Other minerals---------- 69
Apatite---------- 69
Apophyllite---------- 69
Copper---------- 69
Epidote---------- 70
Hydrogrossular---------- 71

Discussion---------- 71
Factors controlling hydrothermal alteration---------- 71
Permeability---------- 72
Temperature---------- 73
Fluid composition ---------- 74
Rock composition---------- 75
Summary and conclusions---------- 79
References cited---------- 83-86
Appendixes:
1. Lithologic description of drill core USGS-N2 from within the caldera of Newberry volcano---------- 87-90
2. Lithologic description of drill core GEO-N1 from the south flank of Newberry volcano---------- 91-92

FIGURES

1. Map showing location of Newberry volcano and major Quaternary volcanic centers in Cascade Range of western United States and British Columbia, Canada---------- 3
2. Generalized geologic map of Newberry caldera---------- 4
3. Map showing location of geothermal exploration drill holes at Newberry volcano---------- 5
4. Comparison of lithologic units in upper part of USGS-N2 drill hole with those of RDO-1 drill hole---------- 9
5. Distribution of hydrothermal alteration minerals in core from lower two-thirds of USGS-N2 drill hole---------- 10
6. Photograph of fine-grained thin-bedded volcaniclastic sandstone drill-core specimen from 315.1-m depth in USGS-N2 drill hole---------- 11
7. Generalized paragenetic sequence of selected hydrothermal minerals in core from USGS-N2 drill hole---------- 11
8. Photographs of drill-core samples from upper and middle parts of USGS-N2 drill hole---------- 15,16
9. Photographs of drill-core samples from lower part of USGS-N2 drill hole---------- 17,18
10. Photomicrographs showing fluid inclusions in hydrothermal quartz crystals from lower part of USGS-N2 drill hole---------- 21
11. Diagram showing fluid-inclusion T_h values for quartz and calcite specimens from lower part of USGS-N2 drill hole---------- 22
12. Distribution of hydrothermal alteration minerals in cuttings samples from drill hole RDO-1---------- 23
13. Diagram showing fluid-inclusion T_h values for quartz specimens from RDO-1 drill hole---------- 24
14. Distribution of hydrothermal alteration minerals in core from drill hole GEO-N1---------- 25
15. Generalized paragenetic sequence of hydrothermal alteration minerals deposited in flank drill holes of Newberry volcano---------- 28
16. Distribution of hydrothermal minerals in core from drill hole GEO-N2---------- 29
17. Diagram showing fluid-inclusion Th values for quartz and calcite specimens from GEO-N2 drill hole-------- 30
18-20. Distribution of hydrothermal alteration minerals in core
18. From GEO-N3 drill hole---------- 31
19. From GEO-N4 drill hole---------- 33
20. From GEO-N5 drill hole---------- 34
21. Scanning electron micrograph of fracture filling that contains crystals of sphalerite and later massive siderite---------- 35
22. Scanning electron micrograph of botryoidal chalcedony open-space deposit with clusters of late quartz crystals---------- 35
23. Distribution of hydrothermal alteration minerals in core from SF NC-01 drill hole---------- 37
24. Photomicrograph of opal with disseminated pyrite crystals---------- 38
25. Diagram showing fluid-inclusion T_h values for quartz and calcite from SF NC-01 drill hole---------- 38
26. Distribution of hydrothermal alteration minerals in SF NC72-03 drill hole---------- 39
27. Diagram showing fluid-inclusion T_h values for quartz and calcite from SF NC72-03 drill hole---------- 40

28-36. Scanning electron micrographs of Newberry drill-core samples showing:
28. Large trapezohedral analcime crystal deposited later than smectite in altered volcaniclastic sandstone---- 42
29. Phacolitic chabazite crystals and fractured and flaking faujasite crystals---- 44
30. Lath-shaped clinoptilolite crystals partly coated by smectite and fibrous mordenite(?)---- 45
31. Fibrous to acicular dachiardite crystals in altered lithic tuff---- 45
32. Bundle of stubby acicular erionite crystals and smectite deposited in pore spaces of basaltic sediment---- 46
33. Fractured and flaking faujasite crystals---- 46
34. Tabular to blocky heulandite crystals---- 47
35. Fibrous mordenite crystals---- 47,48
36. Spherical aggregate of platy gyrolite crystals in volcaniclastic sandstone---- 48
37. $CaCO_3$-$MgCO_3$-$FeCO_3$+$MnCO_3$ ternary diagram for electron microprobe analyses of carbonate minerals from USGS-N2 drill core---- 49
38. Scanning electron micrograph of blocky and discoidal aggregates of rhombic ankerite-dolomite crystals---- 50
39. Scanning electron micrograph of columnar aggregates of rhombic ankerite-dolomite crystals---- 50
40. Scanning electron micrographs and photograph of calcite crystals---- 52,53
41. Photomicrograph showing cross section of discoidal aggregate of siderite crystals---- 53
42. $CaCO_3$-$MgCO_3$+$FeCO_3$-$MnCO_3$ ternary diagram for electron microprobe analyses of discoidal siderite crystal aggregate---- 53
43. Scanning electron micrographs and photograph showing different morphologies of siderite crystal clusters---- 54-56
44. Scanning electron micrographs showing clusters of smectite crystals---- 57
45. Scanning electron micrographs showing mixed-layer chlorite-smectite crystal aggregates---- 58
46. Scanning electron micrographs and photograph of aggregates of chlorite crystals---- 61
47. Scanning electron micrograph of botryoidal opal---- 62
48. Scanning electron micrograph of hemispherical aggregates of bladed cristobalite crystals deposited on calcite---- 62
49. Photomicrographs of vesicle fillings in basaltic breccia fragments---- 63
50. Scanning electron micrographs of pyrrhotite and pseudomorphous replacement of pyrrhotite by pyrite and marcasite---- 64
51. Part of phase diagram for Fe-S system below 350˚C showing electron microprobe compositions of monoclinic pyrrhotite---- 65
52-55. Scanning electron micrographs showing:
52. Octahedral pyrite crystal and marcasite crystals with a cockscomb habit---- 66
53. Blocky anhydrite crystals partly coated by mixed-layer chlorite-smectite rosettes---- 67
54. Backscatter image of intergrown tabular jarosite crystals---- 67
55. Hexagonal tabular natrojarosite crystals---- 68
56. Photograph of part of large cavity filling of red botryoidal hematite and later colorless calcite---- 68
57-60. Scanning electron micrographs showing:
57. Hexagonal, tabular to columnar apatite crystals with later chlorite---- 69
58. Striated grain of native copper partly filling vesicle---- 69
59. Clusters of euhedral twinned epidote crystals---- 70
60. Subhedral hydrogrossular crystals in volcaniclastic sandstone---- 72
61. AFM diagram showing chemical variation of basaltic to rhyolitic core samples and surface rocks from Newberry volcano---- 75
62. Chemical variation diagrams showing differences between precaldera and postcaldera rocks from Newberry volcano---- 76
63. SiO_2 vs. CaO diagram for chemical analyses of rocks from geothermal drill holes and outcrops at Newberry volcano---- 77
64. MgO variation diagrams for chemically analyzed rocks from geothermal drill holes and outcrops at Newberry volcano---- 77,78

65. H_2O vs. SiO_2 diagram for chemically analyzed rocks from Newberry volcano---------- 78
66. Zr variation diagrams for major- and selected trace- element contents of rocks from Newberry volcano---------- 79-81

TABLES

1. Geothermal drill holes at Newberry volcano selected for hydrothermal mineralogy studies---------- 8
2. Chemical analyses of USGS-N2 drill-core samples---------- 12,13
3. Spectroscopic trace-element analyses of USGS-N2 drill-core samples---------- 14
4. INAA trace-element analyses of USGS-N2 drill-core samples---------- 14
5. Electron microprobe analyses of phenocryst and groundmass plagioclase crystals from USGS-N2 drill core---------- 19
6. Fluid-inclusion heating/freezing data for Newberry volcano drill-core samples---------- 20
7. Chemical analyses for drill-core samples outside Newberry caldera---------- 26,27
8. Electron microprobe analyses of zeolite minerals from USGS-N2 drill core---------- 43
9. Electron microprobe analyses of carbonate minerals from USGS-N2 drill core---------- 49
10. Trace-element composition of carbonate and sulfide minerals from USGS-N2 drill core---------- 51
11. Electron microprobe analyses of phyllosilicate minerals from USGS-N2 drill core---------- 60
12. Electron microprobe analyses of sulfide minerals from USGS-N2 drill core---------- 65
13. Trace-element analyses for drill-core samples outside Newberry caldera---------- 70
14. Electron microprobe analyses of epidote from 916.7-m depth in USGS-N2 drill core---------- 71
15. Optical and crystallographic data for epidote from 916.7-m depth in USGS-N2 drill core---------- 72

Library of Congress Cataloging-in-Publication Data

Bargar, Keith E.
Hydrothermal minerology of core from geothermal drill holes at Newberry Volcano, Oregon / Keith E. Bargar and Terry E.C. Keith.
p. cm -- (U.S. Geological Survey professional paper ; 1578)
Includes bibliographical references.
Supt. of Docs. no.: I 19. 16: 1578
ISBN 0-607-91905-1
1. Hydrothermal alteration--Oregon--Newberry Volcano Region. 2. Minerals--Oregon--Newberry Volcano Region. 3. Geothermal resources--Oregon--Newberry Volcano region. I. Keith, Terry E.C. II. Title. III. Series.
QE390.5.B375 1999
551.2'3'09795--dc21 99-32015
CIP

HYDROTHERMAL MINERALOGY OF CORE FROM GEOTHERMAL DRILL HOLES AT NEWBERRY VOLCANO, OREGON

By Keith E. Bargar and Terry E. C. Keith

ABSTRACT

Twenty geothermal exploration drill holes, funded by both industry and various government agencies, were completed between 1976 and 1986 on the flanks and within the caldera of Newberry volcano, central Oregon. These holes were drilled in order to evaluate the geothermal energy potential of this young Cascade volcano. Part of the evaluation process involved studies of the hydrothermal alteration mineralogy in nine of the drill holes. Geothermal drill holes GEO-N1, GEO-N4, and GEO-N3 were located on the south, east, and north flanks of the volcano, respectively. Four holes (GEO-N5, GEO-N2, SF NC-01, and SF NC72-03) were drilled on the west flank of Newberry volcano, and two holes (USGS-N2 and RDO-1) were completed within the volcano's caldera.

Maximum temperatures measured at the bottoms of the flank drill holes GEO-N1, GEO-N3, GEO-N4, and GEO-N5 were below 100˚C. Fractures, vesicles, spaces between breccia fragments, and glassy drill-core samples usually exhibit little or no hydrothermal alteration in the upper parts of these drill holes. Similar open spaces in the lower parts of the drill holes contain low-temperature hydrothermal minerals (carbonates, silica minerals, zeolites, clay minerals, sulfates, iron oxides, and sulfides) that could have formed at the temperatures measured during drilling. Temperatures in the three remaining flank drill holes (GEO-N2, SF NC-01, and SF NC 72-03) exceeded 150˚C at the hole bottoms. The extent of hydrothermal alteration in these drill holes is low to moderate, and the hydrothermal minerals include laumontite, quartz, and mixed-layer chlorite-smectite that are consistent with temperatures above 150˚C.

The extent of hydrothermal alteration is greater in some intracaldera drill-hole specimens from depths where the measured temperatures were significantly higher than temperatures encountered at equivalent depths within the flank drill holes. Measured temperatures above about 300-m depth in the USGS-N2 drill hole ranged between about 18 and 39˚C, and hydrothermal alteration minerals are nearly absent in the drill core. The temperatures increased from 31˚C at 300-m depth to 265˚C at 930-m depth, and hydrothermal alteration is slight to extensive. The more pervasive alteration occurs along fractures and fracture margins and in the more permeable brecciated and volcaniclastic zones. Hydrothermal zeolites, apophyllite, gyrolite, carbonates, apatite, hydrogrossular, clay minerals, silica minerals, sulfides, sulfur, anhydrite, epidote, and iron oxides and hydroxides were identified. Temperatures in the RDO-1 drill hole were greater than 158˚C at about 350.5-m depth. Many of the hydrothermal alteration minerals (analcime, aragonite, siderite, rhodochrosite, calcite, smectite, chlorite, quartz, mordenite, pyrite, pyrrhotite, and hematite) occur at shallower depths than in the nearby USGS-N2 drill core.

The most important controls of hydrothermal alteration in the Newberry volcano drill holes are permeability, temperature, and fluid composition. Hydrothermal fluids flow more readily through the interflow breccias and have altered these breccias and other volcaniclastic layers where initial permeability was highest; massive lava flows having low permeabilities are generally unaltered or only slightly altered except where fractured or vesicular.

Fluid-inclusion studies of quartz and calcite crystals from the lower parts of the three west-flank drill holes indicate that past temperatures were hotter. Temperatures were significantly hotter-commonly by 20 to 40˚C and by as much as 160˚C-in the SF NC72-03 drill hole, which is near the ring fracture on the west side of the volcano. The ring fractures may provide conduits for movement of deep geothermal water to shallower levels. Hydrothermal alteration minerals identified from the two intracaldera drill holes suggest that past temperatures could have been similar to the measured temperatures. However, fluid-inclusion heating studies indicate that temperatures within both drill holes have been significantly hotter (by as much as 80˚C in RDO-1 and by ~100˚C at the bottom of USGS-N2) than the measured temperatures. Lacustrine deposits in the upper parts of these drill holes suggest that transient higher past temperatures may have resulted from higher pressure caused by the additional weight of an intracaldera lake about 100 to 150 m deep.

The few published chemical analyses of waters from the Newberry volcano drill holes and the low measured temperatures in the upper parts of all the drill holes indicate that descending cold meteoric waters exert a substantial control over any alteration in the shallower levels of the drill holes. Limited fluid-inclusion melting-point temperature measurements suggest that the geothermal waters become more saline with depth, increasing from 0 at about 801-m depth to 1.9 weight percent NaCl equivalent near the bottom of the USGS-N2

drill hole. Salinity also appears to be higher near the caldera ring fractures where it ranges from 0.2 weight percent NaCl equivalent in GEO-N2 to as much as 0.7 weight percent NaCl equivalent in SF NC72-03.

Comparison of major- and trace-element contents of chemically analyzed rocks from the GEO-N1, GEO-N5, and SF NC72-03 drill holes with those of published analyses of unaltered surface rocks shows little or no evidence of element mobility resulting from hydrothermal alteration of core from these flank drill holes. Conversely, comparison of the published analyses with chemical data from many USGS-N2 drill-core specimens suggests that hydrothermal alteration caused insignificant to moderate decreases in SiO_2, Na_2O, and K_2O as well as possible slight increases in total Fe and CaO. Considerable scatter of the data for Al_2O_3 may indicate both loss and gain of this element. Gains or losses involving MgO, TiO_2, and total Fe are somewhat difficult to discern because analyses of these elements show strong trends that result from differences in the composition of precaldera and postcaldera lavas and volcaniclastic rocks. The concentration of several trace elements, as well as P_2O_5 and MnO, appears to vary according to whether the rock is basaltic or rhyolitic; trace-element abundance in several USGS-N2 drill-core samples having intermediate compositions appear to complete the differentiation trend.

Possibly the Newberry hydrothermal system is very young and has not evolved to a stage where trace elements and some major elements have been mobilized and reconcentrated in significant amounts. The Newberry hydrothermal system appears to be very youthful because unaltered glassy rocks are present at elevated temperatures. The lack of indications of self-sealing, together with the absence of multiple or cross-cutting fracture systems, also provides evidence that the hydrothermal system is young.

INTRODUCTION

Newberry volcano is in central Oregon about 60 km east of the north-south-trending crest of the Cascade Range (fig. 1). This broad shield-like volcano rises only about 1,100 m above the surrounding terrain, but its extensive deposits have a volume of approximately 450 km^3 that is spread over an area of about 1,600 km^2 (MacLeod and Sherrod, 1988). Enclosed within the 5- by 7-km summit caldera of Newberry volcano are the scenic Paulina and East Lakes (fig. 2). Hot springs on the northeast shore of Paulina Lake have temperatures of 50 and 52˚C (Sammel, 1983). Temperatures as high as 62˚C are reported for hot springs along the south shoreline of East Lake, and a temperature of 35.5˚C was measured in a warm-water well in a campground on the east side of Paulina Lake (Mariner and others, 1980). Weak fumaroles are also present on the northeastern edge of the Big Obsidian Flow (fig. 2), which is the youngest of several Holocene silicic lava flows and eruptive centers within the caldera (Peterson and Groh, 1969; Friedman, 1977). The thermal features and abundant evidence of at least 25 eruptions of silicic volcanic rocks in the Holocene epoch (as young as 1,350 years B.P.) (MacLeod and others, 1995) make this large complex volcano an attractive target for geothermal energy exploration.

Since 1976, numerous geologic and geophysical studies (summarized by Fitterman, 1988), including several deep drill holes, have been completed at Newberry volcano in an attempt to understand the volcano's structure and geothermal system. The location of all of the geothermal drill holes in the vicinity of Newberry caldera are shown on a map published by Olmstead and Wermiel (1988) and in figure 3 of this report. Access to information obtained from these drill holes varies (table 4 in MacLeod and others, 1995), depending partly on whether private or public funds were used to complete the holes.

This report describes the hydrothermal alteration of core and drill cuttings from the two drill holes within Newberry caldera (USGS-N2, and RDO-1) and seven core holes (GEO-N1, GEO-N2, GEO-N3, GEO-N4, GEO-N5, SF NC-01, and SF NC72-03) located outside the caldera rim. Core samples were not recovered from the upper part of USGS-N2, so drill hole USGS-N3 was completed nearby to obtain samples and information on the shallow part of the stratigraphic section. Brief observations on core from USGS-N1, CE NB-3, and CE NB-4 drill holes on the northeast, southeast, and northwest flanks of the volcano (fig. 3) also are included.

The 932-m-deep USGS-N2 drill hole is by far the hottest of all of the Newberry drill holes; in fact, the 265˚C near-bottom temperature is hotter than temperatures reported for any other geothermal drill hole in the Cascade Range within the United States. Only the Meager Mountain area in British Columbia, Canada (fig. 1), where 270˚C is reported from a 3,000-m-deep drill hole (Souther, 1985), has a higher reported temperature. Interpretations of the Newberry volcano hydrothermal system rely heavily on data from the USGS-N2 drill hole. Some preliminary data on the hydrothermal alteration of this drill core were reported by Bargar and Keith (1984). Light stable-isotope measurements on selected mineral and whole-rock samples from USGS-N2 drill core indicate that the hydrothermal minerals probably precipitated from the present geothermal waters (Carothers, Mariner, and Keith, 1987). On the basis of hydrothermal mineralogical data, Keith and others (1984a, b) and Keith and Bargar (1988) concluded that Newberry volcano has a young evolving geothermal system. A comparison of hydrothermal mineralogy in the RDO-1 drill hole with that in the USGS-N2 drill core suggests that rocks within the caldera become less altered at equivalent depths as distance increases from the southern ring fracture (Keith and others, 1986).

Preliminary hydrothermal alteration studies (Bargar and Keith, 1986) show only minor low-temperature alteration, consistent with temperatures reported by Swanberg and Combs (1986) for the GEO-N1 drill hole on the southern flank of Newberry volcano. Wright and Nielson (1986) compared electrical resistivity anomalies with alteration in drill core

GEO N-1 and advised caution in interpretation of electrical geophysical surveys because of an inability to distinguish between rocks that have been altered by high-temperature fluids (USGS-N2) and rocks subjected to low-temperature alteration (GEO-N1). Similar low temperatures are reported for drill holes on the north (GEO-N3), east (GEO-N4), and southwest (GEO-N5) flanks of the volcano (Swanberg, Walkey, and Combs, 1988; Walkey and Swanberg, 1990).

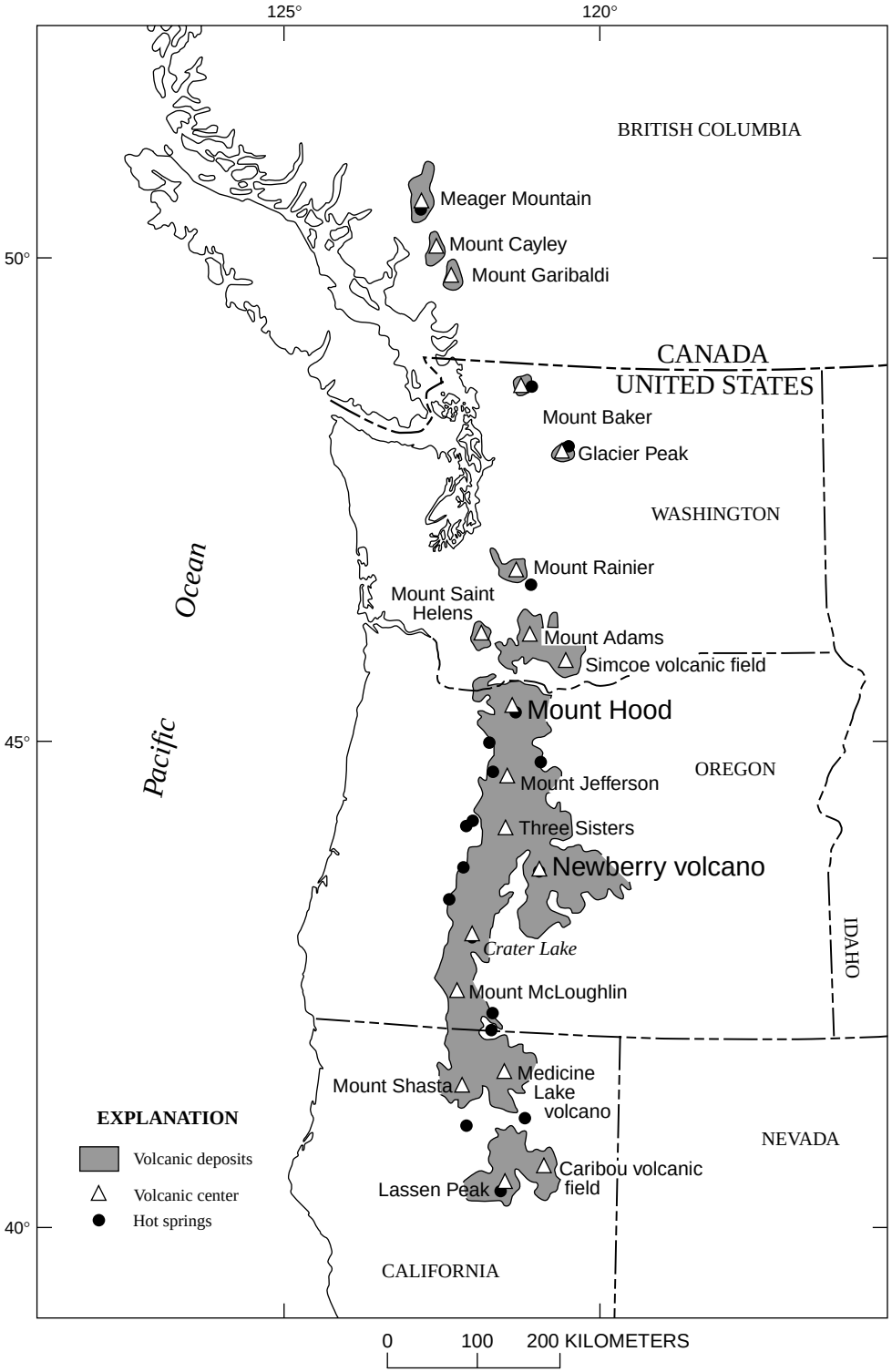

Figure 1.—Map showing location of Newberry volcano and major Quaternary volcanic centers in Cascade Range of western United States and British Columbia, Canada (Sherrod and Smith, 1990).

Higher temperatures and more intensive hydrothermal alteration are reported for Newberry's west-flank drill holes GEO-N2 (Walkey and Swanberg, 1990), SF NC-01, and SF NC72-03 (Arestad, Potter, and Stewart, 1988). In 1990, Newberry volcano was designated as the Newberry National Volcanic Monument (Public Law 101-522) (Collins, 1991). Because future geothermal exploration and possible development of the Newberry geothermal system will be restricted to areas outside the national monument boundaries, the west flank of the volcano may be of considerable interest to the geothermal industry.

ANALYTICAL METHODS

Drill cuttings were sampled at either 3- or 6.1-m intervals during drilling of the RDO-1 drill hole and were logged by M.W. Gannett and A.F. Waibel, who used a binocular microscope at the drill site (Keith and others, 1986). The authors examined the entire USGS-N2 drill core (plus the adjacent offset drill core USGS-N3) by hand lens and collected a subset of the USGS-N2 core, consisting of about 640 specimens that are representative of rock units, vug fillings, fracture coatings, and whole-rock alteration, for laboratory studies of the hydrothermal alteration. GEO-Newberry Crater, Inc., logged and photographed the GEO-N1 and GEO-N3 drill cores and sent a split of both cores to Energy and Geoscience Institute of the University of Utah (EGI). Subsets of the splits of these two cores (262 specimens from GEO-N1 and 118 specimens from GEO-N3), including vein or fracture and vug fillings, and both altered and unaltered representative samples of stratigraphic intervals, were obtained from the EGI core library for this study. GEO-Newberry Crater, Inc., also logged and photographed the GEO-N2, GEO-N4, and GEO-N5 drill cores and made the drill-core and drill-hole data from all of their Newberry drill holes available for this study. The company had acquired the geothermal assets of Santa Fe Geothermal, Inc., at Newberry volcano, which included core from drill holes SF NC72-03, and SF NC-01, and data from them was also available. Photographs provided by GEO-Newberry Crater, Inc., for each core box (drill holes GEO-N2, GEO-N4, GEO-N5, SF NC-01, and SF NC72-03) were used to locate possible alteration zones. These zones were inspected, and representative core samples (88 specimens from GEO-N2, 72 from GEO-N4, 59 from GEO-N5, 95 from SF NC-01, and 118 from SF NC72-03) were collected for this investigation (Bargar and others, 1990); they included fresh rock and hydrothermally altered drill core (vug fillings, fracture coatings, and whole-rock samples). Unfortunately, we were unable to spend the time necessary to thoroughly examine all the core from these five drill holes.

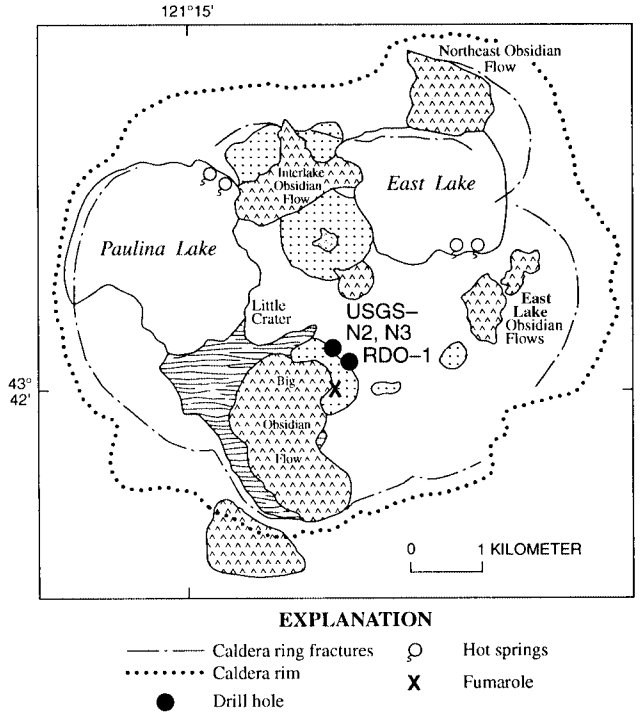

Figure 2.—Generalized geologic map of Newberry caldera, Oregon (after MacLeod and others, 1995) showing locations of drill holes USGS-N2, USGS-N3, and RDO-1, hot springs, fumarole, caldera ring fractures, caldera rim, and some of the younger volcanic deposits. Northeast Obsidian Flow and obsidian flow southwest of Big Obsidian Flow are Pleistocene. Unit in which fumarole is heated may be latest Pleistocene or Holocene; remainder of units in figure are Holocene (post-Mazama ash bed, about 6,845±50 C^{14} yr BP), relative ages of which are provided by MacLeod and others (1995).

Subsets of specimens from the nine Newberry geothermal drill holes were obtained for this study at several different times between 1982 and 1990. Prior to the collection of samples, a lithologic log for each drill hole was made available, usually by the drilling organization. From these logs, we selected subsets of appropriate samples for various types of laboratory analyses. Some core specimens from the USGS-N2 and GEO-N1 drill holes were prepared as thin sections for petrography studies. Core specimens were generally selected for chemical analysis on the basis of being representative of either the freshest available rock of a unit or flow of particular interest (not all flow units were analyzed) or a highly altered part of the same flow unit. Major- and trace-element analyses were obtained for drill-core specimens of two lava flows from each of the GEO-N5 and SF NC72-03 drill holes and from several depths in the GEO-N1 and USGS-N2 drill holes. Major elements were analyzed by X-ray spectroscopy and conventional rock analysis methods, and trace elements were analyzed by energy dispersive X-ray fluorescence spectroscopy, optical spectroscopy, and instrumental neutron activation analysis. Techniques for these methods are described in Baedecker (1987). In this report, the chemically analyzed rocks are classified, according to weight percent SiO_2, as basalts (<52 percent), basaltic andesite (52-57 percent), andesite (57-62 percent), dacite (62-67 percent), rhyodacite (67-72 percent), and rhyolite (>72 percent).

The sample subset for each drill hole was examined by binocular microscope, and detailed descriptions of the occurrence of the hydrothermal alteration minerals and their paragenetic relations were noted. At this time, we selected appropriate hydrothermal alteration mineralogy samples for X-ray diffraction (XRD), scanning electron microscope (SEM), fluid-inclusion, and electron microprobe analyses.

The mineralogy of many altered and unaltered drill-core specimens was determined by XRD using a Norelco X-ray diffractometer equipped with a graphite monochrometer and

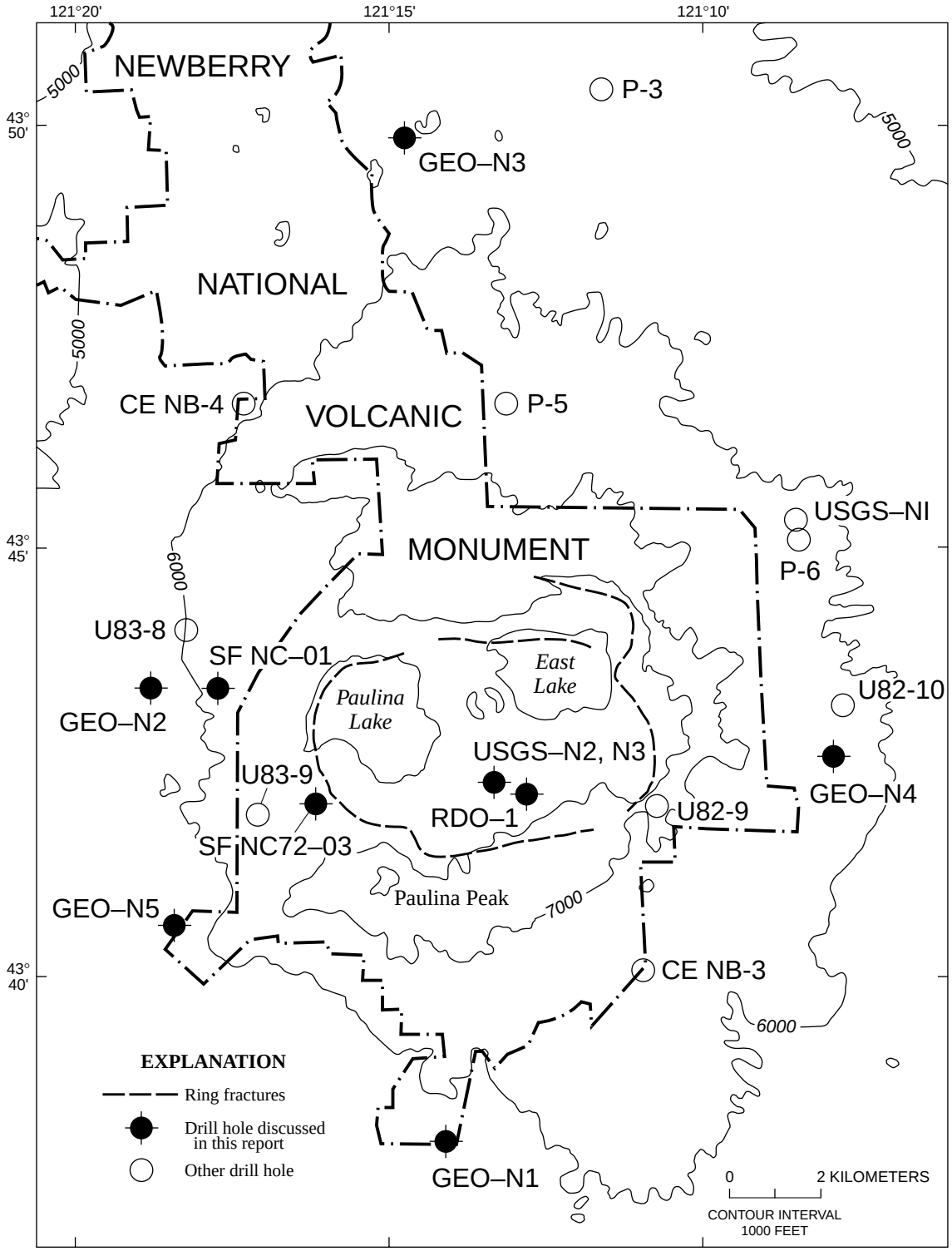

Figure 3.—Map showing location of geothermal exploration drill holes at Newberry volcano (after Olmstead and Wermiel, 1988).

Ni-filtered Cu-Kα radiation. Rock and mineral specimens were prepared as slurries on glass slides and run at 1˚2θ/min; selected zeolite and clay samples were heated in a furnace at 450 or 550˚C and X-rayed a second time or were glycolated by placing the slides in an atmosphere of ethylene glycol at 60˚C for 1 hour before X-raying again. In later analyses, the Norelco XRD was controlled by a Dapple computer automation system.

Several hydrothermal mineral specimens were carbon or gold-palladium coated and mounted in a Cambridge Stereoscan 180 or 250 SEM (equipped with an X-ray energy-dispersive spectrometer or EDS) in order to obtain detailed information on the morphology, paragenesis, and semiquantitative chemistry of very small hydrothermal mineral specimens.

Doubly polished thick sections of hydrothermal quartz and calcite were prepared from as many drill core specimens as possible in order to obtain data on past subsurface temperatures and fluid salinities at Newberry volcano. Measurements of fluid-inclusion homogenization temperatures (T_h) and final melting-point temperature (T_m), determined by the freezing method (Roedder, 1962), for specimens from drill holes GEO-N2, SF NC72-03, SF NC-01, and RDO-1 were made by using a Linkam THM 600 heating/freezing stage and TMS 90 temperature-control system. A Chaixmeca heating/freezing stage was used to obtain fluid-inclusion data for the USGS-N2 drill hole. Successive calibration runs, using synthetic fluid inclusions (Bodnar and Sterner, 1984) and chemical compounds with known melting points recommended in Roedder (1984), suggest that the accuracy of the homogenization temperature (T_h) measurements should be within ±2.0˚C and that the final melting-point temperature (T_m) values should be accurate to at least ±0.2˚C for the Linkam heating/freezing stage. The Chaixmeca heating/freezing stage has similar accuracy. Salinity of the fluids trapped inside the fluid inclusions was calculated, in weight percent NaCl equivalent, by an equation given in Potter, Clynne, and Brown (1978). Selected specimens were crushed with a device manufactured by M.K. Latham Enterprises in order to observe the behavior of the gas bubble when the fluid inclusions were breached. By this means, some information can be obtained about the nature of the vapor phase within the fluid inclusions (Roedder, 1984).

Quantitative chemical analyses for several hydrothermal minerals from the USGS-N2 drill core were obtained with an ARL-EMX electron microprobe by using both natural and synthetic mineral standards. A defocused 15-25 μm beam was utilized at an accelerating voltage of 15 kV, a sample current of 15 nA, and a counting time of 10 seconds.

ACKNOWLEDGMENTS

Our knowledge of Newberry volcano geology, hydrology, and geochemistry was greatly enhanced through discussions with W.W. Carothers, S.E. Ingebritsen, N.S. MacLeod, R.H. Mariner, E.A. Sammel, and D.R. Sherrod. We thank M.J. Johnson, C.A. Swanberg, and W.C. Walkey of GEO-Newberry Crater, Inc. for providing us with preliminary data from the GEO-N1 and GEO-N3 drill holes and allowing us to sample the three other GEO-Newberry Crater, Inc., and the two Santa Fe Geothermal, Inc., drill cores. P.M. Wright of the Energy and Geoscience Institute of the University of Utah permitted us to sample GEO-Newberry, Inc. drill cores GEO-N1 and GEO-N3 and Cal Energy CE NB-3 and CE NB-4 for this study. The assistance of M.H. Price, L. Stevens, and S. McKnight with X-ray diffraction, computer manipulations, and diagrams, S. Wessells with some of the drafting, and R.L. Oscarson with scanning electron microscope studies is gratefully acknowledged. We especially acknowledge the manuscript reviews by J.M. Donnelly-Nolan, R.C. Erd, and D.R. Sherrod, which greatly improved this report.

GEOLOGIC SETTING

Newberry volcano, one of the largest of the Cascade volcanoes, is also one of the largest Quaternary volcanoes in the conterminous United States (MacLeod and Sherrod, 1988). Many physical, chemical, and age similarities between Newberry volcano and the much larger Medicine Lake volcano in northern California suggest that the two volcanoes have similar origins and are related to the Cascade Range of volcanoes (Donnelly-Nolan, 1988). Newberry volcano is at the western end a group of Miocene to Holocene volcanic vents that extend northwestward across much of the southeast quarter of Oregon. Radiometric ages indicate that the volcanic activity is progressively younger toward the west, culminating in the Holocene volcanism at Newberry (Walker, 1974; MacLeod, Walker, and McKee, 1976). The flanks of Newberry volcano are mantled by more than 400 cinder cones and fissure vents, several rhyolitic domes, flows, and pyroclastic deposits, as well as basaltic to basaltic-andesite flows and pyroclastic deposits, all of Quaternary age (MacLeod and others, 1981). Paleomagnetic studies of the surficial basaltic to rhyolitic lava flows extruded from Newberry volcano and of flows recovered from the USGS-N2 drill hole show only normal polarities; thus the volcano probably is younger than 0.7 Ma (MacLeod and Sammel, 1982). Drill holes GEO-N1 and GEO-N3 did penetrate rocks having reversed polarities; however, these older rocks and other nearby, reversely polarized domes and flows may predate Newberry volcano (MacLeod and others, 1995). MacLeod and Sammel (1982) and MacLeod and Sherrod (1988) describe multiple sets of ring fractures within the Newberry caldera, which indicate that caldera collapse may have occurred more than once following major eruptions between about 0.3 and 0.5 Ma. Postdating the last caldera collapse are several intracaldera volcanic deposits, including the Big Obsidian Flow, which overlie

the ~6.8-ka Mazama ash bed (Bacon, 1983; MacLeod and Sherrod, 1988).

Geophysical studies (summarized in Fitterman, 1988) suggest that the interior of Newberry volcano is composed of three distinct zones. The upper zone consists predominantly of younger unaltered silicic to mafic lava flows and tuffs along with their feeder pipes and dikes. In this zone, electrical resistivities are high (Fitterman, Stanley, and Bisdorf, 1988), and seismic velocity (Catchings and Mooney, 1988) and densities (Gettings and Griscom, 1988) are low. An intermediate zone contains older, hydrothermally altered, silicic to mafic lava flows and tuffs, abundant dikes, and some small intrusive pod-like bodies. The geophysical studies show that the intermediate zone has moderate density, intermediate seismic velocity, and low electrical resistivity. Feeder dikes beneath the ring fractures are interpreted from high gravity values. The lowermost zone, characterized by high electrical resistivity, high seismic velocity, and high density, may contain numerous sills, dikes, and small pods that are mostly solidified. Seismic tomography studies by Achauer, Evans, and Stauber (1988) show one low-velocity zone that they interpreted as a small molten magma body about 3 to 5 km beneath the surface of the caldera. A later analysis of compressional-wave-attenuation tomography using the data of Achauer, Evans, and Stauber (1988) led Zucca and Evans (1992) to reinterpret this feature as a recently solidified hot intrusion. Stauber, Green, and Iyer (1988) constructed a three-dimensional velocity picture of the crust beneath Newberry volcano using a teleseismic *P* residual method; they indicate that a high *P* velocity zone, possibly attributable to molten or partially molten intrusions, extends from about 10 to 25 km beneath the caldera and western flank of Newberry volcano. Fitterman (1988) and MacLeod and Sherrod (1988) conclude that Holocene volcanism at Newberry volcano has resulted from the intrusion of many small pods and magma chambers rising from deep within the crust; this model is similar to the one proposed by Donnelly-Nolan (1988) for Medicine Lake volcano.

GEOTHERMAL EXPLORATION

Since 1976, twenty drill holes have been completed at Newberry volcano (Olmstead and Wermiel, 1988) in order to evaluate the geothermal energy potential of this young active volcano. Data for seven of the drill holes has not been released; location, depth, temperature, and other data for ten drill holes are given in table 1. Specimens from three drill holes within the caldera and seven drill holes outside the caldera were obtained in order to better understand the physical and chemical processes occurring at several locations within the volcano. The numerous hydrothermal minerals that precipitated within various parts of the volcano, along with their compositions, provide information about the thermal and chemical conditions present at the time the minerals formed. Fluid-inclusion analyses of hydrothermal calcite and quartz crystals give information about past and present temperatures of hydrothermal alteration.

DRILL HOLES WITHIN THE CALDERA

USGS-N2

In the summer of 1978, the U.S. Geological Survey began drilling the USGS-N2 research drill hole in the south-central part of Newberry caldera (Sammel, 1981) (fig. 3) to obtain stratigraphic, heat-flow, and hydrologic information (Muffler, Bacon, and Duffield, 1982). The drill hole was located at an altitude of 1,935 m about 400 m northeast of the Big Obsidian Flow (fig. 2) and was completed in several stages. During 1978, the hole was drilled to a depth of 312 m by the mud-rotary method; it was progressively deepened by the wireline-coring method during the summers of 1979 and 1981 and was completed to 932-m depth in September, 1981 (MacLeod and Sammel, 1982). In 1980, a second offset drill hole (USGS-N3) was spudded just south of USGS-N2 to provide drill core from the upper part of the stratigraphic section. The USGS-N2 and USGS-N3 drill holes are treated in this report as a single drill hole called USGS-N2. Core recovery from 98-m to about 300-m depth ranged from 40 to 90 percent; below 300-m depth in USGS-N2, core recovery was about 90 percent (MacLeod and Sammel, 1982).

The hydrologic system at Newberry volcano, including data from drill hole USGS-N2, was described by Sammel (1983) and Sammel and Craig (1983). Low temperatures measured in the upper part of USGS-N2 probably are due to dilution by downward-percolating cool meteoric water (Sammel, 1983). Some changes in the temperature-depth profile constructed from the drill-hole data can be correlated with differences in permeability of the various rock units penetrated in the drill hole (Sammel, 1981; MacLeod and Sammel, 1982). The maximum near-bottom temperature measured following drilling was 265˚C (Sammel, 1981; MacLeod and Sammel, 1982). A hypothetical conductive thermal gradient of 285˚C/km is given for the drill hole, and a thermal gradient of 706˚C/km was calculated for the lower 250 m of it (Sammel, 1981; MacLeod and Sammel, 1982). The conductive heat flux for the drill hole is more than 10 times greater than the regional average value (MacLeod and Sammel, 1982).

Drill hole USGS-N2 was flow tested in late September 1981. An initial wellhead pressure of 5,700 kPa decreased to 900 kPa after 20 hours of testing (Sammel, 1981). Sammel (1981) and Sammel and Craig (1983) reported a gas phase that consisted predominantly of CO_2 with minor H_2S, CH_4, and other gas phases. Initially, the dilute fluids collected from the drill hole during flow testing were thought to be contaminated by drilling fluids (Keith and others, 1984b); however, later isotopic studies demonstrated that the drill-hole fluid sample was differ-

Table 1.—Geothermal drill holes at Newberry volcano selected for hydrothermal mineralogy studies.

[m.s.l., mean sea level. —, not available]

Drill hole	Latitude	Longitude	Year drilled	Drilling organization	Drill-collar altitude (m above m.s.l.)	Total depth (m)	Max. temp. (˚C)	References[1]
Drill holes within the caldera								
USGS-N2	43˚ 42.5'	121˚ 13.5'	1978–1981	U.S. Geological Survey	1,935	932	265	1,2,7
USGS-N3	43˚ 42.4'	121˚ 13.5'	1980	do.	1,960	186	—-	2,7
RDO-1	43˚ 42.3'	121˚ 13.3'	1983	Sandia National Laboratories	1,969	424	158+	3,7
Drill holes outside the caldera								
GEO-N1	43˚ 38.3'	121˚ 14.5'	1985	GEO-Newberry, Inc.	1,780	1,387	71	5,6,7
GEO-N2	43˚ 43.6'	121˚ 18.7'	1986	do.	1,779	1,337	164	6,7
GEO-N3	43˚ 4 9.9'	121˚ 14.7'	1986	do.	1,753	1,220	57	5,6,7
GEO-N4	43˚ 42.7'	121˚ 08.2'	1987	do.	1,905	703	18	6,7
GEO-N5	43˚ 40.8'	121˚ 18.6'	1987	do.	1,731	988	69	6,7
SF NC-01	43˚ 43.6'	121˚ 18.0'	1984	Santa Fe Geothermal, Inc.	1,859	1,219	170	4,7
SF NC72-03	43˚ 42.1'	121˚ 19.8'	1983, 1984	do.	1,993	1,372	155	4,7

[1]Sources of data: 1, Sammel (1981), 2, MacLeod and Sammel (1982), 3, Black, Priest, and Woller (1984), 4, Arestad, Potter, and Stewart (1988), 5, Swanberg, Walkey, and Combs (1988), 6, Walkey and Swanberg (1990), 7, MacLeod and others (1995).

ent from the drilling fluid (Ingebritsen and others, 1986). Fluid at the bottom of the drill hole is thought to consist predominantly of steam and CO_2 (Ingebritsen and others, 1986).

LITHOLOGY

A lithologic description of the USGS-N2 drill core is given in appendix 1. A preliminary lithologic log for the drill core (MacLeod and Sammel, 1982) has been slightly modified on the basis of later geochemical and petrographic data (Keith and Bargar, 1988). A stratigraphic column for the upper part of the drill core is shown in figure 4, and a stratigraphic representation of the lower two-thirds of the drill core is shown in the left column of figure 5. Keith and Bargar (1988) divided the rock units of USGS-N2 into three lithologic zones. Zone I comprises the upper 320 m of drill core, which contains lacustrine sediment and unconsolidated pumiceous caldera fill interrupted by a 56-m thick obsidian flow. Zone II extends from 320- to 697-m depth. The section above 501 m consists mainly of lacustrine or fluviatile pumiceous ashy sand and gravel, pumiceous tuff and lithic tuff, tuff breccia, a 10-m-thick rhyodacite sill, and two thin glassy dikes; the section from 501 to 697 m contains coarse dacite breccia and dacite and andesite lava flows. Zone III, which extends from 697- to 932-m depth, is mostly made up of subhorizontal andesite, basaltic andesite, and basalt lava flows and interflow breccias.

HYDROTHERMAL ALTERATION

SURFACE TO 320-M DEPTH

Local palagonitization and some hydration of glass are about the only alteration products seen in the upper 300 m of the drill core, in which the measured temperatures ranged from 18 to 39˚C (Sammel, 1981). XRD analyses also show the presence of minor siderite at 135-m depth, amorphous silica at 181-m depth, and traces of smectite at depths of 174 and 185 m. Beginning at about 300-m depth (fig. 5), scarce zeolites and other hydrous silicates locally replace basaltic

glass in subhorizontal layers of sandstone and siltstone (fig. 6) and fill small fractures and intergranular pore spaces. Calcite and aragonite crystals were deposited later (fig. 7) in steeply dipping fractures as much as 2 mm wide. Although evidence for hydrothermal alteration is lacking for most of the 300- to 320-m interval, a chemical analysis of basaltic glass siltstone at 311.4-m depth shows more than 22 weight percent volatiles. This is the most highly altered core specimen analyzed (table 2). The sample also contains substantially more Cr, Cu, and Ni than any other rock analyzed from Newberry volcano (tables 3 and 4).

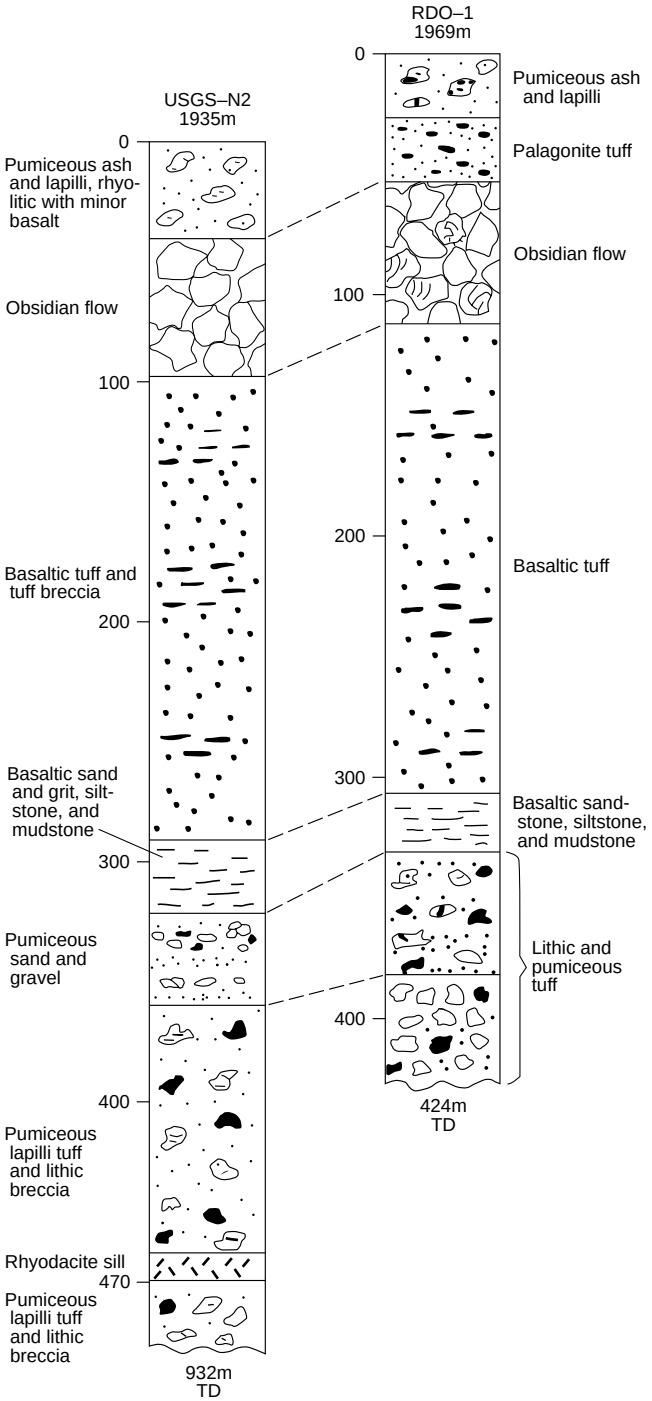

Figure 4.—Comparison of lithologic units in upper part of USGS-N2 drill hole with those of RDO-1 drill hole (after Keith and others, 1986). Drill-hole elevations in meters above mean sea level; TD,Total depth of drill hole.

320- TO 697-M DEPTH

The interval from 320- to 697-m depth is mostly silicic, ranging from rhyolite having a volatile-free SiO_2 value of 73.8 weight percent, in a light-colored pumiceous lithic tuff at 474.6-m depth, to massive and brecciated rhyodacite to andesitic lavas from 501- to 697-m depth that have volatile-free SiO_2 values as low as 60.8 weight percent (table 2 and appendix 1). Rhyolitic to rhyodacitic pumice-rich tuff and lithic tuff from 320- to 501-m depth include abundant amorphous, hydrated glass, detected by XRD, much of which is incipiently to totally replaced by smectite (fig. 8A). Siderite, along with local magnesite and ankerite-dolomite, is abundant as a late-deposited coating on fractures, breccia fragments, and pore-space infilling throughout this interval (figs. 5, 8B, C, and D).

Pumiceous tuff immediately above and below the rhyodacite sill at 460- to 470-m depth has been subjected to more intense, higher temperature alteration due to injection of the sill into wet tuff. The rhyodacite sill is devitrified to a cryptocrystalline mixture of cristobalite and alkali feldspar; however, the perlitic texture remains. Although the rhyodacite sill itself is very dense, secondary permeability is provided by cross-cutting fractures (fig. 8E). Fine-grained quartz, chalcedony, pyrrhotite, pyrite, marcasite, and siderite were deposited along fractures in the sill, and white smectite replaced groundmass of the brecciated parts. The tuff at the upper contact of the sill is baked. A decrease in temperature within the adjacent rock outward from the top and bottom of the sill is reflected by a corresponding decrease in the intensity of alteration, as small amounts of quartz, pyrrhotite, pyrite, calcite, and siderite are deposited in pore spaces, and chlorite and mordenite replace glass in the tuff.

Below the rhyodacite sill, two thin (less than 1-m thick), glassy dikes intersect the pumiceous lithic tuff at depths of 471 m and 479 m. These dike rocks are hydrated and partly replaced by mordenite, and they were injected at sufficiently high temperature to alter the immediately adjacent pumiceous tuff. Thin veinlets lined with calcite and filled with later siderite emanate into the tuff perpendicular to the dike. The contacts of these thin dikes with the tuff are not baked, but the irregular incursion of dike material into the tuff indicates that the tuff was wet and slightly fluidized when intruded.

Rhyodacite, dacite, and andesite lava flows between 501- and 697-m depth are little altered; however, the rock has been bleached in the five breccia zones and adjacent to fractures throughout this interval. Micro-bleaching effects adjacent to the thin veinlets or hairline cracks are seen in thin section. However, thin sections also show that much of the rock is

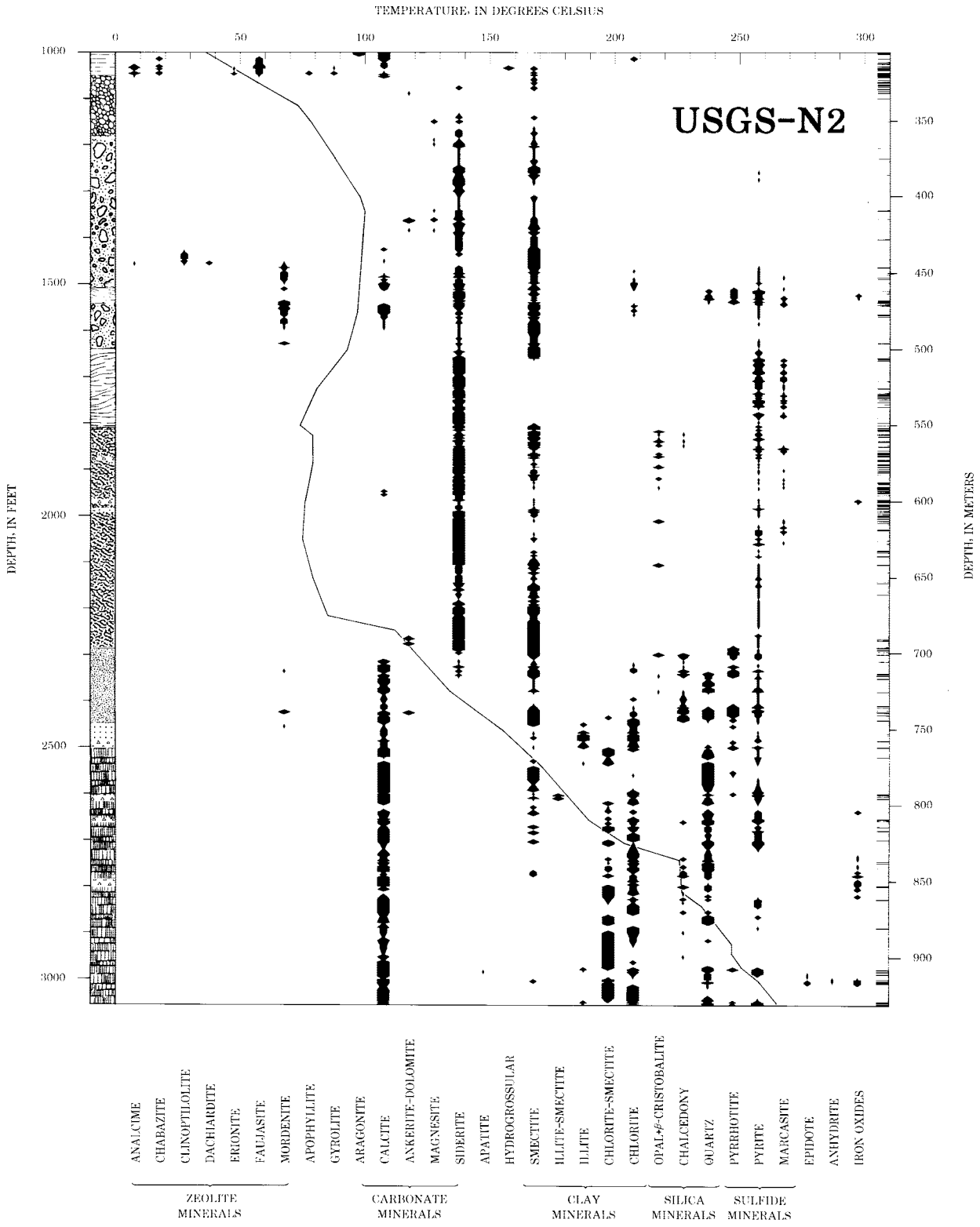

Figure 5.—Distribution of hydrothermal alteration minerals with depth in lower two-thirds of USGS-N2 drill core (after Keith and Bargar, 1988). Left column shows generalized stratigraphic section of rock units in drill hole (MacLeod and Sammel, 1982). Horizontal lines in right column indicate distribution of samples studied. Width of mineral columns shows approximate mineral abundance based on X-ray diffraction and microscope observations. Vertical continuity in mineral presence between samples is assumed except where mineral abundance becomes zero, in which case zero point is arbitrarily placed 0.3 m from last occurrence of the mineral. Solid curve shows measured temperature profile for drill hole (Sammel, 1981; MacLeod and Sammel, 1982).

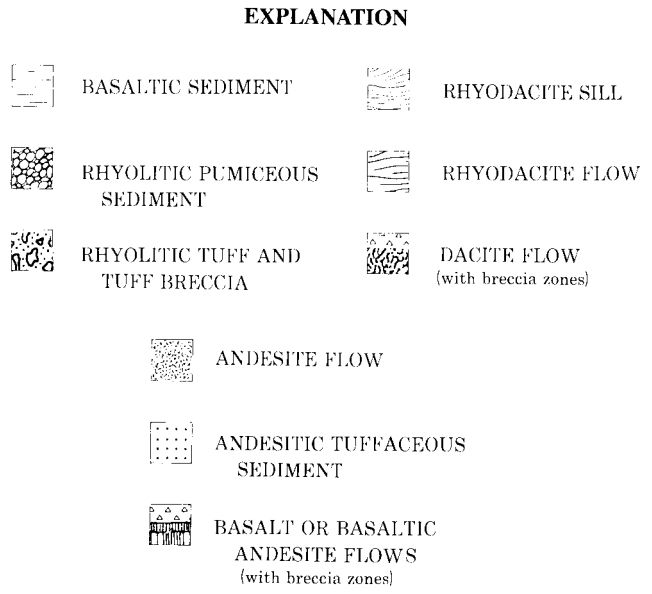

very tight and unaltered, that there was virtually no replacement of primary minerals in the lava flows, and that many vapor-phase cavities lack hydrothermal minerals (fig. 8F). Pyrrhotite was deposited on some fracture surfaces but has been mostly altered to siderite and pseudomorphous marcasite and pyrite (fig. 8G). Scarce opal, cristobalite, and chalcedony were deposited locally on fracture surfaces and in vesicles. Abundant siderite commonly coats fracture surfaces and cements breccia fragments, although much open space between fragments remains in some of the breccias.

The measured temperatures through this zone increased from 40˚C at 300-m depth to 100˚C at about 425-m depth, slowly decreased to 90˚C at 500-m depth, continued to decrease to 75˚C at about 550-m depth, and then increased again to 85˚C at 679-m depth (fig. 5). The temperature increase between depths of 350 m and 500 m in USGS-N2 occurs at a horizon comparable to the position of a 158+˚C hot-water aquifer that was penetrated by drill hole RDO-1 (fig. 12) at a depth of 379.5 m to 397 m. Previous lateral flow of thermal waters between the two holes seems likely (Keith and others, 1986). Mineralogical evidence indicates that the interval of the temperature bulge has been heated to present temperatures or greater by a lateral influx of warm waters. The heating was accompanied by oxidation that resulted in the alteration of pyrrhotite to marcasite, pyrite, and siderite. A residue of the reaction, consisting of sulfur, iron hydroxide, and iron oxide, is present on a fracture surface in the rhyodacite sill. Isotope studies (Carothers, Mariner, and Keith, 1987) show that the siderite in this interval is associated with present temperatures and fluids. Similarly, the presence of iron oxide and natrojarosite and a small temperature inflection measured following drilling suggest that there may have been a major depositional break or an aquifer at 605-m depth in the tuff breccia.

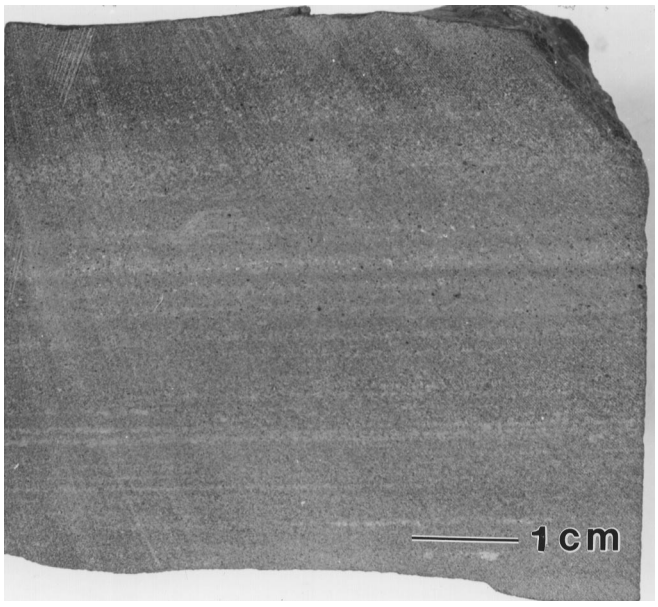

Figure 6.—Fine-grained thin-bedded volcaniclastic sandstone; drill-core specimen from 315.1-m depth in USGS-N2 drill hole. Rock consists of basaltic glass with incipient zeolitization and is of lacustrine origin (MacLeod and Sammel, 1982).

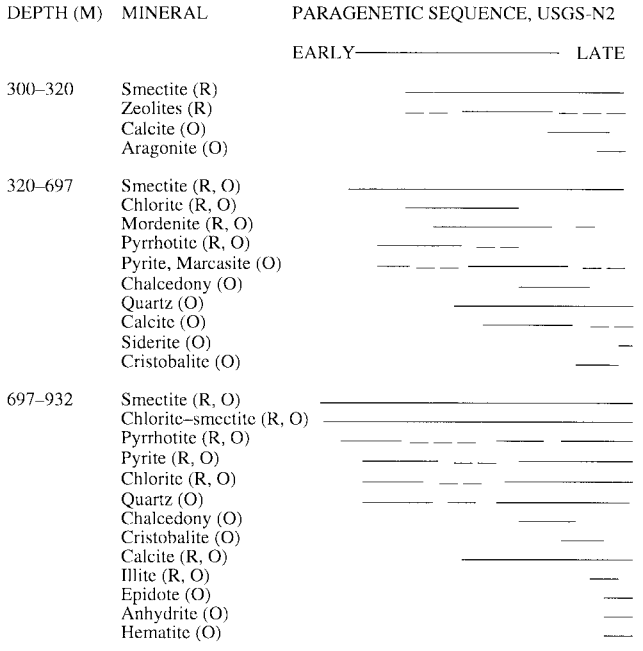

Figure 7.—Generalized paragenetic sequence of selected hydrothermal minerals in USGS N-2 drill core from within caldera of Newberry volcano (after Keith and Bargar, 1988). Most common mineral occurrence in parentheses: O, open-space precipitate; R, replacement of glass or primary minerals. Length of horizontal line has no relation to length of depositional period.

Table 2.—Chemical analyses of USGS-N2 drill-core samples.

Depth (m):	311.4	324.6	400.2	436.5	465.4	469.1	474.6	505.8	652.9	668.7	674.8	689.8	691.0	710.5	734.9	745.2	748.2	752.1
Alteration[2]:	A	F	A	A	A	F	A	F	F	F	F	F	A	A	F	A	A	A
	Major-element analyses (weight percent oxides)[3,4]																	
SiO_2	39.5	65.8	62.1	61.6	70.6	64.6	65.0	66.5	62.3	58.6	62.0	62.0	55.0	61.3	58.2	54.0	57.9	58.5
Al_2O_3	13.0	13.6	14.1	14.5	14.0	13.8	12.8	15.6	16.1	15.8	16.2	16.0	17.0	16.0	15.6	15.0	15.4	16.0
Fe_2O_3	6.62	2.85	4.24	4.38	2.70	3.49	2.29	3.23	5.43	6.97	5.35	5.24	5.57	4.51	8.05	10.1	7.62	8.02
MgO	4.27	1.22	0.86	0.88	0.25	0.78	0.26	0.51	1.58	2.28	1.55	1.57	2.29	1.66	2.19	2.08	1.86	1.82
CaO	7.17	1.45	3.45	1.95	0.58	2.50	1.85	1.72	3.60	5.26	3.63	3.59	3.47	3.55	4.72	5.17	3.97	3.53
Na_2O	2.94	4.15	4.11	3.75	4.63	3.16	2.90	6.10	4.92	4.10	4.73	4.37	3.54	4.03	4.65	3.02	3.49	2.09
K_2O	0.58	3.21	2.65	1.74	3.69	2.83	2.57	2.07	1.90	1.48	1.78	1.74	0.78	1.72	1.56	1.39	1.57	2.30
TiO_2	0.95	0.39	0.62	0.67	0.26	0.54	0.25	0.64	1.09	1.30	1.06	1.06	1.08	1.07	1.48	1.43	1.45	1.31
P_2O_5	0.20	0.07	0.11	0.10	<0.05	0.11	<0.05	0.15	0.36	0.32	0.34	0.34	0.35	0.34	0.61	0.60	0.58	0.47
MnO	0.10	0.06	0.09	0.08	0.10	0.07	0.07	0.12	0.16	0.15	0.16	0.16	0.15	0.09	0.20	0.33	0.16	0.17
H_2O^+	3.56	4.00	3.11	0.41	0.22	2.59	6.43	0.18	1.68	2.13	2.20	2.46	1.90	1.45	0.49	2.59	3.00	2.91
H_2O^-	18.20	1.01	1.56	6.95	1.39	3.47	4.46	0.54	0.33	0.93	0.25	0.47	5.50	2.15	1.78	1.11	1.61	1.40
CO_2	0.98	1.24	2.56	1.83	1.56	0.87	0.62	1.89	0.62	0.73	0.72	0.91	2.42	1.56	0.64	2.87	0.98	1.77
Cl	0.004	0.091	0.057	0.008	0.009	0.004	0.007	0.005	0.042	0.028	0.049	0.052	0.025	0.004	0.005	0.005	0.003	0.004
F	0.02	0.05	0.04	0.04	0.03	0.03	0.05	0.03	0.03	0.04	0.04	0.04	0.14	0.04	0.05	0.05	0.04	0.05
S	<0.01	0.075	<0.01	0.05	0.08	0.03	0.03	0.30	<0.01	<0.01	<0.01	0.02	0.38	0.05	0.03	1.08	0.48	0.12
Total	98.10	99.27	99.66	98.94	100.15	98.88	99.64	99.59	100.16	100.13	100.07	100.02	99.60	99.53	100.25	100.76	100.11	100.46
SiO_2, volatile free[5]:	52.4	70.7	67.2	68.6	72.8	70.3	73.8	68.6	63.9	60.8	64.0	64.5	61.3	65.0	59.5	57.3	61.3	62.0

The paragenetic sequence of secondary minerals (fig. 7) began with the incipient and partial replacement of glass in the tuff by smectite and zeolites between 320- and 505-m depth. Subsequent intrusion of the sill and dikes into wet tuffs caused local baking effects and deposition of the higher temperature alteration minerals pyrrhotite, chlorite, quartz, pyrite, and calcite in small fractures and pore spaces in and adjacent to the sill. Fractures and open-space fillings between about 505- and 697-m depth contain early deposits of pyrrhotite followed by increased oxidation by the present thermal regime to pyrite, marcasite, and siderite. Silica minerals were deposited earlier than carbonate minerals, possibly at the time of pyrrhotite oxidation.

697- TO 932-M DEPTH

Subhorizontal lava flows and breccia units below 697-m depth usually are more mafic (table 2) and include andesite, basaltic andesite, and basalt. The character of hydrothermal alteration in the interval between 697-m depth and the bottom of the drill hole at 932-m depth is different from that of the shallower alteration. Flow breccias, interflow breccias, and pumice layers are altered by replacement of groundmass, especially interstitial glass, to smectite, mixed-layer chlorite-smectite, and chlorite. Locally, plagioclase and mafic phenocrysts have been partly replaced by calcite and (or) clay minerals. Generally the dense parts of the andesite to basalt lava flows are little altered. In contrast, the flow tops and basal flow breccias, vesicular zones, and interflow breccias, as well as a thin interval of pumiceous tuff and tuff breccia, are substantially altered (fig. 5).

The dense andesite flow between depths of 697 m and 758 m is highly fractured and altered to light-green clay minerals from 737- to 745-m depth. Several stages of vein minerals consisting of pyrrhotite, pyrite, clay minerals, quartz, and calcite have been deposited (figs. 9A, B, and C), and there has been partial replacement of calcite by quartz. In spite of extensive alteration and mineral deposition, the fractures are not completely filled, and this zone may have been a young aquifer for lateral migration of thermal waters. The fractured andesite flow overlies interflow breccia and pumice layers that are also extensively altered.

Below 758-m depth, dense massive lava flows are sporadically intersected by steeply dipping hairline fractures that are typically filled with blackish-green clay (mixed-layer chlorite-smectite) and, locally, later calcite (fig. 9D). Wide fractures are scarce, but where present they contain black-green (mixed-layer chlorite-smectite) clay and euhedral quartz and calcite crystals. Vesicles are locally filled with similar blackish-green clay, quartz, and calcite (fig. 9E), and the groundmass in the vesicular zone is more altered due to relatively high permeability. Leaching has occurred in interflow breccias (fig. 9F). In the interval from 697- to 930-m depth, the

Table 2.—Chemical analyses of USGS-N2 drill-core samples—Continued.

Sample No.[1]:	2488	2501	2600	2603.5	2609.5	2631	2655	2661.5	2671	2791.5	2798	2976	2983.5	2988	3049	3051	3054.5
Depth (m):	758.3	762.3	792.0	793.5	795.4	801.9	809.2	811.2	814.1	850.8	852.8	907.1	909.4	910.7	929.3	929.9	931
Alteration[2]:	A	A	F	A	A	F	A	A	F	A	A	F	A	A	F	A	A
Major-element analyses (weight percent oxides)[3,4]																	
SiO_2	50.8	45.9	52.2	46.1	46.5	51.5	46.9	48.5	50.9	48.5	49.9	51.4	46.6	47.2	50.0	48.9	52.4
Al_2O_3	13.4	16.2	15.1	16.4	16.0	15.8	14.8	15.5	16.0	16.6	16.2	16.8	17.1	14.9	16.5	17.6	16.0
Fe_2O_3	11.2	13.0	11.9	12.0	11.2	11.2	11.6	10.3	10.9	11.2	11.1	11.3	11.6	10.4	11.2	11.3	9.22
MgO	2.99	4.01	3.70	3.43	4.15	4.00	4.47	3.60	4.00	4.13	3.91	4.24	3.08	3.52	3.89	4.54	2.62
CaO	5.49	5.63	7.44	5.66	6.98	8.50	6.40	8.93	8.72	7.79	6.97	8.74	7.30	9.11	9.15	7.11	5.77
Na_2O	2.70	2.87	3.94	3.48	3.78	3.83	4.45	3.03	3.63	3.73	4.30	3.93	3.84	3.52	3.14	2.93	3.29
K_2O	0.74	0.25	0.92	0.84	0.41	0.80	0.13	0.31	0.90	0.58	0.54	0.61	0.85	0.60	0.57	0.25	1.33
TiO_2	1.98	2.41	2.31	2.28	2.11	2.08	2.17	1.97	2.04	2.05	1.95	2.10	2.11	1.91	2.03	2.23	1.66
P_2O_5	0.31	0.44	0.43	0.41	0.38	0.36	0.36	0.33	0.36	0.31	0.31	0.31	0.32	0.28	0.31	0.34	0.33
MnO	0.13	0.16	0.19	0.14	0.15	0.16	0.23	0.16	0.17	0.14	0.16	0.21	0.14	0.18	0.16	0.17	0.17
H_2O^+	2.68	3.22	0.79	3.39	3.83	0.04	3.28	2.70	0.11	2.26	2.19	0.45	2.69	2.98	1.55	2.70	2.65
H_2O^-	1.37	1.59	0.88	1.78	0.91	1.54	0.54	0.73	1.97	0.65	0.28	0.73	0.40	0.39	0.43	0.54	1.49
CO_2	3.82	2.52	0.74	3.76	5.02	0.12	4.48	4.55	0.29	2.48	2.37	0.33	2.52	4.96	1.42	0.68	2.34
Cl	0.004	0.005	0.004	0.004	0.004	0.006	0.006	0.004	0.004	0.005	0.005	0.006	0.004	0.003	0.011	0.012	0.006
F	0.03	0.05	0.04	0.04	0.04	0.03	0.03	0.03	0.03	<0.035	0.04	0.03	0.03	0.03	0.02	0.025	0.04
S	3.87	4.2	<0.01	2.3	0.87	<0.01	1.46	0.62	<0.01	<0.01	<0.01	<0.01	<0.01	1.42	0.07	2.56	1.72
Total	101.51	102.46	100.59	102.02	102.33	99.97	101.30	101.26	100.04	101.47	100.23	101.20	98.60	101.40	100.45	101.89	101.04
SiO_2, volatile free[5]:	54.3	48.3	53.2	49.5	50.2	52.4	50.4	52.0	52.1	50.5	52.3	51.6	50.1	50.7	51.5	49.9	55.4

[1] Sample numbers are drill-hole depths in feet.

[2] A, altered rocks, F, freshest available sample from a flow unit.

[3] Analyses of SiO_2 through MnO determined by X-ray spectroscopy. Analysts: A. Bartel, J.S. Wahlberg, J.E. Taggart, and J. Baker, U.S. Geological Survey, Denver, Colo.

[4] Analyses of H_2O^+ through S determined by conventional rock analysis methods. Analysts: N. Elsheimer, L. Espos, and B. King, U.S. Geological Survey, Menlo Park, Calif.

[5] Volatile free SiO_2 values calculated by normalizing to 100 percent after subtracting H_2O^+, H_2O^-, and CO_2.

temperature increased in a quasi-linear fashion from 100˚C to 264˚C (fig. 5).

Near the bottom of the interval, epidote and anhydrite occur in pore spaces and cavities as late-stage deposits (fig. 5). Plagioclase phenocrysts and groundmass have been partly replaced by calcite and probably provided the chemical components for the chlorite and epidote. Microprobe analyses of cross sections of plagioclase phenocrysts (table 5) in the basal lava flows show slight patchy differences in the Na:Ca:K ratios, but the phenocrysts are consistently higher in Ca and lower in Na and K relative to groundmass plagioclase. Significant albitization of plagioclase has not occurred in these rocks. The clay minerals gradually change structurally and chemically with increasing depth and temperature from predominantly smectite to mostly mixed-layer chlorite-smectite with local chlorite.

The bottom 2 m of USGS-N2 drill core, 930- to 932-m depth (fig. 9G), is highly bleached flow breccia and vesicular basalt. Groundmass is partly replaced by pyrrhotite, pyrite, chlorite, quartz, and calcite, and vesicles are partly to totally filled with well-crystallized chlorite, illite, pyrrhotite, pyrite, quartz, calcite, and a small amount of epidote. Plagioclase phenocrysts are partly replaced by calcite and illite; chlorite and epidote fill open spaces left by leaching of the phenocrysts.

Bleaching is conspicuous in the basal parts (approximately 1 m thick) of the lowest two lava flows and decreases rapidly upward into unbleached dense lava. The basal bleaching is due to subhorizontal fluid flow; low vertical permeability restricted fluid access to dense parts of the flows. Bleaching appears to cause little change in mineralogy in the rock, probably only the leaching of iron. However, in some bleached zones pyrrhotite is present, again showing that it forms in low-permeability rocks where fS_2 of fluids is low for a given fO_2 (and fH_2) relative to pyrite (Browne, 1970). Sammel (1981) noted gas, probably CO_2, in the vesicular parts of these lowest two flows during drilling, and the flow test of USGS-N2 produced a fluid that was about 20 weight percent CO_2 (Ingebritsen and others, 1986; Sammel, Ingebritsen, and Mariner, 1988).

The general paragenetic sequence of secondary minerals below 697-m depth in USGS-N2 (fig. 7) began with clay alteration of interstitial glass and replacement of mafic phenocrysts by mixed-layer chlorite-smectite. Locally, small amounts of iron oxide were also deposited early. Small fractures were

Table 3.—Spectroscopic trace-element analyses of USGS-N2 drill-core samples.

[Trace element analyses (in ppm) by optical spectroscopy. Analyst: M. Malcom, U.S. Geological Survey, Denver, Colo. Looked for but not found: Ag, Au, Bi, Cd, Er, Eu, Gd, Ho, Mo, Pr, Sm, Sn, Tb, and U. A, altered; F, freshest available rock from a flow unit]

Sample No.	Depth (m)	Alteration	As	Ba	Be	Ce	Co	Cr	Cu	Dy	Ga	Ge	La	Li	Mn	Nb	Nd	Ni	Pb	Sc	Sr	Th	V	Y	Yb	Zn
1021.5	311.4	A	<20	260	<2	23	30	120	80	11	21	40	12	9	1,100	<8	9	48	<8	35	370	<8	180	20	3	53
1065	324.6	F	<20	760	2	49	<2	<2	9	12	22	20	26	16	520	13	26	<4	9	10	95	8	50	38	5	48
1313	400.2	A	<20	730	2	42	5	<2	11	11	22	<20	23	13	750	8	22	<4	<8	13	160	<8	770	35	4	53
1432	436.5	A	<20	840	2	42	6	<2	14	13	21	<20	24	20	720	12	25	<4	10	15	170	9	83	34	4	60
1527	465.4	A	<20	1400	2	67	<2	<2	8	17	23	<20	31	<4	840	20	32	<4	<8	10	50	14	27	46	6	66
1539	469.1	F	<20	740	2	49	3	<2	11	14	22	<20	25	7	650	12	25	<4	<8	12	150	12	35	38	4	53
1557	474.6	A	<20	720	3	62	<2	<2	7	16	20	<20	31	7	590	16	29	<4	9	9	78	9	5	45	6	57
1659.5	505.8	F	70	660	<2	47	<2	<2	<2	15	24	<20	24	6	980	12	27	<4	<8	15	220	<8	180	41	5	90
2142	652.9	F	<20	570	<2	47	2	<2	3	13	24	30	25	6	1,300	12	27	<4	<8	19	370	<8	24	40	4	88
2194	668.7	F	<20	500	<2	43	11	12	24	14	23	30	22	8	1,200	11	28	8	9	26	360	<8	120	36	4	79
2214	674.8	F	<20	580	<2	46	2	<2	<2	11	21	20	23	6	1,300	13	29	<4	<8	19	380	<8	55	39	4	88
2263	689.8	F	<20	580	<2	45	3	<2	<2	14	27	20	24	5	1,300	13	26	<4	<8	19	370	<8	21	39	4	85
2267	691.0	A	<20	440	<2	51	2	<2	<2	11	25	20	25	9	1,200	12	30	<4	<8	19	360	<8	20	42	5	88
2331	710.5	A	<20	620	<2	50	<2	<2	<2	13	22	20	25	<4	780	15	29	<4	<8	18	360	<8	21	39	5	93
2411	734.9	F	<20	530	<2	47	8	<2	2	15	23	30	23	<4	1,500	13	30	<4	<8	25	370	<8	62	46	5	96
2445	745.2	A	20	460	<2	43	11	<2	<2	14	26	30	23	8	2,400	13	32	<4	9	24	240	<8	55	44	5	110
2455	748.2	A	<20	690	<2	50	6	<2	2	16	28	30	24	<4	1,300	14	31	<4	11	24	480	<8	60	45	5	92
2467.5	752.1	A	<20	800	2	50	6	<2	3	16	28	30	24	11	1,400	15	29	<4	8	24	270	<8	330	45	5	110
2488	758.3	A	80	350	<2	26	27	10	60	10	22	30	15	10	1,100	<8	14	11	17	40	340	<8	310	27	3	68
2501	762.3	A	70	170	<2	34	33	13	44	13	27	40	17	12	1,300	<8	23	11	12	47	380	<8	350	30	3	83
2600	792.0	F	<20	320	<2	29	29	<2	41	14	25	30	17	<4	1,500	<8	23	6	8	43	370	<8	320	32	4	78
2603.5	793.5	A	40	320	<2	30	27	34	41	11	27	30	16	7	1,100	<8	20	10	9	46	300	<8	250	25	3	71
2609.5	795.4	A	30	170	<2	32	28	34	57	10	24	40	15	13	1,200	<8	22	16	<8	38	340	<8	260	28	3	75
2631	801.9	F	<20	290	<2	24	30	35	61	11	24	30	15	6	1,300	<8	21	14	9	45	400	<8	320	28	3	72
2655	809.2	A	<20	900	<2	30	28	19	60	10	27	40	16	11	1,900	<8	20	13	9	39	330	<8	300	26	3	74
2661.5	811.2	A	<20	210	<2	24	26	36	73	13	26	30	16	8	1,300	<8	19	15	9	39	390	<8	280	28	3	68
2671	814.1	F	<20	290	<2	28	29	35	62	12	23	40	15	5	1,400	<8	22	17	<8	44	410	<8	300	29	3	72
2791.5	850.8	A	<20	270	<2	23	31	25	51	12	26	40	12	11	1,100	<8	20	16	8	42	410	<8	310	26	3	71
2798	852.8	A	<20	270	<2	14	29	25	39	9	25	30	12	11	1,300	<8	21	18	<8	40	380	<8	220	25	3	61
2976	907.1	F	<20	240	<2	20	28	23	45	9	23	40	12	5	1,500	<8	18	17	9	41	390	<8	810	25	3	62
2983.5	909.4	A	<20	280	<2	23	29	28	19	11	26	30	12	12	1,200	<8	19	18	11	44	410	280	190	27	3	74
2988	910.7	A	<20	240	<2	22	27	19	31	12	22	30	12	15	1,500	<8	16	14	<8	40	370	<8	210	24	3	63
3049	929.3	F	<20	280	<2	21	30	19	44	11	23	30	12	9	1,300	<8	19	16	9	42	420	<8	470	25	3	69
3051	929.9	A	30	160	<2	22	35	21	54	13	27	40	13	13	1,500	<8	25	18	8	47	400	<8	400	26	3	78
3054.5	931.0	A	30	410	<2	36	21	8	25	13	24	30	18	11	1,400	8	21	7	<8	33	320	<8	620	34	4	75

Table 4.—INAA trace-element analyses of USGS-N2 drill-core samples.

[Trace-element analyses (in ppm) by Instrumental Neutron Activation Analysis (INAA). Analyst: J.S. Mee, U.S. Geological Survey, Denver, Colo. --, not determined. Alteration state (Alt.) A, altered; F, freshest available sample from a flow unit]

Sample No.	Depth (m)	Alt.	Ba	Co	Cr	Cs	Hf	Rb	Sb	Ta	Th	U	Zn	Zr	Sc	La	Ce	Nd	Sm	Eu	Gd	Tb	Tm	Yb	Lu
N2 1021.5	311.4	A	227	22.70	116.0	0.44	2.42	12	< 0.7	0.40	1.18	0.60	61	123	20.80	8.6	18.8	< 10	3.10	0.87	< 8	0.48	0.27	1.94	0.283
N2 1065	324.6	F	792	3.13	2.8	5.40	7.71	91.9	1.38	1.31	8.55	2.87	51.3	309	7.26	26.7	52.8	26.0	6.12	0.98	6.4	1.05	0.61	4.70	0.672
N2 1313	400.2	A	769	5.87	2.3	2.89	7.17	75	0.68	1.08	6.82	2.29	62	324	9.83	23.5	47.0	24.1	5.76	1.25	6.4	0.92	0.54	4.04	0.611
N2 1432	436.5	A	793	6.55	3.2	1.92	7.01	47.6	0.58	1.10	6.68	2.41	61.4	259	10.91	23.2	45.8	26.0	5.69	1.26	5.8	5.8	1.00	0.59	0.620
N2 1527	465.4	A	831	0.62	< 2	1.45	10.70	108	1.23	1.63	10.50	3.60	72	457	7.68	34.6	68.9	32.0	8.50	1.02	8.0	1.52	0.90	6.84	0.974
N2 1539	469.1	F	750	3.96	3.8	9.26	7.06	98	0.57	1.22	7.42	2.55	56	316	8.98	25.3	49.2	24.6	6.20	1.07	6.3	1.00	0.58	4.27	0.661
N2 1557	474.6	A	744	0.72	< 0.8	59.80	9.62	147	1.63	1.50	9.31	3.10	56.3	419	6.40	30.1	61.2	34.0	7.30	0.95	7.6	1.21	0.79	5.60	0.862
N2 1659.5	505.8	F	689	0.94	< 2	0.66	6.96	37	0.46	1.07	4.11	1.43	90	275	11.29	24.6	51.1	30.7	7.37	1.94	7.2	1.15	0.65	4.51	0.700
N2 2142	652.9	F	609	2.81	< 1	1.24	5.93	35	< 0.6	1.01	3.40	1.20	98	244	14.50	24.3	50.0	30.0	7.63	2.05	11.0	1.17	0.70	4.46	0.630
N2 2194	668.7	F	518	11.90	18.5	5.80	5.26	34	< 0.5	0.95	3.27	1.07	92	220	20.00	20.6	42.7	30.6	6.60	1.77	5.1	1.01	0.52	3.80	0.611
N2 2214	674.8	F	596	2.84	< 2	1.11	5.78	32.6	0.20	1.04	3.42	0.96	95	204	14.18	22.7	49.8	31.5	7.15	2.09	7.7	1.12	0.63	4.12	0.640
N2 2263	689.8	F	576	2.53	< 2	1.16	5.50	34	< 0.6	0.98	3.23	1.19	88	191	13.40	23.1	47.3	32.0	7.20	1.94	6.0	1.02	0.63	4.12	0.580
N2 2267	691.0	A	421	2.69	< 3	0.70	5.90	16	0.31	1.03	3.55	1.30	96	236	13.90	23.7	49.9	31.0	7.90	2.08	7.0	1.10	0.48	4.24	0.600
N2 2331	710.5	A	613	2.38	< 2	2.32	5.89	35	< 0.2	1.05	3.41	1.20	103	277	13.50	23.7	48.4	31.0	7.24	1.98	6.0	1.09	0.56	4.35	0.612
N2 2411	734.9	F	545	7.54	< 0.8	1.82	5.80	26	< 0.7	1.18	2.70	1.00	110	198	18.50	22.9	50.0	33.0	8.60	2.30	11.0	1.31	0.72	4.81	0.700
N2 2445	745.2	A	453	11.40	< 4	0.75	5.50	24	0.66	1.06	2.70	0.80	131	228	17.60	21.8	47.0	32.0	8.30	2.08	7.0	1.24	0.70	4.75	0.680
N2 2455	748.2	A	700	7.01	< 3	7.03	5.69	27.7	0.88	1.08	2.60	0.98	94	257	17.60	22.2	47.2	30.6	8.13	2.28	8.0	1.32	0.60	4.61	0.691
N2 2467.5	752.1	A	721	5.70	< 6	1.60	6.60	43	0.45	1.25	3.00	1.20	113	250	17.90	23.5	51.0	32.0	8.40	2.11	11.0	1.27	0.72	5.30	0.730
N2 2488	758.3	A	335	25.80	13.9	0.82	3.36	17.5	1.43	0.68	1.29	0.52	87	121	28.20	12.8	27.3	20.2	5.14	1.52	--	0.87	--	2.93	0.451
N2 2501	762.3	A	213	31.30	19.0	0.54	4.03	< 20	0.80	0.88	1.52	0.70	109	156	34.30	15.7	34.0	22.0	6.40	1.65	7	1.06	0.49	3.58	0.520
N2 2600	792.0	F	338	28.10	2.9	0.45	4.18	16	< 0.9	0.91	1.71	0.60	116	195	32.60	16.0	35.5	28.0	5.97	1.86	4	1.06	0.54	3.57	0.540
N2 2603.5	793.5	A	296	25.50	41.0	0.56	3.65	20	< 1	0.73	1.27	0.50	107	< 200	33.70	13.8	30.2	25.0	5.40	1.44	< 10	0.92	0.25	3.20	0.475
N2 2609.5	795.4	A	171	28.30	41.2	< 0.6	3.51	< 20	< 1	0.64	1.39	<1	105	104	33.00	13.1	28.8	12.0	5.20	1.51	6	0.90	0.40	2.98	0.452
N2 2631	801.9	F	297	28.70	40.6	0.45	3.65	19	< 0.06	0.74	1.30	0.50	103	165	33.00	13.1	29.6	21.6	5.25	1.66	--	0.89	--	3.07	0.483
N2 2655	809.2	A	1,020	27.60	24.5	< 0.4	3.59	< 20	< 0.6	0.85	1.51	0.44	94	189	30.80	14.1	29.6	19.7	5.54	1.29	--	0.90	--	3.10	0.500
N2 2661.5	811.2	A	220	25.60	40.1	0.36	3.47	< 20	0.51	0.69	1.24	0.36	91	130	30.50	13.3	27.6	20.0	5.23	1.72	--	0.87	--	3.03	0.440
N2 2671	814.1	F	236	27.40	40.4	0.56	3.51	16.9	< 0.6	0.74	1.40	0.56	98	140	31.90	12.9	29.1	21.8	5.25	1.63	--	0.95	--	2.89	0.488
N2 2791.5	850.8	A	286	29.90	29.2	0.34	2.83	12	< 0.9	0.49	0.80	<1.	102	<200	31.30	10.5	23.4	< 10	4.43	1.48	< 10	0.88	0.30	2.52	0.384
N2 2798	852.8	A	272	28.40	31.5	< 0.6	2.74	< 10	< 0.9	0.43	1.10	< 0.9	90	< 200	30.40	10.2	22.3	21.0	4.34	1.50	< 7	0.78	0.38	2.67	0.390
N2 2976	907.1	F	255	31.00	33.8	0.43	3.01	12	< 0.9	0.58	1.01	< 1	105	104	33.30	10.6	23.8	17.0	4.59	1.53	5.2	5.2	0.84	0.39	0.409
N2 2983.5	909.4	A	272	28.50	33.3	< 0.4	2.93	19.4	< 0.5	0.54	1.00	<0.4	92	127	32.70	10.7	24.9	< 25	4.65	1.55	--	0.78	--	2.78	0.390
N2 2988	910.7	A	244	27.40	26.7	< 0.6	2.82	< 20	< 0.8	0.48	0.88	<0.9	92	117	29.90	9.9	22.9	< 20	4.14	1.42	< 7	0.79	0.34	2.66	0.365
N2 3049	929.3	F	266	30.70	27.1	< 0.6	2.76	< 20	< 0.9	0.52	0.91	<1	105	< 200	32.50	10.8	24.3	13.0	4.63	1.54	< 7	0.82	0.30	2.69	0.393
N2 3051	929.9	A	194	33.00	29.2	< 0.6	2.93	< 20	< 0.9	0.54	1.10	0.60	116	< 200	34.00	11.0	24.2	< 20	4.76	1.60	< 10	0.83	0.54	2.77	0.426
N2 3054.5	931.0	A	426	19.10	13.7	1.98	4.60	35	0.45	0.81	2.79	0.90	99	183	24.50	17.3	36.1	26.0	5.76	1.58	6	0.92	0.34	3.93	0.580

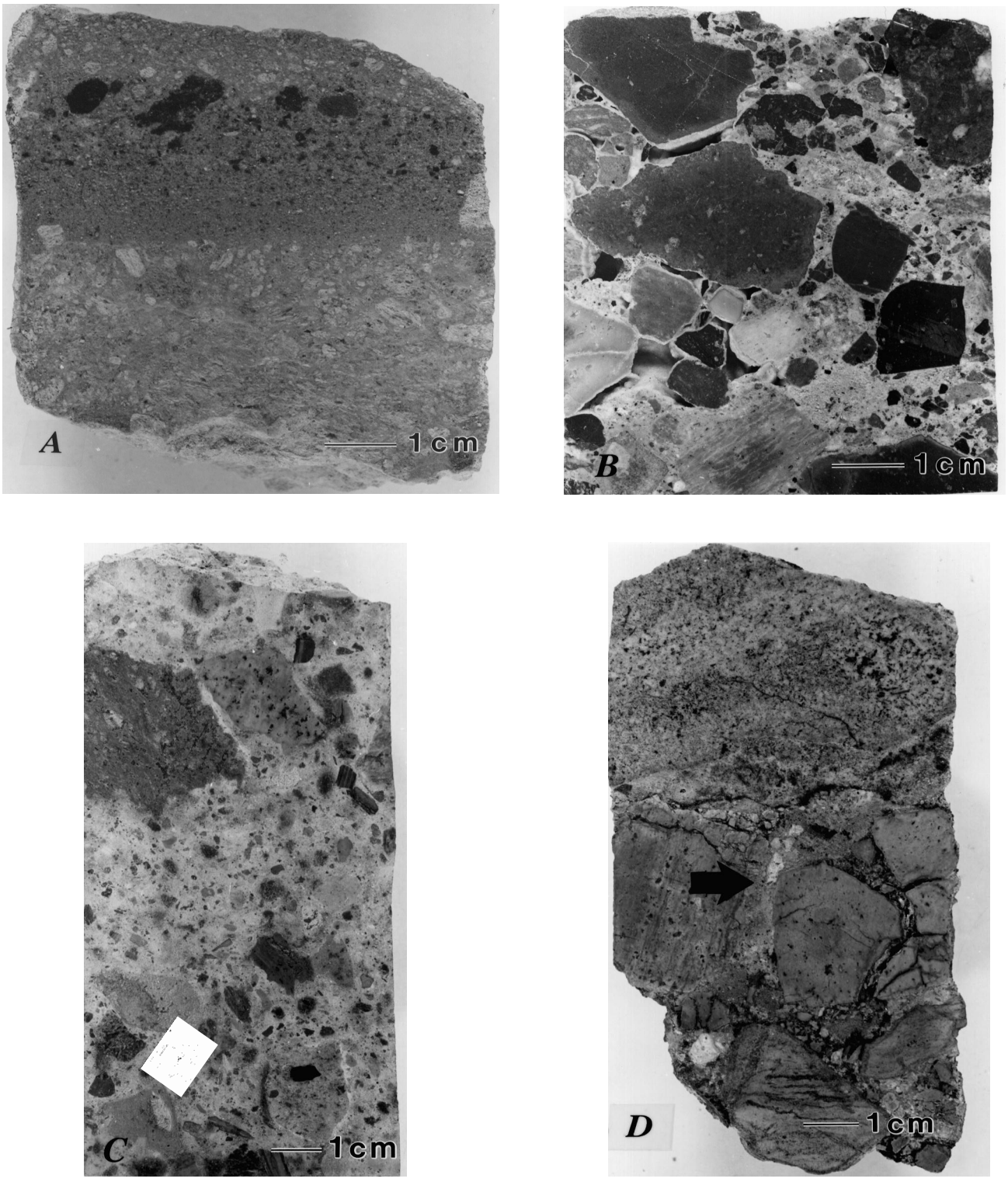

Figure 8.—Drill-core samples from upper and middle parts of USGS-N2 drill hole. A, Pumiceous tuff of unaltered glass with some incipient smectite crystallization, from 351.9-m depth. B, Siderite-cemented lithic-tuff breccia with several unfilled spaces between breccia fragments from 415.1-m depth. C, Pumiceous tuff with incipient smectite replacement and late siderite deposition, from 448.7-m depth. Arrow on specimen points to altered pumiceous glass fragment of siderite and smectite analyzed by XRD. D, Breccia cemented by siderite, from 470.6-m depth. Spaces between breccia fragments are only partly filled. Arrow points to area from which specimen was obtained for XRD analysis. E, Rhyodacite sill from 468.8-m depth; fractures partially filled by secondary minerals. F, Vapor-phase cavities oriented parallel to flow banding in dacite flow from 588.9-m depth. Elongate cavities are coated with vapor-phase tridymite. G, Siderite and pyrite plus marcasite pseudomorphs after pyrrhotite (dark specks) that coat irregular fracture surface in dacite flow at 520.6-m depth.

Figure 8.—Continued.

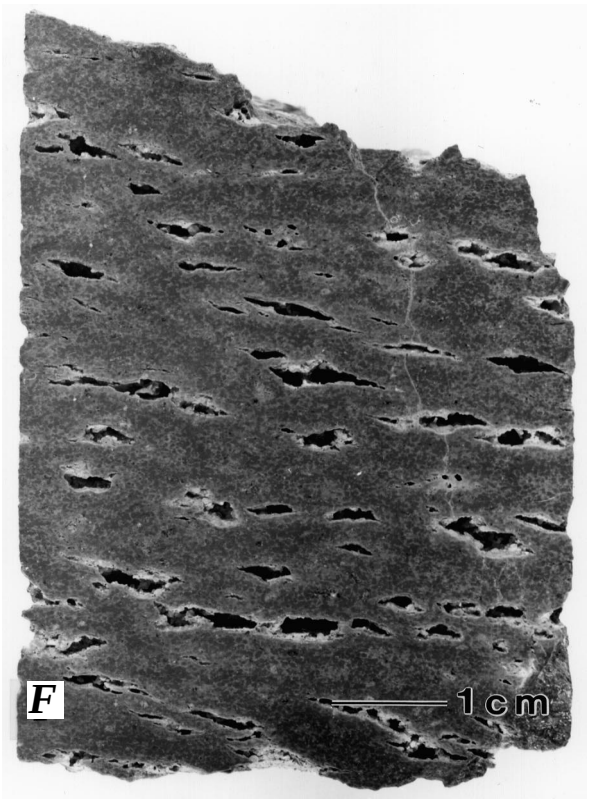

Figure 8.—Continued.

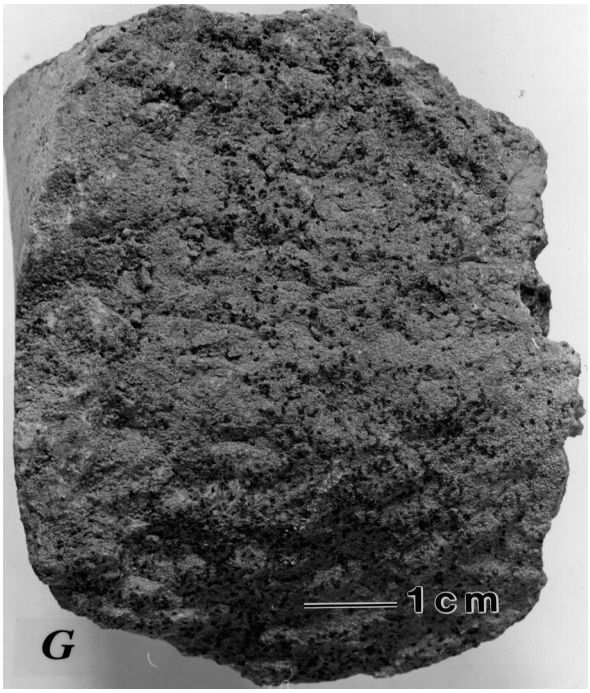

Figure 8.—Continued.

filled with mixed-layer chlorite-smectite and pyrite, which were deposited shortly before and in part were overlapped by deposition of quartz, illite, and the other silica minerals. Most of the calcite precipitated later than quartz and illite, although some codeposition and fluctuating deposition of quartz and calcite appears to have occurred. Anhydrite, epidote, and scarce iron oxide were late minerals deposited in the lower part of the core.

FLUID INCLUSIONS

Quartz and calcite crystals from seven depths (table 6) in the lower 200 m of the USGS-N2 drill core contain mostly secondary, liquid-rich fluid inclusions; the vapor phase ranges from nearly 0 to more than 50 percent of the inclusions. For this study, liquid-rich fluid inclusions having nearly equal vapor-to-liquid ratios (fig. 10A) were selected for heating/freezing measurements. Vapor-rich monophase-vapor and monophase-liquid fluid inclusions occur in some samples. Homogenization temperature (T_h) measurements were obtained for 17 fluid inclusions in one calcite sample and 139 fluid inclusions in nine quartz crystals (table 6). The T_h values, ranging from 173 to 367˚C, are plotted in figure 11 along with the measured temperature profile for the drill hole (Sammel, 1981). Melting-point temperature measurements for 19 fluid inclusions range from 0.0 to -0.2˚C (0 to 0.4 weight percent NaCl equivalent) in samples from 929-m depth and

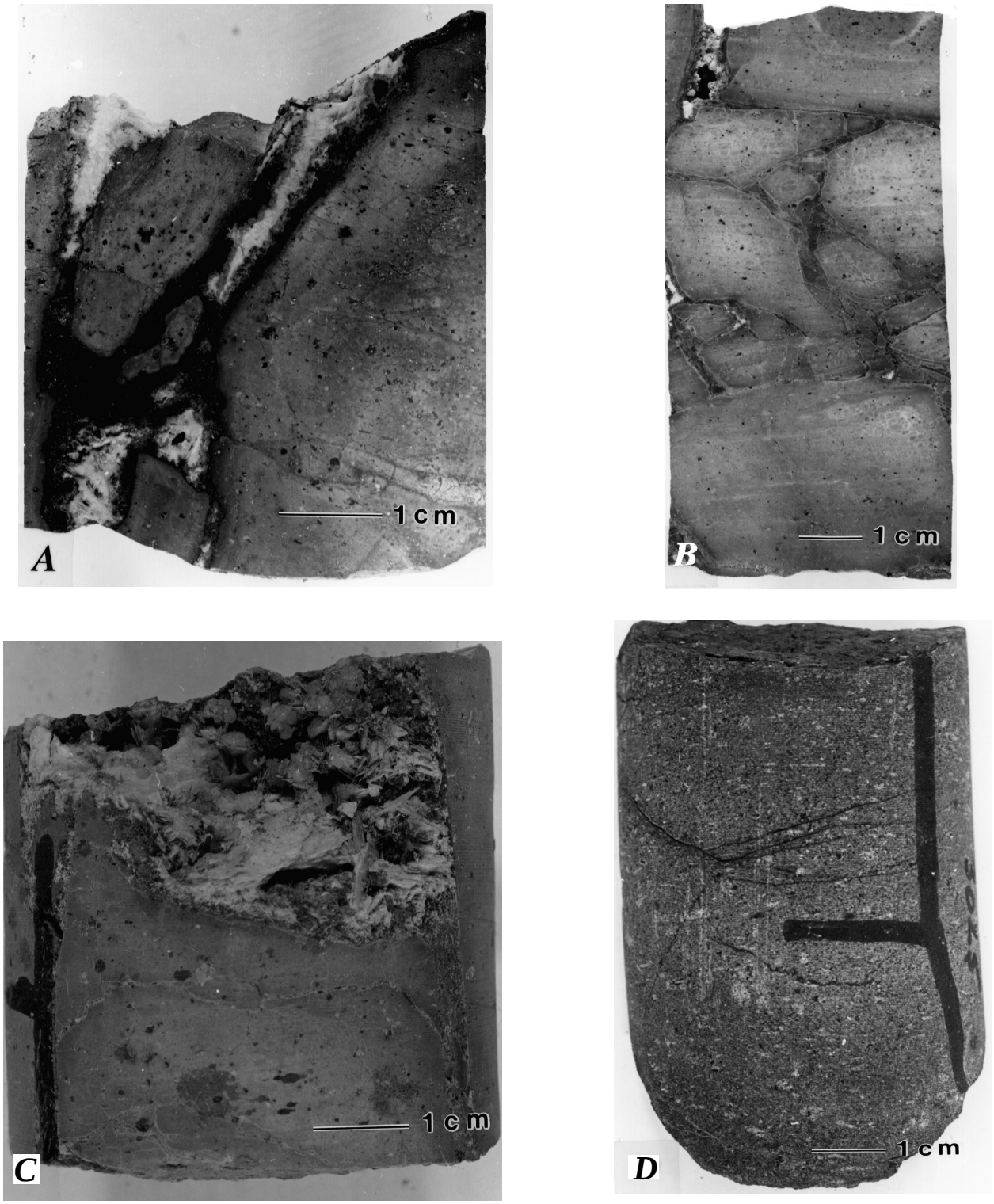

Figure 9.—Drill-core samples from lower part of USGS-N2 drill hole. A, Fractures in altered interflow basaltic-andesite breccia from 741.3-m depth. Filling is chlorite, smectite, pyrrhotite, pyrite, and calcite. B, Partly filled fracture system in altered interflow basaltic-andesite breccia from 742.3-m depth. C, Fracture partly filled with bladed calcite and colorless euhedral quartz crystals in breccia from 742.5-m depth. Note feeder fracture in lower right part of sample. D, Basalt lava flow with hair-line fractures filled by mixed-layer smectite-chlorite, from 922.0-m depth. Rock is self sealed and impermeable. E, Vesicular basaltic andesite lava flow from 835.2-m depth. Vesicles lined or filled with mixed-layer chlorite-smectite, quartz crystals, and rhombic calcite (sample number N2-2740 represents depth in feet). F, Basaltic andesite interflow breccia from 844.3-m depth; mostly leached (light gray areas) but retains dark patches of rock not leached by circulating geothermal fluids. G, Partly leached vesicular basaltic andesite from 930.9-m depth. Vesicles lined with chlorite, quartz, calcite, pyrite, and illite.

Figure 9.—Continued.

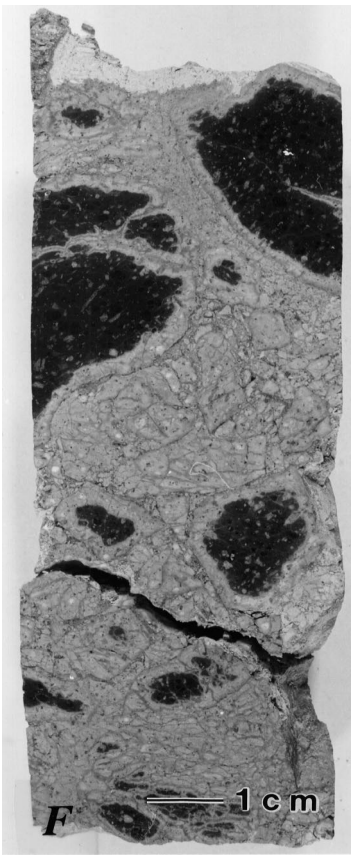

Figure 9.—Continued.

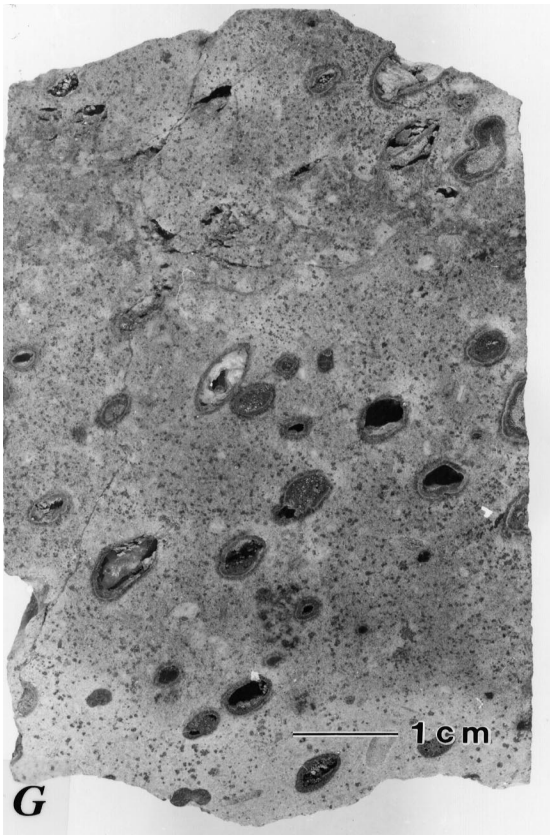

Figure 9.—Continued.

higher. At 931-m depth, the T_m of -0.8 to -1.1°C (1.4 to 1.9 weight percent NaCl equivalent) in 10 fluid inclusions suggests that this lower sample was deposited from a separate more saline fluid than the higher samples. Crushing of a few quartz and calcite fluid inclusions in refractive index oils shows a gradual expansion of the vapor bubble to fill the fluid-inclusion cavity, which indicates the presence of a noncondensible gas such as CO_2 (Roedder, 1984). According to Ingebritsen and others (1986) and Sammel, Ingebritsen, and Mariner (1988), the present bottom fluids from the USGS-N2 drill hole contain high concentrations of CO_2. Hedenquist and Henley (1985) found that the presence of CO_2 in fluid inclusions may result in erroneous T_m values and significantly high salinity estimates, but CO_2 could not account for the difference in T_m measurements between the lowermost and the upper USGS-N2 fluid-inclusion samples.

Taguchi and Hayashi (1982) and Taguchi and others (1984) studied fluid inclusions from drill holes in geothermal areas of Japan and found that at a given depth minimum T_h values are generally the same or slightly warmer than the present measured temperatures; they suggest that minimum T_h values can be used to estimate present temperatures. They also found that maximum T_h values are nearly as high as a theoretical reference boiling-point curve drawn to the present water-table depth. Thus, the fluid-inclusion T_h values often provide a record of decreasing thermal conditions since the

Table 5.—Electron microprobe analyses of phenocryst (ph) and groundmass (gr) plagioclase crystals from USGS-N2 drill core.

Depth (m):	725.1		736.4		916.7		929.9A		929.9B		930.1		931.0	
Crystal:	ph	gr	ph	gr	ph	gr	ph	gr	ph	gr	ph	gr	ph	gr
Analysis No.:	1	2	3	4	5	6	7	8	9	10	11	12	13	14
Major-element analyses (weight percent oxides)														
SiO_2	57.61	58.51	56.64	56.95	48.97	56.78	49.34	52.79	47.58	53.15	48.16	53.52	48.03	53.87
Al_2O_3	26.60	24.98	26.77	25.22	31.79	26.51	31.56	28.33	32.77	28.70	31.93	27.90	32.32	27.75
FeO	0.49	0.64	0.54	0.89	0.68	0.86	0.71	1.15	0.59	0.99	0.53	1.61	0.53	0.68
MgO	0.08	0.10	0.11	0.19	0.09	0.07	0.08	0.30	0.09	0.04	0.12	0.60	0.12	0.09
CaO	10.12	9.30	10.15	9.66	15.08	8.94	15.74	12.54	16.72	12.66	16.98	11.92	16.67	12.62
K_2O	0.17	0.30	0.18	0.30	0.05	0.27	0.11	0.24	0.04	0.27	0.04	0.35	0.02	0.21
Na_2O	6.45	6.98	6.46	7.25	3.16	6.59	2.77	4.52	2.28	4.64	2.41	4.66	2.36	5.12
SrO	0.21	0.25	0.21	0.21	0.19	0.10	0.18	0.15	0.14	0.10	0.15	0.12	0.16	0.14
Total	101.73	101.06	101.06	100.67	100.01	100.12	100.49	100.02	100.21	100.55	100.32	100.68	100.21	100.48
Number of ions on the basis of 32 oxygens														
Si	10.24	10.47	10.15	10.28	9.00	10.24	9.03	9.65	8.75	9.65	8.86	9.72	8.83	9.78
Al	5.57	5.26	5.65	5.37	6.88	5.63	6.81	6.10	7.11	6.14	6.92	5.97	7.00	5.94
Fe	0.07	0.10	0.08	0.13	0.10	0.13	0.11	0.18	0.09	0.15	0.08	0.24	0.08	0.10
Mg	0.02	0.03	0.03	0.05	0.03	0.02	0.02	0.08	0.02	0.01	0.03	0.16	0.03	0.03
Ca	1.93	1.78	1.95	1.87	2.97	1.73	3.08	2.45	3.30	2.46	3.35	2.32	3.28	2.46
K	0.04	0.07	0.04	0.07	0.01	0.06	0.03	0.06	0.01	0.06	0.01	0.08	0.01	0.05
Na	2.22	2.42	2.25	2.54	1.13	2.30	0.98	1.60	0.82	1.63	0.86	1.64	0.84	1.80
Sr	0.02	0.03	0.02	0.02	0.02	0.01	0.02	0.02	0.02	0.01	0.02	0.01	0.02	0.02
An	46.1	41.7	46.0	41.7	72.3	42.3	75.3	59.6	79.9	59.3	79.4	57.4	79.4	57.1
Ab	53.0	56.7	53.1	56.7	27.5	56.2	24.0	38.9	19.9	39.3	20.4	40.6	20.3	41.8
Or	1.0	1.6	0.9	1.6	0.2	1.5	0.7	1.5	0.2	1.4	0.2	2.0	0.2	1.2

host crystals formed. In a few drill holes, the maximum T_h values exceeded the reference boiling-point curve, and Taguchi and Hayashi (1982) and Taguchi and others (1984) indicate that, at the time the fluid inclusions formed, this curve must have been much higher than the current reference boiling-point curve and water table. An extreme example is given by Muramatsu (1984) where the observed T_h values greatly exceed the reference boiling-point curve, and calculations indicate the erosion of about 900 m of overburden since the fluid inclusions formed.

Minimum fluid-inclusion T_h values for the lower part of drill hole USGS-N2 generally are close to the present measured temperature curve (fig. 11). However, the maximum T_h values (as much as 367°C at 931-m depth) greatly exceed the theoretical reference boiling-point curve drawn to the present ground surface as shown in figure 11. Except for one quartz sample at 929-m depth, these fluid inclusions uniformly are liquid rich, without any vapor-rich coeval fluid inclusions. The single quartz crystal from 929-m depth has several monophase-vapor fluid inclusions along healed fractures and a few vapor-rich inclusions that appear to be associated with monophase-liquid fluid inclusions (fig. 10B), in addition to abundant liquid-rich inclusions. These coeval(?) monophase-liquid and vapor-rich fluid inclusions may have formed due to necking down rather than boiling conditions (Bodnar, Reynolds, and Kuehn, 1985). Necking down is a process whereby quartz is dissolved and redeposited, changing the shape of the fluid inclusions over a period of time. During this process, large fluid inclusions can be divided into several smaller inclusions; some of these smaller fluid inclusions may contain only a single phase (vapor or liquid) whereas others contain both vapor and liquid with variable vapor-to-liquid ratios as discussed in Roedder (1984). Fluid inclusions that have necked down can often be recognized by thin tube-like connections between fluid inclusions (fig. 10C) or fluid inclusions with short tails (fig. 10D). If the initial T_h mea-

Table 6.—Fluid-inclusion heating/freezing data for Newberry volcano drill-core samples.

[Dashed (–) where no values to report]

Drill hole No.	Sample depth (m)	Host mineral	Measured temperature[1]	Number of T_m measurments	T_m (°C)[2]	Salinity (weight-percent NaCl equivalent)	Number of T_h measurments	Range of T_h (°C)[3]	Mean T_h (°C)[3]
Drill holes within the caldera									
USGS-N2	768	Quartz	167	0	–	–	15	173–323	261
Ditto	801	do.	197	5	0.0	0.0	—	–	
Ditto	801	do.	197	2	0.0	0.0	24	252–342	277
Ditto	801	do.	197	3	-0.1	0.2	9	267–315	296
Ditto	810	Calcite	190	0	–	–	17	232–289	248
Ditto	840	Quartz	226	0	–	–	23	214–324	276
Ditto	842	do.	226	0	–	–	21	270–308	291
Ditto	929	do.	265	9	-0.1, -0.2	0.2, 0.4	12	258–302	283
Ditto	931	do.	265	5	-0.8, -0.9	1.4, 1.6	18	288–367	318
Ditto	931	do.	265	5	-1.0, -1.1	1.7, 1.9	17	281–311	305
RDO-1	335	Quartz	135	0	–	–	9	210–252	241
Ditto	381	do.	158+	6	-0.4	0.7	11	226–246	236
Ditto	381	do.	158+	8	-0.7	1.2	19	230–246	239
Drill holes outside the caldera									
GEO-N2	925	Quartz	107	4	*	*	4	110–195	133
Ditto	948	do.	110	0	–	–	13	108–153	119
Ditto	1,077	Calcite	126	3	*	*	4	130–133	131
Ditto	1,077	do.	126	0	–	–	7	127–163	139
Ditto	1,077	do.	126	0	–	–	11	125–128	126
Ditto	1,223	Quartz	144	5	-0.1	0.2	22	133–168	153
SF NC-01	900	Calcite	126	3	-0.2	0.4	18	131–133	132
Ditto	900	do.	126	1	0.0	0.0	9	124–134	128
Ditto	900	Quartz	126	7	*	*	18	119–136	122
Ditto	930	Calcite	130	0	–	–	13	126–129	127
Ditto	1,095	do.	153	0	–	–	9	135–168	147
Ditto	1,149	do.	160	0	–	–	13	145–188	162
Ditto	1,149	do.	160	0	–	–	10	159–187	175
Ditto	1,149	do.	160	6	-0.1	0.2	14	152–188	173
Ditto	1,216	Quartz	170	0	–	–	13	164–214	184
SF NC72-03	945	do.	99	5	*	*	6	98–109	103
Ditto	945	do.	99	2	*	*	5	99–114	107
Ditto	1,185	Calcite	130	0	–	–	23	162–212	191
Ditto	1,275	Quartz	145	0	–	–	6	143–292	260
Ditto	1,287	Calcite	145	0	–	–	21	190–248	218
Ditto	1,287	do.	145	1	-0.4	0.7	11	211–271	245
Ditto	1,344	do.	152	0	–	–	15	247–284	274
Ditto	1,344	do.	152	0	–	–	9	267–315	289

[1]Measured temperature sources: USGS-N2 from Sammel (1981) and MacLeod and Sammel (1982); RDO-1 from Black, Priest, and Woller (1984); GEO-N2 from Walkey and Swanberg (1990); SF NC72-03 and SF NC-01 from Arestad, Potter, and Stewart (1988).

[2]Melting-point temperatures (T_m) and salinities not reported for samples designated by * because these fluids are metastable and recorded values are unreliable.

[3]Homogenization temperatures (T_h) not reported for one sample from 801-m depth in USGS-N2 because fluid inclusions all decrepitated at about 130°C.

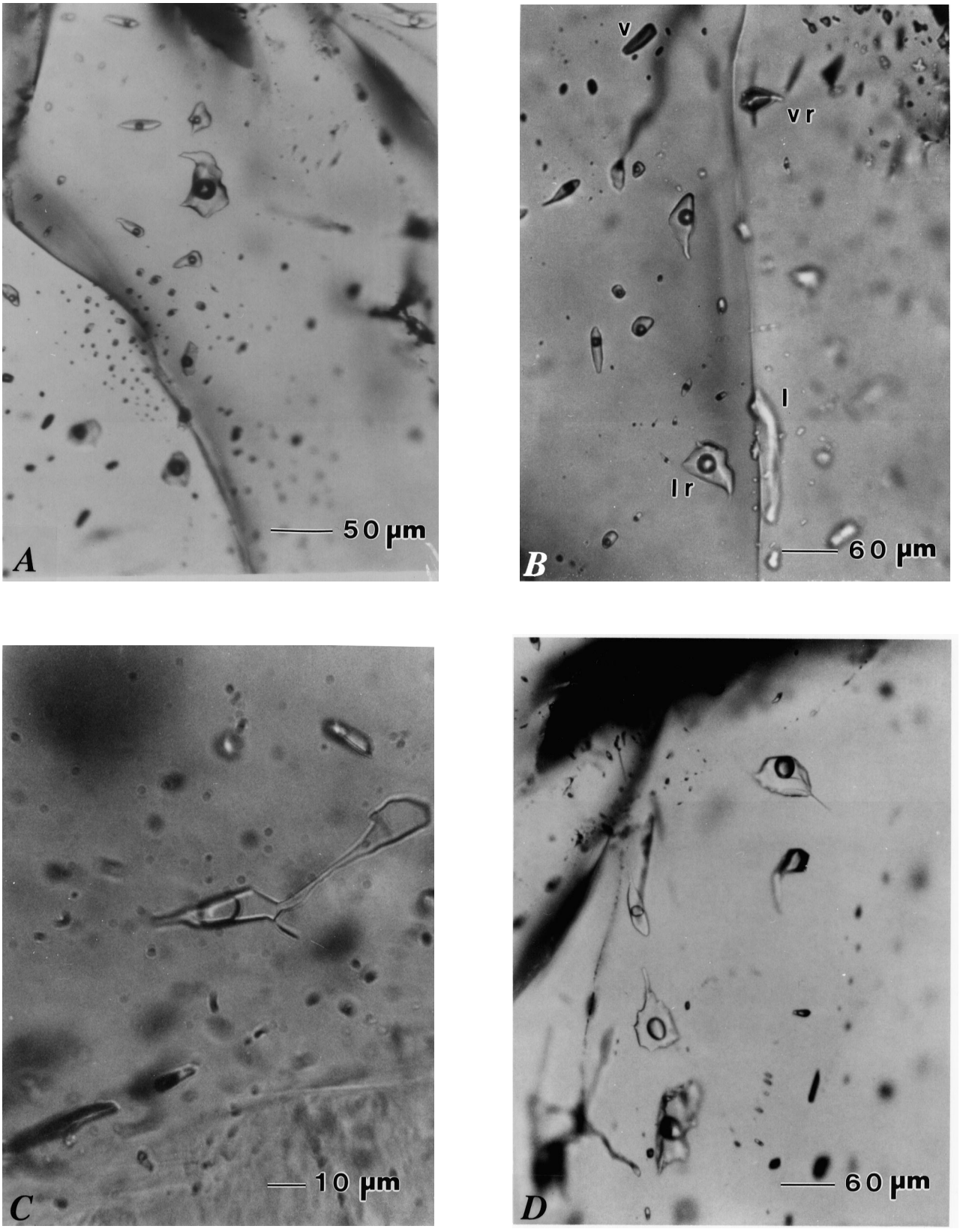

Figure 10.—Fluid inclusions in hydrothermal quartz crystals from lower part of USGS-N2 drill core. A, Liquid-rich fluid inclusions from 928.7-m depth. B, Coeval(?) liquid-rich (lr), monophase-vapor (v), vapor-rich (vr), and monophase-liquid (l) fluid inclusions from 928.7-m depth. C, Liquid-rich fluid inclusion that is almost completely necked down, from 800.9-m depth. D, Liquid-rich fluid inclusions plus vapor-rich fluid inclusion from 928.7-m depth; tails are characteristic of necking down.

surements that plot above the boiling-point curve were due to boiling conditions, the data would be easy to explain. However, in order to unequivocally demonstrate boiling conditions it is necessary for coeval vapor-rich and liquid-rich fluid inclusions to homogenize at the same temperature (Roedder, 1984); no such evidence was observed in this study.

Adjusting the boiling-point curve in order to account for the highest T_h in drill core from USGS-N2 would require about 1,140 m of erosion. If a mean T_h value (318˚C for one set of fluid inclusions in table 6), at 931-m depth, is utilized, the calculations become much more reasonable and removal of only about 160 m of overburden would be required. Williams (1935) indicated, that while fluvial and glacial erosion undoubtedly occurred at Newberry, the effects of these two agents are fairly minimal; erosion by glaciers and water probably would not account for removal of even 160 m of overburden. Lack of glacial moraines at Newberry (Williams, 1935; MacLeod and others, 1995) also suggests that glacial ice cover probably was not extensive and would not allow raising the theoretical boiling-point curve enough to account for the high T_h (Bargar and Fournier, 1988).

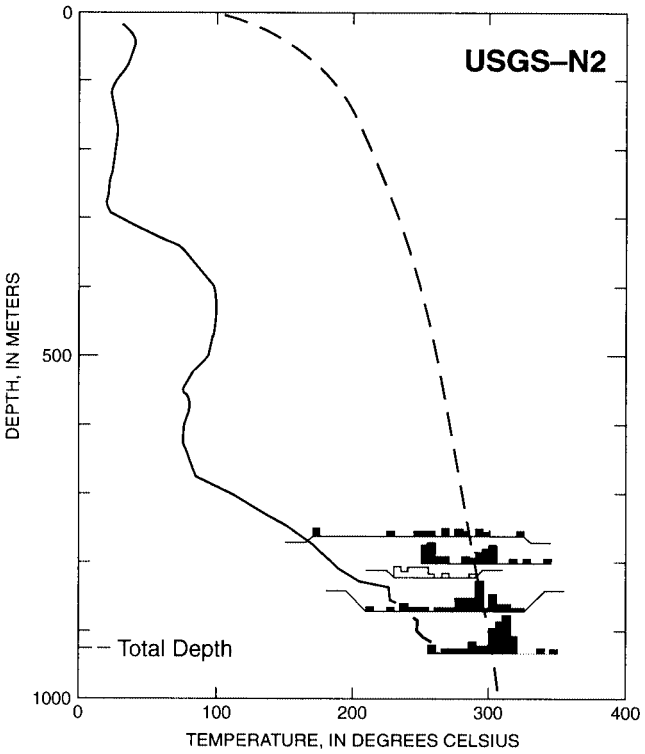

Figure 11.—Fluid-inclusion homogenization temperature (T_h) values for quartz (shaded histograms) and calcite (unshaded histogram) specimens from lower part of USGS-N2 drill core within Newberry caldera. Data are from table 6. Baseline for histograms is sample depth. Dashed line shows a theoretical, reference boiling-point curve for pure water assuming hydrostatic conditions controlled by an overlying column of cold water. Measured temperature data (solid line) from Sammel (1981).

Alternatively, T_h exceeding the present reference boiling-point curve might result from localized high pressure due to bounding impermeable lava layers. Many fractures in the lower part of the USGS-N2 drill core are completely filled, and local pressures might have been closer to lithostatic rather than hydrostatic at the time these fluid inclusions formed. However, a preferred explanation is that at the time the fluid inclusions formed, the caldera of Newberry volcano was filled by a deep intracaldera lake. The presence of a lake is indicated by lacustrine sediments from 290- to 320-m depth in the USGS-N2 drill core (MacLeod and others, 1995). A depth of 160 m for this previous intracaldera lake is reasonable considering that the present-day Paulina Lake is 80 m deep, and it may have been at least 60 m deeper in past times (MacLeod and others, 1995). Another Cascade intracaldera lake at Mount Mazama (Crater Lake), Oregon, presently is 622 m deep (Nelson, Carlson, and Bacon, 1988).

Mineralogical and textural data for USGS-N2 drill core indicate that temperatures higher than about 265˚C could not have persisted for a long time. If temperatures had been as hot as 318˚C (mean T_h at 931-m depth in USGS-N2) for very long, chlorite would be deposited instead of mixed-layer chlorite-smectite, epidote would probably be more abundant, and actinolite and (or) prehnite would probably be present (Bird and others, 1984). In addition, oxygen isotope data for quartz and calcite from the USGS-N2 drill core do not support such high temperatures (Carothers, Mariner, and Keith, 1987). If a deep intracaldera lake was present within Newberry caldera, subsequent volcanic activity probably caused the lake to be at least partially drained so that higher temperature owing to the high pressure of the lake water was relatively short-lived.

RDO-1

During the fall of 1983, a second intracaldera drill hole (RDO-1), located about 0.5 km southeast of USGS N-2 at 1,969-m elevation (figs. 2 and 3), was rotary drilled to a depth of 424 m by Sandia National Laboratories (Keith and others, 1986). This hole penetrated a shallow hot-water aquifer with a temperature exceeding 158˚C between depths of 379 and 397 m (Black, Priest, and Woller, 1984). On the basis of drill cuttings, Keith and others (1986) determined that the same hydrothermal minerals found in USGS N-2 were deposited at shallower depths in drill hole RDO-1. This suggests that past temperatures also were greater at higher levels in drill hole RDO-1, which is closer to the ring fractures in the southern part of Newberry caldera (fig. 3). Modeling studies by Sammel (1983) suggest that the thermal water reached near-surface strata or a few localized surface hot springs by movement along ring fractures or vents for Holocene extrusive rocks.

LITHOLOGY

Drill cuttings from RDO-1 were studied by M.W. Gannett and A.F. Waibel (unpub. data, 1983) and Keith and others

(1986). The upper 20.7 m of drill cuttings consist of white to tan pumice with some clasts of lava and welded tuff. From 20.7- to 39.6-m depth, the drill cuttings are mostly basaltic vesicular-glass lapilli in a palagonite matrix. A thin layer of reworked epiclastic volcanic material occurs at 39.6- to 41.2-m depth. A thick obsidian flow lies between 41.5- and 111.3-m depth. From 111.3- to 307.9-m depth, the RDO-1 cuttings consist of basaltic vesicular-glass lapilli with clinopyroxene, plagioclase, and minor orthopyroxene crystals, as well as lithic inclusions in the tuff. Clayey to sandy volcanic sediments occur between depths of 307.9 m and 328.6 m; primary and devitrification minerals identified by XRD include plagioclase, K-feldspar, and cristobalite. From 328.6- to 424.0-m depth are lithic and pumiceous tuffs that M.W. Gannett and A.F. Waibel (unpub. data, 1983) subdivided into six units on the basis of differences in the amount of lithic and pumiceous material in the tuffs. Most X-rayed samples contain primary plagioclase and (devitrification?) K-feldspar and cristobalite. A good correlation can be made between rocks of Sandia National Laboratories drill hole RDO-1 and the upper part of the USGS N-2 drill core (Keith and others, 1986) (fig. 4).

HYDROTHERMAL ALTERATION

Above 285-m depth in the RDO-1 drill cuttings, the only secondary minerals Keith and others (1986) found appear to be deuteric and consist of minor colorless to white amorphous silica and thin greenish clay vesicle coatings. They also identified traces of smectite and pyrite between depths of 285 m and 307.9 m. In the lower part of the drill hole, hydrothermal alteration minerals (smectite, chlorite, quartz, mordenite, and pyrite) occur both as replacement of groundmass and phenocrysts and as open-space deposits in fractures, vesicles, and intergranular pore spaces; calcite, pyrrhotite, and small amounts of analcime, aragonite, siderite, rhodochrosite, and hematite are open-space fillings (Keith and others, 1986) (fig. 12).

Keith and others (1986) indicated that hydrothermal alteration is most intense between depths of 379.5 m and 397 m. Iron sulfide minerals appear to be early deposits along with smectite; mordenite, calcite, quartz, and chlorite were deposited later, although some of these minerals may be codepositional (Keith and others, 1986).

FLUID INCLUSIONS

Drill cuttings from depths of 335 m and 381 m in RDO-1 contain small (<1 mm) broken quartz crystals containing fluid inclusions. The fluid inclusions formed along healed fractures, but it is uncertain if they are secondary or pseudosecondary because no complete crystals were located. The inclusions primarily are liquid rich with vapor bubbles forming about 5 to 10 percent of the volume. The quartz crystal from 335-m depth also contains some monophase-vapor inclusions and closely associated monophase-liquid inclusions; these single-phase fluid inclusions may have formed due to necking down as described by Roedder (1984). The monophase inclusions are in close proximity to the liquid-rich fluid inclusions used in this study. However, the monophase inclusions are more equant,

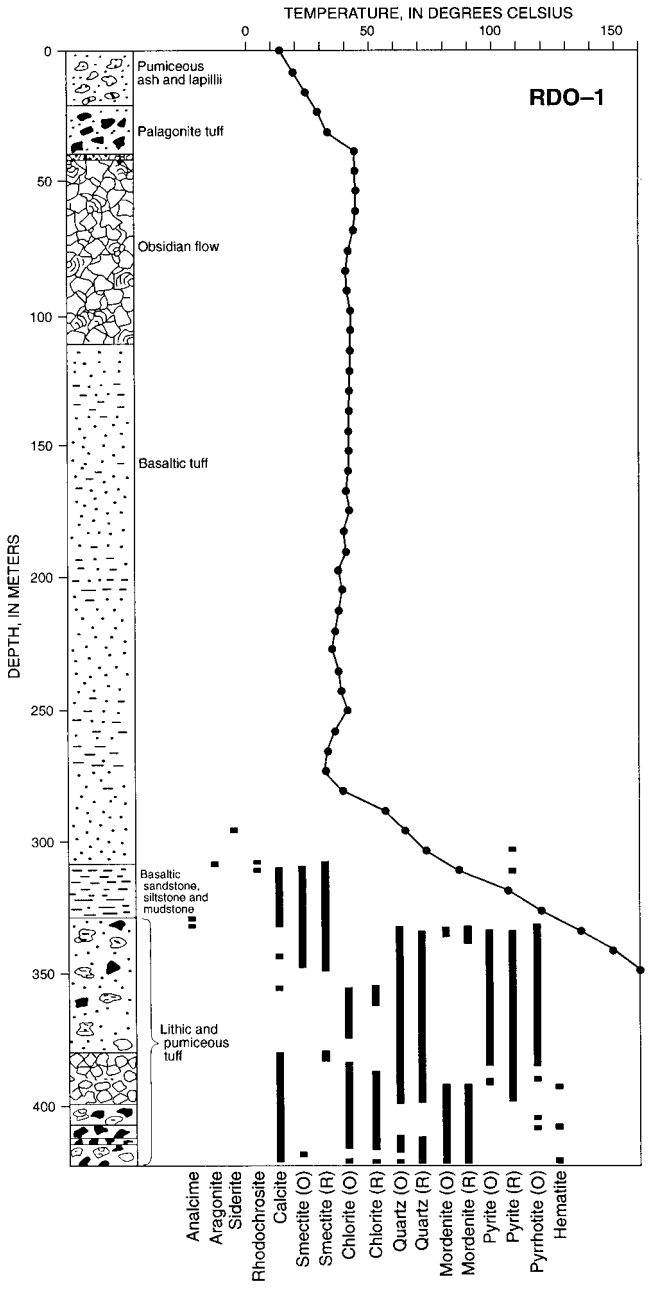

Figure 12.—Distribution of hydrothermal alteration minerals with depth in drill hole RDO-1 (after Keith and others, 1986). Left column shows lithologic log for drill chips. Temperature data (Black and others, 1984) shown as points connected by a solid line. Most common mineral occurrence in parentheses: O, open-space precipitate; R, replacement of glass or primary minerals.

are faceted, and approach a negative crystal appearance unlike the apparently unrelated set of elongate, flattened, liquid-rich inclusions for which T_h and T_m measurements were obtained.

Melting-point temperatures were not measured for the quartz crystal at 335-m depth because the small fragment was polished only on one side and the clarity within the crystal is not sufficient for T_m measurements. In addition, the fluid inclusions were mostly less than 10 μm in size, and the exact temperature at which the last ice melted could not be seen. T_m values for fluid inclusions from the two quartz samples from 381-m depth are -0.4 and -0.7˚C, which corresponds to fluid salinities of about 0.7 and 1.2 weight percent NaCl equivalent, respectively.

Homogenization temperature measurements for 39 liquid-rich fluid inclusions in the three hydrothermal quartz crystals ranged from 210 to 252˚C and averaged about 238˚C (table 6). These temperatures greatly exceed the highest measured temperature of more than 158˚C for the RDO-1 drill hole (Black, Priest, and Woller, 1984) and indicate that past temperatures were considerably warmer than these measured temperatures. In fact, about half of the T_h values of fluid inclusions from 335-m depth plot above a reference boiling-point curve drawn to the present ground surface (fig. 13). The presence of monophase-vapor fluid inclusions and liquid-rich fluid inclusions are not thought to suggest boiling conditions because the two types of fluid inclusions do not appear to be coeval. T_h values reported in table 6 are for liquid-rich fluid inclusions with nearly constant vapor-to-liquid ratios. If boiling conditions did not exist when these fluid inclusions formed, the theoretical reference boiling-point curve at the time the fluid inclusions formed must have originated at a somewhat higher elevation (water table) than at present because of a deep intracaldera lake (as discussed above for USGS-N2 fluid inclusions). Two quartz crystal fragments from 381-m depth contain only liquid-rich fluid inclusions with nearly constant vapor-to-liquid ratios, and T_h values all plot at slightly lower temperatures than the present reference boiling-point curve (fig. 13).

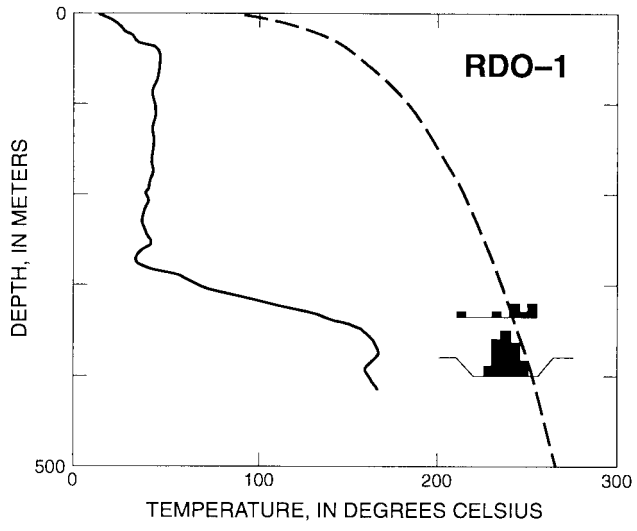

Figure 13.—Fluid-inclusion T_h values for quartz specimens from RDO-1 drill hole within Newberry caldera. Explanation is the same as for figure 11. Measured temperature data from Black, Priest and Woller (1984).

DRILL HOLES OUTSIDE THE CALDERA

GEO-N1

In 1985, GEO-Newberry Crater, Inc. completed the GEO-N1 drill hole on a cost-sharing basis with the U.S. Department of Energy (Earth Science Laboratory, 1986, 1987). GEO-N1 was sited at an altitude of 1,780 m (Walkey and Swanberg, 1990) about 4.9 km south of the southern rim of Newberry caldera (fig. 3) near the vent of a Holocene basalt flow (Swanberg, Walkey and Combs, 1988) and within a soil mercury anomaly shown by Priest and others (1983). The hole was rotary drilled to 148-m depth and cored to a depth of 1,387 m (Swanberg and Combs, 1986; core recovery was about 95 percent (Earth Science Laboratory, 1986).

LITHOLOGY

A generalized stratigraphic description of the GEO-N1 drill core, partly based on data provided by GEO-Newberry Crater, Inc. (Earth Science Laboratory, 1986), is given in appendix 2. The lithologic log of GEO-Newberry, Inc. (see Earth Science Laboratory, 1986) contains detailed lithology notes and tentative rock nomenclature that generally will be followed in this report. Modifications of the descriptions are based on chemical analyses, our observations of the entire split of drill core housed in the EGI core library, and additional drill-core samples collected at the GEO-Newberry Crater, Inc., core-storage facility in Bend, Oregon. Several variations of a stratigraphic column for the GEO-N1 drill core were reported previously in Bargar and Keith (1986), Swanberg and Combs (1986), Wright and Nielson (1986), and Swanberg, Walkey, and Combs (1988).

The GEO-N1 drill core consists mostly of lava flows; associated flow breccia, ash-fall, and ash-flow material occur between lava flows (appendix 2). Most lava flows in the upper ~1,125 m of drill core are basalts and basaltic andesites (fig. 14). Below that depth the analyzed flows (table 7) are basaltic andesites, andesites, or rhyodacites. Primary minerals in the lava flows vary with the chemical composition of the lava but predominantly consist of plagioclase with varying amounts of olivine, clinopyroxene, orthopyroxene, and magnetite. Devitrification cristobalite is identified in many XRD analyses of the drill-core samples. Several shallow lava flows contain vapor-phase tridymite, alkali-feldspar(?), and magnetite that has altered to hematite. Groundmass K-feldspar along with trace amounts of primary quartz were identi-

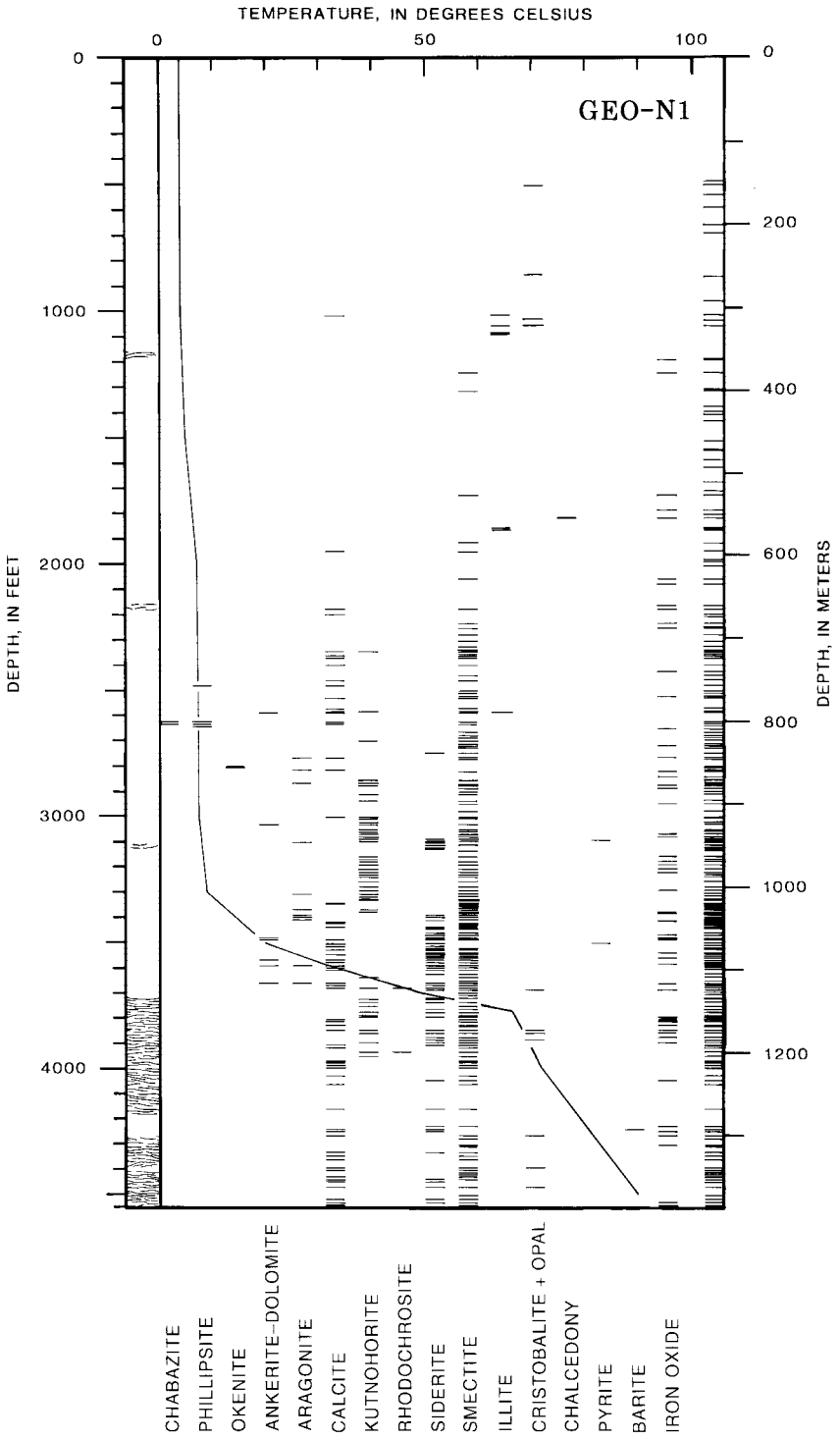

Figure 14. —Distribution of hydrothermal alteration minerals with depth in geothermal drill core GEO-N1 on south flank of Newberry volcano. Left column shows generalized stratigraphic section of rock units in drill hole: Basaltic-to-andesitic (<62 weight percent SiO_2) intervals are unpatterned, and dacitic to rhyolitic intervals (>62 weight percent SiO_2) have wavy pattern. Right column shows distribution of samples studied. Solid curve shows measured temperature with depth in drill hole (after Swanberg and Combs, 1986; Swanberg, Walkey, and Combs, 1988; Walkey and Swanberg, 1990; Wright and Nielson, 1986).

Table 7.—Chemical analyses for drill-core samples outside Newberry caldera.

[Major-element chemical analyses by X-ray spectroscopy; analyst for most samples: T. Frost, U.S. Geological Survey, Denver, Colo. Samples denoted by * analyzed by D.F. Siems and J.E. Taggart, U.S. Geological Survey, Denver, Colo. FeO, H_2O^+, H_2O^-, and CO_2 determined by conventional rock analysis methods; analyst: S.T. Pribble, U.S. Geological Survey, Menlo Park, Calif. Volatile free SiO_2 values calculated by normalizing to 100 percent after subtracting LOI or H_2O^+, H_2O^-, and CO_2. LOI, loss on ignition. —, not determined]

Sample No.:	GEO-N1 593	GEO-N1 2307.5	GEO-N1 2442	GEO-N1 2588.5	GEO-N1 2767	GEO-N1 2819.5	GEO-N1 3060	GEO-N1 3083	GEO-N1 3126.5	GEO-N1 3330	GEO-N1 3391
Depth (m):	180.7	703.3	744.3	789.0	843.4	859.4	932.7	939.7	953.0	1,015.0	1,033.6
Major-element analyses (weight percent oxides)											
SiO_2	55.0	51.3	48.7	49.0	50.8	50.3	52.0	50.4	50.7	52.3	59.6
Al_2O_3	16.5	15.4	16.8	16.9	17.5	17.1	18.3	14.9	15.6	18.0	14.6
Fe_2O_3	9.45	12.1	9.65	9.75	9.52	9.42	8.67	9.72	10.6	8.72	9.02
MgO	4.1	4.6	7.9	7.3	6.5	6.9	4.7	4.0	3.1	5.7	1.8
CaO	7.81	8.42	9.38	9.60	9.85	9.45	9.22	7.61	7.90	8.90	4.72
Na_2O	4.1	4.0	2.9	2.9	3.2	3.1	3.3	3.7	4.1	3.3	4.5
K_2O	1.10	0.70	0.51	0.45	0.62	0.62	0.69	0.54	1.14	0.63	1.96
TiO_2	1.28	2.10	1.14	1.28	1.27	1.26	1.06	1.48	1.57	1.10	1.29
P_2O_5	0.37	0.37	0.28	0.24	0.23	0.25	0.19	0.27	0.31	0.24	0.17
MnO	0.14	0.19	0.15	0.14	0.15	0.15	0.14	0.12	0.20	0.16	0.10
LOI (900°C)	0.01	0.25	2.50	2.24	0.25	1.50	1.70	7.12	4.10	1.00	1.45
Total	99.86	99.43	99.91	99.80	99.89	100.05	99.97	99.86	99.32	100.05	99.21
SiO_2, volatile free	55.1	51.7	50.0	50.2	51.0	51.0	52.9	54.3	53.2	52.8	61.0

fied in some XRD analyses of the silicic lava flows. GEO-N1 lava flows commonly are vesicular at the top and bottom, dense in the interior, and have intervening fractured intervals consisting of steeply dipping tight fractures. Ash and cinder layers and lithic tuffs from the upper part of the drill hole appear to have good permeability where unaltered. At deeper intervals, below 830-m depth, ash-flow tuffs are pervasively altered to smectite and the present permeability is presumably much lower. K-Ar ages for ten selected rocks from the GEO-N1 drill hole range from 0.027 Ma (late Pleistocene) near the top of the drill hole to 1.63 Ma (approximately the late Pliocene-early Pleistocene boundary) in the lower part of the drill hole (Swanberg, Walkey, and Combs, 1988). In addition, a ^{14}C date of 5,835±195 years B.P. was obtained for charcoal collected from a shallow surface excavation near the top of the GEO-N1 drill hole (Swanberg and Combs, 1986; Swanberg, Walkey, and Combs, 1988).

HYDROTHERMAL ALTERATION

A maximum temperature of about 90°C at the bottom of the GEO-N1 drill hole was reported by Walkey and Swanberg (1990). Hydrothermal alteration minerals identified from the drill core are consistent with these low temperatures. Although the temperature gradient begins to increase at about 1,000-m depth, there are no changes in hydrothermal mineralogy at that depth. Twelve moderate to steeply dipping basaltic dikes (as much as an apparent core thickness of about 12 m) between the depths of 622 m and 719 m indicate the presence of a transient heat source during the time the dikes intruded the volcanic pile. The dikes occur near the upper stratigraphic limit of the formation of most hydrothermal alteration minerals in the GEO-N1 drill core. Chilled margins are preserved for some of the dikes, but there is no evidence of significant alteration directly adjacent to the contacts.

The earliest deposited secondary minerals in drill hole GEO-N1 are high-temperature vapor-phase tridymite and vapor-phase or deuteric(?) magnetite and hematite, which formed during cooling of the lava flows and pyroclastic intervals. A few scattered occurrences of ~10Å illite in the upper half of the drill core probably formed during cooling of the volcanic deposits and also may be deuteric. During late-stage cooling and prehydrothermal circulation of meteoric waters, amorphous iron hydroxides or iron oxides and amorphous clay-like deposits were precipitated.

Table 7.—Chemical analyses for drill-core samples outside Newberry caldera—Continued.

Sample No.:	GEO N1 3505	GEO N1 3657.5	GEO N1 3775.5	GEO N1 3909	GEO N1 4238*	GEO N1 4243*	GEO N1 4398*	GEO N5 1976*	GEO N5 3146*	SF NC 72-03 2122*	SF NC 72-03 2807*
Depth (m):	1,068.3	1,114.8	1,150.8	1,191.5	1,291.7	1,293.3	1,340.5	602.3	958.9	646.8	855.6
Major-element analyses (weight percent oxides)											
SiO_2	52.5	53.8	68.7	68.0	70.4	70.8	63.0	74.6	69.0	67.4	50.8
Al_2O_3	16.3	16.0	14.5	14.3	13.7	13.8	14.3	13.2	14.1	14.7	17.5
Fe_2O_3	10.4	9.68	3.74	3.95	2.56	2.73	2.66	0.58	1.29	3.04	4.03
FeO	---	---	---	---	0.74	0.60	2.40	0.93	2.00	1.42	4.60
MgO	4.7	4.5	0.46	0.60	0.33	0.24	1.16	0.18	0.48	0.51	5.77
CaO	8.98	7.23	1.40	1.90	1.20	1.10	2.83	0.79	1.46	2.13	8.93
Na_2O	3.7	4.1	5.6	5.1	4.73	4.76	4.51	4.29	4.96	4.99	3.18
K_2O	0.67	0.93	3.07	3.12	3.61	3.61	2.52	4.19	3.48	2.78	0.38
H_2O^+	---	---	---	---	0.23	0.33	3.53	0.13	0.10	0.28	0.86
H_2O^-	---	---	---	---	0.49	0.46	1.10	<0.01	0.19	0.95	2.19
TiO_2	1.41	1.46	0.58	0.54	0.38	0.39	0.76	0.15	0.32	0.55	1.03
P_2O_5	0.20	0.38	0.12	0.16	0.07	0.07	0.19	<0.05	0.08	0.14	0.24
MnO	0.16	0.16	0.03	0.07	0.08	0.05	0.10	0.03	0.18	0.08	0.14
CO_2	---	---	---	---	0.47	0.27	0.01	<0.01	1.82	0.67	0.44
LOI (900°C)	0.75	1.73	1.13	1.60	---	---	---	---	---	---	---
Total	99.77	99.97	99.33	99.34	98.99	99.21	99.07	99.14	99.46	99.64	100.09
SiO_2, volatile free	53.0	54.8	70.0	69.6	72.0	72.1	66.7	75.4	70.9	69.0	52.6

Hydrothermal smectite and carbonate minerals were deposited later than vapor-phase minerals. Smectite alteration of the pyroclastic layers occurred prior to carbonate deposition. Most open-space smectite also formed earlier than the carbonate minerals; however, locally, smectite was deposited later than carbonate minerals (fig. 15). The numerous carbonate phases are not confined to discrete zones. Instead, the minerals vary from fracture to fracture. Such abrupt changes are especially true for calcite and kutnohorite. The fluids from which these minerals were deposited appear to have varied somewhat in chemical composition in adjacent fractures. It is likely that fluctuations in cation content (Mg, Ca, Mn, and Fe) occur over a period of time because as many as four different carbonate minerals (aragonite, siderite, calcite, and dolomite) were deposited in a single open-space filling. Aragonite is always the last carbonate mineral to be deposited, but, locally, it appears to have been converted to the more stable calcite phase. Some replacement of plagioclase by calcite occurs near 1,200-m depth.

Silica minerals, zeolite minerals, and okenite all formed later than some smectite; only one sample was found that contains early cristobalite in association with later smectite, siderite, and calcite. Pyrite formed later than hydrothermal hematite in the single vein occurrence, and it formed later than smectite but earlier than carbonate minerals in the disseminated occurrences.

The hydrothermal minerals in drill core GEO-N1 compose a mineral suite that is similar to the minerals occurring at temperatures of less than 100°C in the upper 650 m of the USGS-N2 drill core. In both drill holes, hydrothermal silica, zeolite, carbonate, and clay minerals were deposited from migrating fluids, mostly in open spaces of vugs, fractures, and voids in flow breccias. Permeable ash-flow tuff and lithic tuff locally display more extensive alteration of glass to smectite.

GEO-N2

Drill hole GEO-N2 was spudded at an elevation of 1,779 m on the west flank of Newberry volcano about 2.8 km outside the western rim of the caldera (fig. 3). The drill site apparently was chosen on the basis of a geophysical anomaly; the sites for most of the west flank drill holes at Newberry volcano were selected because of electromagnetic or surface resistivity anomalies (Walkey and Swanberg, 1990). A temperature profile for the geothermal well (drilled by GEO-Newberry Crater, Inc.) shows a bottom-hole temperature of 167°C (Walkey and Swanberg, 1990). The SiO_2 content of

sampled fluids increases substantially near the bottom of the GEO-N2 drill hole, which Walkey and Swanberg (1990) conclude is due to the influx of thermal fluids.

LITHOLOGY

Lithologic descriptions and chemical data for the GEO-N2 drill core have not been published by GEO-Newberry Crater, Inc. Drill-core samples obtained for this study emphasize secondary alteration and are not sufficient to provide more than a very generalized description of the stratigraphy of the GEO-N2 drill core; therefore, a detailed stratigraphic column for the drill hole is not included in this report. The core samples consist of basaltic to rhyolitic lava flows with intervening flow breccia, lithic tuff, and volcanic sandstone. Breccias produced by hydrofracturing and tectonic processes are also present. At least one thin basaltic dike intrudes a vesicular mafic lava flow at 1,186-m depth. Some of the collected samples display flow banding and vapor-phase partings; many samples are fractured or contain spherical to elliptical vesicles. Plagioclase is the dominant primary mineral; some magnetite and clinopyroxene(?) are present, and groundmass quartz and K-feldspar occur in the silicic lava flows. In most samples, glass is devitrified to cristobalite. Some lava flows also contain concentrations of tridymite, K-feldspar, and magnetite as vapor-phase minerals. Spaces between breccia fragments, vesicles, and fractures are usually partly to completely filled by hydrothermal alteration minerals.

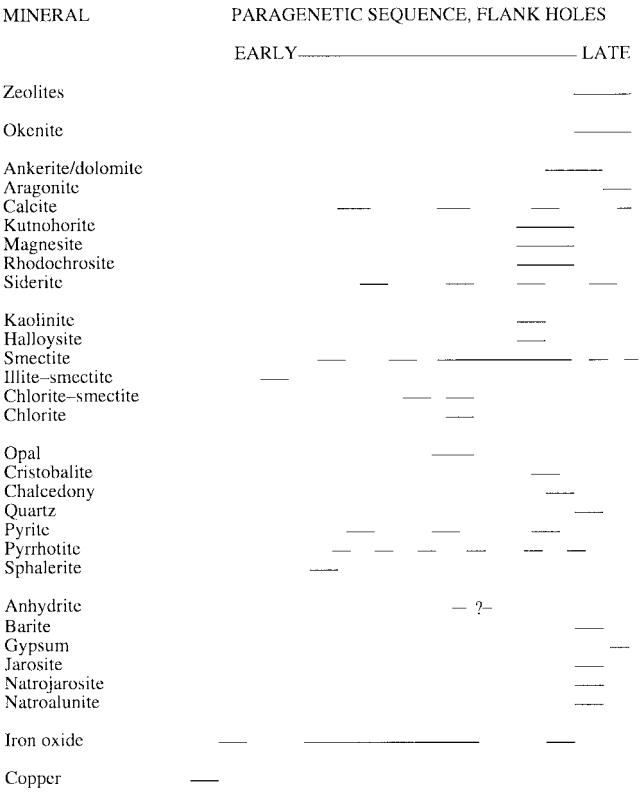

Figure 15.—Generalized paragenetic sequence of hydrothermal alteration minerals deposited in flank drill cores of Newberry volcano. Queried where very uncertain.

HYDROTHERMAL ALTERATION

One of the earliest secondary minerals in the GEO-N2 drill core appears to be native copper (fig. 16) which occurs in vesicles of one sample from 1,186-m depth; presumably, the copper was deposited as a vapor-phase mineral during cooling of the basalt dike host. Octahedral, vapor-phase magnetite crystals that formed in some vesicles at 1,180.2-m depth are partly covered by later mixed-layer chlorite-smectite deposits.

Various colors of smectite (white, bluish, green, orange, brown, black) are deposited in vesicles, on fractures, and between breccia fragments of core from this drill hole; smectite also occurs as altered glass in some lithic tuffs from the GEO-N2 drill core. Smectite was deposited in several generations and can be seen to be both earlier and later than cristobalite in a sample at 679.1-m depth. Texture of the smectite deposits varies from waxy to fibrous. Other open-space clay minerals in this drill core include light- to dark-green mixed-layer chlorite-smectite which also can be fibrous or waxy in texture. A few green clay vesicle-filling samples show no expansion in XRD analyses following glycolation and are chlorite.

Siderite is the earliest carbonate mineral in the GEO-N2 drill core. Some siderite forms tiny caramel-colored rhombic crystals or columnar stacks of rhombic crystals, but most commonly it occurs as hemispheres that may be either earlier or later than smectite. In some places, similar-appearing altered(?) hemispheres consist of minerals such as smectite, mixed-layer chlorite-smectite, hematite, calcite, magnesite, or ankerite-dolomite. Rhodochrosite was detected along with ankerite-dolomite on two XRD analyses of a carbonate patch at 224.9-m depth and with bladed calcite(?) that is replaced by quartz at 1,031.7-m depth. Open-space bladed, blocky, and needle-like calcite crystals were also observed, and some of them formed later than smectite and chalcedony.

Colorless, white or bluish botryoidal vesicle fillings of some GEO-N2 samples were identified as cristobalite in XRD analyses, and many of these deposits formed later than siderite. XRD analyses show that other similar siliceous botryoidal open-space deposits consist of chalcedony. Colorless euhedral quartz crystals formed later than the other silica deposits and are locally associated with earlier smectite or ankerite-dolomite.

Bladed pyrrhotite and green mixed-layer chlorite-smectite in the groundmass of the drill core from 1,104.6-m depth appear to have formed from altered mafic minerals. The pyrrhotite itself is partly oxidized. Fractures and vesicles of a few samples near the bottom of the drill hole are coated by crystals of pyrite, some of which are slightly oxidized at 1,278.3-m depth.

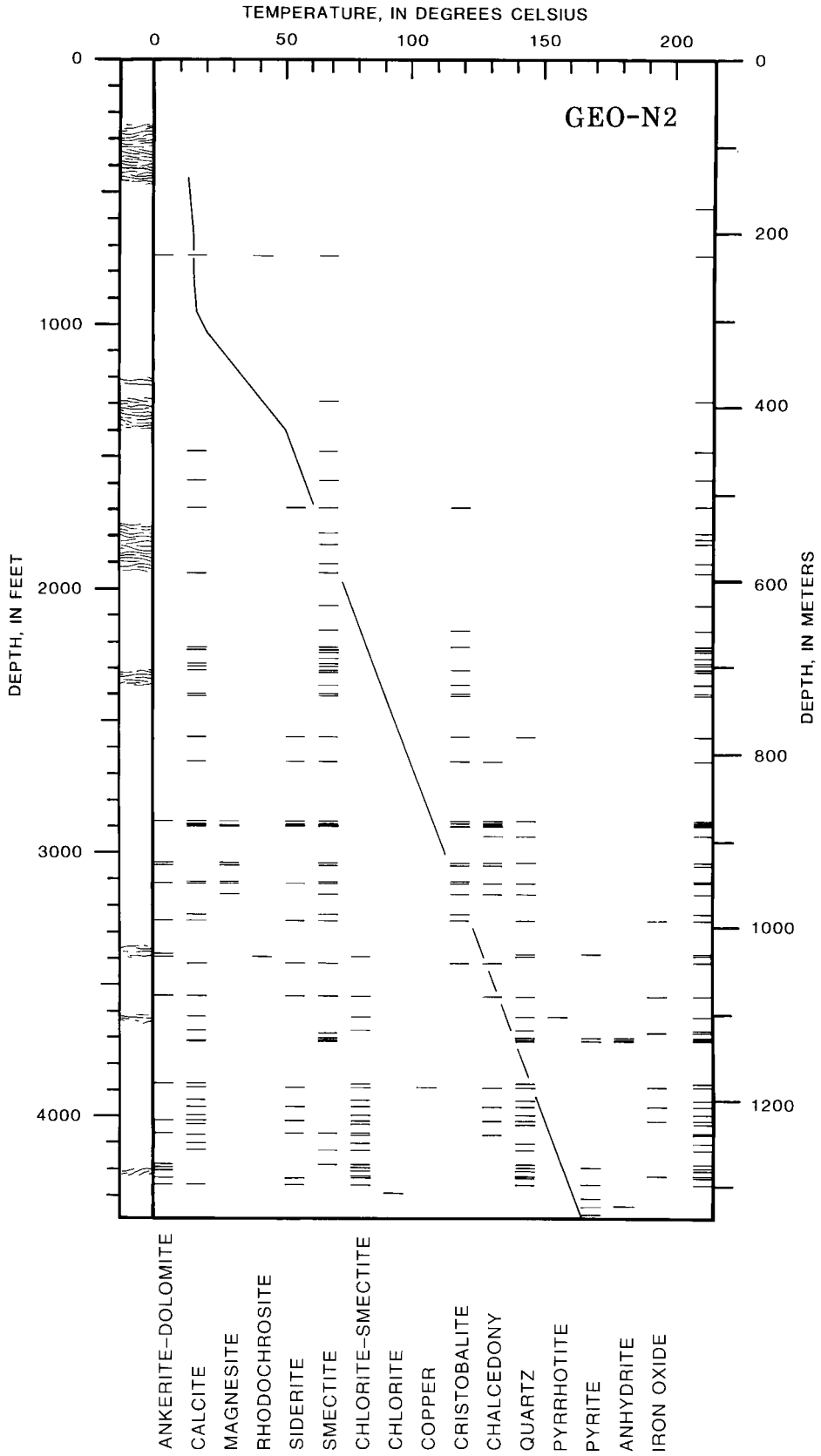

Figure 16.—Distribution of hydrothermal alteration minerals with depth in geothermal drill hole GEO-N2 on west flank of Newberry volcano. Explanation is same as for figure 14. Measured temperature data from Walkey and Swanberg (1990).

Colorless, tabular, anhydrite crystals were deposited in vesicles and fractures at depths of 1,128.4 to 1,131.4 m and at 1,323.1-m depth. Hematite or amorphous iron oxide deposits in the groundmass of some samples stain vapor-phase crystals and sulfides owing to alteration of mafic crystals. At 1,122.3-m depth, a brick-red iron oxide fracture deposit formed later than smectite and an unidentified carbonate mineral.

FLUID INCLUSIONS

Double-polished thick sections for four open-space deposits of hydrothermal quartz and calcite from the GEO-N2 drill core contain monophase-liquid and liquid-rich fluid inclusions having a vapor phase consisting of only about 1 to 2 percent. The fluid inclusions usually occur along healed fractures and appear to be secondary inclusions.

Melting-point temperatures for most of the specimens either could not be determined or were very erratic; T_m values range between -0.3 and +5.8˚C. In many of the fluid inclusions, the vapor bubble disappeared during freezing and only reappeared following melting of the ice, which suggests the presence of metastable fluids (Roedder, 1984). One quartz sample from 1,223-m depth yielded consistent T_m values of -0.1˚C, which indicates that the salinity of this fluid is about 0.2 weight percent NaCl equivalent (Potter, Clynne, and Brown, 1978).

Only 61 T_h measurements were obtained from the 6 mineral chips that were heated. Minimum T_h values for three of the sample depths plot very close to the measured temperature curve given in Walkey and Swanberg (1990) (fig. 17). Two T_h measurements from the lowermost sample plot as much as 11˚C lower than the measured temperature curve, which suggests that past temperatures may have been somewhat lower at this depth. Maximum T_h measurements indicate that the fluid in this drill hole previously has been in the range of about 20 to 40˚C warmer than the present measured temperatures; a single T_h value of 195˚C at 925-m depth may be significant, although additional data would be necessary before reaching any conclusions regarding this value.

GEO-N3

Drill hole GEO-N3, located at an elevation of 1,753 m about 9.7 km north of the northern rim of Newberry caldera, was completed in 1986 (Swanberg, Walkey, and Combs, 1988; Earth Science Laboratory, 1987). The hole was drilled by the rotary method to 138-m depth and cored by wireline method to a total depth of 1,220 m; core recovery ranged from 50 to 95 percent (Earth Science Laboratory, 1987). A maximum temperature of 57˚C was recorded at the bottom of the drill hole (Earth Science Laboratory, 1987).

LITHOLOGY

Drill core from the upper half of the GEO-N3 hole was not sampled for this study because the core specimens appeared to be devoid of secondary mineralization (fig. 18). According to W.C. Walkey (written commun., 1987), the upper part of the drill core consists largely of basaltic to basaltic andesite lava flows with some glassy obsidian flows, interflow breccia, air-fall tuff, ash-flow tuff, scoria, and a few thin dikes. Most of the lower half of the drill core consists of basaltic to basaltic andesite lava flows, scoria, and interbedded ash-flow tuff, although more silicic flows and glassy interflow breccias occur from about 974- to 1,137-m depth. The bottom of the GEO-N3 drill core is composed of basaltic to basaltic andesite lava flows, scoria, and interbedded ash-flow tuff.

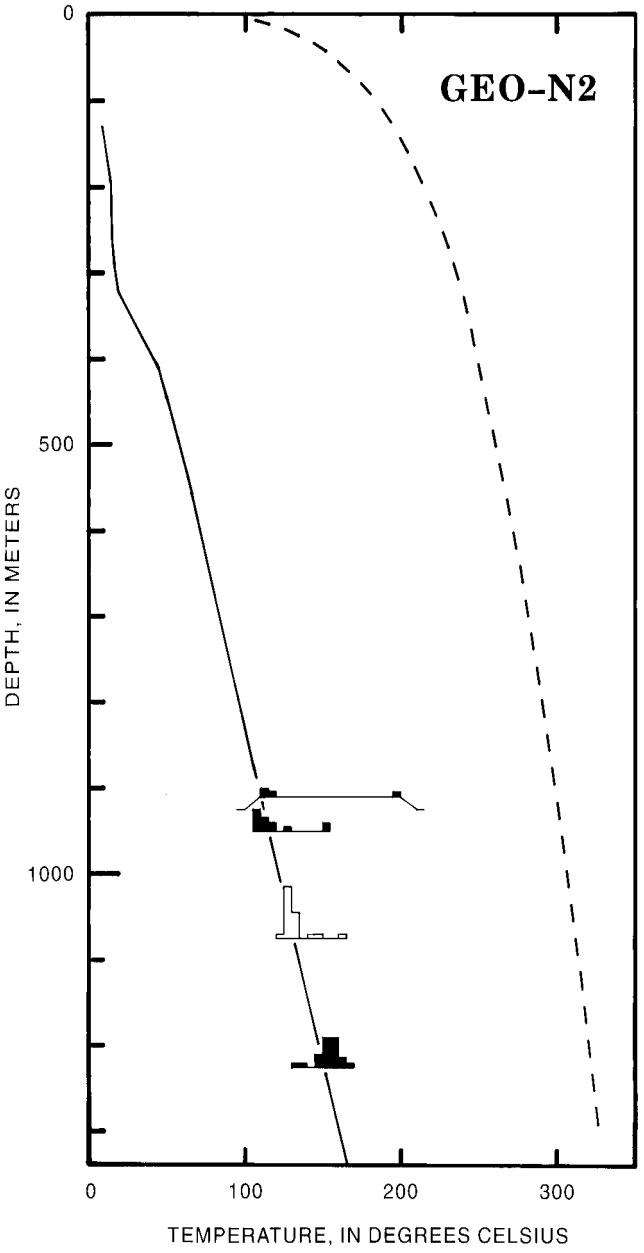

Figure 17.—Fluid-inclusion T_h values for quartz and calcite specimens from GEO-N2 drill core. Explanation is same as for figure 11. Measured temperature data from Walkey and Swanberg (1990).

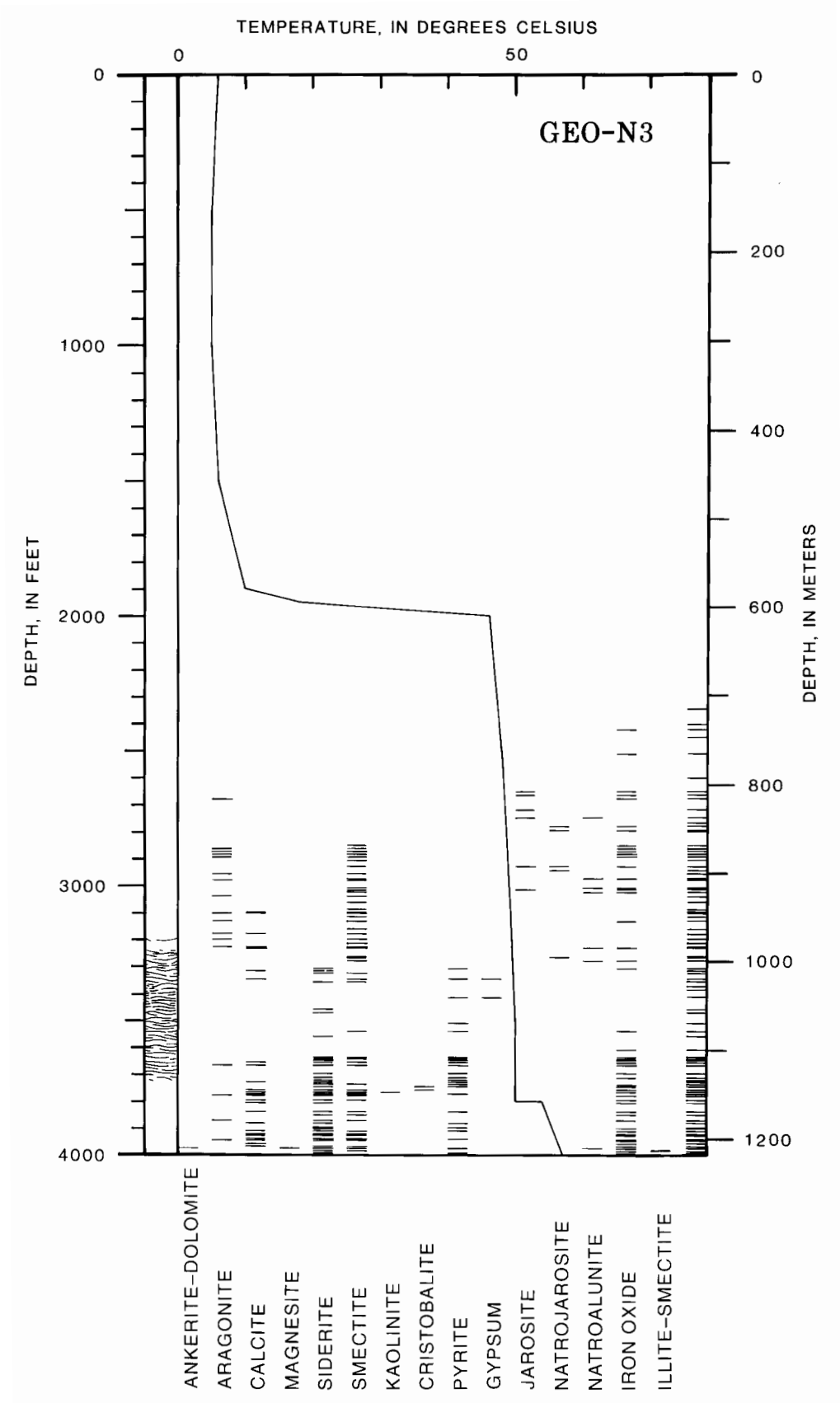

Figure 18.—Distribution of hydrothermal alteration minerals with depth in GEO-N3 drill core on north side of Newberry volcano. Explanation is same as for figure 14. Measured temperature data from Swanberg, Walkey, and Combs (1988), and Walkey and Swanberg (1990).

Swanberg, Walkey, and Combs (1988) reported K/Ar ages for seven GEO-N3 drill core samples that range between about 0.109 Ma and 1.54 Ma.

Primary mineralogy of the mafic lava flows is dominantly plagioclase, with some clinopyroxene and magnetite. Devitrification cristobalite was identified by XRD analyses of several whole-rock samples. The more silicic lava flows contain K-feldspar and vapor-phase tridymite in addition to plagioclase and magnetite. Some magnetite appears to be of secondary origin (vapor-phase?), although much of these deposits has been altered to hematite. Textures of the more silicic lava flows tend to be glassy, dense, or flow banded, while the mafic flows are more open with diktytaxitic, vesicular, or scoriaceous textures. The denser lava flows typically are unaltered; however, where the flows are vesicular, are scoriaceous, or contain vertical to horizontally oriented fractures, the open spaces are partly to completely filled by secondary minerals.

HYDROTHERMAL ALTERATION

Secondary mineralization in the GEO-N3 drill core consists mostly of deposition in vesicles, fractures, and open spaces between breccia fragments. Black sooty, clayey, or botryoidal magnetite in fractures and vesicles was deposited earlier than other secondary minerals and probably is of deuteric origin. Some magnetite open-space fillings are partly altered to hydrothermal(?) hematite. In addition, hematite stains several scoria units, and tuff beds and was deposited as hexagonal vapor-phase crystals. The only other iron-oxide mineral in this drill core is minor goethite, which probably is a low-temperature hydrothermal deposit.

Three samples contain illite or mixed-layer illite-smectite in association with the iron-oxide minerals. The clay minerals appear to be authigenic and do not result from drill mud contamination. One mixed-layer clay sample at 1,219.0-m depth appears to be associated with cooling of a 5-mm-wide glassy dike(?) that intruded the lava flow. The two other clay deposits may have a similar higher temperature origin.

Colorless, botryoidal cristobalite occurs in two vesicle fillings. Sulfate minerals (jarosite, natrojarosite, and natroalunite), deposited in a few vesicles, fractures, and open spaces of scoria, suggest acid-sulfate hydrothermal conditions. Kaolinite in a vesicle filling at 1,148.0-m depth is compatible with formation in an acid environment.

Pyrite crystals appear to be closely associated with siderite and smectite, although the order of deposition for these three minerals may not always be the same. Caramel-colored hemispherical crystal aggregates of siderite sometimes have a black magnetite core. Some other caramel-colored siderite hemispheres, observed in cross sections cut parallel to the planar view, consist of alternating concentric rings of caramel and white- or cream-colored calcite or manganoan calcite. XRD analysis of one siderite sample at 1,211.6-m depth shows the presence of magnesite and ankerite-dolomite (or possibly kutnohorite). Colorless acicular aragonite crystals were deposited later than other secondary minerals in open spaces of the GEO-N3 drill core.

GEO-N4

GEO-Newberry Crater, Inc. completed a single core hole (GEO-N4) at a surface elevation of 1,905 m 3.2 km outside the caldera rim on the east flank of Newberry volcano (Walkey and Swanberg, 1990). The maximum bottom-hole temperature of this drill hole is about 30˚C at a depth of 703 m (Walkey and Swanberg, 1990).

LITHOLOGY

Except for two dacitic lava flows, the drill core consists of basalt, basaltic andesite, and andesite lava flows, lithic- to vitric-pumiceous tuff, scoria, and volcaniclastic debris flows (C.A. Swanberg and W.C. Walkey, written commun., 1990). Plagioclase and magnetite are the dominant primary minerals; minute quartz peaks are present in a few XRD analyses. Pyroxene probably is present, but no peaks were observed in XRD. Vapor-phase tridymite and devitrification cristobalite occur in several XRD analyses.

HYDROTHERMAL ALTERATION

The GEO-N4 drill core samples contain only minor secondary alteration (fig. 19). Glassy tuffs are mostly fresh, and fractures and vesicles are only partly filled. Initial secondary mineralization of the GEO-N4 drill core consists of open-space deposits of vapor-phase minerals, such as tridymite and hexagonal hematite crystals. Amorphous iron oxide (deuteric?) stains several tuffs, cinders, scoria, and other volcanic rocks in the drill core. The earliest hydrothermal minerals appear to be light-yellow to dark-caramel-colored spherical and hemispherical clusters of siderite. Some of the spheres are broken and show a sequence of concentric shells consisting of alternating siderite and calcite (reacts with HCl). Smectite was mostly deposited later than siderite, but occasional smectite deposits are earlier, which suggests that one or possibly both of the minerals formed during two generations. Colorless acicular aragonite crystals were deposited later than other associated hydrothermal minerals.

GEO-N5

Drill hole GEO-N5 is located on the southwest flank of Newberry Volcano 3.9 km outside the caldera rim at an elevation of 1,731 m (Walkey and Swanberg, 1990). The drill hole was completed to 988-m depth and had a bottom-hole temperature near 80˚C (Walkey and Swanberg, 1990).

LITHOLOGY

The GEO-N5 drill core consists of nearly equal proportions of silicic (dacitic to rhyolitic) (table 7) and mafic (basaltic to andesitic) (fig. 20) lava flows, obsidian flows, flow breccias, and obsidian breccias, intercalated lithic-vitric tuff, scoria, debris flows, palagonitic soils, air-fall tuff, and a few dikes (C.A. Swanberg and W.C. Walkey, written commun., 1990). Many of the samples collected for this study are flow banded or vesicular. Glass frequently is devitrified to cristobalite or is hydrothermally altered, but several samples contain unaltered glass. XRD analyses of mafic whole-rock samples show plagioclase and cristobalite, whereas in the silicic rocks K-feldspar and cristobalite were identified in most analyzed samples. Silicic rocks also contain vapor-phase mineralization consisting of tridymite and alkali-feldspar and quartz (granophyric?). Open spaces between breccia fragments, vesicles, and fractures contain small amounts of hydrothermal alteration minerals.

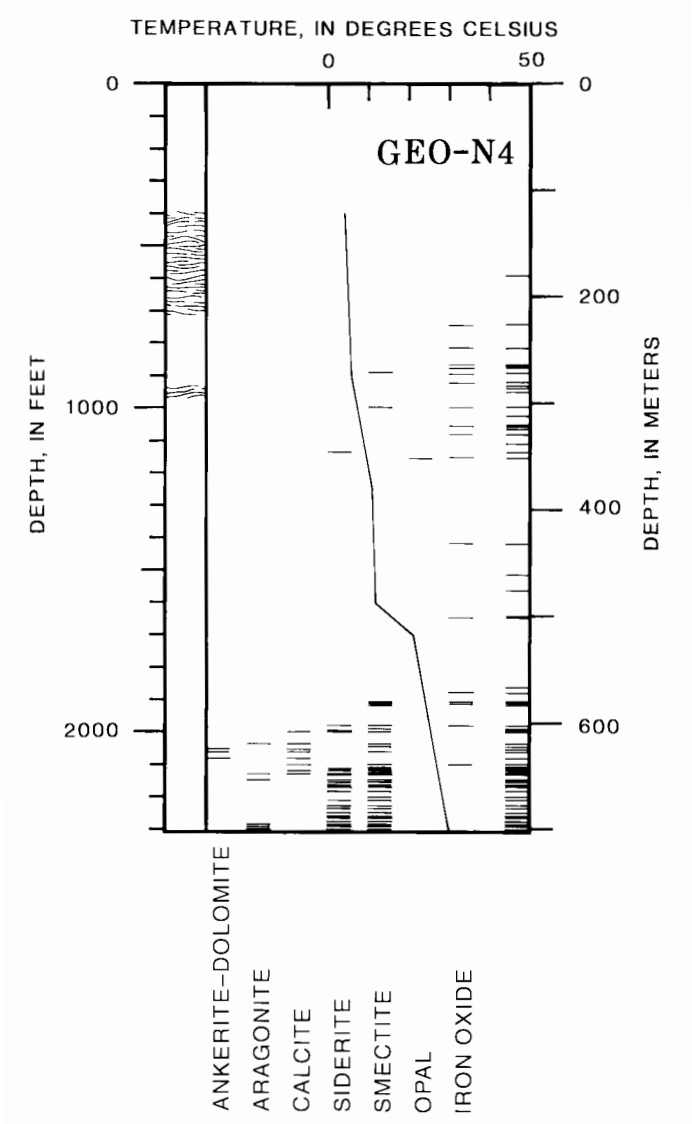

Figure 19.—Distribution of hydrothermal alteration minerals with depth in GEO-N4 drill core on northeast side of Newberry volcano. Explanation is same as for figure 14. Measured temperature data from Walkey and Swanberg (1990).

HYDROTHERMAL ALTERATION

A few intervals in the GEO-N5 drill core contain subhorizontal cavities in which vapor-phase crystals of tridymite, alkali feldspar, cristobalite, and magnetite (mostly altered to hematite or amorphous iron oxide) were formed during cooling of the lava flows. Between depths of about 622 m and 646 m, a silicic lava flow also has euhedral quartz crystals lining the vapor-phase cavities; the quartz probably is granophyric (Keith and Muffler, 1978) because it formed before vapor-phase K-feldspar and tridymite.

Various colors (yellow, orange, brown, pink, red, or black) of iron oxide staining are scattered throughout the GEO-N5 drill core. Red, iron-oxide stained cindery intervals or breccias marking the upper or lower parts of some of the lava flows undoubtedly are deuteric and formed during cooling of the lava flows. Most of these iron oxide deposits are amorphous in XRD analyses, although sporadic poorly crystalline hematite was identified. Magnetite usually occurs as tiny primary groundmass crystals or vapor-phase deposits; however, at 972.3-m depth vesicles are lined with black, spherical, or hemispherical deposits of magnetite (partly altered to red iron oxide) that also may be deuteric. XRD analyses show that soft red clayey material lining a few vesicles and fractures consists of both smectite and hematite and probably is of hydrothermal origin.

A thin carbonate vein at 789.4-m depth contains a few black sphalerite crystals (fig. 21) that formed earlier than the siderite and calcite vein filling. In the upper half of the drill core, virtually all of the obsidian and ash glass is unaltered. Much glass in the lower half of the drill core remains unaltered, but some tuffaceous beds are altered to smectite (halloysite in lithic tuff at 583.1-m depth). Blue-green mixed-layer illite-smectite with disseminated pyrite crystals was deposited on vapor-phase minerals in a cavity at 785.2-m depth. Pyrite is frequently deposited in fractures and vesicles that also contain siderite. Brown, red, green, gray, white, and orange smectite coats many fractures and vesicles and appears to have been deposited in more than one generation; some open-space smectite is earlier than calcite, whereas smectite coats calcite in other deposits. Both siderite and calcite may also have been deposited in more than one generation. In some samples calcite appears to form from siderite with the release of iron oxide; however, in other samples siderite crystals are deposited on top of calcite. The two carbonate minerals commonly are deposited as hemispherical crystal clusters or concentric rings in tight fractures. Both minerals occur as rhombic crystals or massive deposits; siderite may form disc-shaped crystal clusters, whereas in some occurrences calcite needles were deposited. Circular buff car-

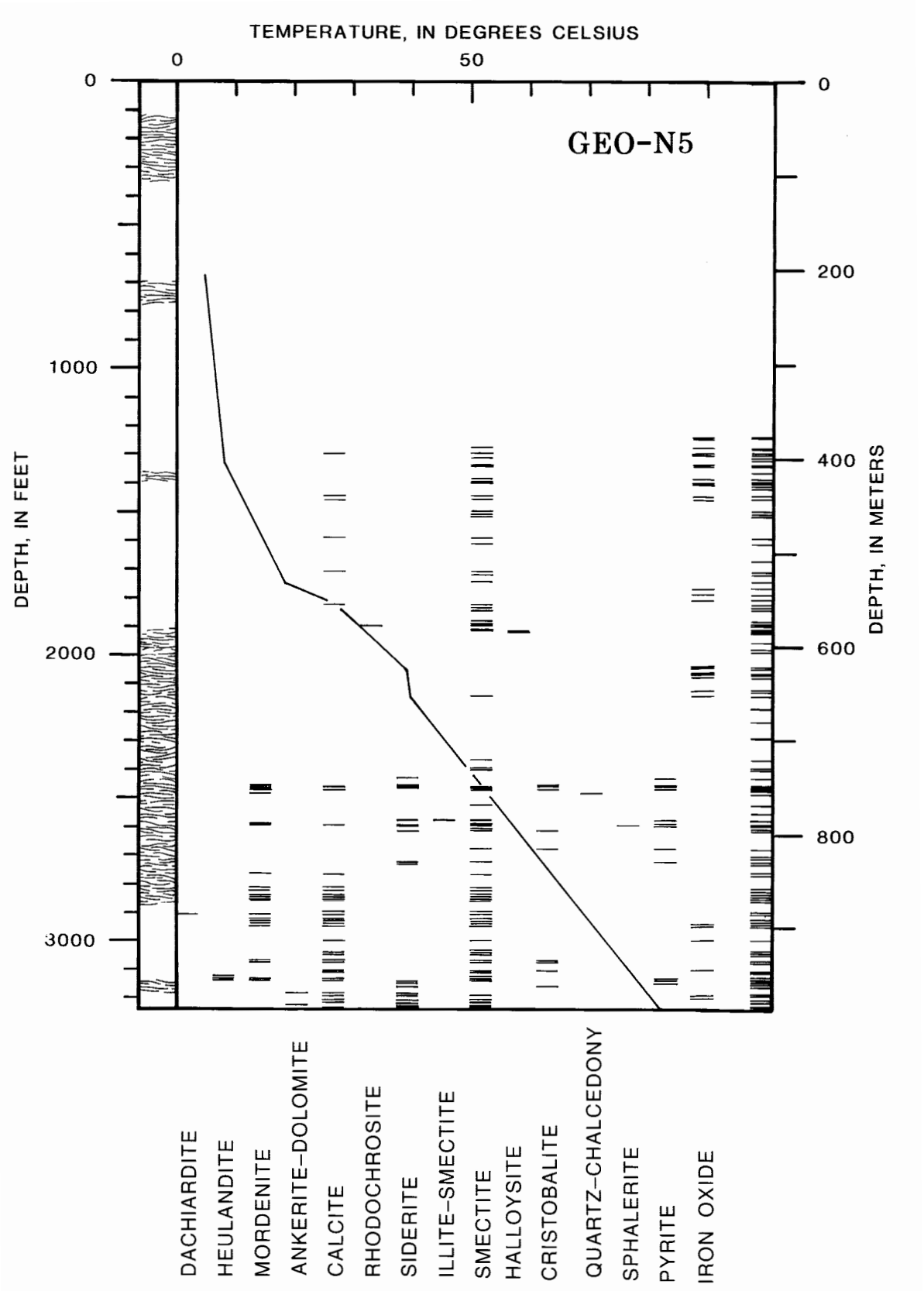

Figure 20.—Distribution of hydrothermal alteration minerals with depth in GEO-N5 drill core on southwest side of Newberry volcano. Explanation is same as for figure 14. Measured temperature data from Walkey and Swanberg (1990).

bonate deposits on a fracture at 576.7-m depth were identified as rhodochrosite in XRD analysis. Colorless, rhombic crystals from two open-space deposits near the bottom of the drill hole were identified as ankerite or dolomite by XRD analysis. Vesicles in one silicic core sample from 756.5-m depth are lined by light-gray botryoidal chalcedony and a few later quartz crystals (fig. 22). Similar frosted botryoidal silica-vesicle deposits, some of which are later than calcite, were identified as cristobalite by XRD. Three zeolite minerals (dachiardite, heulandite, and mordenite) appear to be late deposits in fractures, vesicles, and open spaces between breccia fragments in the lower part of the GEO-N5 drill core; mordenite, along with smectite, also replaces glass in tuffs and breccias.

SF NC-01

Drill hole SF NC-01 was spudded in 1984 at an elevation of 1,859 m about 2 km outside the western rim of Newberry caldera by Santa Fe Geothermal, Inc. (previously known as Occidental Geothermal, Inc.) (Arestad, Potter, and Stewart, 1988; Walkey and Swanberg, 1990). The drill hole was completed to 1,219-m depth and had a near-bottom-hole temperature of 170˚C (Arestad, Potter, and Stewart, 1988).

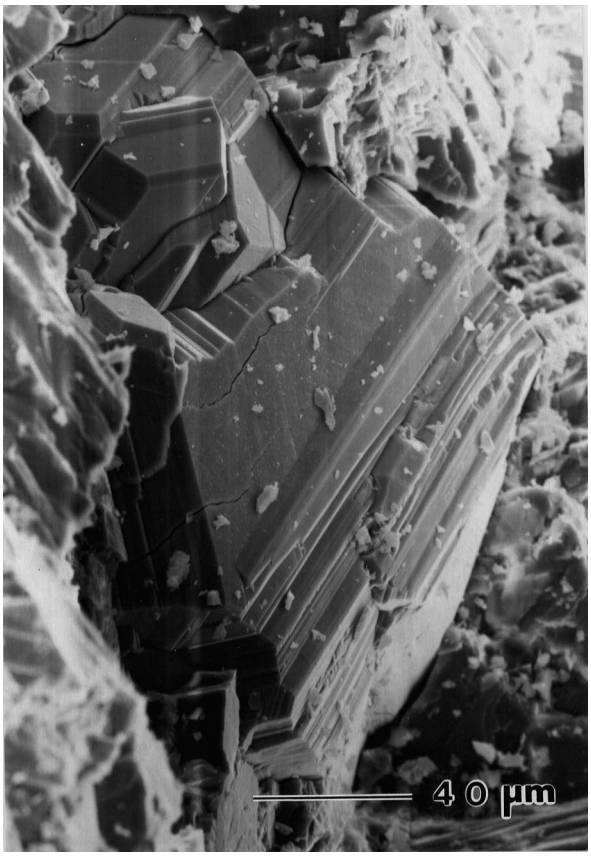

Figure 21.—Scanning electron micrograph of fracture filling at 789.4-m depth in GEO-N5 drill core; contains a few sphalerite crystals and later massive siderite.

LITHOLOGY

The drill hole penetrated mafic (basalt and basaltic andesite) lava flows and cinders in the upper 183 m (Arestad, Potter, and Stewart, 1988). From 183- to 762-m depth, some basaltic andesite and andesite lava flows and cinders are present, but the volcanic ash and lithic tuff intervals, volcanic breccia, and dense and vesicular lava flows are mostly of dacite and rhyodacite composition (Arestad, Potter, and Stewart, 1988). Below 762-m depth the drill core consists of a sequence of andesitic, vesicular to dense lava flows, cinders, and interflow breccias that are increasingly mafic in composition toward the bottom of the drill hole (Arestad, Potter, and Stewart, 1988). XRD analyses show that plagioclase and magnetite are the primary minerals in the mafic rocks; other minerals undoubtedly are present, but were not detected by XRD. Devitrification cristobalite was identified in XRD patterns for both mafic and silicic drill core samples. The silicic rocks contain K-feldspar and quartz, in addition to plagioclase and magnetite. Concentrations of vapor-phase minerals consist of euhedral tridymite and K-feldspar crystals that were deposited within subhorizontal to subvertical linear cavities, usually with some remaining open space.

HYDROTHERMAL ALTERATION

Unaltered glass matrix and obsidian clasts do occur in poorly indurated tuffs from the upper part of the SF NC-01

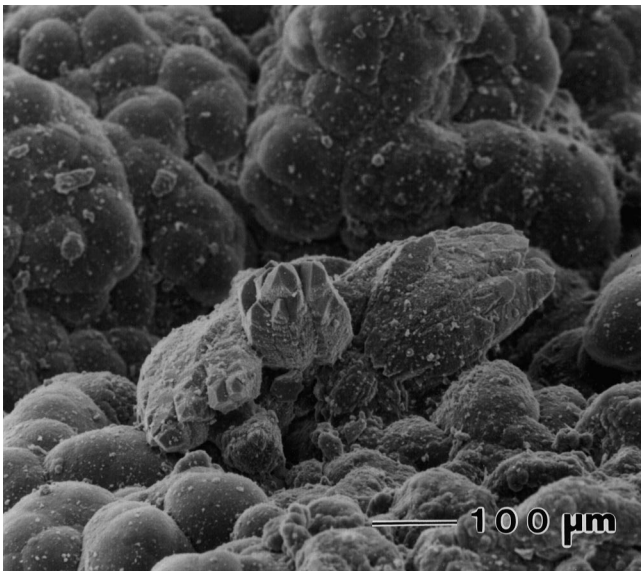

Figure 22.—Scanning electron micrograph of botryoidal chalcedony open-space deposit with clusters of late quartz crystals (center), from 756.5-m depth in GEO-N5 drill core.

drill hole; however, hydrothermal alteration of these deposits is more extensive with depth. Open spaces of vapor-phase partings, fractures, vesicles, and between breccia fragments usually contain hydrothermal mineral deposits below about 200-m depth in the drill hole (fig. 23). One of the earliest deposited minerals frequently is a clay that is dominantly smectite throughout the upper 1,000 m of drill-core samples. While smectite may be orange, brown, gray, white, or green, the majority of smectite samples are green. Some open-space fillings consist of two or more layers or generations of different-colored smectite deposits. Obsidian and pumice intervals are mostly unaltered in the upper half of the drill core, but glass in sampled ash layers from the bottom half of the drill hole are altered to smectite. A few clay deposits between about 277-m and 290-m depth are amorphous in XRD analyses. One of these clay deposits from a fracture at 277-m depth contains tiny disseminated pyrite crystals and later disc-shaped aggregates of siderite. Beneath this cream-colored amorphous clay is colorless to dark-brown isotropic opal (refractive index <1.47), which also contains disseminated pyrite crystals (fig. 24). Below 1,000-m depth, few smectite deposits were seen in the drill core; however, the dominant clay mineral there is green mixed-layer chlorite-smectite. Open spaces between breccia fragments at 1,124.4-m depth are partly filled by green botryoidal chlorite-smectite. One white clay vesicle filling and one green clay fracture deposit consist of mixed-layer illite-smectite as seen in XRD analyses. Three green clay deposits were identified as chlorite by XRD. At 1,120.4-m depth, a wormy-looking cluster of green chlorite crystals (similar to those in figure 45B) was deposited between breccia fragments.

Beneath clay layers in several fractured and vesicular drill-core samples are coatings of yellow-brown-orange-red amorphous iron oxide or red hematite. Massive vapor-phase magnetite in a vesicle at 1,191.2-m depth has red hematite staining, and the groundmass mafic crystals are altered to iron oxide.

Scattered open-space fillings in the upper 1,000 m of the drill core contain crystals or crystal aggregates (some hemispherical) of siderite that appears to have formed during two generations. The earlier siderite deposit is sometimes caramel colored and was followed by light-yellow siderite in a sample from 758.0-m depth. A few samples such as the hemispherical deposits at 617.5-m depth have an intervening smectite layer and later light-yellow siderite. Some samples contain more than one generation of calcite. Colorless rhombic calcite crystals formed earlier than siderite at 758.0-m depth but were deposited later than siderite in several other samples. Vesicles in a lava flow at 1,204.7-m depth are filled, in order of paragenesis, by (1) a botryoidal calcite layer, (2) green clay, (3) colorless calcite, (4) chalcedony, and (5) quartz crystals. Other drill-core samples contain blocky calcite crystals that were deposited later than quartz crystals. Calcite morphology includes massive, bladed, blocky, and scalenohedral forms. Calcite (reacts with HCl) at least partly replaces plagioclase phenocrysts near the bottom of the drill hole. Ankerite-dolomite, the only other carbonate mineral in the SF NC-01 drill core, was identified by two XRD analyses of calcite-bearing samples.

A few botryoidal silica open-space deposits above 1,000-m depth consist of cristobalite. Spherical clusters of cristobalite crystals also coat calcite at 900.0-m depth. The cristobalite open-space fillings appear either to be gradually converted to chalcedony or to consist of alternating chalcedony and cristobalite layers; XRD analyses show that several of the bluish-frosted, banded silica deposits consist of both minerals. Colorless, euhedral, quartz crystals formed later than many of the botryoidal silica deposits.

Two vesicular samples from just above 1,000-m depth contain late deposits of white fibrous mordenite. The only other zeolite mineral identified in this drill core is colorless, fibrous to acicular laumontite, which occurs at 1,120.4-m depth along with earlier wormy-looking green chlorite and blocky calcite.

FLUID INCLUSIONS

Fluid inclusion data were obtained for nine sample chips from five sample depths in the SF NC-01 drill hole. Two bladed calcite samples from 900-m depth have abundant monophase-liquid and liquid-rich fluid inclusions (about 1 to 2 percent vapor) that appear to have formed along crystal growth planes parallel to the crystal faces and may be primary. Most other fluid inclusions in this drill hole appear to have formed along healed fractures and are secondary. At 1,216-m depth, a quartz deposit may be later than fluid inclusions along a healed fracture, in which case the fluid inclusions would be pseudosecondary.

Only ten usable T_m measurements, ranging between -0.2 and 0.0˚C, were obtained for hydrothermal calcite and quartz from depths of 900 m and 1,149 m, and the salinity of these fluid inclusions is about 0 to 0.4 weight percent NaCl equivalent. The vapor phase of fluid inclusions from one hydrothermal quartz sample from 900-m depth all disappeared at about -42˚C during freezing. In seven of the continuously monitored fluid inclusions, the vapor bubble suddenly reappeared at temperatures between +1.7 and + 4.9˚C, but melting of the last piece of ice was not observed; these fluids probably are metastable and do not provide a reliable estimate of the fluid salinity (Roedder, 1984). Melting-point temperatures were not attempted for several samples because the fluid inclusions were too small, because leakage occurred during heating, or because the samples were too cloudy for accurate measurements.

Homogenization temperature measurements for 117 fluid inclusions in quartz and calcite from five sample depths straddle the measured temperature curve of Walkey and Swanberg (1990) (fig. 25). From these measurements, it appears that the rocks sampled in this drill core have been subjected to past temperatures that ranged from as much as about 20˚C lower than the present measured temperatures to about 45˚C higher than the down-hole temperature measurements.

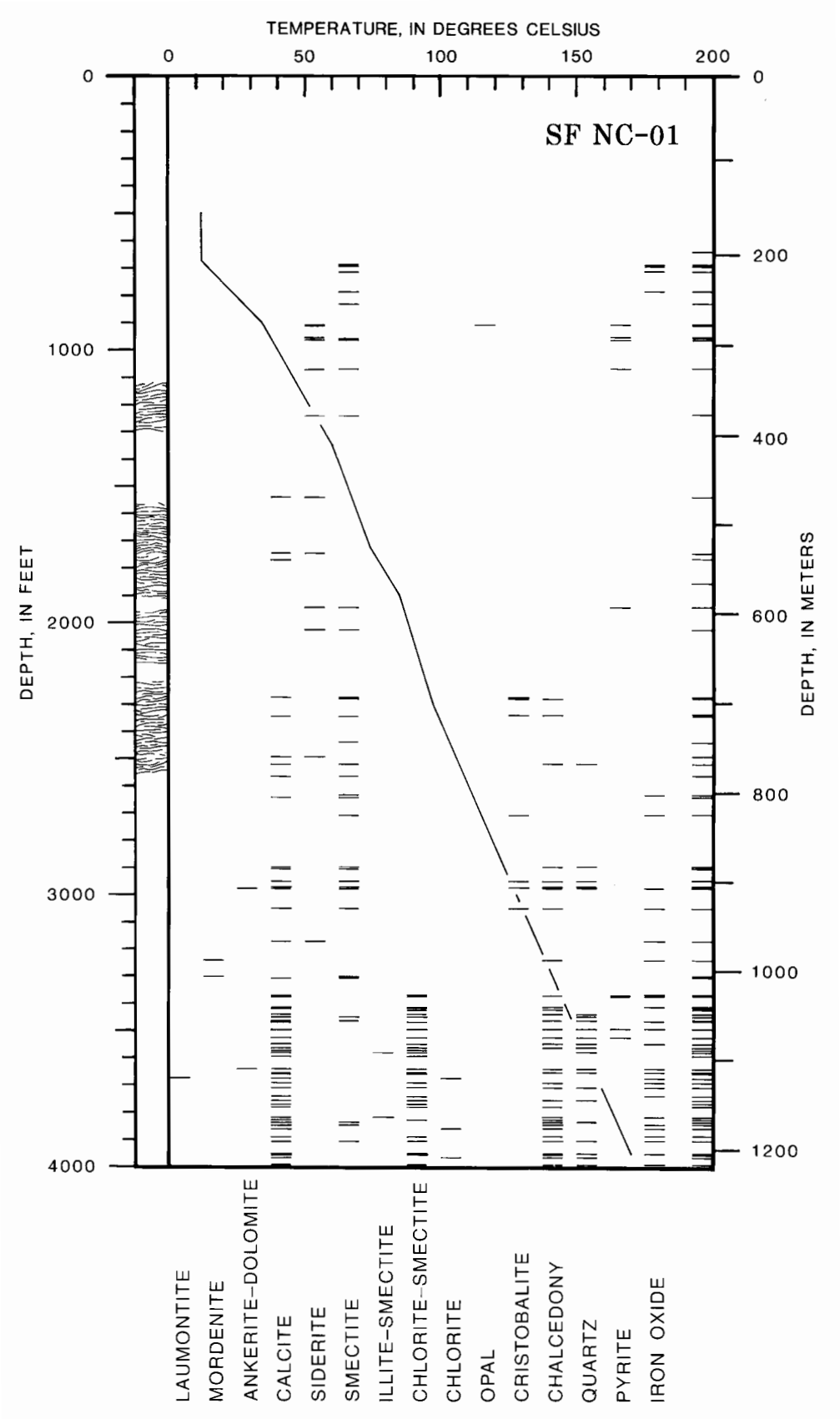

Figure 23.—Distribution of hydrothermal alteration minerals with depth in SF NC-01 geothermal drill hole on west flank of Newberry volcano. Explanation is same as for figure 14. Measured temperature data from Arestad, Potter, and Stewart (1988) and Walkey and Swanberg (1990).

SF NC72-03

Santa Fe Geothermal, Inc., began drilling the SF NC72-03 hole at an altitude of 1,993 m, very near the caldera rim on the west side of Newberry volcano (fig. 3) in 1983 and completed it in 1984 (Arestad, Potter, and Stewart, 1988; Walkey and Swanberg, 1990). A near-bottom temperature of 155˚C was measured in the 1,372-m-deep drill hole and an average geothermal gradient of 137˚C/km is given (Arestad, Potter, and Stewart, 1988).

LITHOLOGY

A generalized stratigraphic column for this drill hole shows basaltic to rhyolitic rocks consisting of massive to very vesicular lava flows, pumice, lahars, vitrophyre, cinders, lithic tuff, and interflow breccia (Arested, Potter, and Stewart, 1988). The more siliceous volcanic rocks occur between about 160- to 240-m depth and 550- to 700-m depth (fig. 26, table 7). Several thin microdiorite sills(?) were encountered at depths of 924 to 929 m, 1,141 m, 1,279 m, and 1,356 m. Plagioclase is the dominant primary mineral; mafic minerals appear to have been altered to clay and hematite, although magnetite is seen in some whole-rock XRD analyses. Silica minerals (primary quartz, devitrification cristobalite, and vapor-phase tridymite) are found in the silicic volcanic rocks.

HYDROTHERMAL ALTERATION

The shallowest sample collected for this study was from about 480-m depth. Hydrothermal minerals were found lining vesicles and fractures and between breccia fragments of virtually every sample examined below that depth. A few fractures and vesicles in the SF NC72-03 drill core contain small amounts of massive to spherical secondary magnetite that usually is at least partly altered to red hematite or amorphous iron oxide. Red iron oxide is an early alteration mineral in many open-space hydrothermal deposits in this drill core and may consist of completely altered vapor-phase or deuteric magnetite. Some red cindery interflow deposits are oxidized to amorphous iron oxide, and groundmass mafic minerals in some lava flows have red iron oxide staining. At 762-m depth, a ~2-cm-thick reddish clay interval consists of smectite and hematite as shown by XRD analysis. There is some evidence for a later stage of red iron oxide alteration in a few botryoidal samples, such as at 1,164.9-m depth where red iron oxide appears to be later than both calcite and dark-green smectite.

Many fractures, vesicles, and open spaces between breccia fragments contain an early deposit of light- to dark-green,

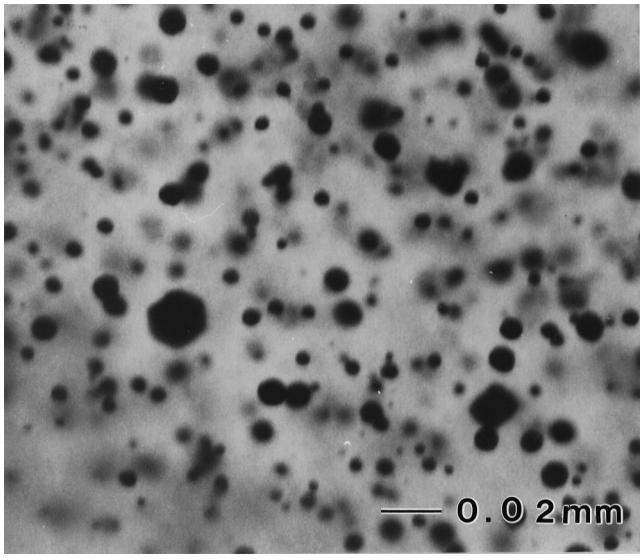

Figure 24.—Opal with disseminated cubic, pyritohedral, and rounded to irregular-shaped pyrite crystals (0.02 mm or less in size) from 227.1-m depth in SF NC-01 drill core.

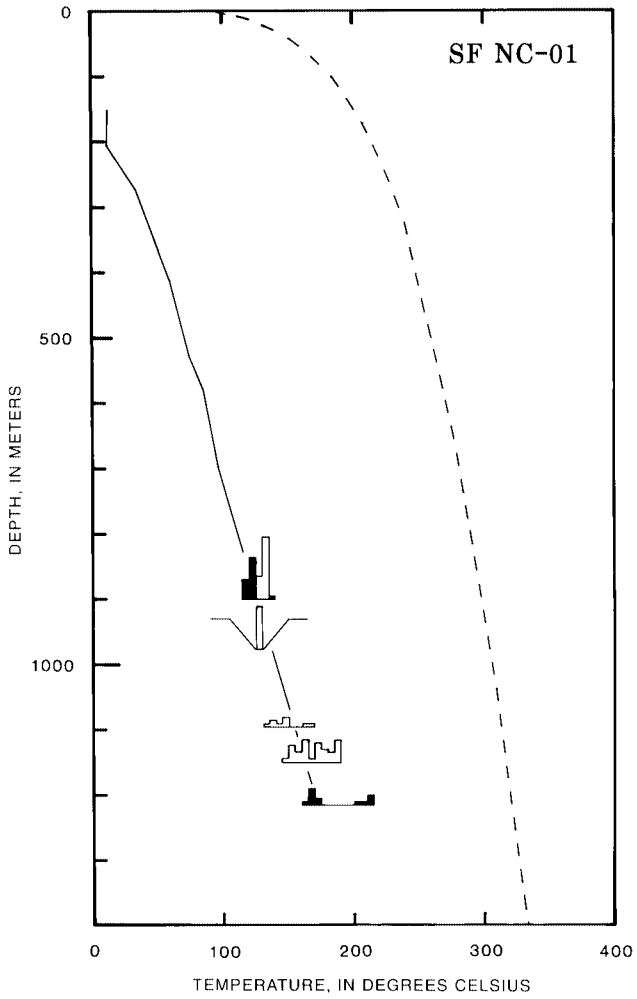

Figure 25.—Fluid-inclusion T_h values for quartz and calcite from SF NC-01 drill hole. Explanation is same as for figure 11. Measured temperature data from Arestad, Potter, and Stewart (1988) and Walkey and Swanberg (1990).

brown, red, orange, or white smectite. Several samples contain evidence for more than one generation of smectite deposition; at 766.0-m depth, vesicles are coated by three different colors of clay deposits. Similarly, a ~1.5-cm vesicle at 1,015.6-m depth is filled by green clay, later pyrite, a second generation of green clay, and finally bluish chalcedony. A few green clay deposits were identified in X-ray analyses as chlorite and mixed-layer chlorite-smectite. One vesicle-filling white clay in a dark-red iron oxide-altered lava flow at 1,342.0-m depth also is identified as a mixed-layer chlorite-smectite by XRD analysis; a semiquantitative chemical analysis of the white clay by EDS on the SEM shows that there is much more Mg than Fe in the deposit.

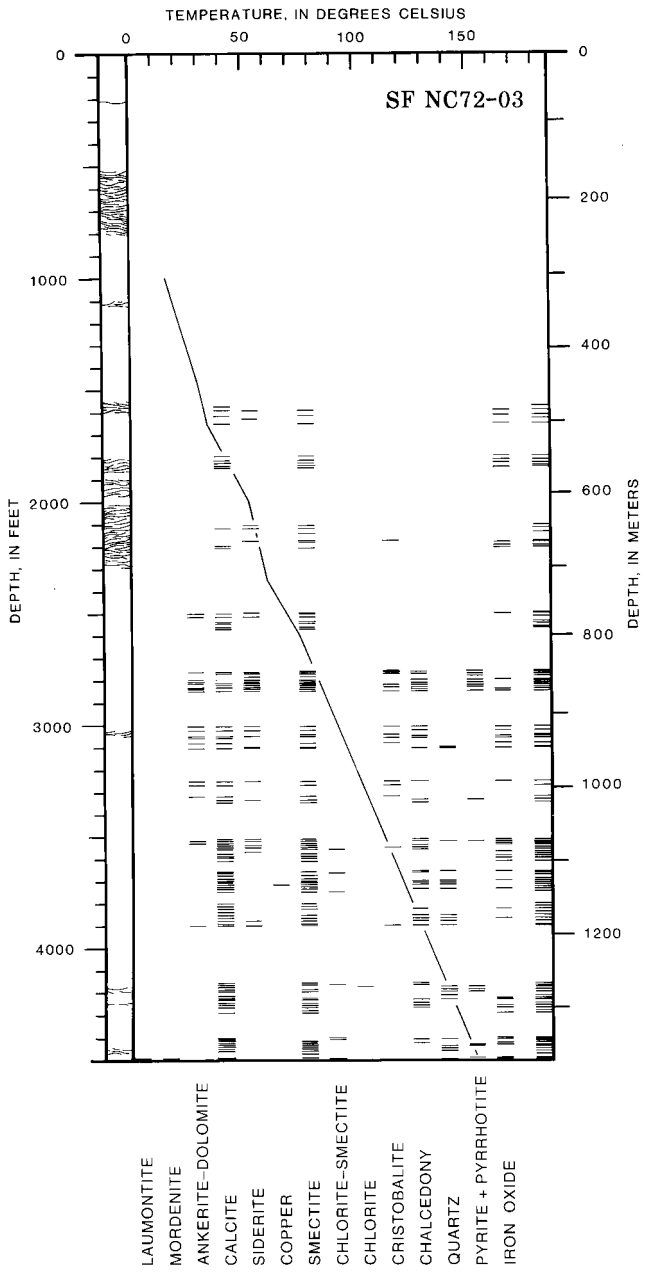

Figure 26.—Distribution of hydrothermal alteration minerals with depth in SF NC72-03 drill hole just outside western ring fracture of Newberry volcano. Explanation is same as for figure 14. Measured temperature data from Arestad, Potter, and Stewart (1988) and Walkey and Swanberg (1990).

Another early deposit in this drill core is siderite, which occurs in open spaces of several samples between depths of 485.2 m and 1,187.2 m. Siderite occurs as individual tiny rhombic crystals, stacks of rhombic crystals, and disc-shaped or hemispherical crystal aggregates and appears to have formed in several generations. Often siderite is closely associated with calcite; at 1,181.6-m depth, botryoidal carbonate deposits consist of alternating layers of white calcite and brown siderite. Calcite, which occurs in most of the collected drill core samples, is much more abundant than siderite. Calcite also formed during more than one episode; early calcite deposits tend to be massive or botryoidal, whereas later generations may consist of bladed, blocky, or scalenohedral crystals. The latest carbonate mineral to be deposited in open spaces of this drill core is ankerite-dolomite, which usually occurs as tiny colorless rhombic crystals between depths of 762.2 m and 1,187.2 m.

White, bluish, frosted, or colorless, massive to botryoidal silica deposits in vesicles and fractures below about 840-m depth usually consist of chalcedony, although several X-ray analyses also show the presence of cristobalite. Tiny colorless euhedral quartz crystals generally are a late deposit; however, quartz is earlier than calcite in vesicles at 1,125.6-m depth, and quartz crystals formed earlier than green clay and calcite in a fracture at 1,356.1-m depth.

One vesicle at 1,131.0-m depth contains an early-deposited grain of native copper. At 1,351.5-m depth, a fracture surface contains a few hexagonal, bladed, iron sulfide crystals that may be pyrrhotite(?). Small amounts of tiny pyrite crystals are deposited in open spaces of a few drill-core samples; sometimes, the minute crystals are disseminated in clay or silica deposits. At the very bottom of the drill core, open spaces between breccia fragments are filled by quartz, calcite and late white prismatic laumontite crystals. A single vesicle in this core sample also contains colorless acicular crystals that might be mordenite(?).

FLUID INCLUSIONS

Fluid inclusions were located in five prepared double-polished thick sections of hydrothermal quartz and calcite crystals from open-space deposits of the SF NC72-03 drill core. All of the fluid inclusions appear to be secondary; most are liquid-rich inclusions, but the shallower samples contain monophase-liquid fluid inclusions. Vapor-bubble volume varies from about 1 to 2 percent in the shallowest sample, to about 5 to 10 percent in the intermediate-depth samples, and to about 15 percent in the deeper samples.

Many of the fluid inclusions were too small for T_m determinations. At 945-m depth, the vapor bubbles disappeared during freezing and reappeared only after the temperature was raised to +0.1 to +2.5˚C, indicating that the

fluid is metastable (Roedder, 1984). A T_m value of -0.4˚C (0.7 weight percent NaCl equivalent) was only observed for a single fluid inclusion from 1,287-m depth. Melting-point temperatures for the flank drill holes are too sparse to warrant drawing any sweeping conclusions concerning the salinity of the fluid from which the calcite and quartz crystals formed. However, the available fluid-inclusion salinity data appear to suggest a slight fluid salinity increase near the ring fracture system on the west side of Newberry volcano. Fluid moving up the fracture probably is slightly saline but becomes diluted by mixing with meteoric water during lateral movement outward from the caldera.

Ninety-six T_h measurements were obtained from fluid inclusions in eight quartz and calcite samples from five depths in the SF NC72-03 drill core (fig. 27). The shallowest sample, at 945-m depth, has minimum T_h values that plot very close to the measured temperature curve and range up to about 15˚C higher. Nearly all of the remaining T_h measurements plot much higher than the temperatures measured during drilling (Walkey and Swanberg, 1990). Homogenization temperatures from near the bottom of the drill hole are about 160˚C higher than the measured temperature curve, indicating that rocks recovered from this drill hole have cooled considerably since the hydrothermal quartz and calcite crystals were formed.

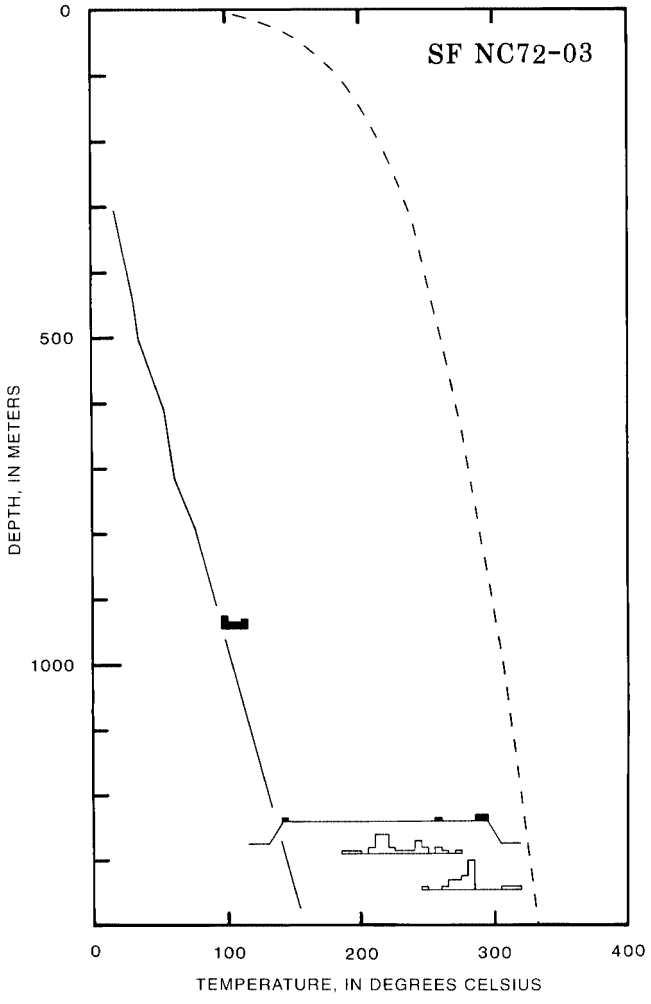

Figure 27.—Fluid-inclusion T_h values for quartz and calcite from SF NC72-03 drill hole. Explanation is same as for figure 11. Measured temperature data from Arestad, Potter, and Stewart (1988) and Walkey and Swanberg (1990).

OTHER DRILL HOLES

The locations of several other geothermal drill holes on the flanks of Newberry volcano that were not studied for this report are shown on figure 3. Some of these holes were very shallow and would not be expected to contain substantial hydrothermal alteration. In 1976, three temperature-gradient drill holes (maximum depth about 61 m) were spudded by Phillips Petroleum Company on the north and northeast flanks of Newberry volcano (P-3, P-5, and P-6) (Olmstead and Wermiel, 1988). Results from these wells were never released.

In September 1977, the U.S. Geological Survey completed drill hole USGS-N1 to a depth of 386 m at an altitude of about 1,900 m on the upper northeast flank of Newberry volcano (Sammel, 1981; MacLeod and Sammel, 1982). The maximum temperature recorded in this drill hole was only 17˚C at 384-m depth (Blackwell, Black, and Priest, 1981; MacLeod and Sammel, 1982). According to MacLeod and Sammel (1982), geothermal gradients for the drill hole (about 50˚C/km) are lower than the mean regional gradient (65°C/km) estimated by Blackwell and others (1978). The drill core consists of rhyolitic to basaltic lava flows and interbedded ash-flow tuffs, ash-fall deposits, breccia, volcaniclastic sediments, and cinders (Sammel, 1981; MacLeod and Sammel, 1982). Magnetic studies indicate that these rocks have not been heated by geothermal fluids (Griscom and Roberts, 1983). No alteration was observed in thin sections, nor was any alteration of this drill core reported by MacLeod and Sammel (1982).

In 1982 and 1983, Union Oil Company of California drilled four 610-m-deep drill holes on the east and west flanks of Newberry volcano (U 82-9, U 82-10, U 83-8, and U 83-9). Results from these drill holes remain unpublished.

California Energy Company, Inc., drilled two holes (1,325 m and 1,225 m deep) on the south and northwest slopes of Newberry volcano in 1986 (Olmstead and Wermiel, 1988) (CE NB-3 and CE NB-4). Drill core from these holes are available for study at the Energy and Geoscience Institute of the University of Utah core storage facility in Salt Lake City, Utah. We made a cursory hand-lens examination of core from the deeper parts of the two holes. Core samples from CE NB-3 contain iron-oxide coatings on fractures, calcite breccia infillings, open-space deposits of green smectite(?), and undifferentiated (Mg, Fe, Ca, or Mn?) carbonate minerals in vesicles and other open spaces between 1,216-m depth and the hole bottom at 1,325 m. Drill-core specimens from CE NB-4 contain similar hydrothermal mineral deposits from 1,162-m depth to the hole bottom at 1,225 m. The hydrothermal mineralogy and extent of alteration in these drill cores are similar to those of the

other flank drill holes located at similar distances from the caldera ring fractures. No samples were obtained for laboratory mineralogy studies.

HYDROTHERMAL MINERALOGY OF DRILL-CORE SPECIMENS

Secondary minerals deposited along fractures and in vesicles in the shallow levels of the Newberry drill cores, especially in flank drill holes, probably are not of hydrothermal origin. Yellow, green, or pale-blue-gray, soft amorphous clay-like open-space deposits in the upper, low-temperature part of a few drill holes are similar in appearance and texture to hydrothermal smectite coatings and may be a precursor smectite-clay phase. Low-temperature zones may also contain minor white, frosted, or colorless amorphous silica deposits that are similar to hydrothermal opal. Some orange-reddish amorphous iron oxide staining may result from low-temperature oxidation of primary magnetite. These types of deposits are also found in fresh lavas as a result of degassing during cooling (the cooler stages).

Some drill-core samples contain tridymite vapor-phase mineralization and sometimes other minerals such as magnetite or ilmenite that formed during initial degassing of lava flows. Reddish iron oxide (amorphous iron oxide, iron hydroxide, or hematite) open-space deposits or pervasive staining of some tuffs, as well as botryoidal, massive, or powdery black magnetite found in some fractures and vesicles (drill hole GEO-N3) probably also formed during later cooling stages of the lava flows and ejecta.

DRILL HOLES WITHIN THE CALDERA

In the upper 300 m of USGS-N2 drill core, alteration minerals are notably sparse; X-ray diffraction analyses show the presence of minor siderite at 135-m depth, amorphous silica at 181-m depth, and traces of smectite at depths of 174 m and 185 m. Measured temperatures in the rhyolitic ash, obsidian, and basaltic tuff, breccia, and sedimentary intervals penetrated in this part of the drill hole ranged from 18 to 39˚C (Sammel, 1981). Below 300-m depth, the measured temperatures ranged from 31˚C at 300-m depth to 265˚C at 930-m depth (Sammel, 1981) (fig. 5), and hydrothermal alteration is slight to extensive, the more pervasive alteration occurs along fractures and fracture margins and in the more permeable brecciated and volcaniclastic zones (Keith and Bargar, 1988). The following minerals were identified in the rhyolitic to basaltic breccia, tuff, sediments, and lava flows recovered from the lower two-thirds of the hole: hydrothermal zeolite minerals (analcime, chabazite, clinoptilolite, dachiardite, erionite, faujasite, and mordenite), apophyllite, gyrolite, carbonate minerals (ankerite, aragonite, calcite, dolomite, magnesite, and siderite), apatite, hydrogrossular, clay minerals (smectite, mixed-layer illite-smectite, illite, mixed-layer chlorite-smectite, and chlorite), silica minerals (opal, cristobalite, chalcedony, and quartz), sulfide minerals (pyrrhotite, pyrite, and marcasite), sulfur, anhydrite, epidote, and iron oxides and hydroxides (hematite, goethite, and lepidocrocite) (fig. 5).

The RDO-1 drill hole, located about 0.5 km southeast of drill hole USGS-N2, encountered temperatures greater than 158˚C at about 350.5-m depth (fig. 12) (Black, Priest, and Woller, 1984; Keith and others, 1986). Many of the hydrothermal alteration minerals (analcime, aragonite, siderite, rhodochrosite, calcite, smectite, chlorite, quartz, mordenite, pyrite, pyrrhotite, and hematite) occur at shallower depths in the RDO-1 hole than in the USGS-N2 drill hole (Keith and others, 1986).

DRILL HOLES OUTSIDE THE CALDERA

Measured temperatures for drill holes on the north, south, east, and southwest flanks of Newberry volcano (GEO-N1, GEO-N3, GEO-N4, and GEO-N5) were less than 100˚C. Thin fracture coatings, vesicle fillings, spaces between breccia fragments, and glassy drill-core samples from these holes usually exhibit little or no secondary alteration in the upper parts of the drill holes. The lower parts of these drill holes contain low-temperature hydrothermal minerals that are compatible with the measured temperatures. Hydrothermal minerals identified from the four drill cores are dominated by carbonate minerals (ankerite-dolomite, aragonite, calcite, kutnohorite, magnesite, rhodochrosite, and siderite), smectite, and hematite, with local minor amounts of silica minerals (opal, cristobalite, and chalcedony), zeolites (chabazite, dachiardite, heulandite, mordenite, and phillipsite), okenite (one occurrence of the calcium silicate hydrate mineral), other clay minerals (mixed-layer illite-smectite and halloysite), sulfates (barite, gypsum, jarosite, natrojarosite, and natroalunite), and sulfides (pyrite and local sphalerite) (figs. 14, 18, 19, and 20). The three remaining flank drill holes (GEO-N2, SF NC-01, and SF NC72-03), located on the west side of Newberry volcano, encountered near-bottom-hole temperatures in excess of 150˚C. Hydrothermal alteration in the three drill holes is slight to extensive (Arestad, Potter, and Stewart, 1988) and reflects the higher temperatures. Hydrothermal minerals identified in one or more of the drill cores include, in addition to several of the above listed minerals, laumontite, mixed-layer chlorite-smectite, chlorite, copper, cristobalite, quartz, anhydrite, and pyrrhotite (figs. 16, 23, and 26).

Figure 15 shows a very generalized paragenetic diagram for hydrothermal mineralogy from all of the Newberry geothermal drill holes located outside the caldera that were sampled for this study. Iron oxides and clay minerals are usually early deposits; carbonate minerals, silica minerals, sulfates, and zeolites were deposited later but do not necessarily coexist. Several minerals, particularly smectite, siderite and calcite, were deposited in more than one generation.

HYDROTHERMAL MINERALS

ZEOLITE MINERALS

Zeolite minerals are sparsely distributed in drill holes on the outer flanks of Newberry volcano; only minor amounts of chabazite, dachiardite, heulandite, laumontite, mordenite, or phillipsite were identified in four of the drill holes (figs. 14, 20, 23, and 26). Except for mordenite, these mostly calcium-rich zeolite minerals were associated with mafic rocks. Somewhat more abundant zeolite minerals in the USGS-N2 drill core occur in two zones at depths of 308.9 to 320 m, and 436.5 to 496.2 m (fig. 5). In the upper zone, analcime, chabazite, erionite, and faujasite were identified as vein fillings and altered glass in basaltic sediments. The lower zone contains analcime, clinoptilolite, dachiardite, and mordenite as open-space deposits and alteration products of glass in rhyolitic tuff and tuff breccia. A few scattered occurrences of mordenite persist to about 748.2-m depth. Traces of analcime and some mordenite were found in drill cuttings from the RDO-1 drill hole (fig. 12).

Electron microprobe and scanning electron microscope (SEM) semiquantitative energy-dispersive X-ray spectroscopy (EDS) analyses of some of the USGS-N2 zeolites show variations in the chemistry of the minerals that partly reflect the chemistry of the rocks in which they reside. Alkali-rich clinoptilolite and dachiardite occur in the more silicic rocks, whereas calcium-rich chabazite, analcime, and erionite are found in mafic rocks. The cation composition of other analcime deposits, faujasite, and mordenite are either variable or inconsistent with the type of rock in which they are found.

Measured temperatures for the depths at which the above zeolite minerals occur appear to be compatible with temperatures at which these zeolites are found in other geothermal areas (Kristmannsdóttir and Tómasson, 1978). Minerals such as analcime, laumontite, and mordenite can form over a wide temperature range that can exceed 200˚C; in Newberry drill cores these zeolite minerals were found at temperatures presently ranging between about 50 and 160˚C. Chabazite, clinoptilolite, heulandite, and phillipsite were identified at present temperatures of about 100˚C or less in the Newberry drill cores, which is consistent with temperatures reported for these minerals in Icelandic geothermal areas (Kristmannsdóttir and Tómasson, 1978). Erionite was found at about 50˚C in one of the Newberry drill cores and is reported at temperatures below 110˚C from Yellowstone National Park (Honda and Muffler, 1970). Dachiardite occurs in two Newberry drill cores at measured temperatures less than about 100˚C, but the mineral has been found at temperatures as high as 200˚C in drill cores from Yellowstone's geothermal areas (Bargar and others, 1987). Faujasite, identified in one of the Newberry drill cores at a temperature of about 50˚C, is thought to form under hydrothermal conditions (Gottardi and Galli, 1985), but it apparently has not been reported from other modern-day geothermal areas.

ANALCIME

Two fine-grained volcaniclastic drill-chip samples at depths of 329 and 332 m in drill hole RDO-1 (fig. 12) contain analcime, as shown by whole-rock XRD analyses. Analcime was found at two locations in the USGS-N2 drill core (fig. 5). In the upper zone (about 313- to 320-m depth; temperature 40-50˚C), euhedral trapezohedral analcime crystals (fig. 28) occur as open-space deposits in coarse basaltic sediments. A trace of analcime also was detected by XRD at 443.8-m depth (temperature ~l00˚C). These low temperatures are reasonable for the formation of analcime, which appears to be somewhat independent of temperature constraints; analcime has been found over a wide temperature range (70-300˚C) in several geothermal drill holes (Honda and Muffler, 1970; Keith, White, and Beeson, 1978; Kristmannsdóttir and Tómasson, 1978). Analcime formation appears to be favored by increasing the pH and Na+ concentration of the associated fluid (Kusakabe and others, 1981).

Electron microprobe analyses of analcime from a depth of 318.5 m (table 8, analyses 4-8) show that the mineral is a sodium-rich pure analcime end member.

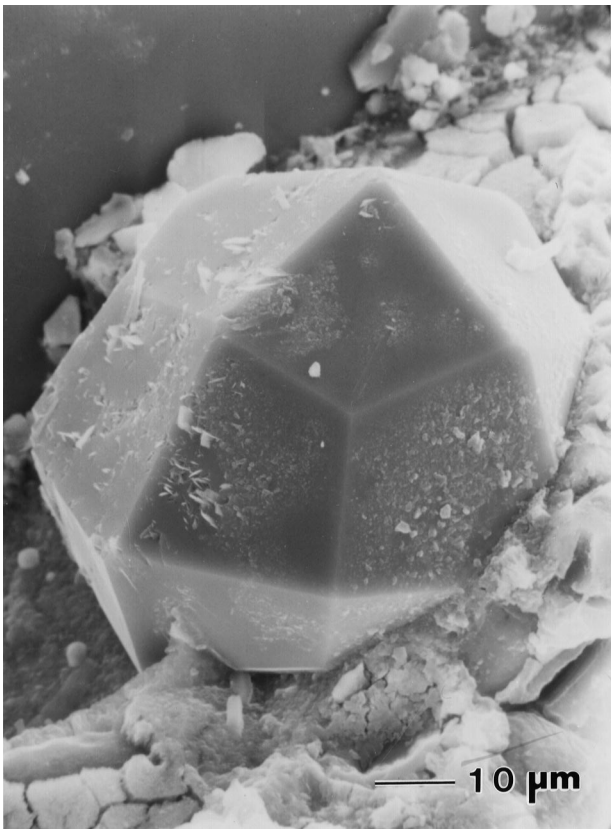

Figure 28.—Scanning electron micrograph of large trapezohedral analcime crystal deposited later than smectite in altered volcaniclastic sandstone at 315.1-m depth in drill core USGS-N2. A second, unidentified zeolite(?) or clay(?) mineral precipitated later than euhedral analcime crystal.

Table 8.—Electron microprobe analyses of zeolite minerals from USGS N-2 drill-core.

Mineral:	Calcian analcime			Analcime					Clinoptilolite			Dachiardite	Faujasite	
Depth (m):	314.6–315.1			318.5					442.3			443.2	314.4	
Analysis No.:	1	2	3	4	5	6	7[1]	8[1]	9	10	11	12	13	14
Major-element analyses (weight percent oxides)														
SiO_2	54.25	56.55	53.26	58.08	58.96	55.48	57.60	56.84	65.94	63.38	65.51	73.30	49.93	47.13
Al_2O_3	21.35	20.50	22.25	22.37	20.16	19.49	19.95	19.78	15.24	14.22	15.51	10.84	20.76	19.54
Fe_2O_3	0.00	0.00	0.02	0.00	0.00	0.18	0.01	0.01	0.28	0.11	0.38	0.06	0.16	0.11
MgO	0.01	0.14	0.07	0.00	0.00	0.13	0.02	0.00	0.22	0.27	0.16	0.00	0.09	0.00
MnO	0.04	0.01	0.04	0.00	0.01	0.04	0.04	0.00	0.00	0.00	0.03	0.02	0.00	0.02
CaO	4.41	4.04	5.75	0.03	0.04	0.11	0.11	0.25	1.19	1.08	0.51	1.15	9.13	3.29
Na_2O	7.36	7.87	6.26	13.16	12.48	11.33	11.89	12.20	6.39	5.80	2.96	5.37	1.93	7.08
K_2O	1.44	1.53	0.96	0.01	0.01	0.01	0.05	0.03	1.71	1.43	8.34	0.14	0.14	2.01
Total	88.86	90.64	88.61	93.65	91.66	86.77	89.67	89.11	90.97	86.29	93.40	90.88	82.14	79.18
Number of atoms on the basis of														
	96 oxygens								72 oxygens			48 oxygens	24 oxygens	
Si	32.74	33.45	32.19	33.09	34.16	33.97	34.09	33.94	28.25	28.50	28.10	20.41	8.06	8.04
Al	15.19	14.29	15.85	15.02	13.77	14.06	13.91	13.93	7.70	7.54	7.84	3.56	3.95	3.93
Fe	0.00	0.00	0.01	0.00	0.00	0.01	0.01	0.00	0.09	0.04	0.12	0.01	0.02	0.01
Mg	0.01	0.01	0.06	0.00	0.00	0.12	0.02	0.00	0.14	0.18	0.10	0.00	0.02	0.00
Mn	0.02	0.01	0.02	0.00	0.00	0.02	0.02	0.00	0.00	0.00	0.01	0.01	0.00	0.00
Ca	2.85	2.56	3.72	0.02	0.02	0.07	0.07	0.16	0.55	0.52	0.23	0.34	1.58	0.60
Na	8.62	9.02	7.34	14.53	14.02	13.45	13.64	14.12	5.31	5.06	2.46	2.90	0.61	2.34
K	1.11	1.16	0.74	0.01	0.00	0.01	0.04	0.02	0.94	0.82	4.57	0.05	0.03	0.22
Si+Al	47.9	47.7	48.0	48.1	47.9	48.0	48.0	47.9	36.0	36.0	35.9	24.0	12.0	12.0
$Si/Al+Fe^{3+}$	2.2	2.3	2.0	2.2	2.5	2.4	2.5	2.4	3.6	3.8	3.5	5.7	2.0	2.0
Bal. error[2]	-1.7	-6.7	1.1	3.1	-2.2	1.3	0.2	-3.7	2.1	4.1	3.2	-2.2	3.4	4.8

[1]Analyses 7 and 8 are averages of 5 and 6 analyses, respectively.

[2]Cation balance error determined by the method of Passaglia (1970).

Additional chemical analyses of analcime from the interval 314.6-315.1-m depth (table 8, analyses 1-3) show substantial amounts of CaO in addition to Na_2O. A continuous solid-solution series exists between Na-bearing analcime and Ca-bearing wairakite (Gottardi and Galli, 1985). Lack of a doublet (400) XRD reflection at 3.41 Å (run at 1/4° 2θ/min.) indicates that this occurrence of the mineral probably should be classified as calcium-rich analcime rather than sodium-rich wairakite (Coombs, 1955). Formation of the calcium-rich analcime specimen probably was due to calcium release during hydrothermal alteration of basaltic sediments at this depth.

CHABAZITE

Chabazite was identified by XRD analysis of fracture and pore-space fillings in samples of basaltic sandstone between depths of 308.9 and 318.5 m in drill hole USGS-N2 (fig. 5). The colorless, intergrown, twinned hexagonal crystals have a phacolitic lenticular habit (fig. 29A and B) and were observed in SEM to be a late deposit on top of faujasite and calcite in a sample from 308.9-m depth. Phacolite (colorless lenticular twinned chabazite) crystals apparently are uncommon in altered rocks of the Cascade Range; instead, the usual crystal habit for chabazite from these rocks is a pseudocubic rhombohedron (fig. 9 in Bargar, 1990). Semiquantitative EDS analysis on the SEM shows that chabazite from 308.9-m depth consists of Si, Al, Ca, K, and Na. Trace amounts of colorless to white twinned pseudocubic rhombohedral chabazite crystals coat fractures along with calcite, smectite, and phillipsite in a mafic lava flow between 801- and 802-m depth in drill core GEO-N1 (fig. 14). In both drill holes, chabazite occurs at depths where measured temperatures were less than 60°C. Chabazite is a characteristic hydrothermal mineral in low-

temperature alteration zones (<75˚C) of Icelandic geothermal areas (Kristmannsdóttir and Tómasson, 1978).

CLINOPTILOLITE

Lath- to acicular-shaped clinoptilolite crystals (fig. 30) were identified by XRD in six samples between depths of 436.5 and 443.8 m (temperature ~99˚C) in drill hole USGS-N2 (fig. 5). All six samples were heated overnight at 450˚C in order to distinguish between clinoptilolite and heulandite by the X-ray method of Mumpton (1960). No change in intensity or position of the (020) X-ray reflection at ~9.0 Å was observed in any of the samples; thus, the mineral was identified as clinoptilolite. The clinoptilolite probably forms as an alteration product of pumiceous fragments in the rhyolitic tuff breccia. Electron microprobe analyses (table 8, analyses 9-11) from 442.3 m show great variation in Na_2O and K_2O contents for different crystals in the same sample. One clinoptilolite crystal (analysis No. 11 in table 8) is high in potassium—8.34 percent. We are unaware of K_2O that high for clinoptilolite from any other hydrothermal deposit. Clinoptilolites with such high K_2O contents usually are produced by sedimentary (Stonecipher, 1978) or diagenetic (Ogihara and Iijima, 1990) processes rather than by hydrothermal alteration. Keith, White, and Beeson (1978) and Bargar and Beeson (1985) reported clinoptilolite K_2O contents of 5.73 and 4.99 weight percent, respectively, in rhyolitic drill-core specimens from thermal areas of Yellowstone National Park.

DACHIARDITE

Clusters of fibrous-, acicular-, or lath-shaped dachiardite crystals (fig. 31) were found in a single sample of rhyolitic tuff from 443.2-m depth in drill hole USGS-N2 (temperature is ~98˚C) (fig. 5). Dachiardite is a fairly rare zeolite mineral that appears to have formed, along with smectite, from alteration of pumice fragments. An electron microprobe analysis (table 8, analysis 12) shows that the Newberry dachiardite is a sodium-rich mineral and probably should be referred to as sodium dachiardite rather than dachiardite (Bargar and others, 1987). One volcanic breccia sample in drill core GEO-N5 contains tiny colorless dachiardite crystals along with mordenite and smectite in open spaces between breccia fragments at 886.7-m depth (temperature ~70˚C) (fig. 20).

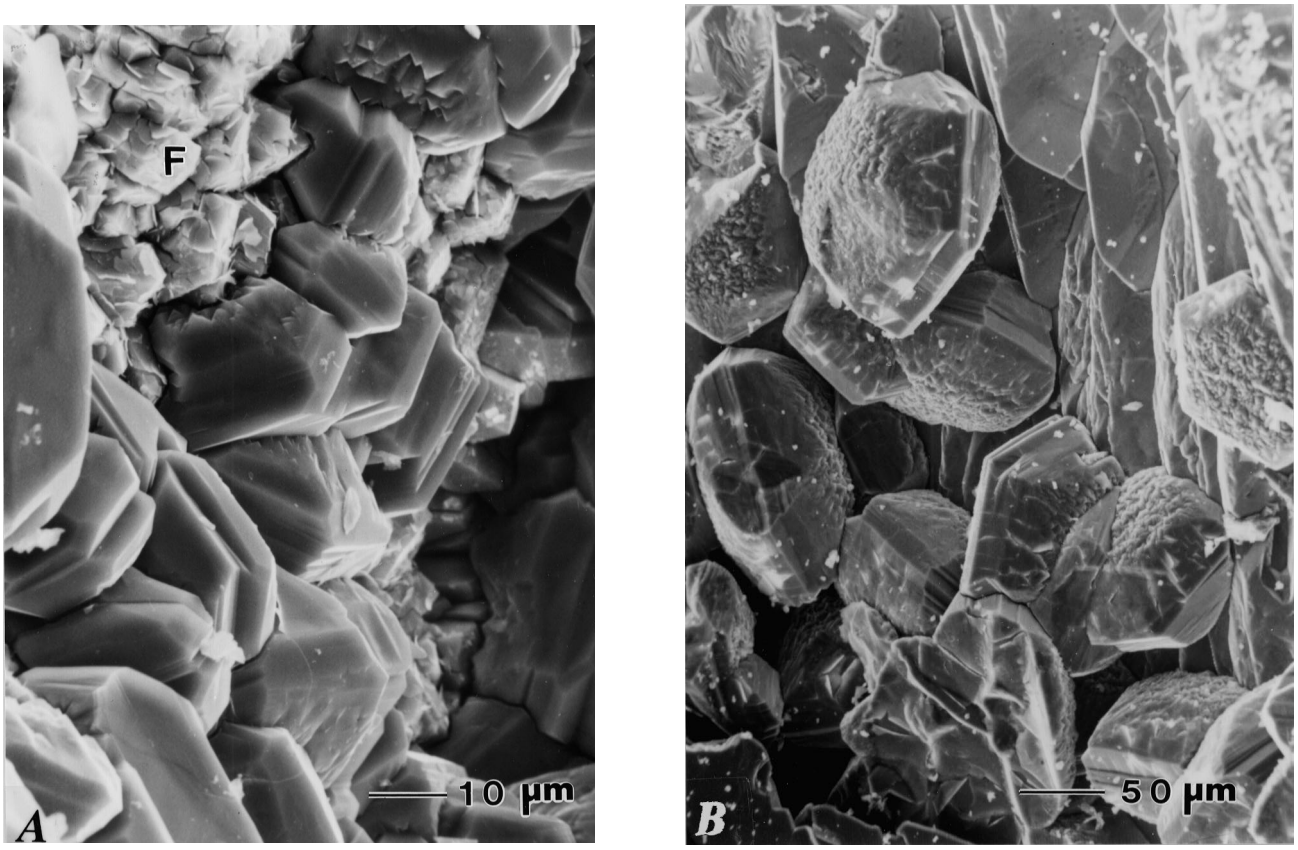

Figure 29.—Scanning electron micrographs of phacolitic chabazite crystals from 308.9-m depth in USGS-N2 drill hole. A, Twinned crystals deposited later than fractured and flaking faujasite (F) that coat veinlet. B, Phacolitic habit of chabazite.

ERIONITE

Bundles of tiny prismatic erionite crystals (fig. 32) appear to have formed by alteration of glass in three samples of basaltic sediments between depths of 315 m and 318.5 m in drill hole USGS-N2 (fig. 5). The presence of Mg, Ca, Fe, K, Na, Al, and Si is indicated by EDS analysis using the SEM. Erionite occurs at a depth where the temperature measured following drilling was about 50˚C. In the drill core from Yellowstone National Park, erionite is found at temperatures <110˚C (Honda and Muffler, 1970).

FAUJASITE

Faujasite, a rare zeolite mineral, was identified by XRD analyses of colorless to white vein fillings and intergranular open-space deposits of 11 porous samples of basaltic sediments between 308.9- to 320-m depth in drill hole USGS-N2 (temperature about 40-50˚C) (fig. 5). Scanning electron micrographs of faujasite from this drill core (fig. 33) suggest crystal deterioration with extensive cracking and flaking of the crystal surfaces. Electron microprobe chemical analyses of two faujasite crystals from 314.4-m depth (table 8, analyses 13 and 14) show considerable variability in Na_2O and CaO contents which, according to Gottardi and Galli (1985), is typical for faujasite.

HEULANDITE

One vesicular lava flow in drill hole GEO-N5 contains tiny, colorless, tabular to blocky, euhedral heulandite crystals (fig. 34) in fractures and vesicles in association with smectite, mordenite, and calcite at 951.3- to 954.6-m depth (temperature ~80˚C) (fig. 20). XRD analysis of one multicomponent sample shows a peak at ~9.0 Å; semiquantitative chemical analysis by EDS on the SEM shows Si, Al, and Ca, along with minor K, Mg, and Na, and the mineral is tentatively identified as heulandite rather than clinoptilolite.

LAUMONTITE

Single volcanic breccia samples near the bottoms of drill holes SF NC-01 and SF NC72-03 (1,120.4- and 1,370.1-m depth, respectively) contain tiny, white, prismatic, laumontite crystals deposited in open spaces between breccia fragments in association with earlier quartz, chlorite, calcite, or mixed-layer chlorite-smectite. Measured temperatures at these depths are about 150 to 160˚C (figs. 23 and 26). Laumontite commonly occurs between temperatures of 100 and 200˚C (Kristmannsdóttir and Tómasson, 1978), but it can also form at lower temperatures (McCulloh and others, 1981).

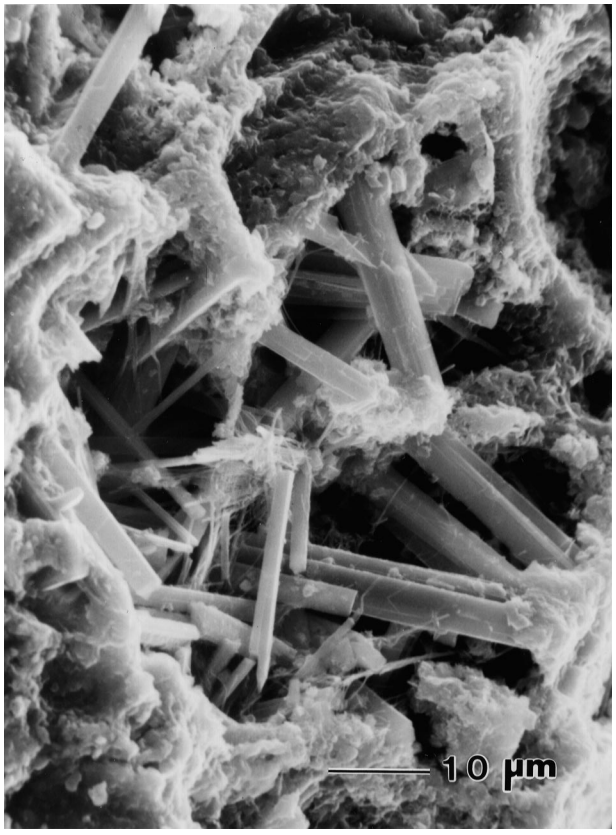

Figure 30.—Scanning electron micrograph of lath-shaped clinoptilolite crystals partly coated by smectite and fibrous mordenite(?), from 442.3-m depth in drill core USGS-N2.

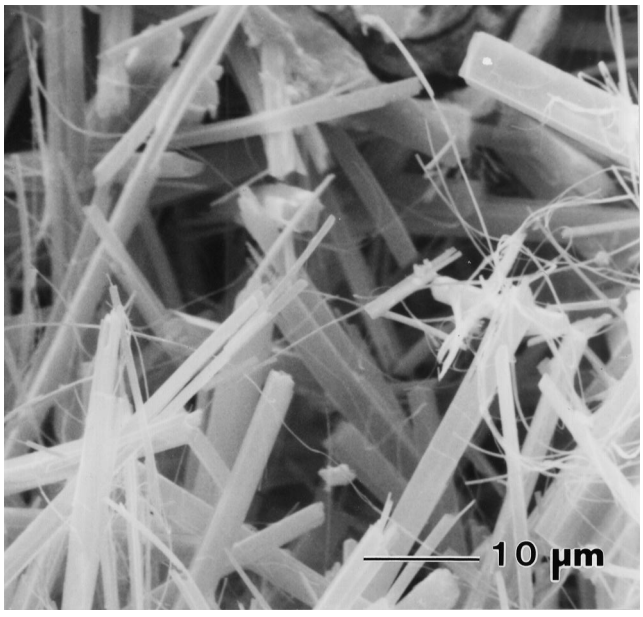

Figure 31.—Scanning electron micrograph of fibrous to acicular dachiardite crystals in altered lithic tuff from 443.2-m depth in USGS-N2 drill core.

MORDENITE

White fibrous radiating hemispherical crystal clusters (fig. 35A) or mattes of acicular mordenite crystals were deposited in vesicles of lava flows, open spaces between breccia fragments, or perlitic cracks of partly altered glass in the lower part of the GEO-N5 drill core (fig. 20). An EDS semiquantitative chemical analysis of this mordenite shows Si, Al, and Ca>Na. The only other mordenite identified in drill cores from the flanks of the volcano occurs near the bottoms of the SF NC-01 and SF NC72-03 drill holes where white fibrous mordenite crystals were deposited in a few cavities. Temperatures measured during drilling of these two holes were about 140 to 150˚C; however, temperatures in the lower part of the GEO-N5 drill hole ranged from about 50 to 80˚C. In Icelandic geothermal areas, mordenite forms over a wide temperature range (~75-230˚C) (Kristmannsdóttir and Tómasson, 1978).

Mordenite, the most abundant zeolite mineral in the USGS-N2 drill core, occurs as open-space deposits from depths of 443.7 to 460.2 m, and 469.1 to 496.2 m, and in three widely scattered samples from between 711.2 and 748.2 m (fig. 5). In the upper zone, mordenite is confined to the uppermost and lowermost part of a rhyodacite sill and rhyolitic tuffs where the fibrous zeolite was produced by alteration of glass. Figure 35B shows tiny fibrous mordenite crystals that formed perpendicular to the walls of a vesicle. A semiquantitative chemical analysis by EDS shows the presence of Si, Al, Ca, and K.

Mordenite was identified in drill cuttings from the RDO-1 drill hole as an open-space filling and in altered tuffs at 332- to 338-m depth along with smectite. Between depths of 393 and 423 m, mordenite is more abundant, and the fibrous to acicular crystals are associated with later-deposited bladed calcite (fig 35C), subhedral quartz crystals, and chlorite in open-space fillings; mordenite also replaces glass in altered pumice and lithic tuffs. Temperatures were not measured at the bottom of the RDO-1 drill hole (Keith and others, 1986) (fig. 12); the maximum temperature at which this mordenite formed must have exceeded 160˚C.

PHILLIPSITE

In drill hole GEO-N1, tiny, colorless, prismatic crystals from a lava flow at 756-m depth and three samples of open-

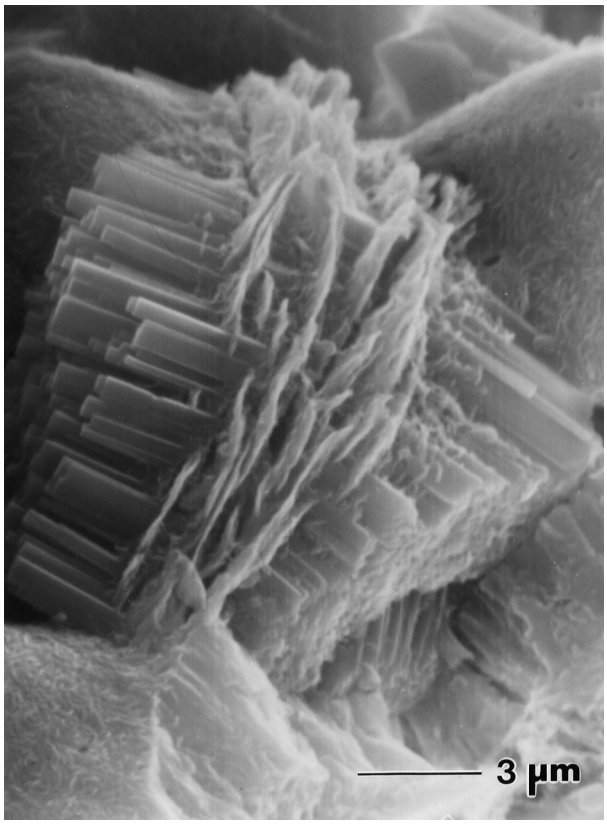

Figure 32.—Scanning electron micrograph showing bundle of stubby acicular erionite crystals and smectite deposited in pore spaces of basaltic sediments from about 315-m depth in USGS-N2 drill core.

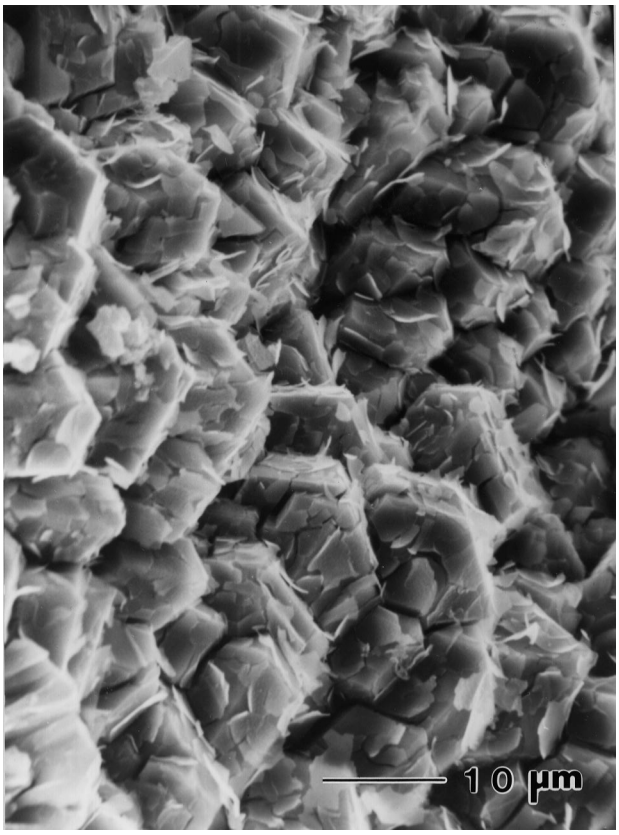

Figure 33.—Scanning electron micrograph of fractured and flaking faujasite crystals from 308.9-m depth in drill core USGS-N2.

space fillings in a lava flow between depths of 801 and 804 m were identified as phillipsite by XRD (fig. 14). Phillipsite occurs with chabazite in two of the samples; calcite and smectite are the only other associated hydrothermal minerals. Measured temperatures at these depths are below 10˚C. Phillipsite formed between temperatures of 60 and 85˚C in Icelandic geothermal areas (Kristmannsdóttir and Tómasson, 1978), but it has been reported at temperatures as low as 37˚C in a drill hole at Surtsey volcano (Jakobsson and Moore, 1986).

CALCIUM SILICATE HYDRATE MINERALS

GYROLITE

Clusters of lamellar gyrolite crystals line a fracture at 314.5-m depth in the drill core from USGS-N2 (fig. 5). Gyrolite also fills pore spaces in basaltic sandstone at 318.5-m depth (fig. 36) along with calcite, smectite, erionite, hydrogrossular, analcime, chabazite, apophyllite, and faujasite. An electron microprobe analysis of gyrolite from 314.5-m depth gave the following percentages of major-element oxides: 54.88 SiO_2, 1.60 Al_2O_3, 0.02 Fe_2O_3, 0.03 MgO, 33.37 CaO, 0.45 Na_2O, and 0.03 K_2O (total weight percent oxides = 90.38). Gyrolite typically is associated with zeolite minerals in basalts (Merlino, 1988). Basaltic drill-hole specimens from a few Icelandic geothermal areas contain gyrolite (Kristmannsdóttir and Tómasson, 1978), and gyrolite occurs in the rhyolitic drill core from one research geothermal drill hole in Yellowstone National Park (Bargar, Beeson, and Keith, 1981). In both of these occurrences, the temperatures were considerably higher than the <50˚C measured temperature at which gyrolite was found in the USGS-N2 drill hole.

OKENITE

Okenite occurs as a soft white vug filling in a basalt lava flow core specimen from 857-m depth in drill core GEO-N1 (temperature <10˚C) (fig. 14). The mineral appears to be rare in modern geothermal systems but typically is found in ba-

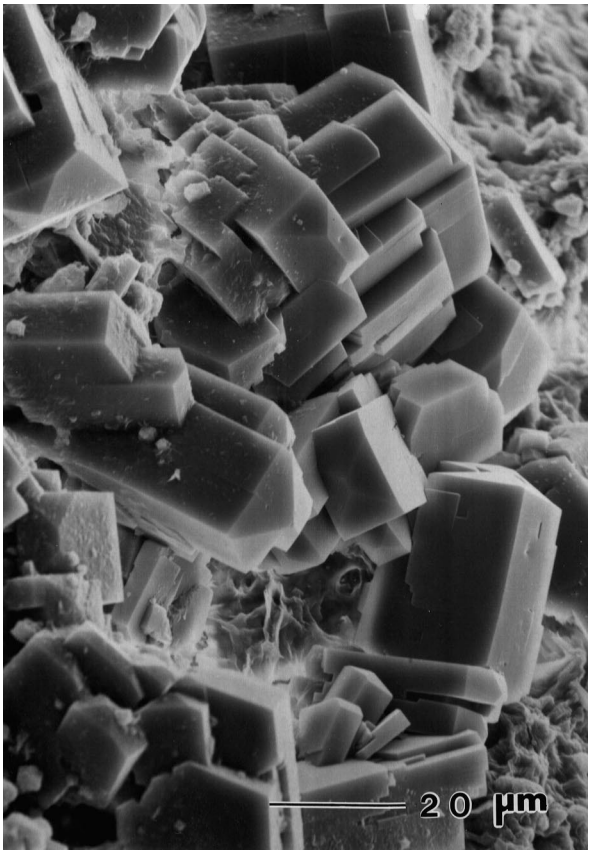

Figure 34.—Scanning electron micrograph of tabular to blocky heulandite crystals from 951.3-m depth in drill core GEO-N5. Associated smectite appears to have been deposited both earlier and later than heulandite.

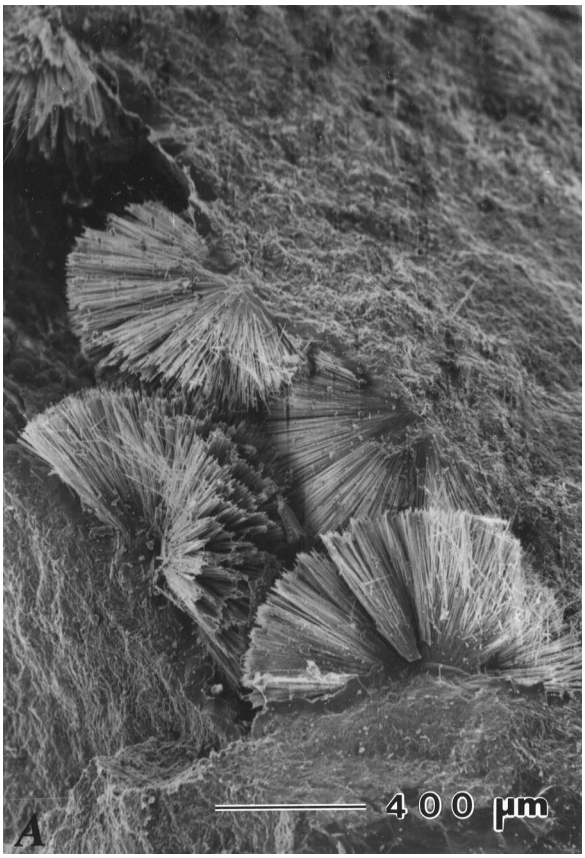

Figure 35.—Scanning electron micrographs of mordenite crystals from Newberry volcano. A, Clusters of radiating fibrous mordenite crystals that partly fill open space in core from 748.4-m depth in GEO-N5 drill hole. B, Vesicle completely lined by short mordenite fibers at 496.2-m depth in USGS-N2 drill core. C, Fibrous and acicular mordenite crystals and later bladed calcite from about 393-m depth in drill cuttings from RDO-1 drill hole.

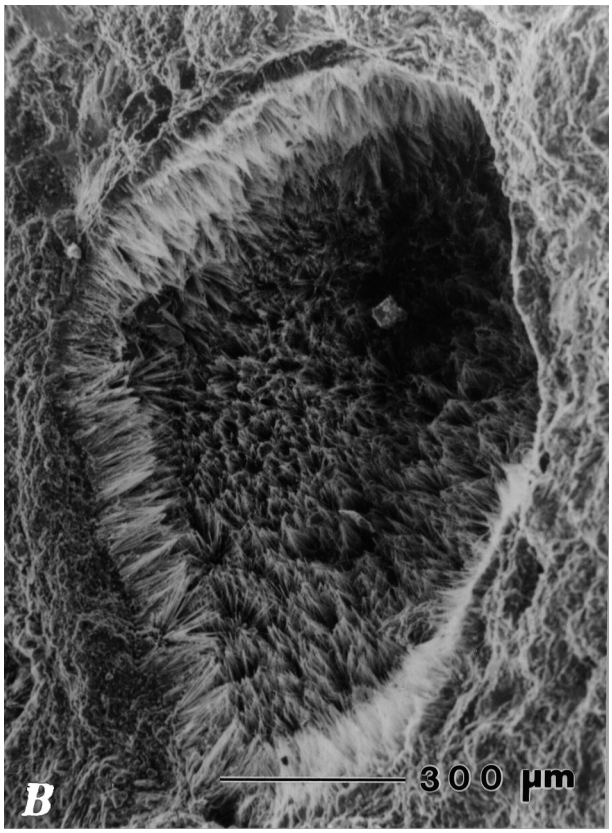

Figure 35.—Continued.

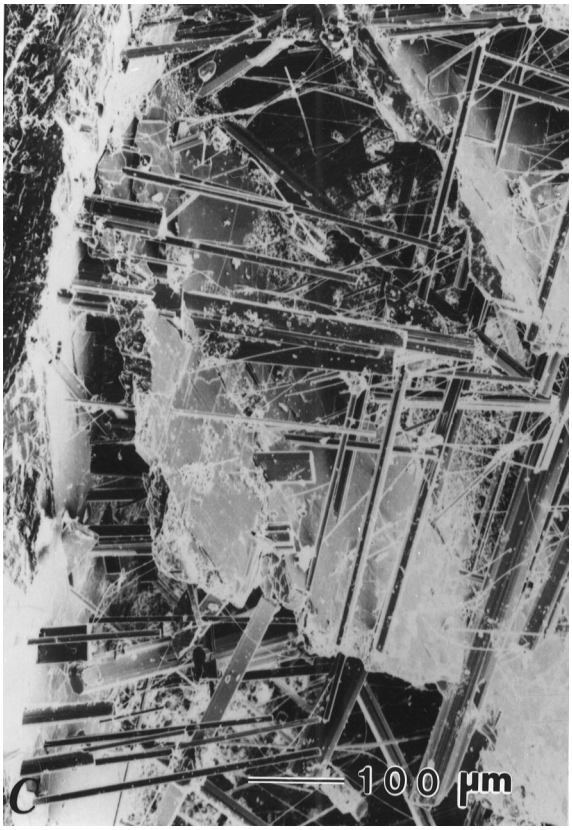

Figure 35.—Continued.

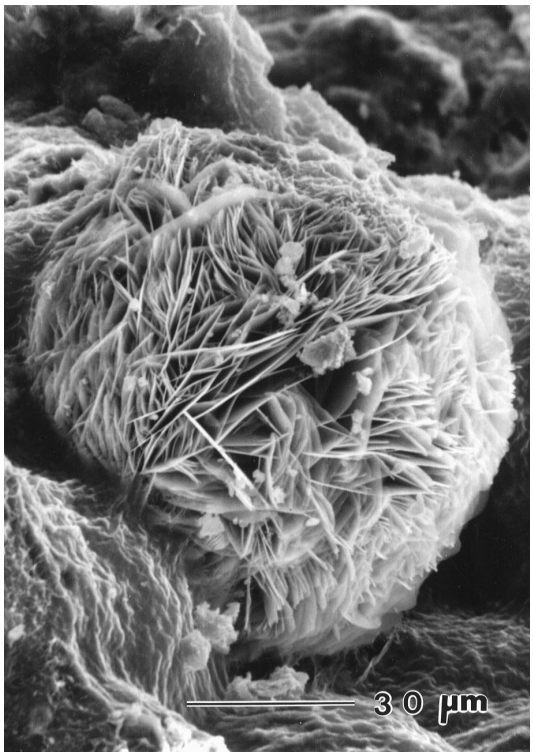

Figure 36.—Scanning electron micrograph of spherical aggregate of platy gyrolite crystals in smectite-altered volcaniclastic sandstone from 318.5-m depth in drill core USGS-N2.

salt cavities in association with zeolite minerals (Heller and Taylor, 1956). Platy okenite crystals have also been reported from a single cavity (temperature ~130˚C) in a rhyolitic drill-core specimen from Yellowstone National Park (Bargar, Beeson, and Keith, 1981).

CARBONATE MINERALS

Every geothermal core hole, both on the flanks of Newberry volcano and within the caldera, contains at least three carbonate minerals that were deposited in vesicles, on fractures, or between breccia fragments. Calcite and siderite are the most abundant of the carbonates; other minerals include aragonite, ankerite-dolomite, kutnohorite, magnesite, and rhodochrosite. Most mineral identifications were made by XRD analyses. XRD identification of carbonate minerals is based on the mineral powder diffraction file of the Joint Committee on Powder Diffraction Standards (JCPDS). No internal standard was used in any of the XRD measurements; however, accuracy of the measurements should be within about ±0.02 Å. The most intense X-ray reflection was found to be significantly different in nearly all the carbonate minerals probably owing to variation in the composition of the minerals. Electron microprobe analyses of several carbonate minerals from the USGS-N2 drill core show considerable vari-

Table 9.—Electron microprobe analyses of carbonate minerals from USGS-N2 drill-core.

[Analysis numbers 4, 5, 7, 11, 13, 15, 16, and 17 contain trace amounts of SiO_2. Analysis number 14 is an average of 6 analyses]

Mineral:	Aragonite	Calcite				Dolomite				Ankerite	Magnesite		Siderite			Ca-, Fe-rhodochrosite	
Depth (m):	305.7	308.4	452.8	716.9					415.1				450.2	565.7	693.7	590.6	
Analysis No.:	1	2	3	4	5	6	7	8	9	10	11	12	13	14	15	16	17
Major-element analyses (weight percent oxides)																	
MgO-----	0.75	0.11	0.52	0.58	1.07	22.36	23.67	16.69	15.98	14.45	41.64	43.68	6.65	5.53	12.12	1.39	0.76
CaO------	53.78	55.11	48.91	46.96	39.68	28.17	26.04	30.78	30.78	31.33	3.76	3.72	8.68	3.95	2.53	8.99	14.21
MnO-----	0.19	0.10	2.19	5.77	8.92	0.17	0.15	0.36	0.41	0.67	0.18	0.00	1.82	3.04	2.02	15.31	28.58
FeO------	0.20	0.17	3.41	3.32	7.57	1.49	2.45	5.84	6.76	8.37	3.12	1.25	40.45	48.14	40.97	32.43	13.78
SrO------	0.06	0.08	0.00	0.02	0.00	0.06	0.05	0.02	0.00	0.06	0.04	0.00	0.00	0.00	0.08	0.00	0.00
BaO------	0.08	0.05	0.02	0.14	0.10	0.13	0.02	0.13	0.03	0.11	0.05	0.00	0.09	0.09	0.13	0.01	0.05
CO_2[1]----	43.31	43.58	42.40	43.35	42.50	47.60	47.90	46.22	45.99	45.96	50.46	51.36	40.00	40.54	41.64	37.93	38.18
Total--	98.37	99.20	97.45	100.27	99.84	99.98	100.28	100.04	99.95	100.95	99.25	100.01	97.69	101.29	99.49	96.06	95.56
Number of atoms on the basis of 6 oxygens																	
Mg--------	0.04	0.01	0.03	0.03	0.06	1.03	1.08	0.79	0.76	0.69	1.80	1.86	0.36	0.30	0.64	0.08	0.04
Ca--------	1.95	1.99	1.81	1.70	1.47	0.93	0.83	1.05	1.05	1.07	0.12	0.11	0.34	0.15	0.10	0.37	0.58
Mn--------	0.01	0.00	0.06	0.17	0.26	0.01	0.00	0.01	0.01	0.02	0.00	0.00	0.06	0.09	0.06	0.50	0.93
Fe--------	0.01	0.00	0.10	0.09	0.22	0.04	0.06	0.16	0.18	0.22	0.08	0.03	1.24	1.45	1.21	1.05	0.44
Sr--------	0.00	0.00	0.00	0.00	0.00	0.00	0.00	0.00	0.00	0.00	0.00	0.00	0.00	0.00	0.00	0.00	0.00
Ba--------	0.00	0.00	0.00	0.00	0.00	0.00	0.00	0.00	0.00	0.00	0.00	0.00	0.00	0.00	0.00	0.00	0.01
C---------	2	2	2	2	2	2	2	2	2	2	2	2	2	2	2	2	2

[1]CO_2 was determined by stoichometric calculation.

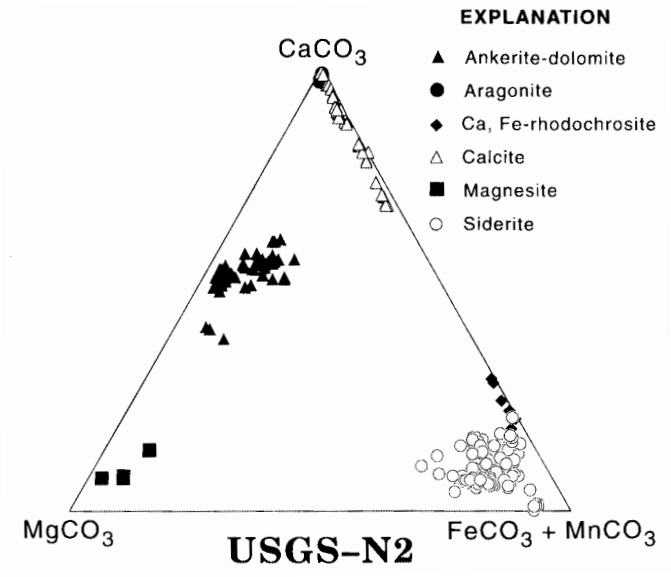

Figure 37.—$CaCO_3$-$MgCO_3$-$FeCO_3$+$MnCO_3$ ternary diagram for electron microprobe analyses of carbonate minerals from USGS-N2 drill core.

ability in the Mg, Ca, Mn, and Fe cation content (table 9 and fig. 37). In fact, two of the carbonate minerals (ankerite and dolomite) were found to be very close both structurally and morphologically and are not readily distinguishable except by their Mg:Fe ratio (Deer, Howie, and Zussman, 1966).

ANKERITE-DOLOMITE

Colorless to white rhombic ankerite-dolomite crystals or massive fillings were deposited in open spaces between breccia fragments, vesicles, or fractures in all seven of the flank drill cores and in the USGS-N2 core hole within the Newberry caldera (figs. 5, 14, 16, 18, 19, 20, 23, and 26). Morphology of the crystalline deposits varies from individual rhombs to disk-shaped (fig. 38), columnar (fig. 39), or hemispherical clusters of rhombic crystals. XRD analyses of these carbonate deposits have a major (104) reflection ranging between about 2.89 Å (dolomite) and 2.90 Å (ankerite) making it difficult to determine which of the two minerals is present from the X-ray analysis. Electron-microprobe analyses of crystals from three samples from the USGS-N2 drill core (table 9, analyses 6-10) indicate that the crystals are inhomogeneous and range from ferroan dolomite to ankerite. The crystals are

slightly Ca-rich in most analyses; however, in three analyses Mg is greater than Ca, and the chemical data plot outside the ankerite-dolomite field (fig. 37). Minor Mn, Sr, and Ba were detected in the electron-microprobe analyses. Trace-element analysis of one sample from USGS-N2 (table 10) also shows the presence of minor Zn, as well as measurable Ce, Co, Ga, and Yb. Measured temperatures at the depths where ankerite-dolomite was found in the drill holes range from <10 to ~150˚C. Dolomite was found in one drill-core sample from Yellowstone National Park at a depth where the measured temperature was 190˚C (T.E.C. Keith, unpub. data, 1991). In some Salton Sea geothermal drill holes, dolomite and ankerite are reported at depths where measured temperatures range from less than 100˚C to more than 200˚C (Muffler and White, 1969) or even as high as about 250˚C (McDowell and Paces, 1985).

ARAGONITE

Aragonite occurs in core samples of three drill holes from the north, east, and south flanks of Newberry volcano (figs. 14, 18, and 19) and is found in both of the intracaldera drill holes (figs. 5 and 12). Colorless acicular (as long as ~2.0 cm) aragonite crystals or fan-shaped aggregates of aragonite crystals were deposited in scattered vesicles and fractures where the measured temperatures are <50˚C. In a few samples, vesicles are completely filled by colorless, massive aragonite; however, white powdery or cauliflower-like aragonite deposits were also verified by XRD analyses. Electron-microprobe analysis of aragonite from one sample in the USGS-N2 drill core (fig. 37 and table 9 analysis 1) suggests minor substitution of Sr, Ba, Mn, Mg, and Fe for Ca in the aragonite structure.

CALCITE

Calcite was found in all of the Newberry drill cores; it usually is the predominant carbonate mineral, but siderite is more abundant in the USGS-N2 and GEO-N4 drill holes. Vesicles, fractures, and open spaces between breccia fragments contain white massive or colorless crystalline calcite deposits. Calcite replaces plagioclase phenocrysts near the bottoms of the GEO-N1 and USGS-N2 drill holes. Crystal morphology of the calcite is variable and ranges from individual thin-bladed crystals (fig. 35C) to equant (fig. 40A) or needle-like crystals (fig. 40B). Some calcite is associated with

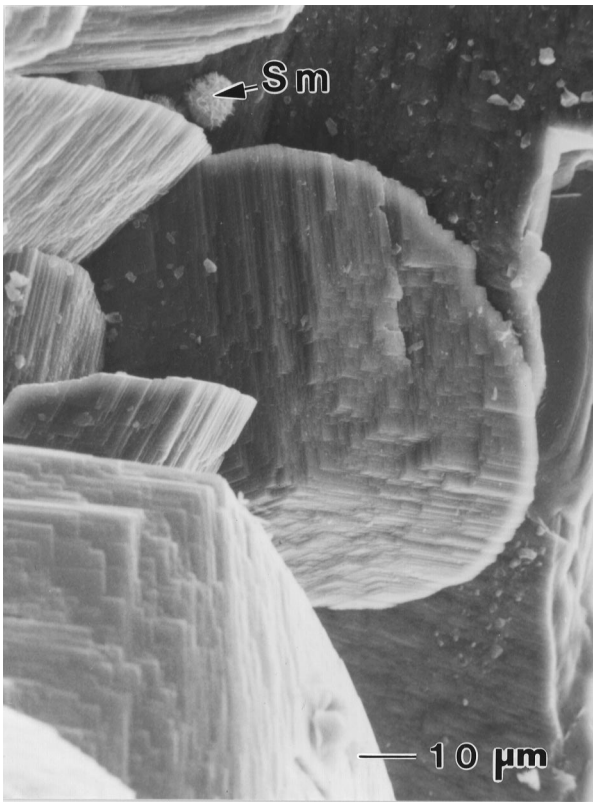

Figure 38.—Scanning electron micrograph of blocky and discoidal aggregates of rhombic ankerite-dolomite crystals and a small spherical cluster of smectite (Sm) crystals from 693.7-m depth in USGS-N2 drill core.

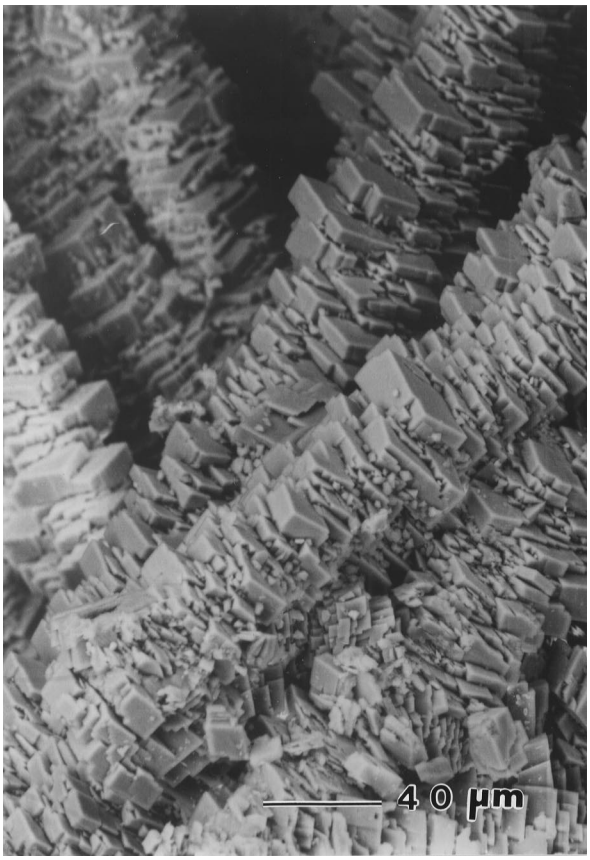

Figure 39.—Scanning electron micrograph of columnar aggregates of rhombic ankerite-dolomite crystals from 841.6-m depth in SF NC72-03 drill core.

Table 10.—Trace element composition (in ppm) of carbonate and sulfide minerals from USGS-N2 drill core.

[Analyses by emission spectroscopy, Analysts: P.H. Brigg and J. Cornell, U.S. Geological Survey, Denver, Colo. –, not determined]

Mineral:	Calcite	Dolomite + ankerite	Siderite	Pyrrhotite	Pyrite
Depth (m):	768.1	415.1	570.0	713.2	930.1
Ag	<2	<2	<2	<2	<2
As	-	-	-	140	930
Ba	3	57	14	-	-
Bi	-	-	-	<10	<10
Cd	<2	<2	5	<2	2
Ce	<4	5	17	<4	13
Co	2	7	9	23	335
Cr	-	-	-	1	12
Cu	-	-	-	3	447
Eu	<2	<2	<2	<2	<2
Ga	<4	6	26	-	-
Gc	-	-	-	-	-
Ho	<4	<4	<4	<4	<4
La	<2	<2	8	<2	6
Mn	793	1,720	22,100	51	129
Mo	-	-	-	<2	<2
Nd	<4	<4	10	<4	5
Ni	-	-	-	<2	74
Pb	<2	<2	14	16	22
Sn	-	-	-	<20	20
Sr	328	123	7	-	-
Ta	-	-	-	<40	<40
Th	<4	<4	4	<4	<4
U	<100	<100	<100	<100	<100
V	-	-	-	5	98
W	-	-	-	-	-
Y	<1	-	-	2	13
Yb	-	1	13	<1	1
Zn	5	47	97	10	242

earlier and later red iron oxide and green (iron-rich?) smectite (fig. 40C); it is surprising that siderite did not form rather than calcite in the presence of abundant iron.

The most intense XRD (104) peak for calcite typically ranges from about 3.02 to 3.05 Å. However, some of the Newberry calcite deposits have their most intense X-ray reflection between 2.99 and 3.01 Å, which indicates that the mineral contains significant manganese (Krieger, 1930; Bargar and Beeson, 1984). In the drill core from USGS-N2, the Mn content appears to increase with increasing depth (table 9 analyses 2-5, and fig. 37); significant Fe and Mg also are present in some of the analyzed samples. The trace elements Ba and Sr occur in minor amounts along with detectable Co and Zn (tables 9 and 10).

KUTNOHORITE

Colorless, white- to light-yellow, botryoidal, acicular, or massive vesicle and fracture fillings in the lower half of the GEO-N1 drill core were identified as kutnohorite (fig. 14). These deposits have a major (104) XRD reflection at about 2.91 to 2.98 Å; the wide range in peak position is a function of Ca or Mg as the predominant cation (Gabrielson and Sundius, 1965; Tsusue, 1967). Kutnohorite has the dolomite structure (Frondel and Bauer, 1955); however, the X-ray peaks that are characteristic of dolomitic structure may be too weak to detect, at least in Ca-kutnohorite (Gabrielson and Sundius, 1965). Consequently, some difficulty occurred in distinguishing between calcite and kutnohorite because abundant manganese in the calcite structure expands the range of positions of the most intense X-ray reflection from ~3.03 Å (typical calcite) to about 2.95 Å (Krieger, 1930). In this study, carbonate minerals were identified as kutnohorite if the most intense X-ray peak ranged between 2.91 and 2.98 Å and as calcite if the reflection occurred from 2.99 to 3.05 Å. Kutnohorite and calcite in the GEO-N1 drill core were not deposited in distinctive zones; instead, the two minerals overlap in their distribution throughout the lower half of the drill hole (fig. 14). In some fractures or vugs, calcite and kutnohorite are found together or are closely associated with one or more additional carbonate minerals (ankerite-dolomite, aragonite, rhodochrosite, or siderite). This distribution suggests that the cation content of the fluids that deposited these carbonate minerals probably varied somewhat with time.

MAGNESITE

Magnesite was found by X-ray diffraction analyses of a few scattered rhyolitic volcaniclastic and tuffaceous samples from 349.3 to 365.2-m depth and between depths of 409.0 and 421.8 m in the USGS-N2 drill core (fig. 5). Magnesite also occurs in vesicles of one sample from near the bottom of the GEO-N3 drill core (fig. 18) and was deposited in vesicles, fractures, and between breccia fragments of a few samples between 876.3- and 961-m depth in the GEO-N2 drill hole (fig. 16). Many of the samples also contain closely associated siderite, ankerite-dolomite, and calcite. According to electron-microprobe analyses (fig. 37 and table 9 analyses 11 and 12) of magnesite from the USGS-N2 drill core, the mineral is not a pure magnesium carbonate; substantial Ca and Fe and minor Mn, Sr, and Ba are present in an analysis of the mineral.

RHODOCHROSITE

Rhodochrosite is a sparse hydrothermal mineral in the drill cores from Newberry volcano. Samples collected from three of the flank drill holes (GEO-N1, GEO-N2, and GEO-N5) (figs. 14, 16, and 20) contain vesicle or fracture fillings of

colorless to light-yellow, bladed, columnar, or botryoidal carbonate deposits that have an intense XRD reflection between 2.82 and 2.86 Å. Closely associated minerals are ankerite-dolomite, kutnohorite, and siderite. Both drill holes within the caldera contain rhodochrosite; caramel-colored botryoidal coatings of clastic fragments at 308- to 311-m depth in samples from the RDO-1 drill hole (fig. 12) were identified by XRD as rhodochrosite. Some disk-shaped and spherical clusters of siderite crystals from the USGS-N2 drill core have a dark, nearly opaque core that is surrounded by concentric rings when viewed in cross section (fig. 41). Two beam scans, ~90° apart, from core to rim across a slabbed surface of a spherical crystal cluster at 590.6-m depth were made with the electron microprobe. The results show that the core is Mn- and Ca-rich (Ca-Fe rhodochrosite) and Fe- and Mg-poor (fig. 42 and table 9 analysis 17). The Mn and Ca content decreases toward the rim, and Mg and Fe increase outward and are most concentrated in the rim.

SIDERITE

All of the Newberry geothermal drill cores (except the RDO-1 drill cuttings) examined for this study contain siderite deposits in vesicles, fractures, and open spaces between breccia fragments. The siderite varies greatly in color from pale yellow to caramel to dark reddish orange, and the color appears to reflect the chemical composition of the mineral. Lighter caramel or pale-yellow siderite crystals have their most intense (104) XRD reflection at about 2.82 Å, corresponding to siderite with high manganese content (Rosenberg, 1963). In darker caramel-colored siderite crystals (Fe-rich), the most intense X-ray reflection occurs between about 2.78 and 2.80 Å.

Morphology of siderite in the Newberry drill cores is varied. Occasionally, massive vesicle fillings or individual rhombic siderite crystals are found; however, siderite more commonly forms randomly oriented disk-shaped aggregates of rhombic crystals (fig. 43A). Just as common are spherical or hemispherical crystal clusters that differ in the size or arrangement of the rhombic crystals (fig. 43B, C, D, and E). Rarely, siderite crystals form unusual shapes such as columns of stacked crystals, fan-shaped crystal aggregates, boomerang-shaped crystal aggregates, crystal aggregates arranged in an open-textured configuration resembling lace, or a rather staghorn-shaped arrangement of clustered siderite

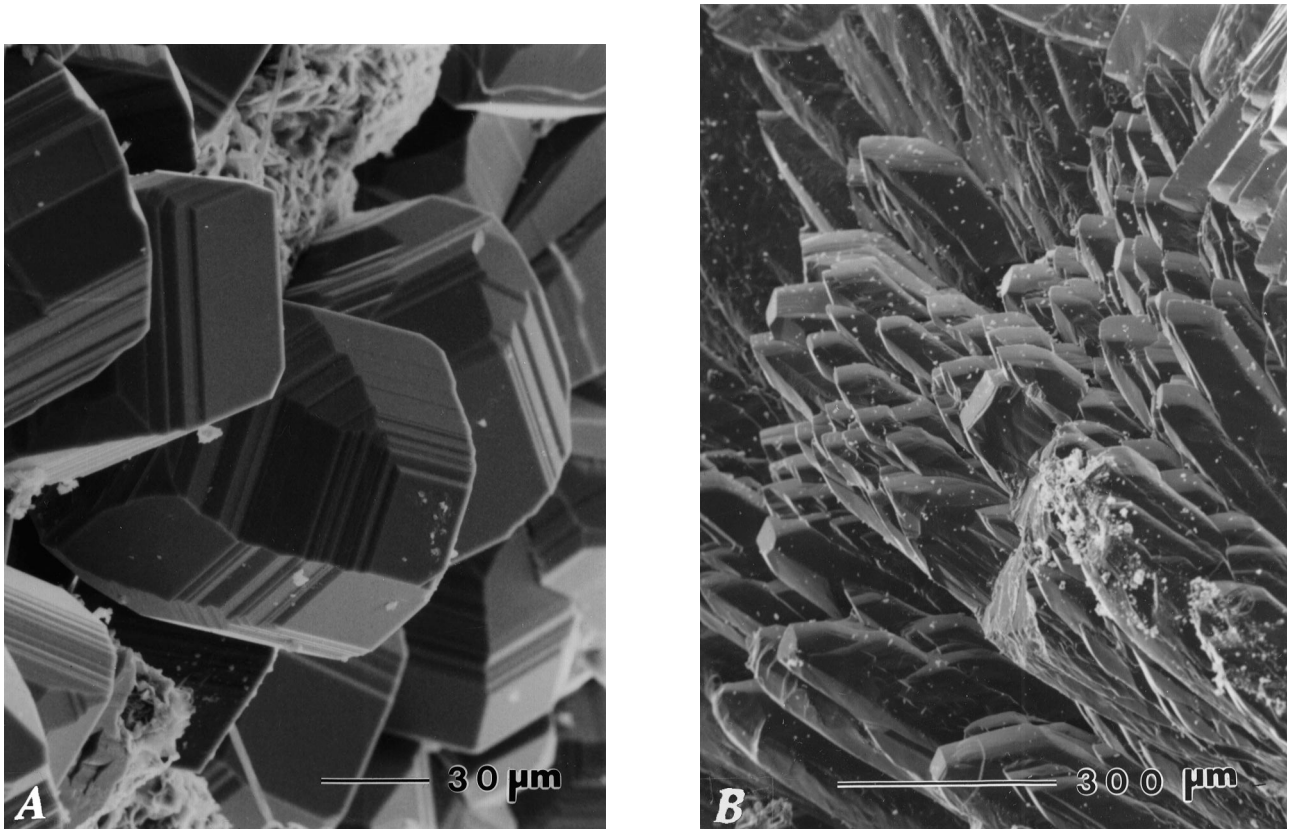

Figure 40.—Scanning electron micrographs and photomicrograph of calcite crystals from Newberry volcano. A, Blocky aggregates of calcite crystals and associated chlorite that line fracture at 847.6-m depth in USGS-N2 drill core. B, Needle-like rhombic calcite crystals from fracture filling in basaltic sandstone at 308.9-m depth in USGS-N2 drill core. C, Photomicrograph of ~1-cm-long vesicle filling of multiple alternating layers of calcite (Cc), green (iron-rich?) smectite (Sm), and red iron oxide (Fe). From 906.8-m depth in drill core SF NC-01.

crystals (fig. 43F). XRD analyses of some of the exotically shaped deposits indicate that the predominant mineral is siderite; however, other carbonate minerals such as ankerite-dolomite, kutnohorite, and magnesite also are locally present. A group of concentric rings on a fracture surface (fig. 43G) consists of alternating dark layers of siderite and lighter layers of calcite or aragonite that react with HCl. Similar concentric rings or hemispherical shells of carbonate deposits in other drill cores sometimes have a core of clay or even black magnetite or reddish iron oxide.

There is considerable inhomogeneity of Mg, Ca, Mn, and Fe contents in individual siderite crystals and crystal clusters (fig. 37 and table 9 analyses 13-16). Some siderite crystals contain substantial Sr and Ba. Trace-element analysis of a siderite sample from 570.0-m depth in drill core USGS-N2 (table 10) also showed small amounts of Cd, Ce, Co, Ga, La, Nd, Pb, Th, Yb, and Zn.

CLAY MINERALS

KAOLINITE AND HALLOYSITE

Halloysite and smectite were identified by XRD from an ash-flow tuff core sample at 950-m depth in the GEO-N1 drill hole (Wright and Nielson, 1986). A peach-colored tuffaceous deposit that is completely altered to halloysite was

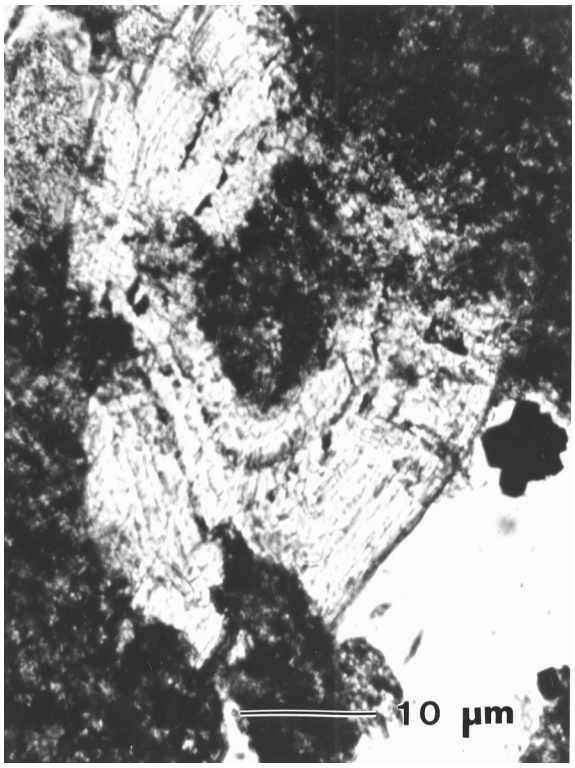

Figure 41.—Cross section of discoidal aggregate of siderite crystals from 659.9-m depth in USGS-N2 drill core. Core of crystal aggregate is rich in Mn and Ca (Ca-Fe rhodochrosite); Mg and Fe content increases progressively away from core toward rim.

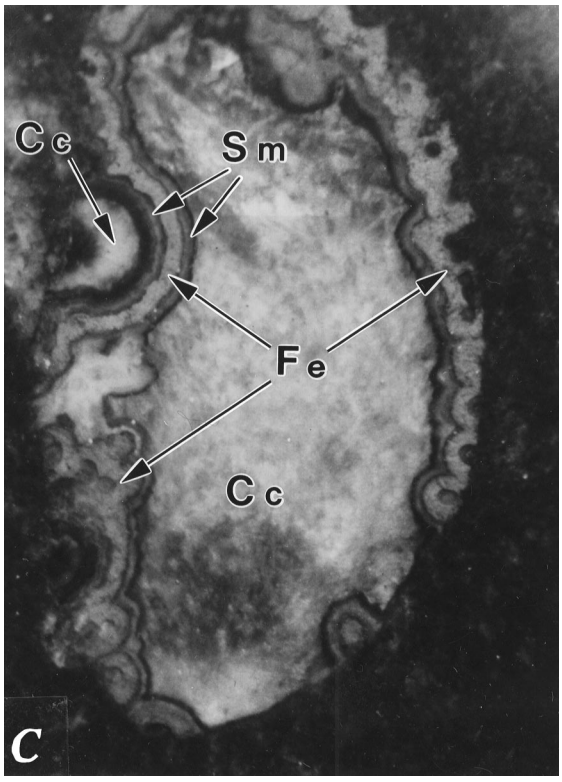

Figure 40.—Continued.

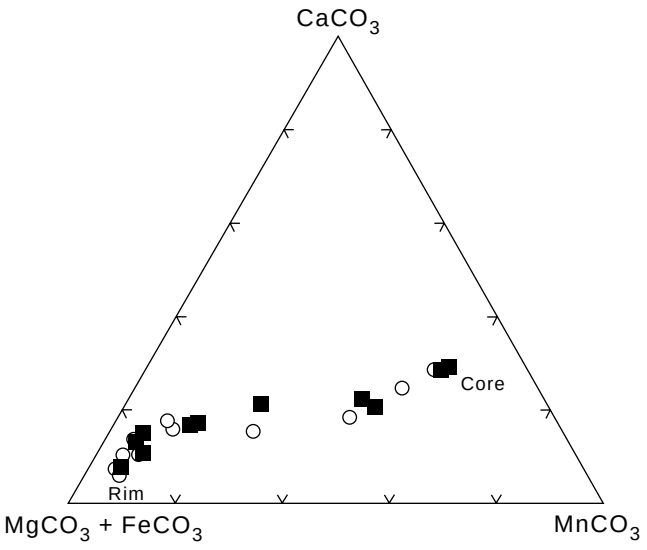

Figure 42.—$CaCO_3$-$MgCO_3$+$FeCO_3$-$MnCO_3$ ternary diagram for electron microprobe analyses of discoidal siderite crystal aggregate from 590.6-m depth in USGS N-2 drill core. Two traverses, represented by solid squares and open circles, were made 90˚ apart from core to rim of crystal aggregate.

found at 583.1- to 586.0-m depth in core hole GEO-N5 (fig. 20). The only other kaolinite-group mineral (~7Å XRD peak that is destroyed by heating at 550˚C for 1/2 hour, Starkey, Blackmon, and Hauff, 1984) found in the Newberry drill cores occurs in basalt vesicle fillings at 1,148.0-m depth in drill core GEO-N3 (fig. 18) where magnetite, smectite, kaolinite, siderite, and calcite (in order of formation) were identified in XRD analyses. Measured temperatures at the depths where kaolinite-group minerals were identified in all three drill holes are less than 50˚C. The origin of these scarce kaolin deposits from the flanks of Newberry volcano is uncertain; however, several sulfate minerals were deposited at a little shallower depth than kaolinite in the GEO-N3 drill core, and nearby drill-core samples contain pyrite. Possibly local acidic conditions were created by the oxidation of pyrite (Steiner, 1977) in rock adjacent to the drill-core sample. If so, the acidic conditions must have been very brief because siderite was deposited somewhat later than the kaolinite. Wright and Nielson (1986) suggest that the GEO-N1 ash-flow tuff alteration may result when extrusive volcanic material interacts with local ground water or geothermal water; if so, the formation temperature undoubtedly was much higher than the measured temperatures.

SMECTITE

Smectite is the most abundant clay mineral in all of the Newberry drill holes; white-yellow, blue-green, brown-black, massive to crystalline clay deposits coat open spaces of vesicles and fractures, fill voids between breccia fragments, and replace glass in tuffaceous samples and the matrix of lava flows. Paragenetic relations between smectite and other hydrothermal minerals frequently show more than one generation of smectite deposition. Detailed XRD studies of smectite show (001) basal reflections that range from poorly crystalline (low broad X-ray peaks) to well-crystallized with sharp (001) X-ray peaks that generally fall within the range from ~13 to 16 Å; the basal spacing expands to between ~16 and 18 Å after exposure to ethylene glycol vapors at 60˚C for 1 hour and contracts to ~10 Å after heating at 550°C for 30

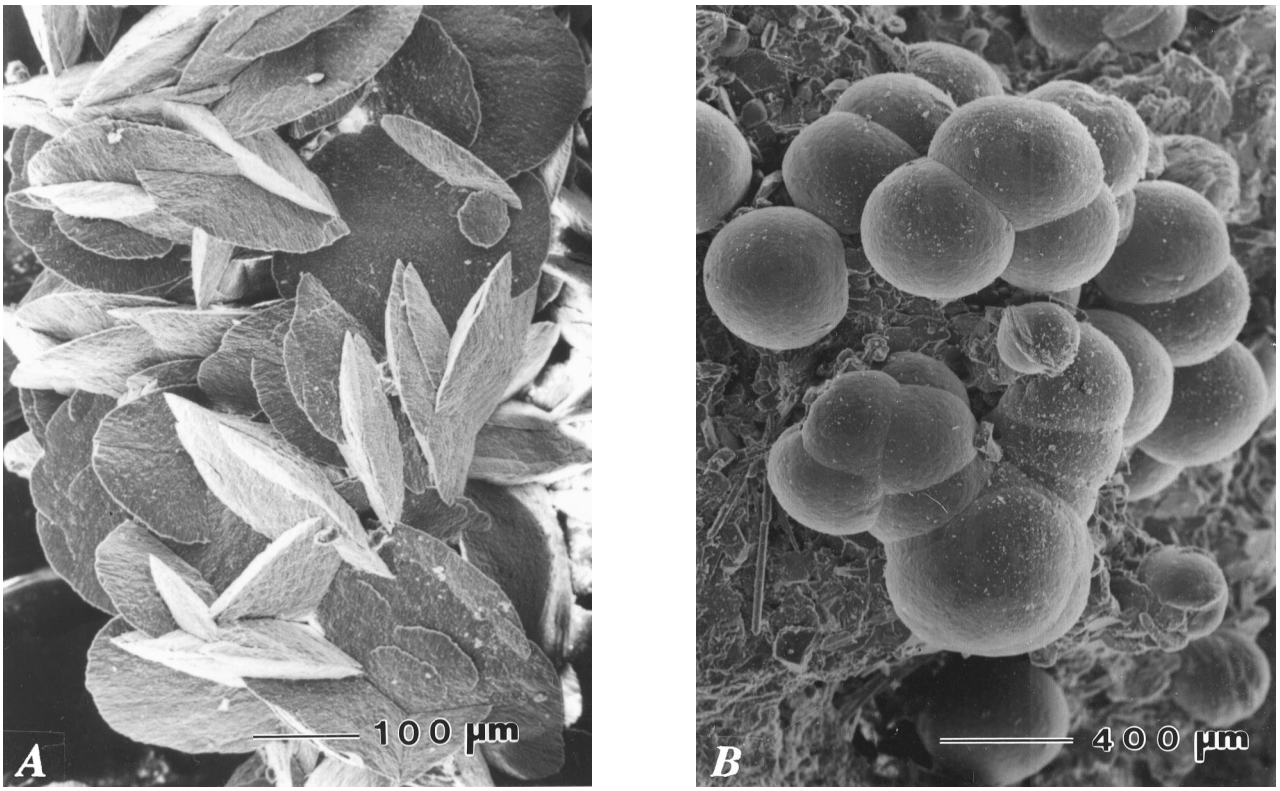

Figure 43.—Scanning electron micrographs and photograph of siderite morphologies at Newberry volcano. A, Cluster of discoidal aggregates of siderite crystals coating fracture at 565.7-m depth in drill core USGS-N2. B, Cluster of spherical aggregates of siderite crystals deposited on vapor-phase parting at 603.2-m depth in drill core GEO-N4. Very tiny individual crystals are not discernible at this scale. C, Spherical aggregates of rhombic siderite crystals from 1,291.7-m depth in GEO-N3 drill core. Small parts of overlapping rhombic siderite crystals can be distinguished. Areas between some spherical siderite crystal clusters contain scattered individual rhombic siderite crystals. D, Roughly spherical aggregates of rhombic siderite crystals from depth of 690.2 m in GEO-N4 drill core. E, Rosette of rhombic siderite crystals filling part of vesicle at 1,296.6-m depth in drill core GEO-N1. F, Branching aggregate of siderite crystals that resembles antler or staghorn from 987.9-m depth in drill core GEO-N5. G, Photograph showing group of concentric rings deposited on fracture surface at 648.9-m depth in drill core GEO-N4. Rings consist of alternating dark siderite and light calcite or aragonite (reacts with HCl).

Figure 43.—Continued.

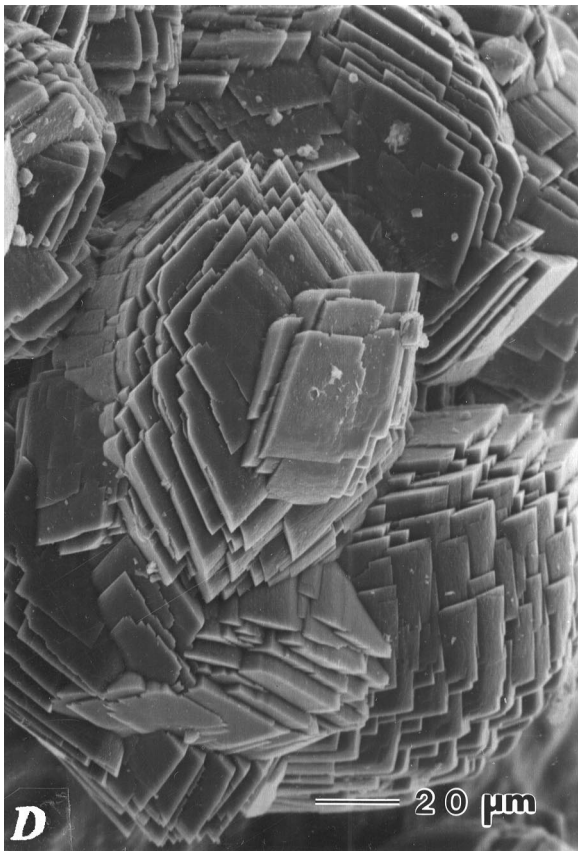

Figure 43.—Continued.

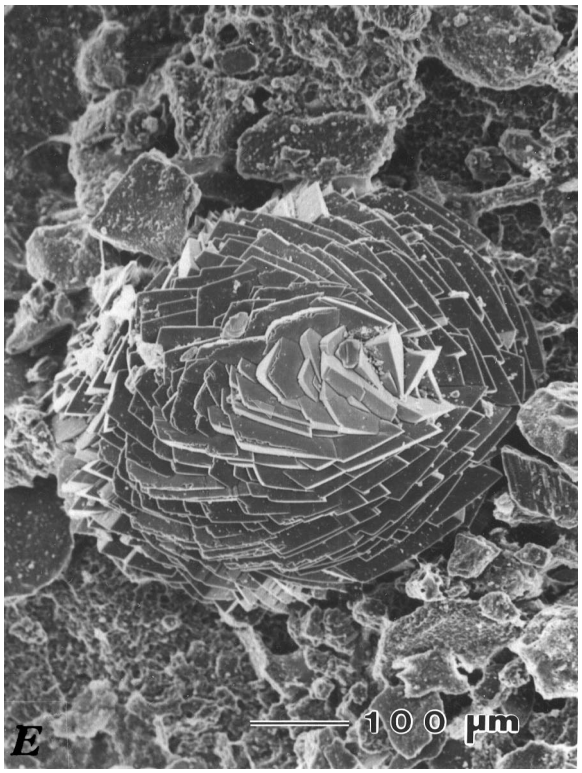

Figure 43.—Continued.

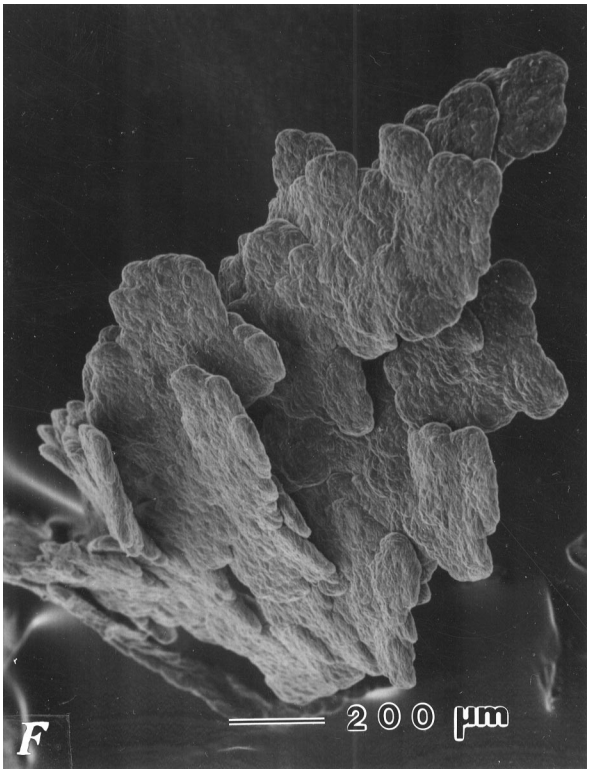

Figure 43.—Continued.

minutes. The range of unglycolated (001) basal reflections suggests that there is some variation in the exchangeable cations (Grim, 1968). Semiquantitative chemical analyses of several clay samples by EDS shows the presence of Si, Al, and Fe in all the samples analyzed; Ti, Mg, Ca, Na, and K are also present in one or more of the analyzed clays. The mean index of refraction for one of the green Fe-rich clay samples, ~1.58 to 1.59, suggests that the smectite species probably is nontronite. Crystal habit generally takes the form of randomly oriented, open-textured, sheet-like or platy crystals (fig. 44A) or densely packed platy crystals (fig. 44B). However, green smectite (identified by XRD) vesicle fillings in one sample from the GEO-N2 drill core have a fuzzy or fibrous surface coating (fig. 44C). According to Phillips and Griffen (1981), nontronite may sometimes have a fibrous crystal habit.

MIXED-LAYER ILLITE-SMECTITE

Light-green and white mixed-layer illite-smectite was identified as fillings between breccia fragments and as an alteration product of phenocryst plagioclase in a narrow, very altered breccia zone at depths of 793.5 and 795.5 m in drill core USGS-N2 (fig. 5). XRD data for two samples show a $(001)_I/(001)_S$ spacing of ~10.7 Å that contracts to ~9.7 Å (smectite peak not seen) after exposure to ethylene glycol for 1 hour at 60˚C. These two samples appear to be randomly interstratified illite-smectite (Hower, 1981). A third sample has a peak at ~11.4 Å that splits into ~16.4 and ~9.0 Å peaks after glycolation and is probably an allevardite-ordered interstratified illite-smectite (Hower, 1981). All three samples appear to have about 80 to 90 percent illite layers (Hower, 1981; Horton, 1985). According to data given in Horton (1985), these mixed-layer clays could have formed very near the present measured temperature of about 180˚C.

Three of the flank drill cores contain mixed-layer illite-smectite deposits. A low, broad, asymmetrical, XRD reflection at about 10.8 Å, which separates into two reflections at about 9.8 and 12.0 Å following glycolation, was seen for a single sample at 1,219.0-m depth in the GEO-N3 drill core (fig. 18). The mineral is tentatively identified as an allevardite-ordered mixed-layer illite-smectite (Hower, 1981). It is associated with a 0.5-cm-wide vertical glassy dike(?) that is mostly altered to magnetite, hematite, pyrite(?), siderite, and gray-green mixed-layer illite-smectite. A blue-green clay deposit on a vapor-phase cavity containing tridymite crystals at 785.2-m depth in drill core GEO-N5 (fig. 20) has a ~11.5 Å peak that splits into ~17 and ~9.7 Å peaks following glycolation and is a randomly interstratified mixed-layer illite-smectite (Hower, 1981). Both the GEO-N3 and GEO-N5 clay deposits occur at depths where the measured temperatures are <60˚C. One sample is associated with vapor-phase mineralization and the second with a narrow glassy dike; both samples probably are deuteric and formed during cooling of the lava flow or intrusion at temperatures that were considerably higher than the measured temperatures. In drill core SF NC-01, a light-green fracture filling from 1,090.3-m depth and white vesicle fillings at 1,164.0-m depth (fig. 23) have XRD peaks at about 12 to 13 Å that split into two peaks at ~13 to 14 Å and at 9.5 to 9.7 Å, respectively, after glycolation. The measured temperature at the depths where the two SF NC-01 allevardite-ordered mixed-layer illite-smectite (about 65-80 percent illite, Hower, 1981) clay samples were deposited is about 150˚C. According to Horton (1985, fig. 9), mixed-layer illite-smectite with about the same illite component occurs in other geothermal areas at about the same temperature.

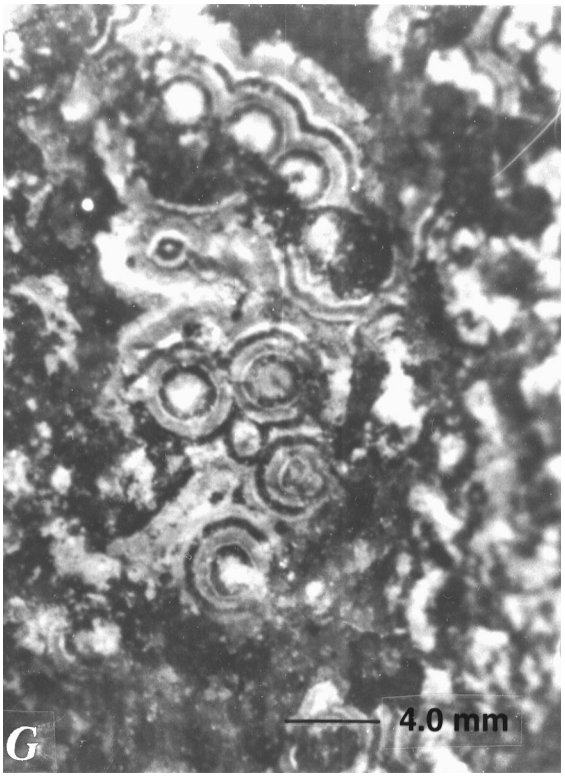

Figure 43.—Continued.

ILLITE

Light-green illite (mean index of refraction ~1.55-1.56), a mica-clay mineral showing no change in the 10 Å XRD peak following glycolation (Grim, 1968), is mostly confined to breccia zones at depths of 752.1 to 761.4 m, 772.4 m, 907.8 to 908.8 m, and 930.1 to 931.8 m in the intracaldera USGS-N2 drill core (fig. 5). Measured temperatures at these depths ranged between about 150 and 265˚C. An EDS semiquantitative chemical analysis of illite from 907.8 m shows the presence of Si, Al, Fe, and K. XRD analyses of lithic tuffs, lava-flow vesicle fillings, and fracture fillings from depths of 310.0 to 362.0 m, 568.1 to 568.5 m, and 789.0 m in drill core GEO-N1 (fig. 14) show that white, yellow, orange, and greenish-brown clay alteration has a very low, broad ~10

Å peak. The basal (001) peak does not shift when the sample is glycolated, indicating that the mineral is illite. Measured temperatures at these depths in the GEO-N1 drill hole are <10˚C; illite undoubtedly did not form at such low temperatures. Wright and Nielson (1986) attributed the formation of halloysite at depths of 948.8 to 951.0 m in this drill hole to the interaction of cooling volcanic deposits and meteoric water. Probably, the illite formed similarly before the extrusive volcanic rocks cooled to the measured drill-hole temperatures.

MIXED-LAYER CHLORITE-SMECTITE

Scattered samples, below 742.5-m depth in drill core USGS-N2 contain green mixed-layer chlorite-smectite or corrensite (fig. 5). Ordered interstratified chlorite-smectite is found lining fractures, filling vesicles, and replacing interstitial glass in andesite and basalt. Mixed-layer chlorite-smectite has a sheet-like morphology and occurs as rosettes of platy crystals at 915.2-m depth (fig. 45A). XRD analyses show that ordered interstratified chlorite-smectites from this intracaldera drill core contain higher order 28 to 29 Å X-ray reflections in addition to 14 and 7 Å reflections that exhibit a slight expansion with glycolation (Hower, 1981). From the X-ray data, this clay mineral appears to contain random proportions of

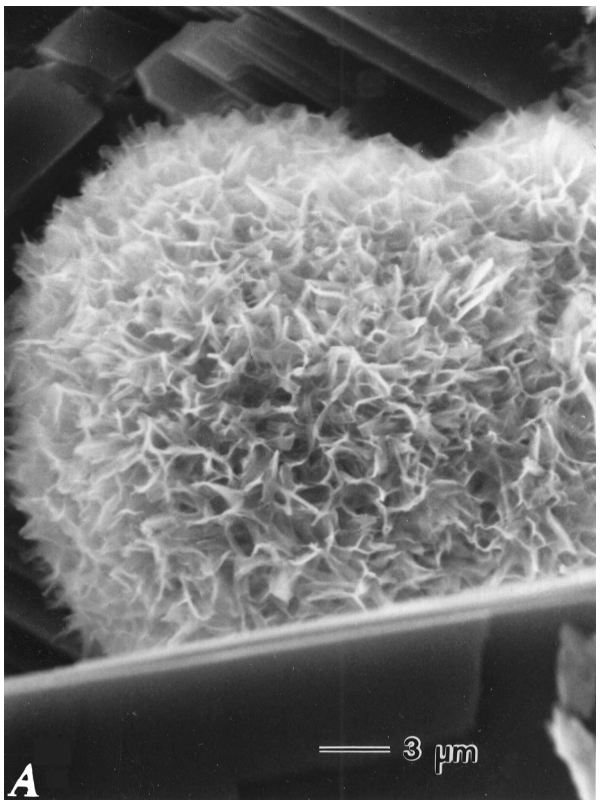

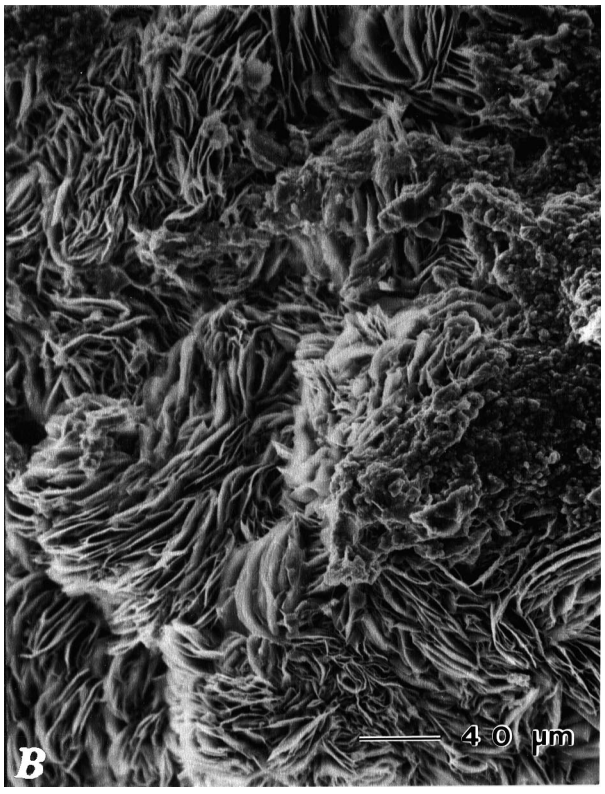

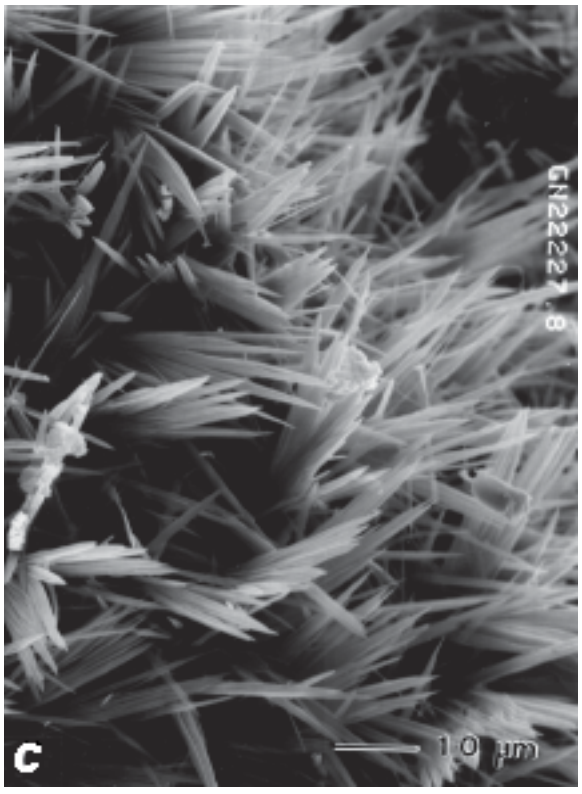

Figure 44.—Scanning electron micrographs of smectite morphologies at Newberry volcano. A, Open-textured spherical aggregate of randomly oriented sheet-like smectite crystals deposited on dolomite-ankerite crystals in open space between breccia fragments at 690.4-m depth in USGS-N2 drill core. B, Vesicle filling of closely spaced dark-green platy smectite crystals from 884.5-m depth in SF NC-01 drill core. C, Olive-green fibrous smectite crystals filling vesicle at 679.0-m depth in GEO-N2 drill core.

chlorite and smectite with no discernible pattern. Electron microprobe analyses of mixed-layer chlorite-smectite from 916.7-m depth (table 11 analyses 10-17) show that the mineral is very rich in Mg and would plot in the talc-chlorite field of the Si vs. Fe/Fe+Mg diagram of Hey (1954, p. 280).

Mixed-layer chlorite-smectite was identified in the lower 200 to 400 m of the three higher temperature (measured temperatures between ~110 and 160˚C) drill holes (GEO-N2, SF NC-01, and SF NC72-03) on the west flank of Newberry volcano (figs. 16, 23, and 26). Vesicles, fractures, and open spaces between breccia fragments are coated with mostly light- to dark-green clay that sometimes has a waxy, botryoidal, or wormy (fig. 45B) texture. EDS semiquantitative chemical analysis of several of the mixed-layer clay deposits generally show Mg, Al, Si, Fe, and variable amounts of Ca. Most of the analyses suggest that Mg content is somewhat greater than Fe; however, one white clay deposit at 1,342.0-m depth in drill core SF NC72-03 (fig. 26) contains Mg, Al, Si, K, Ca, and Fe, with Mg being much more abundant than Fe. All of the mixed-layer chlorite-smectite deposits appear to be well crystallized and have very sharp (001) and (002) XRD peaks at an average of about 14.7 and 7.3 Å that show slight expansion to about 15.3 and 7.5 Å following exposure to ethylene glycol at 60˚C for 1 hour. One sample also has a first-order peak at 29.9 Å, which expands to about 32.4 Å after glycolation and is characteristic of corrensite (Bailey, 1982). Heating to 400˚C for 1/2 hour causes slight contraction of the (001) peak to about 14.0 Å. Hydrothermally altered basaltic rocks in drill holes from the Reykjanes, Iceland, geothermal area contain mixed-layer chlorite-smectite and swelling chlorite that formed between temperatures of 200˚ and 270˚C (Kristmannsdóttir, 1976). Kristmannsdóttir subdivided these interstratified clay minerals into 5 different swelling chlorites and mixed-layer chlorite-smectite. In the present study, several differences were noted for the behavior of the (001) X-ray peak with various treatments, but no systematic study or attempts at subdivision were made.

CHLORITE

Dark-green chlorite precipitated in open spaces and in altered pumiceous to lithic tuff in drill-hole samples between depths of 357 and 424 m in the RDO-1 drill core (fig. 12). At 390-m depth, open-space botryoidal clusters of randomly oriented sheet-like chlorite formed later than calcite. Chlorite appears to be the latest hydrothermal mineral deposited in

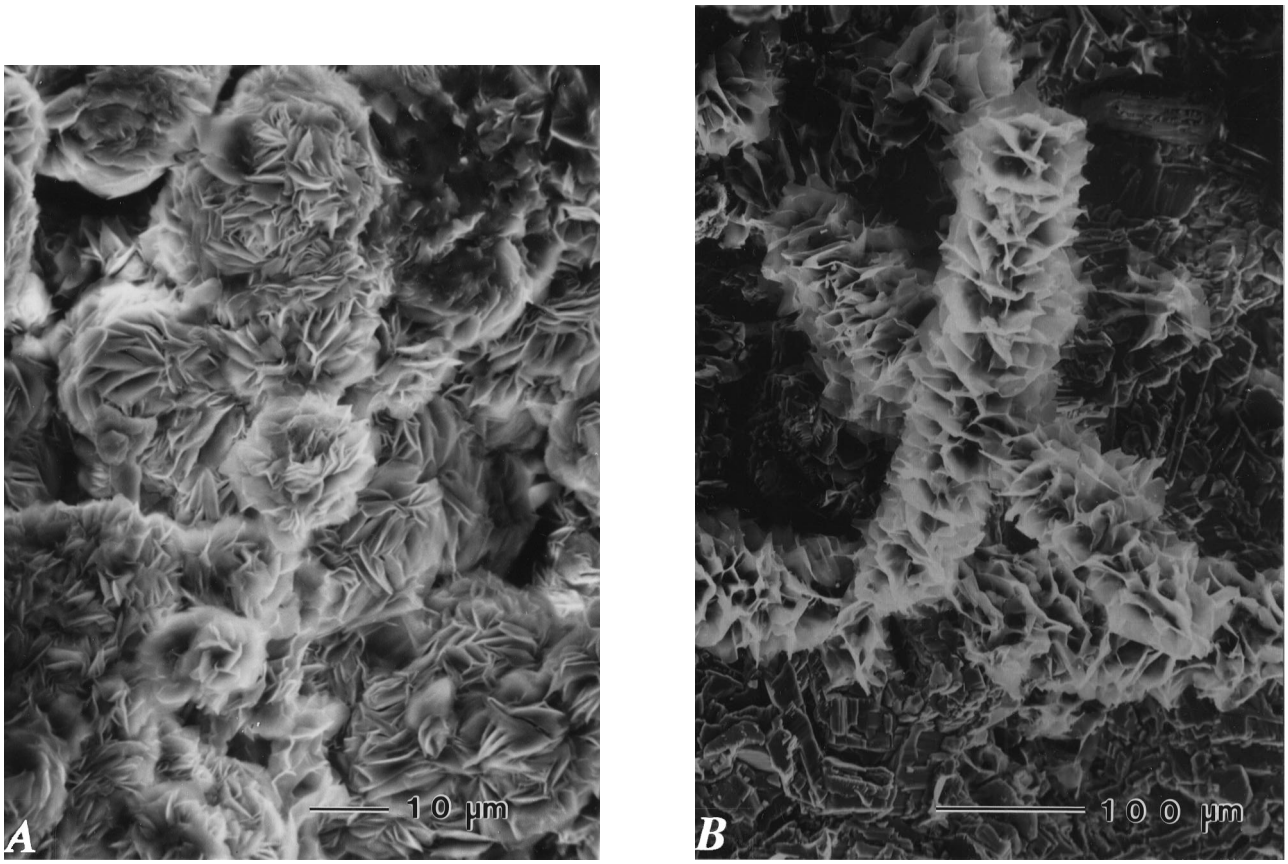

Figure 45.—Scanning electron micrographs of two mixed-layer chlorite-smectite forms at Newberry volcano. A, Rosettes of platy mixed-layer chlorite-smectite crystalline aggregates that coat fracture at 915.2-m depth in USGS-N2 drill core. B, Wormy-textured clusters of mixed-layer chlorite-smectite crystals deposited on calcite in cavity at 1,140.9-m depth in SF NC72-03 drill core.

the RDO-1 drill-hole specimens. The measured temperature for the upper part of the chlorite zone is a little more than 160˚C (fig. 12). Chlorite identified by XRD at depths of 308.9 m, 448.7 to 477.2 m, and below 707.4 m in the USGS-N2 drill core (fig. 5) is primarily an open-space deposit on fractures and in vesicles; it occurs mostly as randomly oriented subhedral platy crystals, rosettes of radiating sheet-like crystals (fig. 46A), or books of euhedral hexagonal platelets (fig. 46B). Electron-microprobe analyses of chlorite from 930.0-m depth (table 11, analyses 1-9) show that it would plot in the pycnochlorite field of a Si vs. Fe/Fe+Mg diagram (Hey, 1954, p. 280). Chlorite, swelling chlorite, and randomly mixed-layer chlorite-smectite have been described in Iceland's Reykjanes geothermal area at temperatures of 200 to 260˚C (Kristmannsdóttir, 1976). In the USGS-N2 drill core, there appears to be a progression of smectite to randomly interstratified chlorite-smectite to ordered interstratified chlorite-smectite to chlorite over the measured temperature range of about 150 to 265˚C (fig. 5).

Chlorite was only identified as fracture coatings, vesicle fillings, and fillings between breccia fragments in the three west-flank drill cores (GEO-N2, SF NC-01, and SF NC72-03) that also contain mixed-layer chlorite-smectite; it also was found as altered mafic minerals in one sample from the SF NC72-03 drill core (fig. 26) . Most of the chlorite deposits consist of randomly oriented platy crystals, but spaces between breccia fragments at 1,120.4-m depth in the SF NC-01 drill core (fig. 23) are partly filled by a matte of intergrown wormy clusters (about 2 mm in length) of sheetlike crystals (fig. 46C; see also fig. 45B). The green clay mineral has (001) and (002) XRD reflections at about 14 and 7 Å that do not expand with glycolation and are not appreciably affected by heating to 400˚C for 1/2 hour. Measured temperatures at the depths where chlorite was found in the west-flank drill holes range between about 140 and 160˚C (figs. 16, 23, and 26); these temperatures correspond well with the minimum temperature for chlorite in the lower part of the USGS-N2 drill core (fig. 5).

SILICA MINERALS

Drill cores from within Newberry caldera and on the flanks of the volcano contain silica minerals that span the range of crystallinity from noncrystalline opal to poorly crystallized cristobalite (XRD peak at 4.11 Å) to better ordered cristobalite (XRD peak at 4.04 Å) to chalcedony—a cryptocrystalline variety of quartz—to well-crystallized quartz. Geothermal drill holes in Yellowstone National Park show the same depositional sequence of silica minerals (Keith, White, and Beeson, 1978). The solubilities of these silica minerals at various temperatures, and indications that the less well-crystallized silica phases can be converted to better-crystallized silica minerals through solid-state recrystallization as in the conversion from opal to cristobalite or from poorly ordered cristobalite to well-ordered cristobalite, are discussed by (Keith, White, and Beeson, 1978). However, solution and redeposition are thought to be required in converting chalcedony to quartz and in the formation of chalcedony from cristobalite (Murata and Larson, 1975). Several silica samples in the Newberry drill cores consist of both chalcedony and cristobalite in XRD analyses. These deposits appear to consist of chalcedony that is enveloped by cristobalite and may result from changing physical or chemical conditions during silica deposition.

OPAL

A few scattered fractures between 554.1- and 641.9-m depth in drill core USGS-N2 (fig. 5) are lined by white powdery to granular, massive orange, or white to colorless botryoidal (fig. 47) noncrystalline opal (isotropic, index of refraction = ~1.46). EDS chemical analysis on the SEM shows only Si. A fracture at 354.0-m depth in the GEO-N4 drill hole (fig. 19) on the east flank of Newberry volcano contains a colorless to frosted botryoidal silica coating that is isotropic and has an index of refraction <1.46; however, a few of the silica fragments viewed in oils have an index of refraction >1.46 and a spotty low-order birefringence that might indicate partial conversion to cristobalite. At 277-m depth in core hole SF NC-01 (fig. 23), a fracture is coated by as much as ~2.5 mm of colorless to dark-brown, massive to botryoidal isotropic silica with an index of refraction <1.47. Gray and cream-colored amorphous clay is a later deposit in the fracture; both the opal and clay fracture coatings contain disseminated, yellowish, cubic and pyritohedral metallic pyrite crystals (see fig. 24). XRD analysis of one white fracture coating at 322.2-m depth in the GEO-N1 drill core (fig. 14) indicates that the material is amorphous and probably consists of opal. Similar, white to light-yellow-green, thin fracture and cavity coatings of three other core samples in the upper part of the GEO-N1 drill core also appear to be opal.

CRISTOBALITE

Colorless to white botryoidal cristobalite (index of refraction = ~1.47, weak birefringence) coats a few fractures from depths of 556.0 to 563.1 m and 700.4 to 725.1 m in the USGS-N2 drill core (fig. 5). XRD analyses of several samples also show the presence of peaks for quartz or cryptocrystalline chalcedony, but none was observed in refractive-index oils.

Cristobalite was identified in six of the flank drill cores (all except GEO-N4). In core hole GEO-N1 (fig. 14), several cavities in samples from depths of 1,124 to 1,172 m, open spaces of two breccia samples at 1,301.3- and 1,339.6-m depth, and a fracture filling at 1,363.4-m depth are partly coated by bluish botryoidal cristobalite. A massive, 2- to 3-mm-thick green fracture filling at 1,178-m depth consists of cristobalite in XRD analysis. Cristobalite also was identified in an X-ray trace of a soft, spongy-clayey, fracture filling at 1,185-m depth.

Table 11.—Electron microprobe analyses of phyllosilicate minerals from USGS-N2 drill core.

Mineral:	Chlorite									Mixed-layer chlorite-smectite							
Depth (m):	930.0									916.7							
Analysis No.:	1	2	3	4	5	6	7	8	9	10	11	12	13	14	15	16	17
Major-element analyses (weight percent oxides)																	
SiO_2	28.05	29.10	28.41	28.15	29.16	28.67	29.19	29.00	28.68	34.24	34.97	37.49	35.01	35.95	35.26	36.11	34.90
Al_2O_3	19.19	17.74	18.43	18.67	18.04	18.26	18.69	18.10	18.38	12.90	13.12	11.78	13.07	12.59	13.06	13.07	12.86
TiO_2	0.02	0.02	0.04	0.01	0.00	0.01	0.71	0.00	0.00	0.00	0.02	0.01	0.00	0.00	0.00	0.00	0.04
FeO	22.74	21.88	20.97	21.12	21.19	21.60	21.38	21.29	21.68	10.15	10.82	10.55	10.35	10.49	10.60	10.55	10.42
MgO	15.62	17.53	16.86	16.94	17.57	17.09	17.22	17.16	16.71	23.35	23.49	23.02	23.73	23.71	23.72	23.96	23.16
MnO	0.57	0.51	0.47	0.56	0.51	0.51	0.48	0.49	0.52	0.36	0.45	0.54	0.36	0.35	0.37	0.38	0.33
CaO	0.10	0.15	0.09	0.07	0.10	0.17	0.10	0.12	0.10	1.07	1.26	2.30	1.19	1.33	1.15	1.46	1.37
Total	86.29	86.93	85.27	85.52	86.57	86.31	87.77	86.16	86.07	82.07	84.13	85.69	83.71	84.42	84.16	85.53	83.08
Number of atoms on the basis of 28 oxygens																	
Si	5.91	6.05	6.00	5.94	6.06	6.00	5.99	6.06	6.02	7.05	7.05	7.40	7.07	7.19	7.08	7.13	7.10
Al_{IV}	2.09	1.95	2.00	2.06	1.94	2.00	2.01	1.94	1.98	0.95	0.95	0.60	0.93	0.81	0.92	0.87	0.90
Al_{VI}	2.67	2.40	2.58	2.58	2.48	2.51	2.50	2.52	2.56	2.18	2.16	2.14	2.18	2.16	2.18	2.18	2.19
Ti	0.00	0.04	0.01	0.00	0.00	0.00	0.11	0.00	0.00	0.00	0.00	0.00	0.00	0.00	0.00	0.00	0.01
Fe	4.01	3.81	3.70	3.73	3.68	3.78	3.67	3.72	3.81	1.75	1.82	1.74	1.75	1.76	1.78	1.74	1.77
Mg	4.90	5.44	5.31	5.32	5.45	5.33	5.26	5.35	5.23	7.17	7.06	6.77	7.14	7.07	7.10	7.05	7.03
Mn	0.10	0.09	0.09	0.10	0.09	0.09	0.08	0.09	0.09	0.06	0.08	0.09	0.06	0.06	0.06	0.06	0.06
Ca	0.02	0.03	0.02	0.02	0.02	0.04	0.02	0.03	0.02	0.24	0.27	0.49	0.26	0.29	0.25	0.31	0.30
Fe/Fe+Mg	0.45	0.41	0.41	0.42	0.40	0.41	0.41	0.41	0.42	0.20	0.21	0.21	0.20	0.20	0.20	0.20	0.20

In the GEO-N2 drill core (fig. 16), vesicles, fractures, and spaces between breccia fragments contain colorless, white, or bluish botryoidal or spherical silica deposits at 514.5-m depth and scattered samples between depths of 656.7 and 1,040.9 m. XRD analyses of these siliceous open-space fillings show the presence of both poorly crystallized cristobalite and well-crystallized cristobalite; the former has a major low broad X-ray peak close to 4.11 Å, and the latter has high sharp peaks near 4.04 Å (Keith, White, and Beeson, 1978). Cristobalite is the dominant mineral above about 810-m depth but also occurs in scattered samples below that depth. Peaks for cryptocrystalline quartz or chalcedony are also present in several X-ray analyses of the botryoidal silica deposits below 810-m depth. Well-crystallized cristobalite was not identified in any of the other flank or intracaldera drill cores.

Frosted to colorless botryoidal cristobalite lines open spaces in scoriaceous drill core material at 1,141.5-m depth and coats vesicles at 1,146.2-m depth in the GEO N-3 drill core (fig. 18). It is the only silica mineral identified in core samples from this drill hole. A few scattered samples below ~750-m depth in the GEO-N5 drill core (fig. 20) show cristobalite in XRD analyses of altered glass in lithic tuff and obsidian breccia, as botryoidal silica deposits in fractures and vesicles, and as fillings between breccia fragments.

The drill core from the SF NC-01 drill hole has a few bluish-gray to frosted botryoidal cristobalite deposits in fractures and vesicles from 693.4- to 930.1-m depth (fig. 23). SEM studies usually show that the botryoidal silica has a smooth surface with no evidence of crystallinity, similar to the opal of figure 47. However, one sample of cristobalite deposited on calcite at 900.1-m depth shows that the botryoidal silica consists of spherical clusters of bladed crystals (fig. 48). A similar habit has been observed for hydrothermal cristobalite in drill cores from Yellowstone National Park (Bargar and Beeson, 1981) and for diagenetic cristobalite in the Miocene Monterey Shale in California (Murata and Larson, 1975).

The SF NC72-03 drill core contains cristobalite between depths of 662.9 and 1,187.2 m (fig. 26). Fractures, vesicles, and open spaces between breccia fragments are partly filled by soft white silica, by colorless, frosted, or bluish-white botryoidal silica, or by similarly colored massive silica deposits. SEM observations of a cristobalite sample from 867.2-m depth shows botryoidal clusters of bladed(?) crystals similar to those in figure 48. Many of these cristobalite deposits contain associated chalcedony.

QUARTZ AND CHALCEDONY

Colorless euhedral quartz crystals (as long as 7 mm) were deposited in vesicles and fractures between depths of 461.5 and 468.9 m and below 713.5-m depth in the USGS-N2 drill

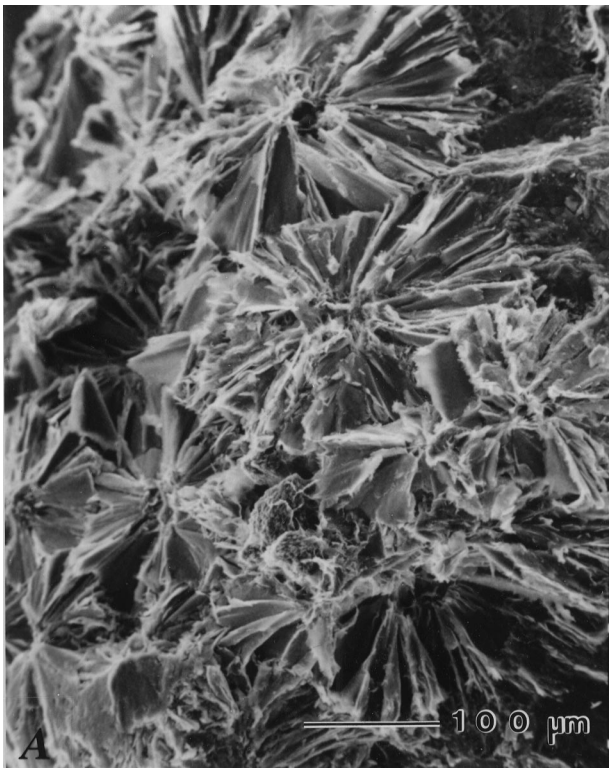

core (fig. 5). A few samples show more than one generation of quartz crystals. The general paragenetic sequence consists of pyrite, green clay (chlorite or mixed-layer chlorite-smectite), ± bluish botryoidal chalcedony (cryptocrystalline quartz), crystalline quartz, bladed or blocky calcite (fig. 49), ± very minute quartz crystals coating calcite. Hydrothermal quartz was identified both in the groundmass of the pumiceous to lithic tuffs and as open-space fillings throughout most of the RDO-1 drill cuttings below 332-m depth. Euhedral open-space quartz crystals (as long as 2 mm) were deposited later than pyrrhotite, mordenite, and calcite but formed earlier than some of the chlorite.

The four west-flank drill holes (GEO-N2, GEO-N5, SF NC-01, and SF NC72-03) all contain quartz crystals in the lower parts of the drill cores (figs. 16, 20, 23, and 26). Most of these quartz deposits consist of tiny euhedral to subhedral crystals that formed on top of botryoidal chalcedony (see fig. 22) in vesicles and fractures or between breccia fragments. However, several core samples contain thin quartz veins or tiny colorless crystals that formed in open spaces without earlier chalcedony deposits.

Colorless, white, or bluish-gray cryptocrystalline chalcedony (mean index of refraction = ~1.53) lines vesicles, coats fractures, and fills space between breccia fragments at depths of 556.0 to 563.1 m, 701.0 to 744.0 m, and at scattered locations between 811.2- and 899.8-m depth in the USGS-N2 drill core (fig. 5). The open-space cryptocrystalline silica deposits generally have a massive, banded, or botryoidal texture and have XRD peaks for chalcedony (quartz) and cristobalite in the upper zone; below ~701-m depth, XRD analyses of the

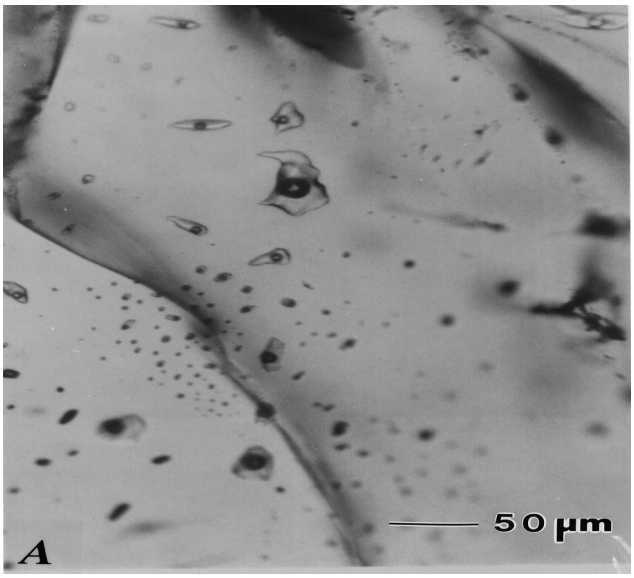

Figure 46.—Scanning electron micrographs and photograph of crystalline chlorite at Newberry volcano. A, Rosettes of sheet-like chlorite crystalline aggregates that coat fracture at 740.7-m depth in drill core USGS-N2. B, Randomly oriented aggregates of stacked, hexagonal, platy chlorite crystals from vesicle filling at 931.0-m depth in drill core USGS-N2. C, Wormy-textured aggregates of chlorite crystals deposited between breccia fragments along with acicular laumontite crystals at 1,120.4-m depth in SF NC-01 drill core.

microcrystalline to microfibrous silica deposits only show the presence of chalcedony. Many of the chalcedony open-space fillings are covered by later-formed tiny quartz crystals.

Five of the flank geothermal drill cores at Newberry volcano contain chalcedony deposits. A single sample of yellowish botryoidal chalcedony coats flow-breccia fragments at 555.2-m depth in drill core GEO N-1 (fig. 14). Scattered vesicle, fracture, or cavity fillings in the lower part of the GEO-N2 drill core (fig. 16) contain colorless, white, or bluish, massive, banded, or botryoidal chalcedony. A few samples in the upper part of the chalcedony zone also have XRD peaks for cristobalite. Vesicle fillings of one core sample from 756.5-m depth in drill hole GEO-N5 (fig. 20) are composed of light-gray botryoidal chalcedony and later, poorly developed quartz crystals (see fig. 22). Open-space fillings in the lower part of core hole SF NC-01 (fig. 23) contain similar colorless, frosted, white, or bluish powdery, massive, banded, and botryoidal chalcedony. Cristobalite also is indicated by XRD analyses of a few samples from the upper part of this chalcedony zone. Vesicles, fractures, and spaces between breccia fragments of samples from the lower part of the SF NC72-03 drill hole (fig. 26) have chalcedony with the same morphology and colors as the above flank drill holes; cristobalite is also identified in XRD analyses of these silica deposits.

SULFIDE MINERALS

PYRRHOTITE

Tabular pseudohexagonal bronze pyrrhotite crystals (as long as 3 mm) (fig. 50A) line fractures and cavities and are disseminated in the USGS-N2 drill core from depths of 460.9 to 466.8 m, 696.2 to 792.5 m, and 907.8 to 931.8 m (fig. 5). Pyrrhotite generally is one of the earliest hydrothermal minerals deposited in these sections of drill core. A few core samples in the upper zone contain replacement pyrite and marcasite that appear to be pseudomorphous after pyrrhotite (fig. 50B). Electron microprobe analyses of four pyrrhotite samples from the two upper pyrrhotite zones are listed in table 12 (analyses 1-4); additional analyses are given by Bargar and Keith (1984; appendix 7). Trace-element analyses show that pyrrhotite from 713.2-m depth contains some As along with minor Co, Cr, Cu, Mn, Pb, V, Y, and Zn (table 10). A plot of atomic percent iron versus temperature (phase diagram for the Fe-S system below 350˚C, fig. 51) indicates that the USGS-N2 pyrrhotite should be monoclinic (type 4c) (Kissin and Scott, 1982). Nine additional samples from the three pyrrhotite zones were X-rayed at 1/4˚/min.; in all nine X-ray

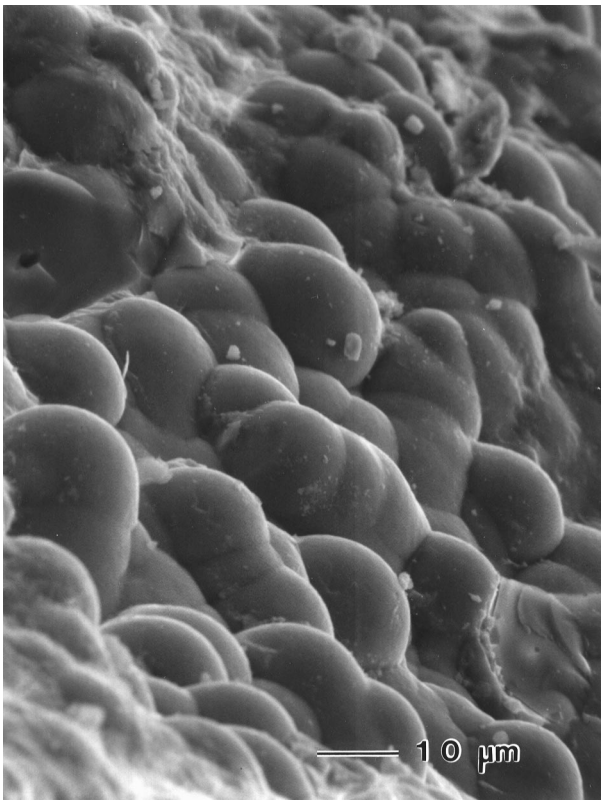

Figure 47.—Scanning electron micrograph of botryoidal opal deposit at 613.3-m depth in USGS-N2 drill core.

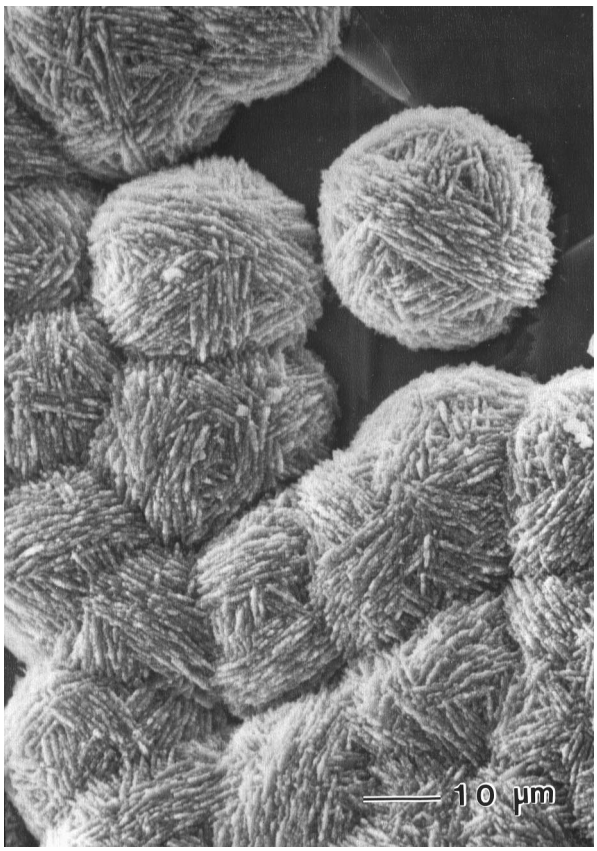

Figure 48.—Scanning electron micrograph of hemispherical aggregates of bladed cristobalite crystals deposited on calcite at 900.1-m depth in SF NC-01 drill core.

diffractograms, doublet X-ray reflections (102) and (202) of nearly equal intensity suggest that a hexagonal component, if present, could only be of minor abundance (Arnold, 1966).

Euhedral bladed pyrrhotite crystals line open spaces of several drill cuttings chips between depths of 332 and 408 m in the RDO-1 drill hole (fig. 12). The pyrrhotite crystals frequently are associated with quartz prisms and appear to be the earliest hydrothermal mineral deposited in the RDO-1 drill-hole material.

The groundmass of a pale-gray-green, bleached, moderately porous dacitic core sample from 1,104.6-m depth in the GEO-N2 drill hole (fig. 16) contains oxidized bladed sulfide that was identified as pyrrhotite by an X-ray-powder camera film. This sample is the only pyrrhotite positively identified in any of the flank drill cores. However, a fracture at 1,351.5-m depth in the SF NC72-03 drill core (fig. 26) contains very tiny hexagonal bladed (pyrrhotite?) crystals like those in figure 50A; EDS analysis using the SEM shows that they are composed of Fe and S.

Browne and Ellis (1970) and Steiner (1977) report finding pyrrhotite in the drill cores from New Zealand geothermal areas at temperatures ranging from 152 to 268˚C. Pyrrhotite in drill cores from Yellowstone National Park occurs at drill hole temperatures of 130 to 152˚C (Bargar and Beeson, 1981). In the USGS-N2 drill hole, the measured temperatures the three pyrrhotite zones were about 97˚C, 110 to 180˚C, and 250 to 265˚C. Measured temperatures in the pyrrhotite zone of the RDO-1 drill hole were above 130˚C. The measured temperatures at the depths where the pyrrhotite was located in drill holes GEO-N2 and SF NC72-03 were about 140, and 150˚C, respectively.

PYRITE

Cubic pyrite crystals are present in the USGS-N2 drill core at depths of 383.7 m, 388.6 m, 446.2 to 828.9 m, and in scattered concentrations below 828.9 m (fig. 5). Pyrite is closely associated with siderite, smectite, and marcasite in the main sulfide zone. Microprobe analyses of six pyrite samples, listed in table 12 (analyses 5-10), show minor Co in addition to Fe and S. Significant amounts of the trace elements As, Co, Cu, and Zn, as well as some Cd, Ce, Cr, La, Mn, Nd, Ni, Pb, Sn, V, Y, and Yb, are present in an analysis of pyrite from 930.1-m depth in the drill hole (table 10). Several samples from between depths of 338 and 399 m in the RDO-1 drill cuttings (fig. 12) contain disseminated pyrite or pyrite in thin veins, but it is not very abundant in any of the samples.

Pyrite is present in all of the flank drill holes except for drill hole GEO-N4. Small patches of disseminated, very

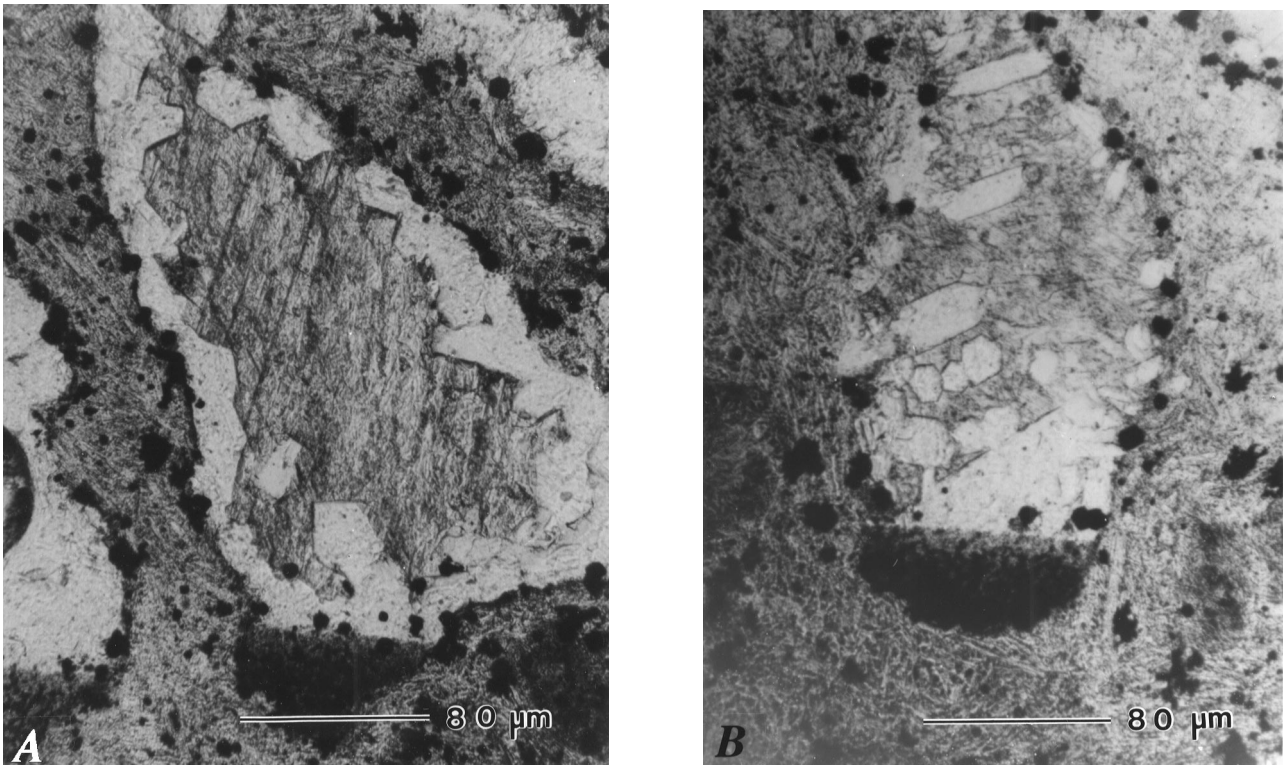

Figure 49.—Vesicle fillings (A and B) in basaltic breccia fragments at 793.1-m depth in USGS-N2 drill core. Bottoms of vesicles have horizontal layer of pyrite and green chlorite; pyrite and traces of chlorite also are deposited along walls of vesicles. Disseminated pyrite and very minor chlorite occurs throughout groundmass of basaltic breccia fragments. Vesicles were later filled with euhedral quartz crystals and finally calcite.

minute (~ 0.02 mm) yellow metallic cubic pyrite crystals were identified only at 943-, 945-, and 1,068-m depths in the GEO N-1 drill core (fig. 14). In the lowest sample, a pyrite veinlet crosscuts iron oxide deposits, and pyrite crystals formed later than smectite in vesicles. Pyrite occurs in three zones (1,030.8 m, 1,128.4 to 1,131.4 m, and 1,278.3 to 1,332.3 m) in the GEO-N2 drill core (fig. 16) as tiny crystals on fractures and in vesicles. Samples from the middle zone also contain colorless anhydrite crystals. Some of the open-space pyrite deposits in the other two zones appear to be slightly oxidized with a surrounding halo of orange-brown staining. Pyrite lines fractures and vesicles and coats open spaces between rock fragments in scattered core samples below 1,009.0-m depth in the GEO-N3 drill core (fig. 18). Most of the pyrite is very fine grained; a few samples have larger cubic crystals that are about 1 mm diameter. At depths of 1,020.2, 1,020.3, and 1,040.0 m, tiny white fibrous gypsum crystals probably formed due to post-drilling oxidation of pyrite.

Tiny cubic pyrite crystals were deposited on fractures, in vesicles, and between breccia fragments in the lower part of the GEO-N5 drill core (fig. 20). At 958.6-m depth, the apparent bladed habit of the pyrite suggests replacement of a precursor sulfide mineral. Pyrite crystals were found in open spaces of three zones in the SF NC-01 drill core (fig. 23). One sample in the upper zone contains a fracture filling with opal and smectite that both contain disseminated cubic and pyritohedral pyrite crystals (see fig. 24). Euhedral to subhedral pyrite crystals (fig. 52A) are commonly associated with siderite and smectite in this drill core. Several samples from the lower half of the SF NC72-03 drill core (fig. 26) contain pyrite on fractures and in vesicles. Some pyrite is disseminated in smectite and cryptocrystalline silica (cristobalite and quartz or chalcedony in X-ray analyses) open-space deposits (see fig. 24).

MARCASITE

Marcasite occurs as cavity and fracture deposits, in close association with pyrite and pyrrhotite, at scattered locations between depths of 452.8 and 627.0 m in the USGS-N2 drill core (fig. 5). Marcasite typically has a tabular-prismatic habit (fig. 50B) and locally shows the characteristic cockscomb morphology of twinned crystals (fig. 52B). Marcasite is

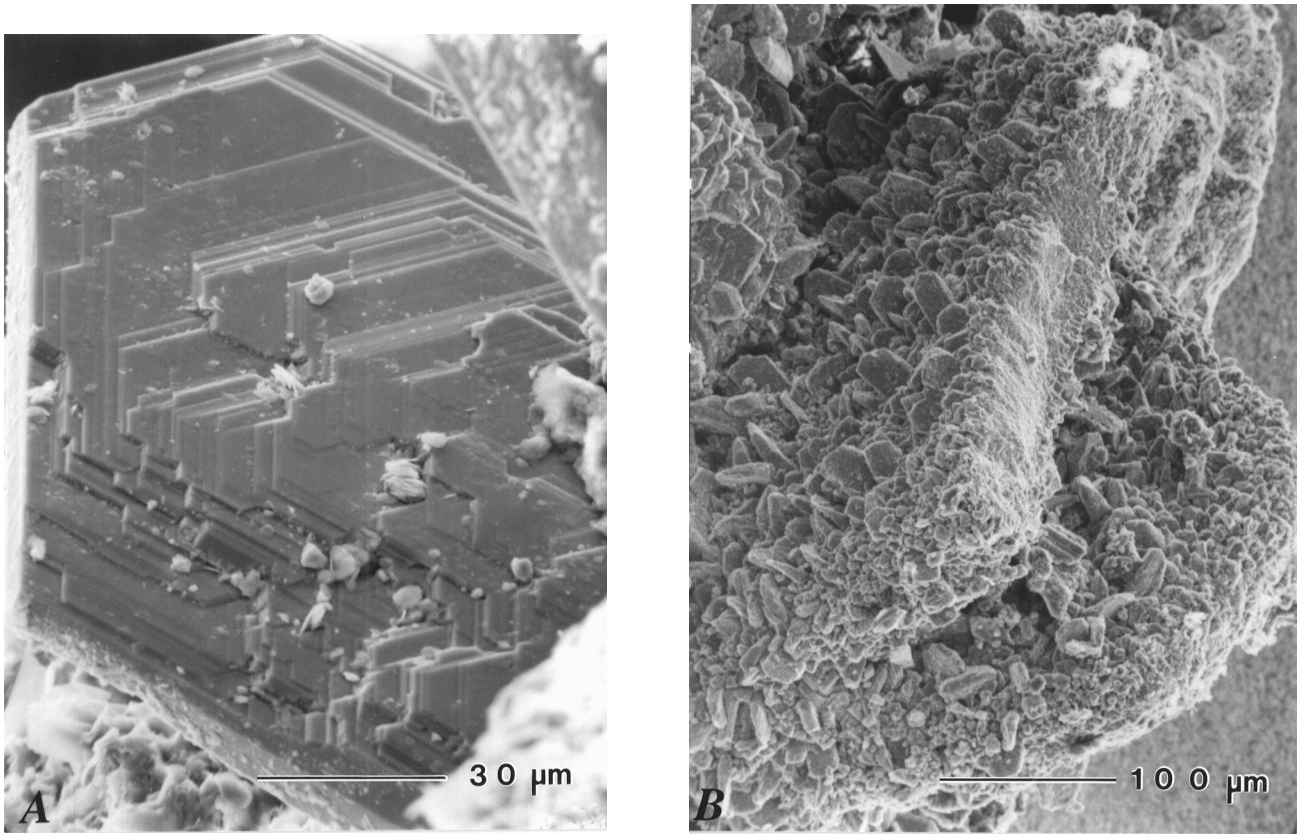

Figure 50.—Scanning electron micrographs of pyrrhotite, marcasite, and pyrite at Newberry volcano. A, Laminar aggregate of hexagonal pyrrhotite crystals and later chlorite partly filling vug at 907.8-m depth in USGS-N2 drill core. B, Pseudomorphous replacement of large bladed pyrrhotite(?) crystals by small tabular marcasite and massive to blocky pyrite (identified by XRD) crystals on fracture at 534.8-m depth in USGS-N2 drill core.

Table 12.—Electron microprobe analyses of sulfide minerals from USGS-N2 drill core.

[Analyses Nos. 1, 2 and 6–10, 3, 5, and 11 are averages of 6, 7, 12, 14, and 9 analyses, respectively; Tr, trace amount]

Mineral:	Pyrrhotite				Pyrite						Marcasite
Depth (m):	463.4	713.7	736.4	740.7	450.2	463.4	639.7	716.9	725.1	930.1	565.7
Analysis No.:	1	2	3	4	5	6	7	8	9	10	11
	Weight percent elements										
Fe ----------	56.60	59.79	59.94	60.14	45.58	43.25	46.01	46.47	46.06	45.92	46.24
Co ----------	0.05	0.05	0.03	0.05	0.01	0.00	0.02	0.03	0.04	0.04	0.00
Ni ----------	0.00	Tr	0.01	Tr	0.00	0.00	0.00	0.00	0.00	0.00	0.00
S ----------	38.45	39.65	39.69	39.62	51.45	50.96	52.44	52.85	52.12	52.99	52.66
Total ----	95.10	99.49	99.67	99.81	97.04	94.21	98.47	99.35	98.22	98.95	98.90

metastable with respect to pyrite at low temperature (Craig and Scott, 1974) and is converted to pyrite at temperatures greater than 160˚C in the Salton Sea geothermal system of California (McKibben, 1979). Marcasite occurs at temperatures of about 80 to 170˚C in drill cores from Yellowstone National Park (Bargar and Beeson, 1984) and at temperatures slightly below ~140˚C at Steamboat Springs, Nevada (Sigvaldson and White, 1962). The present temperature range at which marcasite occurs in the USGS-N2 drill core is ~74 to 98˚C. Several electron microprobe analyses of marcasite from 565.7-m depth (appendix 9 in Bargar and Keith, 1984; and table 12, analysis 11 of this report) show that the mineral is fairly homogeneous with respect to both Fe and S and contains no detectable Co or Ni.

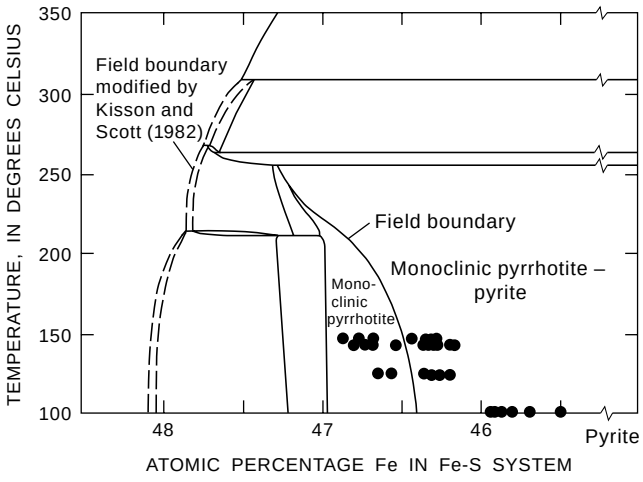

Figure 51.—Monoclinic pyrrhotite and monoclinic pyrrhotite-pyrite fields of phase diagram for Fe-S system below 350˚C (after Kissin and Scott, 1982) showing electron microprobe compositions of pyrrhotite from four depths in USGS-N2 drill core. USGS-N2 temperatures at depths where pyrrhotite was identified are from Sammel (1981).

SPHALERITE

Thin fracture fillings at 789.4-m depth (temperature <60˚C) in the GEO-N5 drill core (fig. 20) contain early black euhedral crystals of sphalerite (see fig. 21) in association with later soft brown siderite and colorless calcite. EDS chemical analysis of the sphalerite using the SEM shows Zn and S with significant Fe and is the basis for the sphalerite identification. Sphalerite occurs at temperatures above 300˚C in geothermal drill holes of the Salton Sea area, California (McKibben and Elders, 1985). Minor sphalerite also has been found in some geothermal areas of New Zealand (Browne, 1969; Browne and Lovering, 1973; Steiner, 1977) at temperatures of 120 to 298˚C. The waters from which the New Zealand sphalerite precipitated have low salinity and only trace amounts of Zn (Browne and Ellis, 1970). The Newberry sphalerite probably formed during some stage of cooling of the volcanic rocks at somewhat higher temperatures than occur at present.

SULFATE MINERALS

ANHYDRITE

Colorless blocky anhydrite crystals formed on fractures at 914.7 m to 915.9 m in drill hole USGS-N2 (fig. 5), along with later mixed-layer chlorite-smectite (fig. 53), where the temperature measured during drilling was about 258˚C. The presence of anhydrite at depth in the Newberry drill cores probably is due to oxidation of H_2S in the fluids. Subsequent fluid chemistry must have changed because the anhydrite appears to have been partly dissolved either before or during deposition of the mixed-layer clay. Anhydrite also was identified in fractures and vesicles of the GEO-N2 drill core at depths of 1,128.4 to 1,131.4 m and at 1,323.1 m (fig. 16). The anhydrite crystals are colorless and tabular, have a mean index of refraction of about 1.57, and

are usually associated with pyrite crystals that appear to be partly oxidized.

BARITE

One cavity at 1,293.4-m depth in the GEO-N1 drill core (fig. 14) contains very tiny colorless crystals that were identified as barite by XRD analysis. Barite characteristically forms in hydrothermal environments associated with metalliferous deposits (Phillips and Griffen, 1981; Krupp and Seward, 1987); it is rarely reported from nonmetalliferous modern geothermal areas.

JAROSITE, NATROALUNITE, AND NATROJAROSITE

Several sulfate minerals were identified in the GEO-N3 drill core (fig. 18). Six samples between depths of 809.2 and 918.7 m have vesicles, fractures, or open spaces in scoria that are coated by yellow, orange, or greenish-yellow, intergrown, finely crystalline hexagonal tabular jarosite crystals (fig. 54). Similar white or yellow, hexagonal, tabular, natrojarosite crystals (fig. 55) line vesicles, fractures, and open spaces of scoria at depths of 846.8 to 851.3 m, 893.1 to 896.5 m, and 995.9 m in the GEO-N3 drill core. Another white or yellow sulfate mineral, natroalunite, also is found in vesicles, fractures, and other open spaces of seven scattered samples between 837.6 m-depth and the bottom of this drill core.

Jarosite [$KFe_3^{+3}(SO_4)_2(OH)_6$], natrojarosite [$NaFe_3^{+3}(SO_4)_2(OH)_6$] and natroalunite [$NaAl_3(SO_4)_2(OH)_6$] are all members of the alunite group of minerals. These minerals generally form in near-surface hydrothermal acid-sulfate or fumarolic conditions (Hemley and others, 1969). The drill core in this zone and above has the appearance of fumarolic conditions with yellowish-orangish-reddish iron oxide deposits and staining in open spaces. However, pyrite occurs in many drill-core samples beneath the sulfate zone. The three alunite-group sulfate minerals, jarosite,

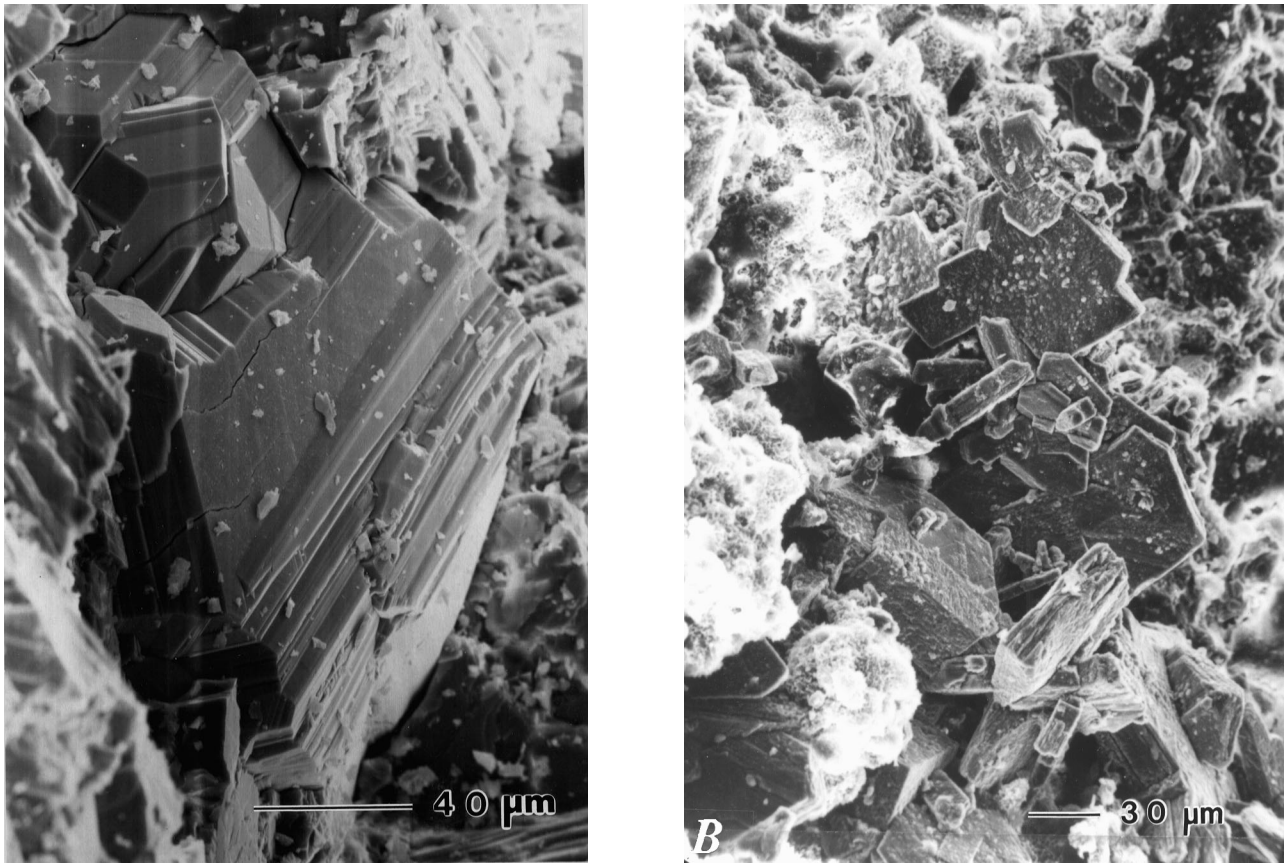

Figure 52.—Scanning electron micrographs of pyrite and marcasite crystals at Newberry volcano. A, Octahedral pyrite crystal with earlier(?) siderite and later smectite coating fracture surface at 326.1-m depth in SF NC-01 drill core. B, Marcasite crystals with cockscomb habit accompanied by later smectite (pyrite and siderite also identified by XRD), from fracture at 565.7-m depth in USGS-N2 drill core.

natrojarosite, and natroalunite, in the GEO-N3 drill hole may have formed from either acid-sulfate conditions due to oxidation of pyrite or precipitation from fumarolic gases.

GYPSUM

Gypsum was identified at depths of 1,020.2 and 1,040.0 m in the GEO-N3 drill core (fig. 18). Sprays of tiny white fibrous gypsum crystals occur in open spaces in association with pyrite. Gypsum probably formed as a result of minor oxidation of pyrite crystals, but we are not certain if the gypsum precipitated before or after the drill core was brought to the surface. Minor gypsum was occasionally observed deposited on top of pyrite crystals in a few of the other drill cores where the mineral does not appear to be related to the present hydrothermal conditions within the drill holes.

IRON OXIDE AND IRON HYDROXIDE MINERALS

Several iron oxide or iron hydroxide minerals occur in the drill cores from the flanks of Newberry volcano or from inside the caldera. In the mineral distribution diagrams, these minerals are lumped together under the general heading of iron oxide.

HEMATITE AND LEPIDOCROCITE

Hematite was identified by XRD analyses of material from a few vesicles, fractures, altered mafic minerals, and oxidized zones at depths of 599.8 to 600.5 m, 804.5 m, 833.9 to 860.1 m, and 914.7 to 917.1 m in the USGS-N2 drill core (fig. 5). A narrow zone from 464.5- to 466.0-m depth contains oxidized crusts that coat pyrrhotite crystals. XRD analyses show that the crusts are composed of sulfur, goethite, and lepidocrocite in addition to pyrrhotite, pyrite, and marcasite. Presumably, the two iron oxide minerals and sulfur are by-products of the alteration of pyrrhotite to pyrite and marcasite. Red iron oxide stains were observed in three samples from the lower part of the RDO-1 drill hole (fig. 9); the stains are identified as hematite by Keith and others (1986).

GOETHITE

XRD analyses of three brown to orange clayey fracture coatings and breccia open-space fillings from depths of 906.0,

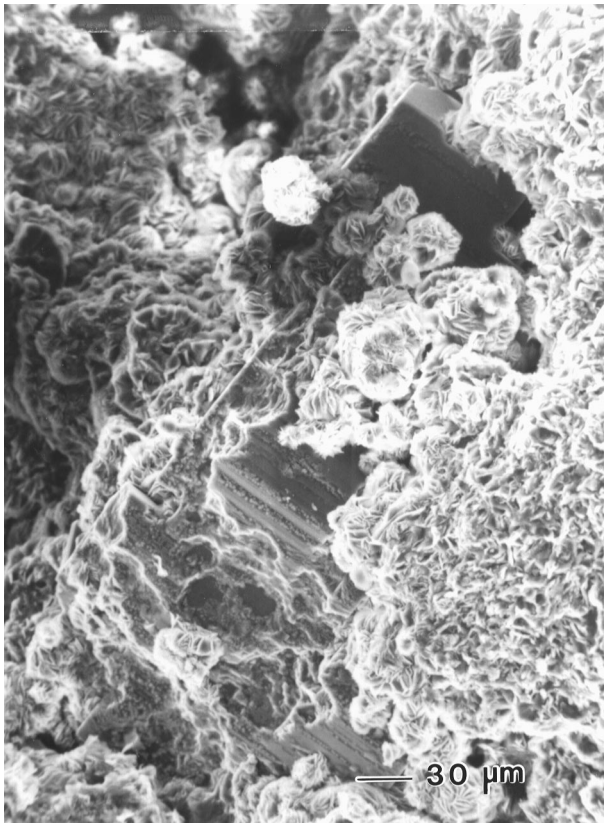

Figure 53.—Scanning electron micrograph of blocky anhydrite crystals partly coated by later mixed-layer chlorite-smecite rosettes on fracture surface at 915.2-m depth in USGS-N2 drill core.

Figure 54.—Backscatter image (on scanning electron microscope) of intergrown tabular jarosite crystals from vesicles at 918.7-m depth in GEO-N3 drill core.

917.7, and 921.6 m in the GEO-N3 drill core show the presence of smectite, natroalunite, and goethite (fig. 18). Goethite is an iron hydroxide mineral that commonly forms due to weathering or low-temperature hydrothermal alteration of iron-rich sulfides and oxides (Deer, Howie, and Zussman, 1966). No sulfide or iron oxide minerals were observed in these drill core samples; either these minerals were completely altered or the goethite and natroalunite formed due to the oxidation of iron sulfide in rock adjacent to the drill-core samples.

MAGNETITE

A few cavities containing euhedral, high-temperature, vapor-phase minerals that formed during cooling of the lava at 1,180.2-m depth in the GEO-N2 drill core (fig. 16) have associated black to red blocky crystals. These crystals may have been high-temperature, vapor-phase, magnetite crystals that are partly to completely altered to red hematite or amorphous iron oxide. Vapor-phase titanomagnetite crystals (significant Ti in EDS analysis using the SEM) also rim a vesicle at 1,299.1-m depth in this drill core.

Several drill-core samples from below 1,132.2-m depth in the GEO N-3 drill hole (fig. 18), at 972.3-m depth in drill hole GEO-N5 (fig. 20), and at depths of 1,136.6, 1,164.9, and 1,288.7 m in drill hole SF NC72-03 (fig. 26) have fractures and vesicles that are lined by black sooty or clayey deposits and black botryoidal precipitates that were identified as magnetite in XRD analyses. Botryoidal magnetite appears to have formed earlier than other secondary minerals, and some of the black magnetite spheres and hemispheres appear to form the core for later botryoidal siderite crusts. The secondary magnetite frequently is partly altered to reddish amorphous iron oxide or hematite (fig. 56). These magnetite open-space deposits probably formed during cooling of the lava flows and are of vapor phase or deuteric origin.

AMORPHOUS IRON OXIDE

Yellow, orange, brown, red, and black iron oxide stains the interflow breccias, scoria deposits, ash layers, and tuffaceous beds in most of the Newberry flank drill cores. XRD analyses of these deposits usually indicate that the iron oxide is amorphous. Most of the staining probably forms by oxidation of primary magnetite during cooling of the volcanic deposits and is deuteric; however, some staining may be due to

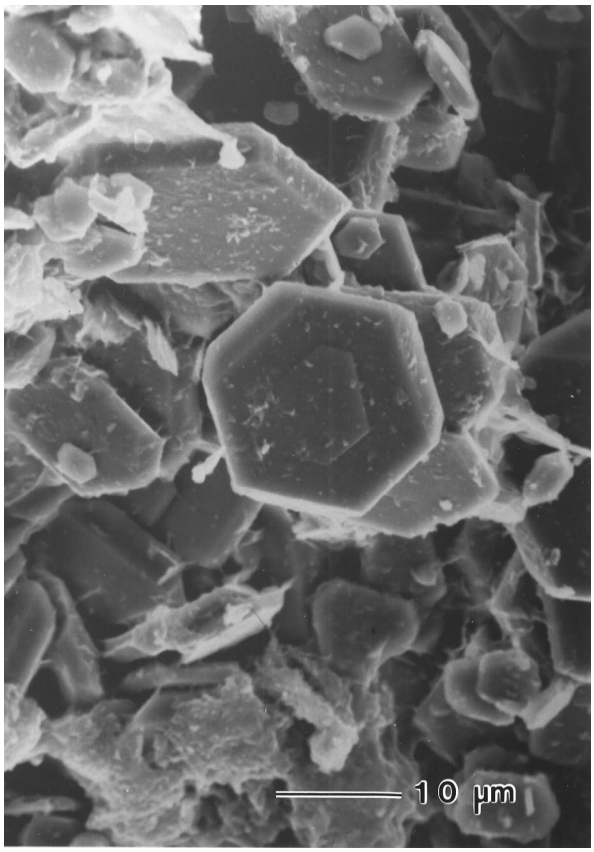

Figure 55.—Scanning electron micrograph of hexagonal tabular natrojarosite crystals from fracture at 995.9-m depth in GEO-N3 drill core; euhedral natrojarosite crystals are partly coated by smectite.

Figure 56.—Part of large cavity filling of red botryoidal hematite (individual spheres are ~0.5 mm in diameter) and later colorless calcite from 1,343.6-m depth in SF NC72-03 drill core.

weathering processes. XRD studies of iron oxide-stained vapor-phase crystals (including magnetite), groundmass magnetite grains, and botryoidal deuteric(?) magnetite deposits generally show the presence of hematite, although sometimes the deposits appear to be amorphous iron oxide. These hematite and amorphous iron oxide deposits could be deuteric or they could form due to weathering or low-temperature hydrothermal alteration. Other clayey hematite fracture and vesicle fillings and altered siderite crystals undoubtedly were produced by hydrothermal alteration.

OTHER MINERALS

APATITE

Crystals of a hexagonal, tabular to prismatic apatite group mineral (fig. 57) line a cavity at 909.8-m depth in the USGS N-2 drill core where the temperature measured following drilling was ~250˚C (fig. 5). Similar euhedral hydrothermal apatite crystals occur in Yellowstone National Park drill core Y-6, where the temperature measured during drilling was about 100˚C (Bargar and Beeson, 1984). Steiner (1977) found hexagonal prismatic hydrothermal apatite crystals (no temperature given) that are pseudomorphous after mafic phenocrysts in the Wairakei geothermal area of New Zealand. Apatite also is present in the Larderello geothermal area, Italy, along with epidote and datolite, which suggests that the minerals precipitated at more than 200˚C (Cavarretta, Gianelli, and Puxeddu, 1980).

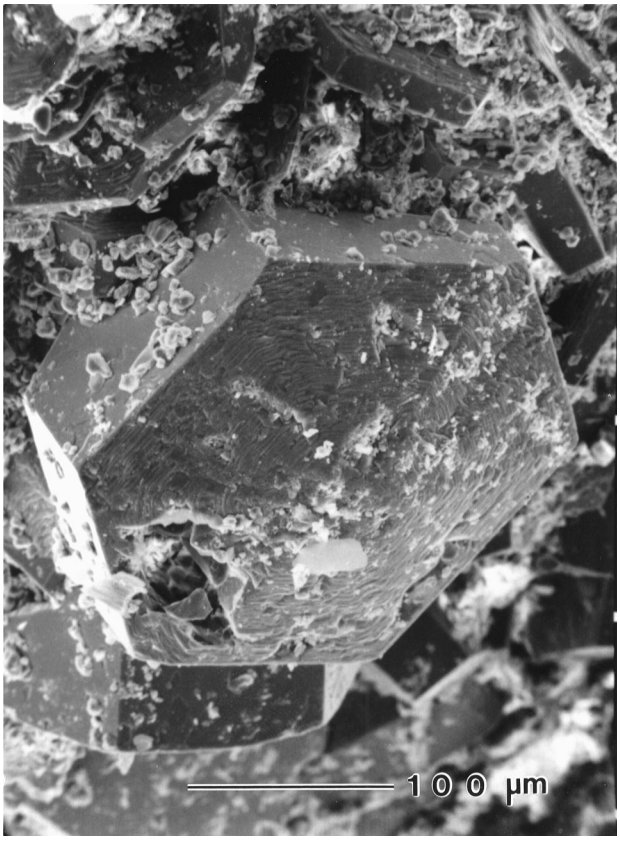

Figure 57.—Scanning electron micrograph of hexagonal, tabular to columnar apatite crystals with later chlorite that line vesicle at 909.8-m depth in USGS-N2 drill core.

APOPHYLLITE

The identification of an apophyllite group mineral at 318.5-m depth in USGS-N2 drill core (fig. 5; temperature ~50˚C) is based on a single multicomponent XRD pattern. To the best of our knowledge, apophyllite has not been reported previously from a geothermal system; however, the mineral is not rare and is frequently associated with zeolite minerals in basalts (Dunn, Rouse, and Norberg, 1978).

COPPER

Native copper was identified in vesicles at 1,186.0-m depth in drill core GEO-N2 (fig. 16) and at 1,131.0-m depth in the SF NC72-03 (fig. 26) drill core (fig. 58). Both drill holes are on the west flank of Newberry volcano. Measured temperatures at the copper-bearing sample depths of the two drill holes are about 120 to 150˚C. Fluid-inclusion homogenization temperatures in quartz and calcite from the SF NC72-03 drill hole range from near the present conditions up to about 311˚C. Native copper has been observed in a few other geothermal drill holes in the Cascade Range of Oregon (Bargar, 1980, 1990; Bargar, Keith and Beeson, 1993; Keith and Boden, 1981). Native copper commonly occurs in basaltic lavas owing to chemical reactions be-

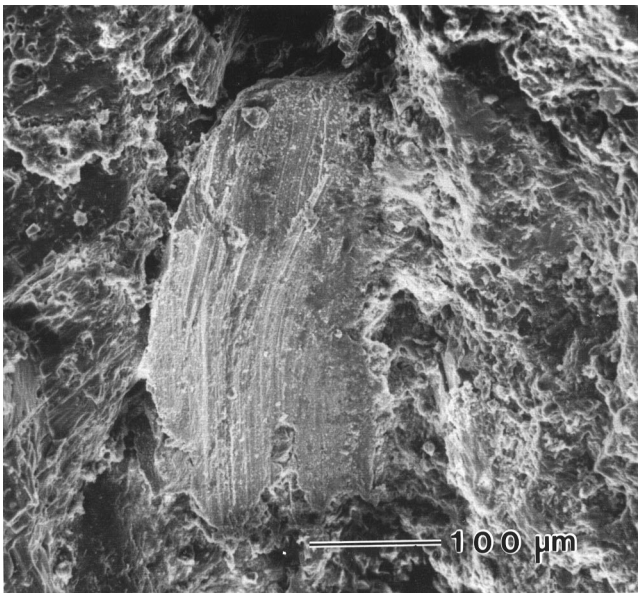

Figure 58.—Scanning electron micrograph of striated grain of native copper partly filling vesicle at 1,131.0-m depth in SF NC72-03 drill core.

tween copper-bearing low-temperature hydrothermal waters and hematite or other iron-bearing minerals (Hurlbut, 1971). In the USGS-N2 drill-hole samples, the more silicic lavas have lower Cu values (sample nos. 1065 to 2467.5 in table 3). The Cu concentration for one basalt specimen from the SF NC72-03 drill hole is greater than Cu values for more silicic drill core samples from the flank drill holes (table 13).

Table 13.—Trace element analyses (in ppm) of drill-core samples outside Newberry caldera.

[Determined by energy dispersive X-ray fluorescence spectroscopy. Analysts: J. Kent and E. Bell, U.S. Geological Survey, Menlo Park, Calif.]

Sample No.:	GEO-N1 4238	GEO-N1 4243	GEO-N1 4398	GEO-N5 1976	GEO-N5 3146	SF NC 72-03 2122	SF NC 72-03 2807
Depth (m):	1,291.7	1,293.3	1,340.5	602.3	958.9	646.8	855.6
Ba	1,000	1,000	780	1,100	860	970	285
Ce	60	84	84	50	68	90	44
Cr	<20	<20	<20	<20	<20	<20	110
Cu	16	18	18	14	20	16	66
La	<30	32	32	<30	36	56	<30
Nb	16	18	16	14	20	16	<10
Ni	<10	<10	<10	<10	<10	10	100
Rb	86	82	84	112	82	70	14
Sr	100	92	225	52	96	200	680
Y	58	60	50	36	58	52	16
Zn	60	72	86	54	76	84	66
Zr	400	405	325	205	355	315	110

EPIDOTE

Euhedral yellow-green epidote crystals (fig. 59) line vugs and fractures from depths of 911.5 to 912.6 m and 916.4 to 916.7 m in the USGS-N2 drill core (fig. 5). The twinned epidote crystal clusters occur in association with earlier quartz and calcite and later(?) chlorite or mixed-layer chlorite-smectite; some core samples also have patches of reddish hematite. Multiple electron microprobe chemical analyses across three epidote crystals (table 14) suggest some Fe-Al substitution with very slight Fe enrichment and Al depletion near the centers of two of the crystals. Selected optical and crystallographic data for epidote from 916.7-m depth in the USGS-N2 drill hole are given in table 15 (R.C. Erd, written commun., 1991).

The measured temperature at which epidote was found in the USGS-N2 drill hole was about 258˚C, which is well above the 230˚C minimum stability limit given for epidote that forms at low-pressure conditions characteristic of geothermal areas (Seki, 1972). Bird and others (1984) subsequently documented calc-silicate temperature data from several well-studied natural systems and indicated that epidote most commonly is deposited at temperatures between 200 and 250˚C.

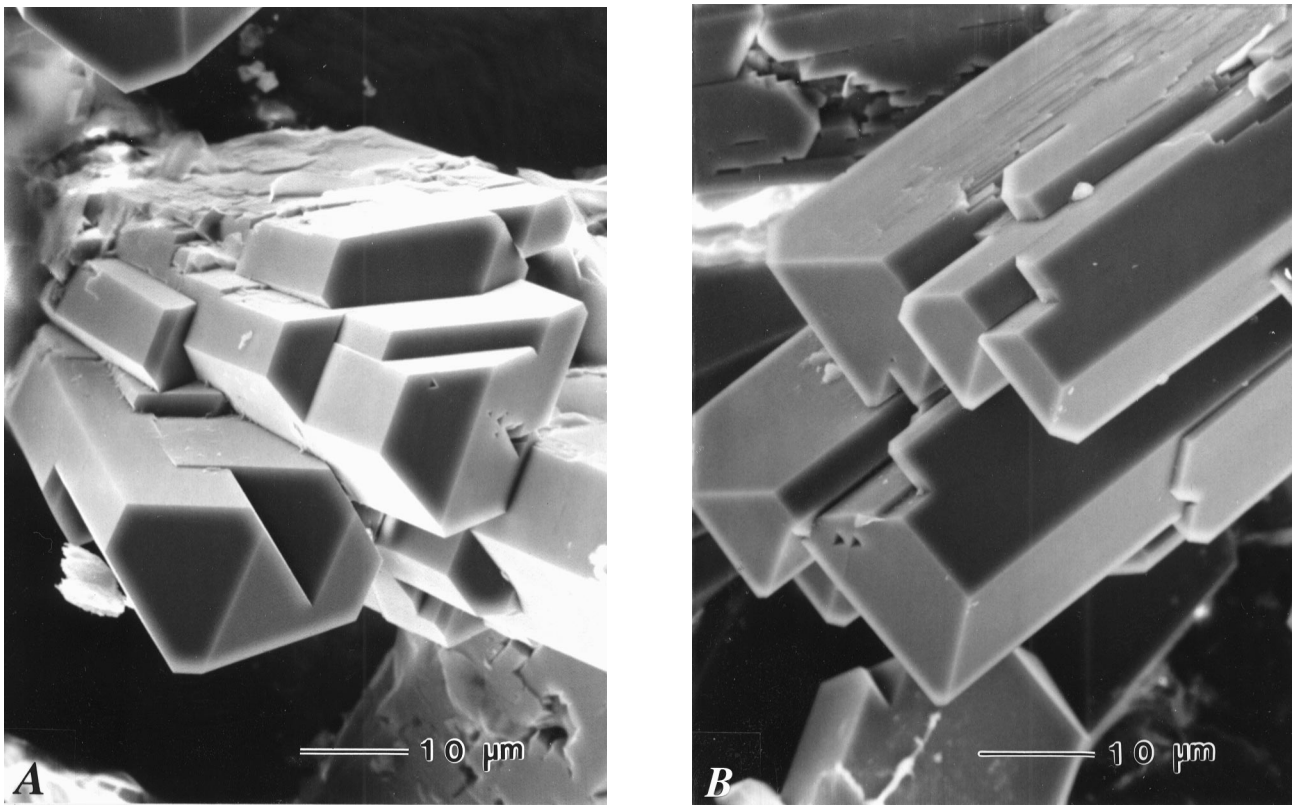

Figure 59.—Scanning electron micrographs showing clusters of euhedral twinned epidote crystals (A and B) from cavity at 916.4-m depth in USGS-N2 drill core.

Table 14.—Electron microprobe analyses of epidote from 916.7-m depth in USGS-N2 drill core.

Crystal No.:	1					2					3				
Analysis No.:	1	2	3	4	5	1	2	3	4	5	1	2	3	4	5
Major-element analyses (weight percent oxides)															
SiO_2	37.03	37.29	37.16	37.05	37.28	37.38	37.29	37.38	37.17	37.10	37.22	36.64	37.35	37.56	37.18
Al_2O_3	20.48	20.27	20.20	19.81	20.26	21.15	22.34	20.42	19.62	21.97	20.38	19.97	20.28	20.11	22.75
TiO_2	0.31	0.28	0.27	0.22	0.27	0.20	0.05	0.22	0.31	0.01	0.31	0.31	0.27	0.12	0.13
Fe_2O_3	16.76	16.64	17.02	16.81	17.08	15.40	14.82	17.04	17.35	15.06	16.31	16.90	17.02	16.74	13.55
MgO	0.13	0.14	0.15	0.10	0.06	0.09	0.07	0.16	0.11	0.08	0.09	0.12	0.15	0.18	0.08
MnO	0.17	0.17	0.24	0.13	0.12	0.12	0.37	0.17	0.16	0.15	0.11	0.13	0.18	0.61	0.59
CaO	22.90	22.92	22.75	22.99	23.04	23.28	22.95	22.79	22.99	23.16	22.91	22.67	22.87	22.73	22.29
Total	97.78	97.71	97.79	97.11	98.11	97.62	97.89	98.18	97.71	97.53	97.33	96.74	98.12	98.05	96.57
Number of atoms on the basis of 12.5 oxygens															
Si	3.00	3.02	3.01	3.03	3.01	3.02	2.99	3.02	3.02	2.99	3.03	3.01	3.02	3.03	3.01
Al_{IV}	0.00	0.00	0.00	0.00	0.00	0.00	0.01	0.00	0.00	0.01	0.00	0.00	0.00	0.00	0.00
Al_{VI}	1.96	1.94	1.93	1.91	1.93	2.01	2.10	1.94	1.88	2.08	1.95	1.93	1.93	1.92	2.17
Fe	1.03	1.02	1.04	1.03	1.04	0.94	0.90	1.03	1.06	0.91	1.00	1.04	1.04	1.02	0.83
Ti	0.00	0.01	0.00	0.00	0.00	0.00	0.00	0.00	0.00	0.00	0.00	0.00	0.00	0.00	0.00
Mg	0.02	0.02	0.02	0.01	0.01	0.01	0.01	0.02	0.01	0.01	0.01	0.01	0.02	0.02	0.01
Mn	0.01	0.01	0.02	0.01	0.01	0.01	0.03	0.01	0.01	0.01	0.01	0.01	0.01	0.04	0.04
Ca	1.99	1.99	1.98	2.01	2.00	2.02	1.97	1.97	2.00	2.00	2.00	1.99	1.98	1.97	1.93
Ps (mol %)[1]	34.4	34.5	35.0	35.0	35.0	31.9	30.0	34.7	36.1	30.4	33.9	35.0	35.0	34.7	27.7

[1]Pistacite (Ps) component determined by calculation of Fe/Fe+Al.

HYDROGROSSULAR

A whole-rock XRD analysis of reddish basaltic sediments from about 315-m depth in drill hole USGS-N2 (fig. 5) gives a pattern nearly identical to that of tricalcium aluminate hexahydrate [$Ca_3Al_2(OH)_{12}$] or nonsilicic hydrogrossular (Zabinski, 1966). The X-ray pattern is very similar to that of synthetic $Ca_3Al_2(OH)_{12}$ (JCPDS 24-217). SEM studies of the USGS-N2 sample show that the mineral forms tiny dodecahedral(?) crystals (fig. 60) in pore spaces of the caldera-fill materials.

According to Zabinski (1966), a true silica-free hydrogrossular has not been found to occur naturally. However, Passaglia and Rinaldi (1984) described a hydrogrossular group mineral (katoite) which has much lower silica content than other members of this garnet group. A single electron microprobe analysis of the USGS N-2 drill core materials gives (in weight percent oxides) 4.30 SiO_2, 38.24 Al_2O_3, 1.97 TiO_2, 13.99 FeO, 0.38 MgO, 0.05 MnO, and 38.69 CaO (total oxides = 97.62). This analysis is substantially lower in silica than the katoite analysis and has extraordinarily high alumina and iron contents compared with reported analyses of hydrogrossular (Passaglia and Rinaldi, 1984).

Garnet has been reported from several modern geothermal systems where it apparently formed at temperatures above 300°C (Bird and others, 1984). The measured temperature at which the USGS-N2 garnet occurs is only about 50°C, and there is no evidence that temperatures in this part of the drill core ever approached 300°C. Zabinski (1966) indicates that hydrogrossular of composition $Ca_3Al_2[OH]_{12}$ may form as a crystalline phase in the hydration of Portland cement. Cement and other foreign materials are routinely used in completing geothermal drill holes in the Cascade Mountains. The hydrogrossular crystals found in the USGS-N2 drill core sample appear to be a late phase and may have been introduced during drilling.

DISCUSSION

FACTORS CONTROLLING HYDROTHERMAL ALTERATION

Factors that influence the distribution and kind of mineral assemblages present in hydrothermal systems include permeability, rock and water composition, temperature, pressure, and duration of hydrothermal alteration (Browne and Ellis, 1970). These factors are largely interdependent, but the effects of one or more of the factors can exert a dominant influence in the location and extent of hydrothermal alteration. Permeability of the rocks controls the access of thermal fluids, which cause hydrothermal alteration of the rocks and precipitation of secondary minerals in open spaces. Obviously rocks that have very restricted permeability or are completely impervious to fluids will be only slightly altered. Crystallinity of the host rock is of

Table 15.—Optical and crystallographic data for epidote from 916.7-m depth in USGS-N2 drill core.

[Determined by R.C. Erd, U.S. Geological Survey, Menlo Park, Calif. (written commun., 1991)]

Specimen No.:	N2-3007.5
Crystal Size:	
Length (*Y*) ----------	0.21 mm
Width (*X*) ----------	0.055 mm
Width (*Z*) ----------	0.063 mm
Indices of refraction:	
α ----------	1.745 ±0.003
β ----------	1.774 ±0.003
γ ----------	1.787 ±0.003
Birefringence (γ - α) ----------	0.042
$2V_X$ ----------	68 ±1° measured
Dispersion ----------	*r* > *v*, strong
Pleochroism ----------	*X* = light greenish brown *Y* = greenish brown *Z* = yellow-green *Y* ≥ *Z* > *X*
Optical orientation ----------	*X* : *c* = + 8° *Y* : *b* *Z* : *a* = + 33°

importance because glass is altered more easily than crystalline rock. Chemical composition of the host rock determines the availability of cations to form alteration minerals. Similarly, the cation and anion content of the fluids interacting with the rocks influences the composition of alteration minerals. Temperature may be the most significant factor in hydrothermal alteration because many of the chemical reactions require elevated temperatures. Pressures at the depths penetrated by most of the Newberry flank drill holes probably are not sufficient to greatly affect the hydrothermal alteration (Browne and Ellis, 1970). However, the effects of past higher pressure within the caldera, possibly owing to an overlying deep intracaldera lake, apparently resulted in higher fluid-inclusion homogenization temperatures than can be accounted for by the present geothermal system. Duration of the hydrothermal alteration at Newberry volcano is not precisely known. Hydrothermal alteration is undoubtedly occurring at the present time and likely extended back through the Holocene and probably into the late Pleistocene following the first volcanic eruptions from Newberry volcano.

Data on the factors controlling hydrothermal alteration are most complete for the USGS-N2 drill hole, which was studied in much greater detail than the others (Keith and Bargar, 1988). Conclusions based on the study of the USGS-N2 drill core may also be applicable to the other drill cores.

PERMEABILITY

On the flanks of Newberry volcano, pronounced lateral and vertical permeability were expected prior to drilling on the basis of the available information concerning the types of rocks that constitute this volcano (Black, 1983). Lava flows in the flank drill holes generally are vesicular at the top and bottom and dense in the interior; intervening intervals contain steeply dipping hairline fractures. Volcanic deposits between most lava flows include flow breccia, vitric tuff, lithic tuff, volcanic sandstone, and scoria or cinders. Fractures, vesicles, and void spaces between breccia fragments are partly to completely filled in the lower parts of the seven sampled drill holes located outside the caldera. Partial filling of the open spaces reduces permeability somewhat but does not completely eliminate the passage of water through the rocks. The upper parts of most of these flank drill holes contain unfilled open spaces. Ash and cinder layers and tuffaceous strata appear to have high permeability where unaltered; at deeper

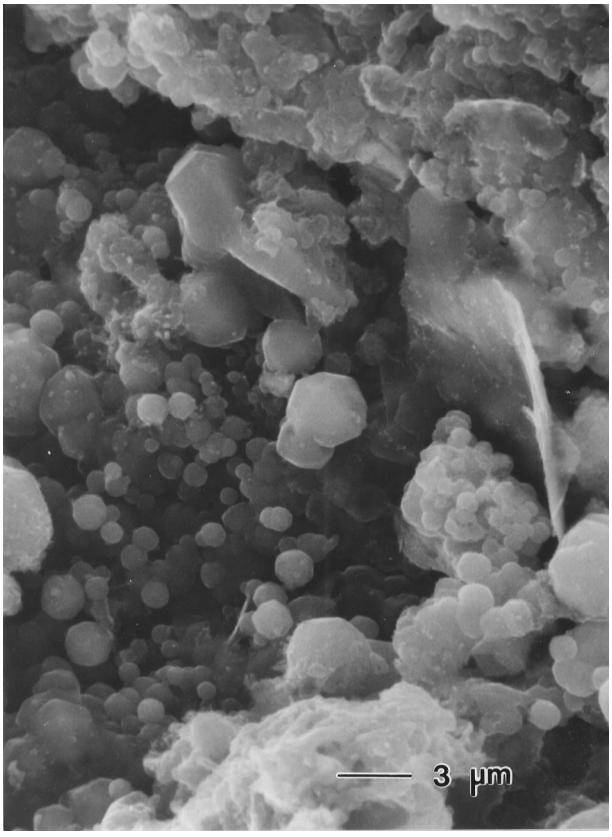

Figure 60.—Scanning electron micrograph of subhedral hydrogrossular crystals in volcaniclastic sandstone from 314.6-m depth in USGS-N2 drill core.

intervals some of these deposits are pervasively altered to clay, and the present permeability is presumably quite low.

MacLeod and Sammel (1982) indicated that vertical permeabilities within Newberry caldera are low except for fluid movement along faults, brecciated intrusion conduits, and ring fractures. They further suggest that lateral fluid flow is restricted to permeable zones having access to vertical fracture zones that contain water. In the USGS-N2 drill hole, several intervals appear to have maintained substantial subhorizontal permeability, allowing passage of both cold meteoric and thermal fluids (MacLeod and Sammel, 1982). High to moderate primary permeability was present in tuff, tuff breccia, and flow breccia, and, more locally, in highly vesicular parts of lava flows. Primary permeability within lava flows was very low because of the dense, fine-grained crystalline nature of the rocks. Consequently, the lava-flow interiors are much less altered than the more permeable rock units. Secondary permeability in dense lava flows was provided by hairline fractures that were rapidly sealed by deposition of hydrothermal minerals (mostly clay minerals), which resulted in a decrease or cessation of fluid flow through many rock units penetrated by the drill hole (especially below 697-m depth). These dense lava flows may form an impermeable cap for a deeper thermal convection system for the USGS-N2 area, as proposed by Sammel, Ingebritsen, and Mariner (1988).

Unfilled open spaces in the drill-chip samples suggest that permeability of most of the volcanic units penetrated by the RDO-1 drill hole is quite high. Below 307.9-m depth, hydrothermal minerals are deposited in open spaces and replace glass, which locally reduces the permeability. Vesicles may be completely filled by mordenite and chlorite, but bladed calcite and euhedral quartz crystals only partly fill open spaces and the rock remains pervious. The presence of unaltered pumice and the high permeability led Keith and others (1986) to suggest that the volcanic units penetrated by the RDO-1 drill hole are in an early stage of hydrothermal alteration.

TEMPERATURE

Temperature profiles for the seven drill holes on the flanks of Newberry caldera are shown in figs. 14, 16, 18, 19, 20, 23, and 26. Hydrothermal alteration minerals from drill holes GEO-N2, SF NC-01, and SF NC72-03 (figs. 16, 23, and 26), located on the west side of the volcano, include carbonate minerals, iron oxide, and smectite, in addition to higher temperature minerals such as quartz, mixed-layer chlorite-smectite, and chlorite. Measured bottom-hole temperatures for these drill holes are higher than 150˚C, and fluid-inclusion studies of calcite and quartz (figs. 17, 25, and 27) show that the past temperatures were significantly hotter than the present-day temperatures. This is especially true near the ring fracture, where fluid-inclusion homogenization temperatures (T_h) are mostly greater than 200˚C and some are above 300˚C.

Measured temperatures throughout the GEO-N1, GEO-N3, GEO-N4, and GEO-N5 drill holes, located on the south, north, east, and southwest flanks of the volcano, are less than 100˚C. Hydrothermal alteration mineralogy of the four drill holes is dominated by carbonate minerals, smectite, and iron oxide (figs. 14, 18, 19, and 20). The presence of these minerals and lack of higher temperature minerals, such as quartz, chlorite, or mixed-layer illite-smectite (except for a single sample at the bottom of the GEO-N3 drill hole), indicate that temperatures resulting from circulating thermal fluids probably never were very much hotter than the highest temperatures measured following drilling.

Temperatures in three other geothermal drill holes (USGS-N1, CE NB-3, and CE NB-4) on the flanks of Newberry volcano were below 100˚C. Hydrothermal alteration in these drill cores either is absent or is similar to that of the other low-temperature flank drill holes.

Measured temperatures in the USGS-N2 drill hole correlate closely with the temperature ranges indicated by hydrothermal minerals deposited throughout the drill core (fig. 5). Clay minerals are the best indications of temperature in the drill core. Smectite forms at lower temperatures; mixed-layer chlorite-smectite is deposited at intermediate temperatures; and chlorite precipitates at higher temperatures. However, these clay minerals are not strictly dependent on temperature. The structure of clay minerals may vary depending on whether the clay replaces glass or fills open spaces. Clay minerals with different structures may even coexist; mixed-layer chlorite-smectite in the groundmass interstices coexists with chlorite vesicle fillings at the bottom of the USGS-N2 drill core. Above 697-m depth, the hydrothermal alteration mineralogy suggests that temperatures probably have not been higher than the present measured temperatures except in the contact zones of the rhyodacite sill and thin dikes. Alteration is more intense in these zones, and the hydrothermal minerals were formed at higher temperatures than the secondary minerals in the adjacent tuffs. Alternatively, the present temperature maximum of about 100˚C between 400- and 425-m depth (fig. 5) suggests a lateral influx of thermal water. This water probably was as hot as the waters that deposited the chlorite-quartz-calcite-mordenite assemblage below 355-m depth in drill hole RDO-1 (Keith and others, 1986). Minimum fluid-inclusion T_h values for the lower part of drill hole USGS-N2 generally are warmer or nearly coincident with the measured temperature curve (fig. 11). However, the maximum T_h values of the liquid-rich fluid inclusions (as high as 367˚C at 931-m depth) greatly exceed the theoretical reference boiling-point curve. It appears likely that these high-T_h measurements resulted from increased pressure in the vicinity of the USGS-N2 drill hole at the time the fluid inclusions formed because of an overlying deep intracaldera lake. Lacustrine sediments between 290- and 320-m depth in the USGS-N2 drill core tend to support this hypothesis.

In the RDO-1 drill hole, smectite occurs between depths of about 308 m and 350 m where the temperature measured during drilling was about 80 to 150˚C (fig. 12). Chlorite was identified below the smectite zone where temperatures probably exceeded 158˚C (Keith and others, 1986). The present

aquifer temperature for the lower part of the RDO-1 drill hole is presumed to be greater than 158˚C (Black, Priest, and Woller, 1984). However, T_h measurements of liquid-rich fluid inclusions in hydrothermal quartz crystals at 335- and 381-m depth suggest that past temperatures were as high as about 252˚C (fig. 13). These high-T_h values plot above a reference theoretical boiling-point curve drawn to the present ground surface, and they appear to support the conclusion that the fluid inclusions formed at a time when the pressure was greater because of a deep intracaldera lake. Present temperatures in the RDO-1 drill hole are hotter than at the same depths in the USGS-N2 drill hole. The RDO-1 drill hole is closer to the southern ring fracture, which suggests that hot fluids probably move upward along the ring fractures and then spread out laterally within the caldera-fill deposits.

FLUID COMPOSITION

Complete chemical analyses of fluids from the seven flank Newberry geothermal drill holes are lacking. The only published water-chemistry data for these drill holes are given in Swanberg, Walkey, and Combs (1988) and Walkey and Swanberg (1990) who reported silica values for fluids collected from drill holes GEO-N1, GEO-N2, and GEO-N3. For drill hole GEO-N1, Swanberg, Walkey and Combs (1988) indicated that the use of fluid chemistry is inconclusive in locating depths of geothermal fluids. On the other hand, they indicated that SiO_2 data for the lower part of the GEO-N3 drill hole do show the presence of a geothermal fluid. Also, according to Swanberg, Walkey, and Combs (1988), low values for SiO_2 and other fluid constituents throughout much of the GEO-N3 drill hole suggest a dilution effect by a rain curtain of cold descending groundwater. High concentrations of SiO_2 and other fluid constituents for two parts of the GEO-N2 drill hole are interpreted by Walkey and Swanberg (1990) as showing the presence of pore fluids rather than circulating geothermal waters.

Melting-point temperature (T_m) measurements of fluid inclusions in quartz and calcite from the GEO-N2, SF NC-01, and SF NC72-03 drill cores are sparse (table 6). The limited data show values of 0.2, 0 to 0.4 , and 0.7 weight percent NaCl equivalent for the salinities of these respective drill holes. The data suggest a slight increase in the fluid salinity with decreasing distance toward the ring fracture system on the west side of Newberry volcano. Slightly saline fluid moving up the ring fractures would be quickly diluted by mixing with meteoric water during lateral movement outward from the caldera.

T_m values for fluid inclusions in two quartz samples from 381-m depth in the RDO-1 drill core indicate that the fluid salinities are in the range of about 0.7 to 1.2 weight percent NaCl equivalent. Near the bottom of the USGS-N2 drill hole, salinities of the fluid inclusions are less than 0.4 weight percent NaCl equivalent except for the lowermost sample at 931-m depth where the salinities are about 1.4 to 1.9 weight percent NaCl equivalent. The highest salinity water in USGS-N2 drill hole fluid-inclusion specimens appears to represent fluid that has been least diluted by meteoric water. The RDO-1 drill hole is closer than the USGS-N2 drill hole to the southern ring-fracture system, which might account for higher salinity, hotter fluids at shallower levels in the RDO-1 well.

Chemical analyses of water from the RDO-1 drill hole were not obtained before the well was abandoned. Dilute liquid (pH ranging from 5.3 to 6.1) sampled at the separator during a 20-hour flow test of the USGS-N2 drill hole (Sammel, 1981; Keith and others, 1984b) was steam condensate that probably originated as a mixture of steam and CO_2 in the bottom 2 m of the drill hole (Carothers, Mariner, and Keith, 1987; Ingebritsen and others, 1986). However, it is uncertain whether the steam originated from a true two-phase fluid system in the rock formation or resulted from flow testing. The high CO_2 content of the sampled bottom fluid may indicate high partial pressure of CO_2 (pCO_2) in porous zones throughout the USGS-N2 drill hole. This high pCO_2 could account for the scarcity of epidote (Browne, 1978) at higher temperatures near the bottom of the drill core, as well as the paucity of zeolites (Muffler and White, 1969) at lower temperatures in the glassy tuffs of the upper part of the drill core where zeolites would be expected to be abundant.

Fluids with elevated oxygen fugacity (fO_2) are suggested by the formation of iron oxide at permeable horizons (fig. 5) and by deposition of sulfate minerals—natrojarosite (not shown in fig. 5) and anhydrite—at depths where the influx of more oxidized thermal meteoric water has occurred. However, such oxidation can result from boiling fluids in an open system. At 250˚C, only 2 percent boiling is necessary to cause extensive separation of gases (H_2S and CO_2) from the liquid to the extent that the volume of vapor is equal to the volume of liquid, leaving the liquid in an oxidizing state (Ellis, 1970; Drummond and Ohmoto, 1985). On the basis of evidence from New Zealand (Tulloch, 1982), the bladed morphology of calcite crystals might indicate that boiling occurred in more permeable intervals of the USGS N-2 drill core. However, colorless bladed calcite crystals also occur near the bottom of the SF NC72-03 drill hole where the temperature does not appear to have ever exceeded the boiling point.

The occurrence of pyrrhotite has been attributed to high H_2 levels relative to H_2S and O_2 in the Broadlands geothermal field, New Zealand (Browne, 1970; Browne and Ellis, 1970), and at Krafla, Iceland (Steinthórsson and Sveinsbjörnsdóttir, 1981). At the Broadlands field, pyrrhotite crystallizes in low-permeability rocks in a chemical environment caused by confined boiling (Browne, 1970). At Krafla, the early deposition of pyrrhotite is interpreted as being indicative of the underlying magmatic processes (Steinthórsson and Sveinsbjörnsdóttir, 1981). Pyrrhotite occurs in low-permeability rocks of the lower part of the USGS-N2 drill core, as well as in the rhyodacite sill between 460- and 470-m depth. Fluid samples were not collected near the depth of the sill; however, magmatic sulfurous gases may have accompanied the intrusion of the rhyodacite sill and were confined to the

sill following its emplacement. Pyrrhotite in the rhyodacite sill is depleted in Fe and S relative to pyrrhotite in the deeper part of the drill core. This depletion, as well as alteration to pyrite and marcasite (and siderite), is caused by the introduction of thermal meteoric waters that are more oxidizing than the initial fluids. Pyrrhotite from the lower part of USGS-N2 does not appear to be altered. Sulfur isotope ($\partial^{34}S$) values of +1.6 parts per thousand for pyrite from 930-m depth and of +1.7 parts per thousand for pyrrhotite from 713-m depth (Keith and others, 1984b) are within the range of magmatic sulfur.

Bleaching due to hydrothermal alteration of the lowest 2 m of USGS-N2 drill core, as well as at the basal parts of the lower two basalt lava flows, occurs where two-phase fluids are present in a confined-boiling or vapor-dominated zone. The dense basalt lava flows form an impermeable barrier above the permeable basal flow breccias. Local boiling separates steam from the fluid, which is confined to the interflow breccia, and the low-pH steam condensate bleaches the rock at the base of the overlying lava flow. In contrast, the liquid part of the boiling fluid becomes increasingly oxidizing as indicated by a small amount of late iron oxide (hematite) deposition. Increased oxidation moves the fluid into the stability field for hematite, and pyrrhotite and pyrite are no longer deposited. Additional evidence for the increasingly oxidizing hydrothermal fluids is provided by the change from deposition of sulfide minerals to precipitation of late-forming sulfate (anhydrite).

ROCK COMPOSITION

Many published chemical analyses of surface rock samples that were collected on the flanks of Newberry volcano and within its caldera show that the volcano is composed of rocks ranging in composition from basalt to rhyolite (Williams, 1935; Higgins, 1973; MacLeod and Sherrod, 1988; and MacLeod and others, 1995). Higgins (1973) subdivided the rocks of Newberry volcano into four groups (precaldera, syncaldera, postcaldera, and flank) on the basis of the geologic history of the volcano and the geographic position of the rock specimens. However, he observed that chemical analyses of the rocks show two trends: (1) Iron-enriched precaldera rocks and (2) alkali-enriched postcaldera rocks. The differences are attributed to the presence or absence of lake water within the caldera of Newberry volcano. During precaldera conditions, the caldera region was filled by relatively dry lavas and volcaniclastic rocks, whereas the large depression at the volcano's summit has been occupied by lake water following formation of the caldera. A large volume of water overlying the magma chambers greatly affected the lavas' oxygen fugacities, which are influenced by pressure and water content, during differentiation of the magmas (Higgins, 1973). The volume of water trapped within the caldera may have been even greater in the past than that contained within the two present-day 50- and 80-m-deep lakes (MacLeod and others, 1995).

Chemical variation diagrams (Higgins, 1973, figs. 13, 14, and 15) show different trends for several elements in precaldera and postcaldera rocks. An AFM diagram of Higgins' data, as well as data from MacLeod and others (1995), shows a trend toward iron enrichment of the precaldera basaltic rocks and a second trend toward greater magnesium content of the postcaldera rocks (fig. 61). Superimposed on figure 61 are plots of the chemical analyses of rocks from the USGS-N2 drill hole (from table 2) and three flank drill holes (from table 7). This diagram shows that some of the basaltic rocks from the flank drill holes have compositions similar to those of the postcaldera rocks of Higgins (1973), and many of the basaltic USGS-N2 drill-core samples are even more iron enriched than those of Higgins' precaldera basalts. This double trend can also be seen in several other plots (figs. 62A, B, and C) involving different elements (including total Fe vs. MgO, MgO vs. SiO_2, and TiO_2 vs. SiO_2) as indicated by Higgins (1973). These three diagrams are among those that Higgins says are useful to show differences in major-element chemistries of precaldera and post caldera rocks at Newberry volcano.

Trends in the chemical diagrams of figures 61 and 62 appear to be influenced somewhat by hydrothermal alteration; for example, plots of oxides such as MgO and TiO_2 versus SiO_2 suggest some depletion of SiO_2 in the USGS-N2 drill core specimens when compared to the analyses of unaltered rocks given in Higgins (1973) and MacLeod and others (1995). Similarly, a plot of CaO versus SiO_2 (fig. 63) shows SiO_2 loss in most analyzed specimens from the USGS-N2 drill hole. SiO_2 loss coupled with some depletion of CaO in

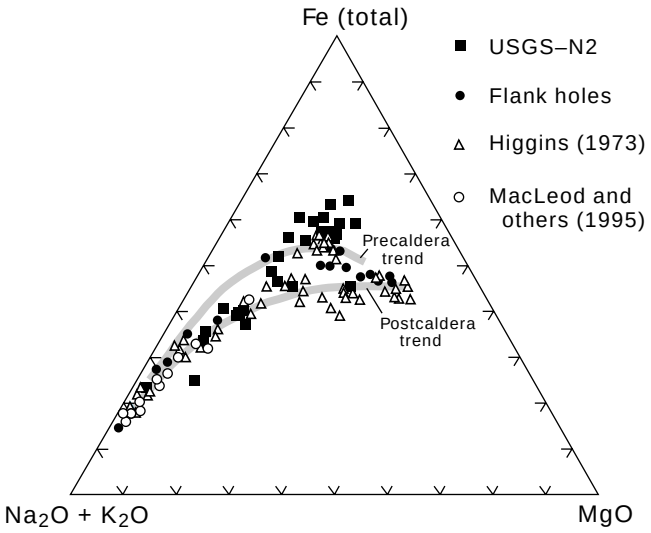

Figure 61.—AFM diagram showing chemical variation of basaltic to rhyolitic rocks from geothermal drill holes on flanks of Newberry volcano and within the caldera (USGS-N2), compared with analyses of surface rock samples from Higgins (1973) and MacLeod and others (1995). Lines showing precaldera and postcaldera trends from Higgins (1973, fig. 13B).

the USGS-N2 drill core samples could have resulted in the observed pronounced trend; however, loss of CaO does not appear to be very great in any of the analyzed USGS-N2 samples when compared with the MgO content of unaltered specimens (fig. 64A). MgO variation diagrams for other oxides of major elements (Al_2O_3, P_2O_5, K_2O, and MnO, figs. 64B, C, D, and E, respectively show minor to considerable scatter for both USGS-N2 and unaltered Newberry rocks that may reflect some gains or losses of these elements during hydrothermal alteration; however, the dispersion of data points more likely results from variations in MgO content of precaldera and postcaldera rocks. An MgO versus Na_2O diagram (fig. 64F) suggests some loss of Na_2O in many of the USGS-N2 drill core specimens. A plot of MgO versus TiO_2 (fig. 64G) suggests that the TiO_2 content of USGS-N2 core samples has not been affected by hydrothermal alteration. Instead, the plot appears to show separate precaldera and postcaldera trends that illustrate Higgins' (1973) concept of a two-trend chemical relation at Newberry volcano.

Evidence for hydrothermal alteration is suggested by the high water content of many of the USGS-N2 analyzed rocks, although several analyses of unaltered Newberry rocks from Higgins (1973) and MacLeod and others (1995) also contain substantial H_2O (fig. 65). One analyzed USGS-N2 specimen from 311.4-m depth contains nearly 22 weight percent total H_2O and is extensively hydrothermally altered. With only 39.5

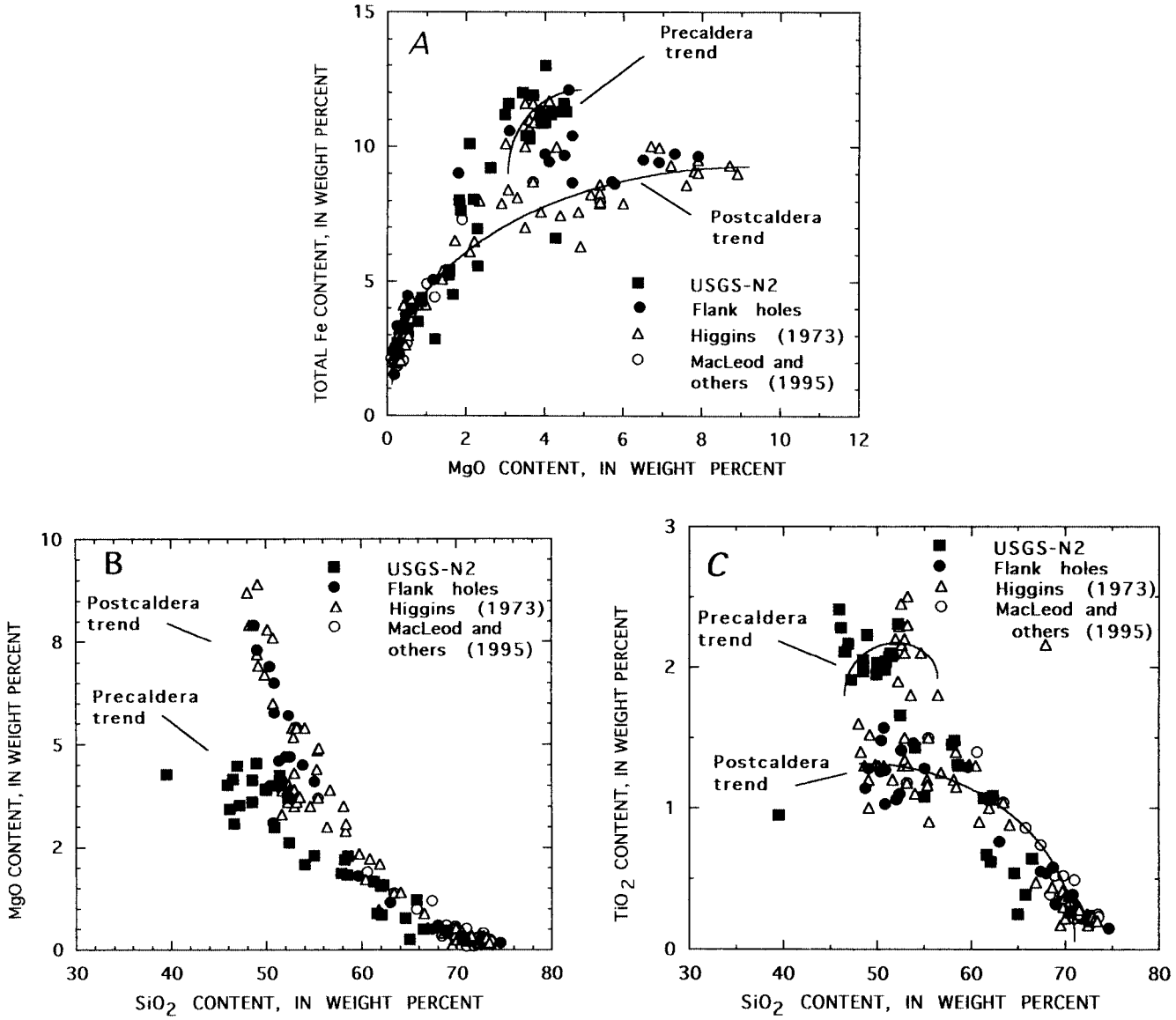

Figure 62.—Chemical variation diagrams for samples from USGS-N2 (table 2) and flank geothermal drill holes GEO-N1, GEO-N5, and SF NC72-03 (table 7) compared with analyses of surface rocks from Higgins (1973) and MacLeod and others (1995). A, MgO vs. total Fe. B, SiO_2 vs. MgO. C, SiO_2 vs. TiO_2.

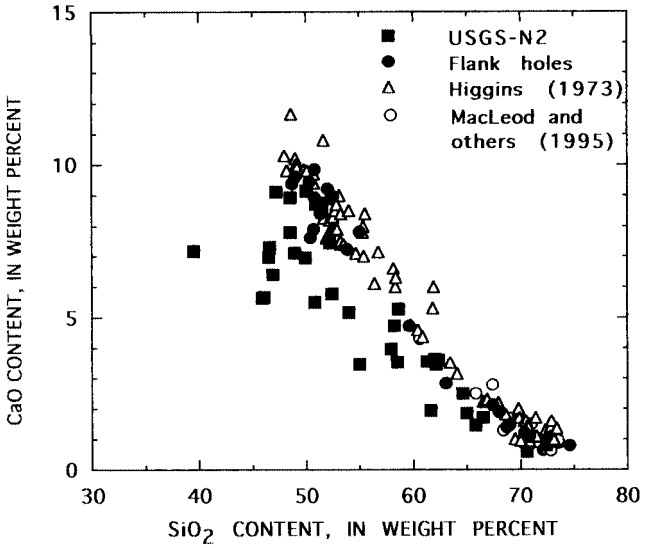

Figure 63.—SiO_2 vs. CaO diagram for chemical analyses of rocks from drill holes USGS-N2, GEO-N1, GEO-N5, and SF NC72-03 and outcrops at Newberry volcano. Diagram shows a loss of SiO_2 resulting from hydrothermal alteration in nearly all analyzed rocks from USGS-N2 core.

weight percent SiO_2, this core sample is extremely depleted in SiO_2 and plots alone on any SiO_2 variation diagram (see figs. 62B, C and 63).

Depiction of the chemical effects of hydrothermal alteration for both major and trace elements typically are shown on variation diagrams of the elements versus immobile elements appear to be little affected by hydrothermal alteration, although data are considerably scattered in some diagrams. Hydrothermal alteration has caused definite loss of Na_2O (F) and possibly some loss of K_2O (D) in rocks from USGS-N2 drill hole. G, MgO vs. TiO_2 diagram clearly shows the double trend of unaltered precaldera and postcaldera rocks.

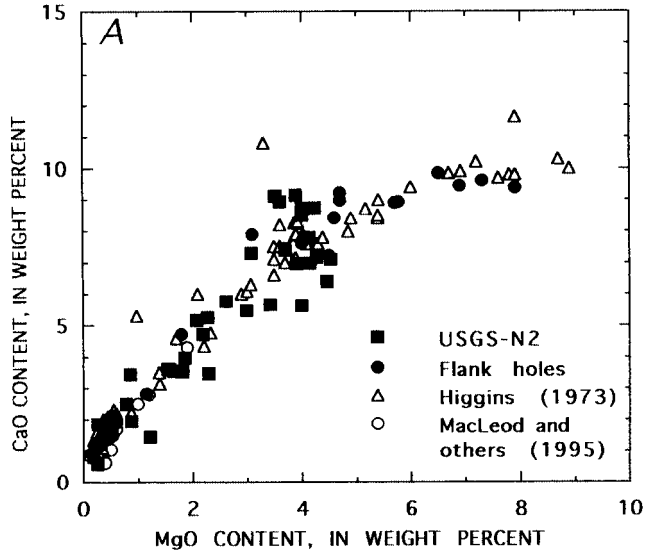

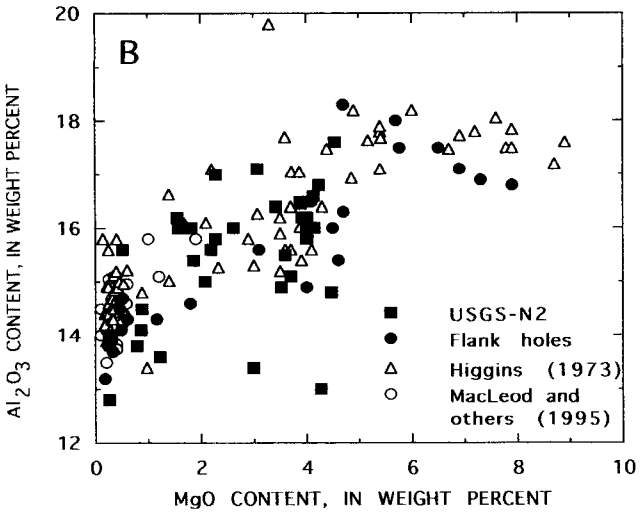

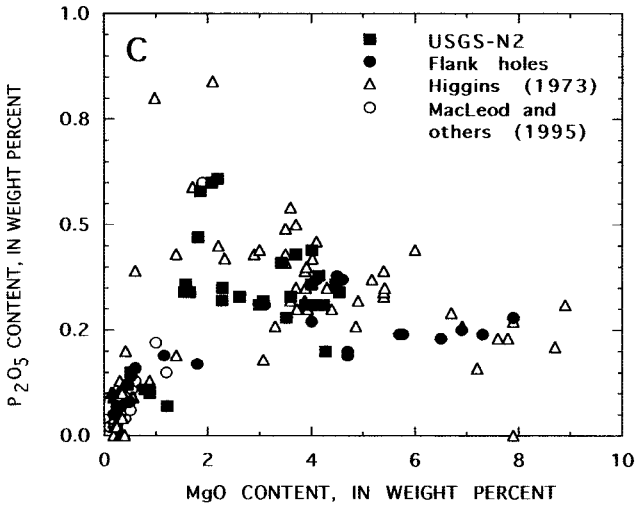

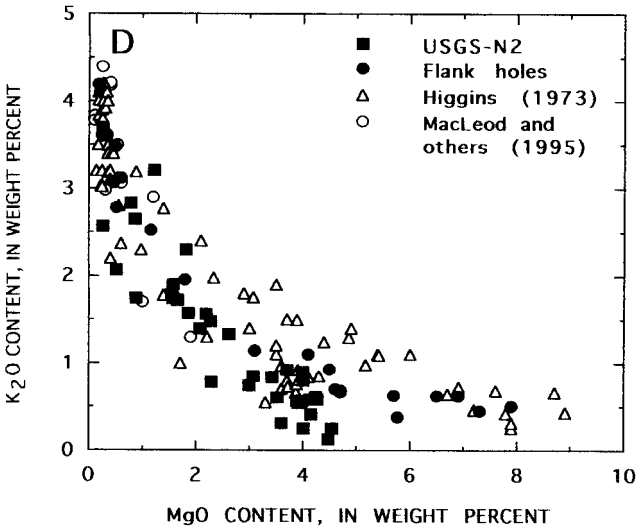

Figure 64.—MgO variation diagrams for chemically analyzed rocks from geothermal drill holes USGS-N2, GEO-N1, GEO-N5, and SF NC72-03 and outcrops at Newberry volcano. A, Comparison of samples from unaltered surface rocks with rocks from geothermal drill holes suggests that little if any CaO has been gained or lost owing to hydrothermal alteration. B-E, Al_2O_3, P_2O_5, K_2O, and MnO

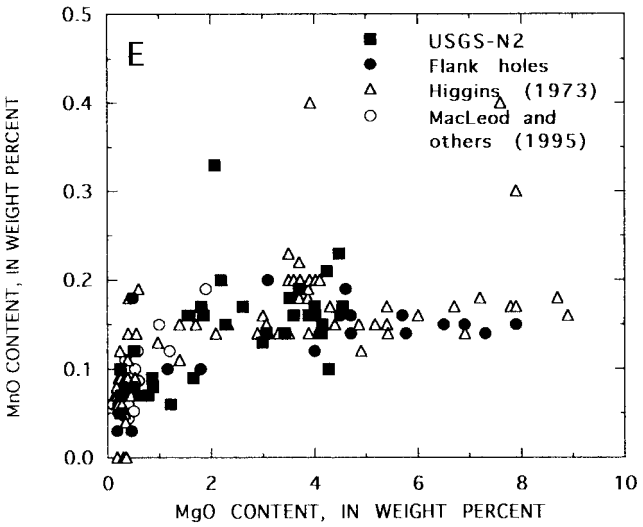

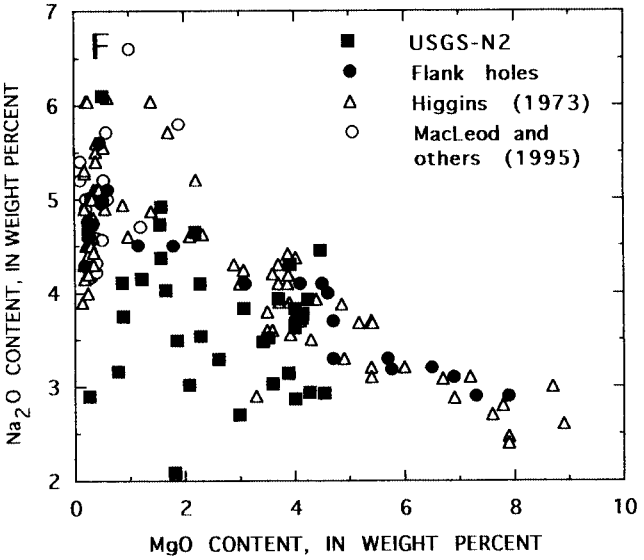

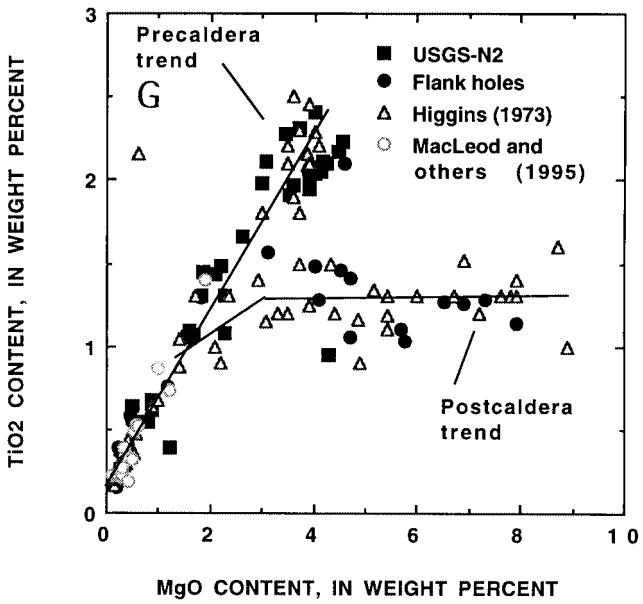

Figure 64.—Continued.

ments, such as Zr or TiO_2 (Finlow-Bates and Stumpfl, 1981). Several plots of Zr versus major and trace elements for the analyzed Newberry drill-core specimens (from tables 2, 3, 4, 7, and 13) were compared with chemical analyses of unaltered Newberry rocks from Higgins (1973) and MacLeod and others (1995). These diagrams show considerable scatter for Al_2O_3 (fig. 66A), apparent loss of SiO_2, Na_2O, and K_2O (figs. 66B, C, and D), and an increase in CaO (fig. 66E) and possibly total Fe(?) (fig. 66F) for several of the USGS-N2 analyzed drill-core specimens. The higher total Fe values in the Zr versus total Fe diagram (fig. 66F), the suggestion of a double trend in a Zr versus TiO_2 diagram (fig. 66G), and a concentration of data points at ~4 weight percent MgO on a Zr versus MgO diagram (fig. 66H) may reflect differences in precaldera versus postcaldera rock chemistry rather than hydrothermal alteration. Higgins (1973) indicated that the abundance of these three elements may have been strongly influenced by the presence (postcaldera) or absence (precaldera) of lake water within the caldera of Newberry volcano.

Higgins (1973) observed that on chemical variation diagrams of some trace elements (Ba, Rb, and Sr) the data plot into two groups according to whether the rocks are basalts or rhyolites rather than of precaldera or postcaldera origin. The data of Higgins (1973) and MacLeod and others (1995) are plotted along with data from tables 3, 4, and 13 of this report as Zr versus Ba, Cu, Rb, Sc, and Sr diagrams (figs. 66I, J, K, L, and M, respectively). Two groupings of the data from Higgins (1973) and MacLeod and others (1995) occur in these diagrams because of differences in trace elements in the basaltic and rhyolitic rocks. Many of the analyzed rocks from

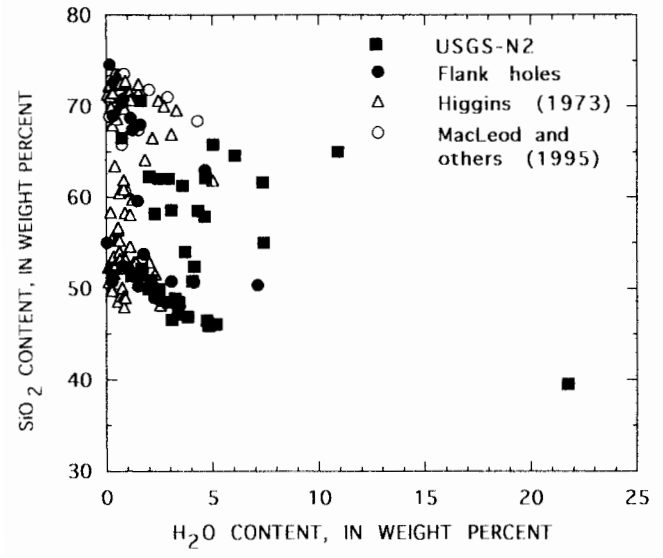

Figure 65.—H_2O vs. SiO_2 diagram for chemically analyzed rocks from Newberry volcano drill holes USGS-N2, GEO-N1, GEO-N5, and SF NC72-03. Diagram shows high H_2O content resulting from hydrothermal alteration in many USGS-N2 drill-core samples.

the USGS-N2 drill hole are of intermediate composition (see table 2), and the separation between basaltic and rhyolitic rocks on these diagrams is at least partly filled to form a nearly continuous differentiation series. Minor to considerable scatter in the data points of the Zr variation diagrams may indicate gains or losses of trace elements owing to hydrothermal alteration (Kristmannsdóttir, 1983); however, substantial scatter of data points also occurs for some trace elements in the unaltered rocks.

For drill holes GEO-N2, GEO-N3, GEO-N4, SF NC-01, and RDO-1, no major or trace element chemical analyses are presently available. Eighteen drill-core samples from drill hole GEO-N1 were analyzed for major elements along with two drill-core samples from each of the GEO-N5 and SF NC72-03 drill holes (table 7). Analyses of selected trace elements were obtained for three of the GEO-N1 samples and the four GEO-N5 and SF NC72-03 samples (table 13). A few of the analyzed drill-core samples from the GEO-N1 hole are slightly altered, but most of them were selected for analysis because they are relatively unaltered. Although the H_2O ($H_2O^+ + H_2O^-$ or LOI) content for four of the flank drill core specimens is greater than 3.0 (table 7; fig. 65), most chemical analyses of specimens from the flank drill holes plot with the unaltered surface-rock samples on SiO_2, MgO, and Zr variation diagrams (figs. 62, 63, 64, and 66). Figures 61 and 62 suggest that both precaldera and postcaldera rocks are represented in core specimens from the flank drill holes.

SUMMARY AND CONCLUSIONS

Numerous geothermal drill holes have been completed at Newberry volcano. Hydrothermal alteration of specimens from several of these drill holes has been studied, and the results are reported here and in previous publications (Bargar and Keith, 1984; Keith and others, 1984a, b; Keith and others, 1986; Bargar and Keith, 1986; Carothers, Mariner, and Keith, 1987; Keith and Bargar, 1988; Arestad, Potter, and Stewart, 1988; Bargar and others, 1990). Holes GEO-N1, GEO-N4, and GEO-N3 were located on the south, east, and north flanks of the volcano, respectively. Four wells (GEO-N5, GEO-N2, SF NC-01, and SF NC72-03) were drilled on the west flank of Newberry. Two drill holes (USGS-N2 and RDO-1) were completed within the volcano's caldera. Of the nine drill cores used for this study, only the USGS-N2 drill core was studied in great detail. The drill holes penetrated basaltic to rhyolitic rocks that have been affected by only mild post-emplacement temperatures (<100˚C) in the upper parts of USGS-N2 and RDO-1 and in all the flank drill holes except for the lower parts of GEO-N2, SF NC-01, and SF NC72-03. Alteration minerals deposited in open spaces (mostly carbonates, smectite, zeolites, iron oxide, and sulfates) reflect these low temperatures. Conversely, the lower parts of the three higher temperature west-flank drill holes (150 to 170˚C) and the two intracaldera drill holes (158+˚C in RDO-1 and 265˚C in USGS-N2) contain alteration miner-

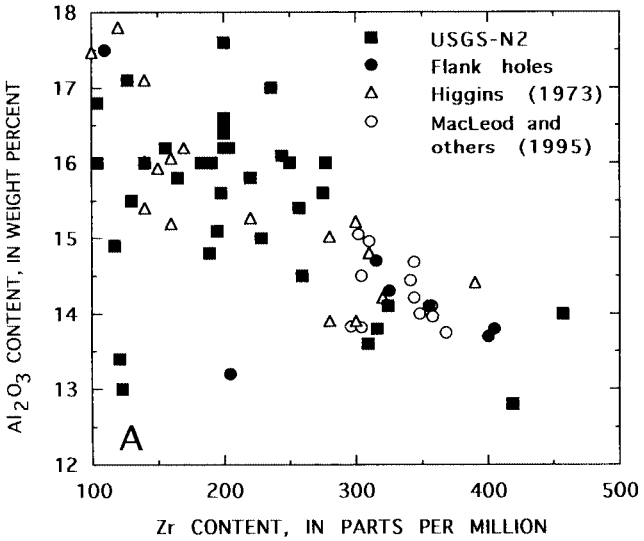

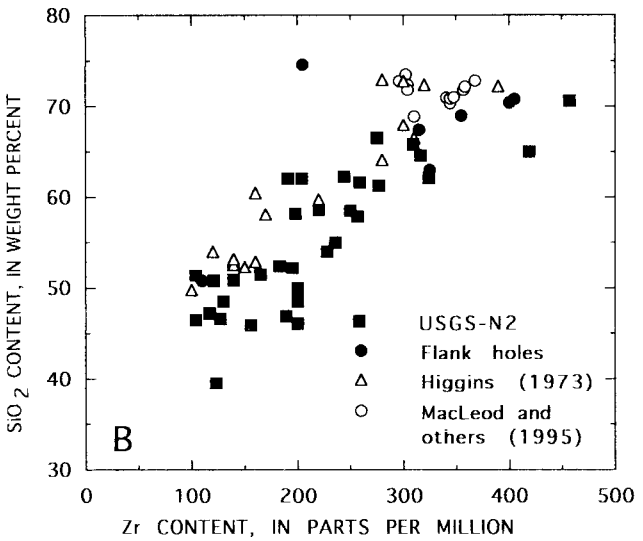

Figure 66.—Zr variation diagrams for major- and selected trace-element contents of rocks from Newberry volcano drill holes USGS-N2, GEO-N1, GEO-N5, and SF NC72-03. Diagrams A to H appear to show more depletion of SiO_2, Na_2O, and K_2O in many samples from USGS-N2 drill core than in samples of unaltered surface rocks. There may be both depletion and enrichment of Al_2O_3, CaO, and total Fe in USGS-N2 specimens; however, there is considerable scatter of data points in some of the diagrams. Scattering of data for total Fe, TiO_2, and MgO may be caused by differences in amounts of these elements in precaldera and postcaldera rocks; this also appears to be especially true for TiO_2. Trace-element contents of basaltic and rhyolitic analyses of Higgins (1973) plot in two groups according to rock type. Plots of trace elements in diagrams I to M reflect many rock compositions intermediate between basalt and rhyolite.

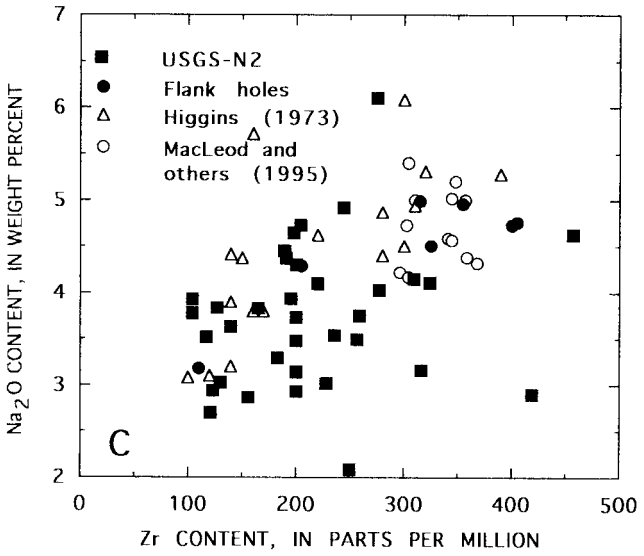

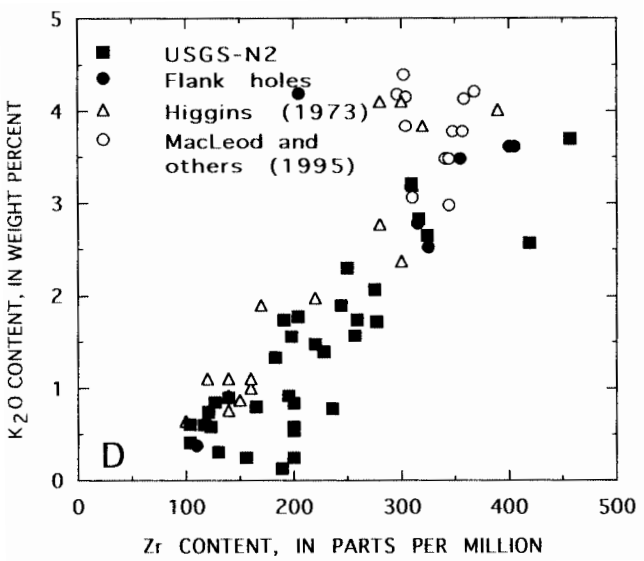

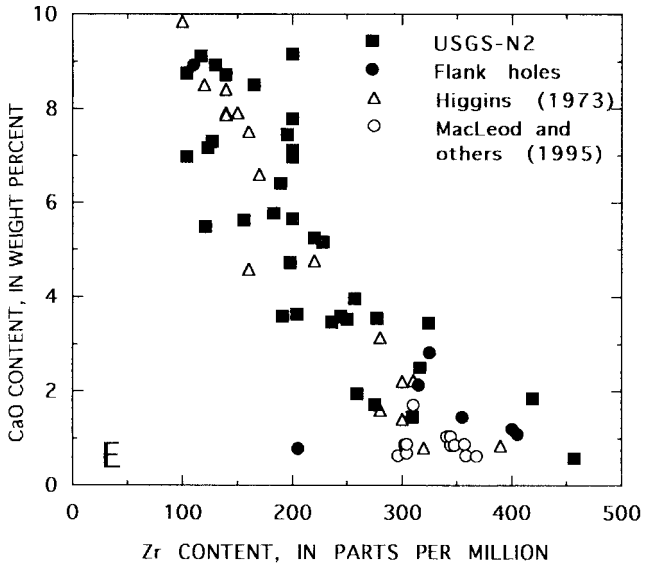

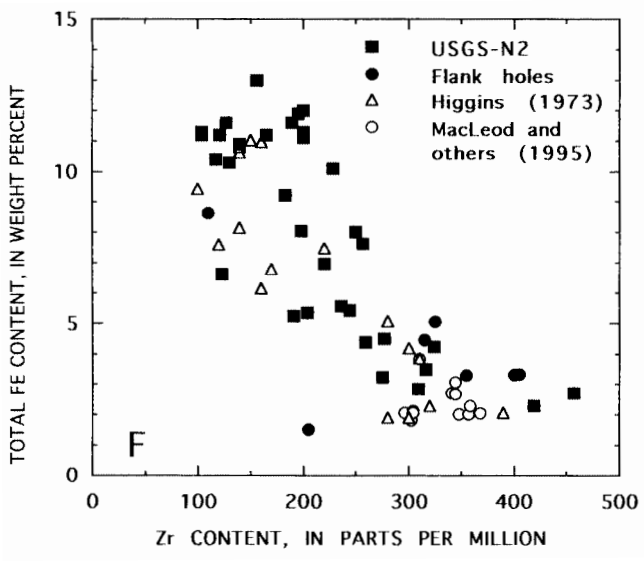

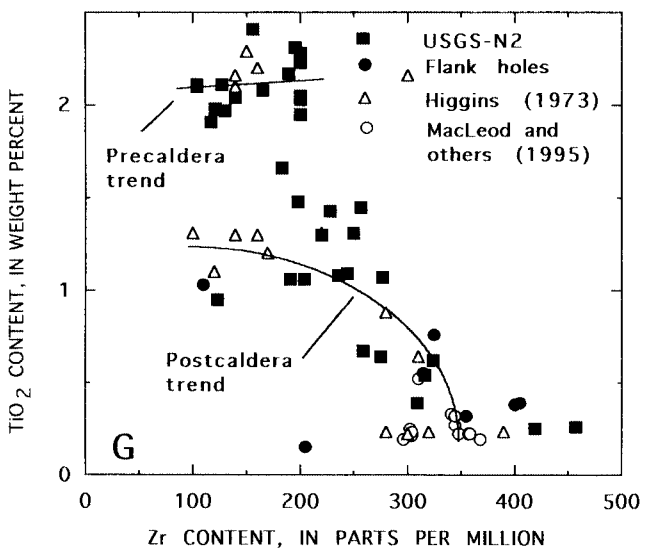

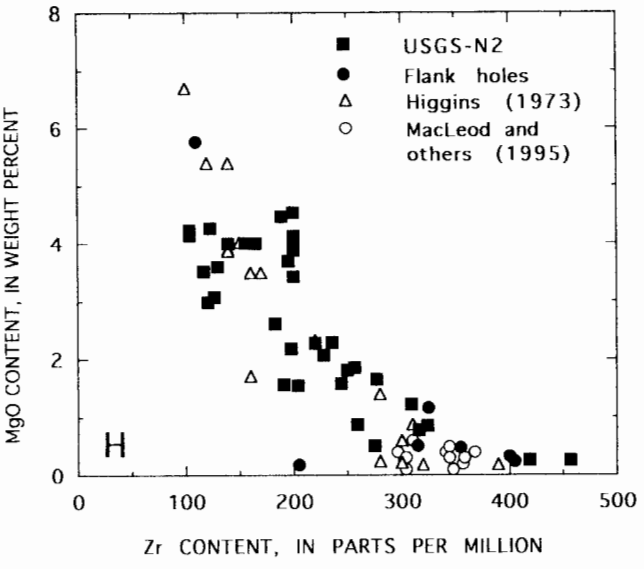

Figure 66.—Continued.

Figure 66.—Continued.

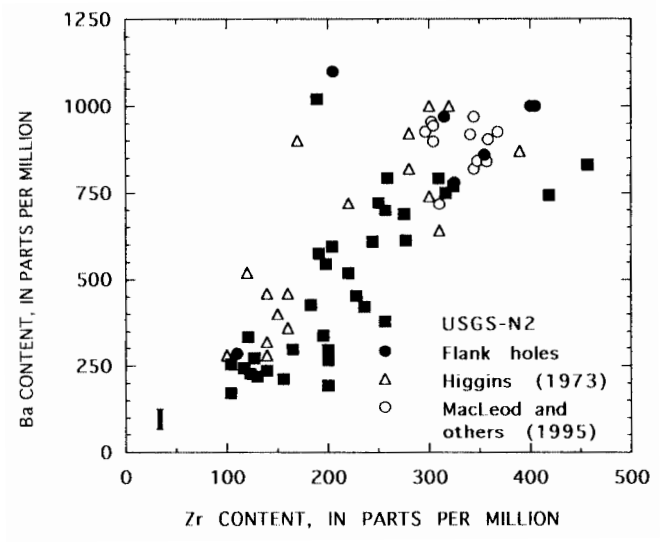

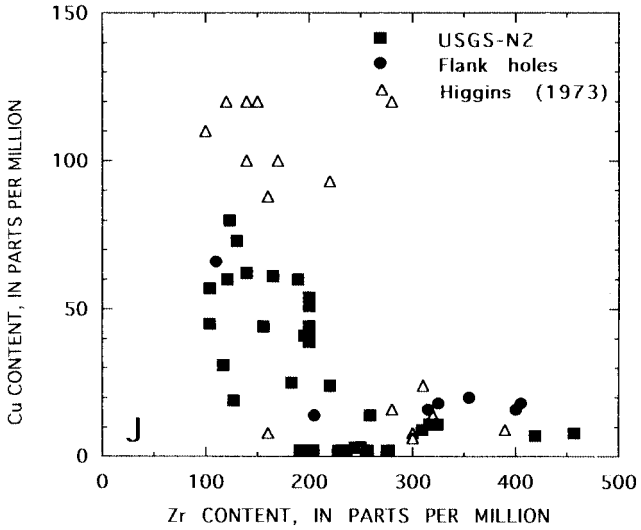

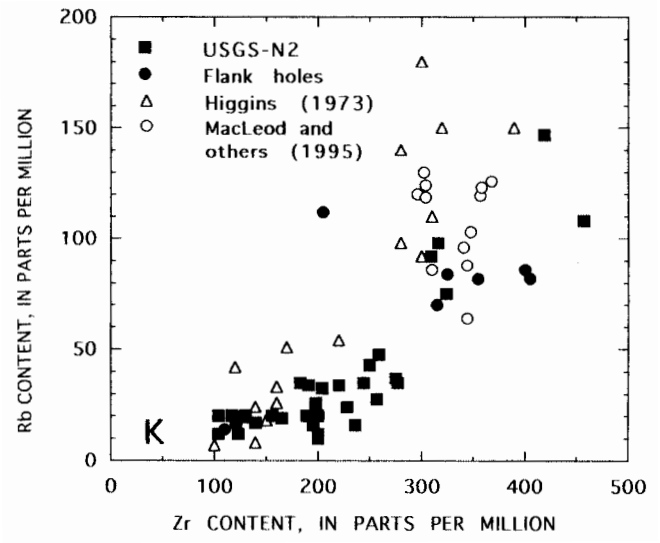

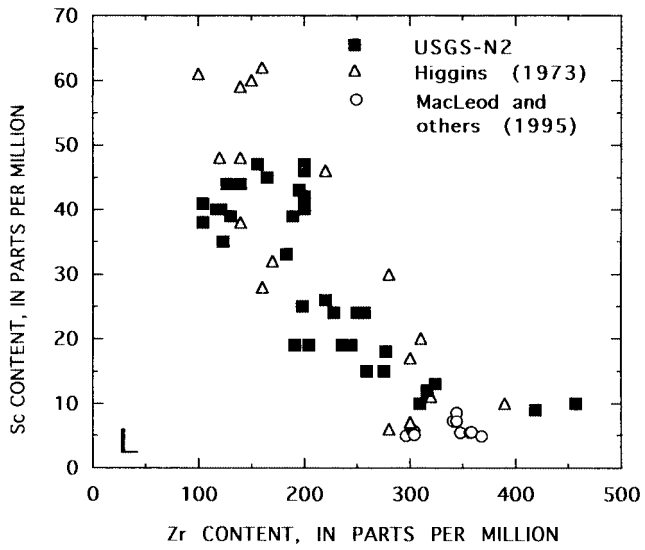

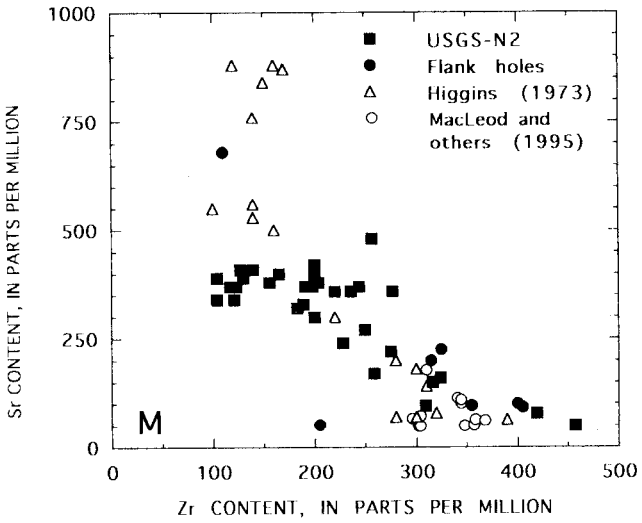

Figure 66.—Continued.

als (quartz, mixed-layer chlorite-smectite, and chlorite) that formed at significantly higher temperatures. The most notable difference in hydrothermal mineralogy between the two intracaldera drill holes is that in RDO-1 alteration minerals (chlorite, quartz, mordenite, pyrite, and pyrrhotite) occur at shallower depths than in USGS-N2 because of significantly higher temperatures at equivalent depths.

Nearly all of the hydrothermal alteration minerals identified in the Newberry drill cores are found in the USGS-N2 drill core. They first appear at a depth of 300 m, where scarce zeolites and smectite replace basaltic glass and the fractures contain late-formed calcite and aragonite. Measured temperatures above 300-m depth did not exceed 35˚C. Hydrothermal alteration between 300- and 697-m depth consists mainly of incipient alteration of pumice to smectite, but much glass remains hydrated and otherwise unaltered. A rhyodacite sill between 460- and 470-m depth intruded wet tuffs and caused local, more intense alteration of the enclosing tuffs to chlorite and mordenite, with open-space deposition of quartz, calcite, pyrrhotite, pyrite, and marcasite. A late hydrothermal heating event throughout the interval resulted in deposition of siderite along fractures, in pore spaces, and as cement in breccias. Measured temperatures between 320- and 697-m depth increase from 35 to 100˚C at 410-m depth and then show a reverse thermal gradient to 74°C at 550-m depth. Temperatures range from 74 to 85˚C at depths from 550 to 675 m.

Hydrothermal alteration from 697-m depth to the bottom of the USGS-N2 drill hole at a depth of 932 m increases with depth and increasing temperature along a steep conductive thermal gradient from 110°C at 697-m depth to 265˚C at 930-m depth. Hydrothermal minerals in this zone are mainly smectite, mixed-layer chlorite-smectite, pyrrhotite, pyrite, calcite, and quartz. As temperatures increase toward the bottom of the drill hole, mixed-layer chlorite-smectite and chlorite become the dominant clay minerals and smectite abundance decreases. Where different clay structures coexist, the mixed-layer clay replaces groundmass and lines thin irregular fractures, whereas the chlorite coats vesicles and appears to be a later deposit. Scarce amounts of epidote, anhydrite, and hematite are late-stage minerals near the base of the section and are compatible with the measured temperatures of 250 to 265˚C. In the highly altered rocks at the bottom of the drill hole, primary plagioclase is partly replaced by calcite and illite.

The most important controls of alteration in USGS-N2 are permeability, temperature, and fluid composition. The massive subhorizontal lava flows that make up the lower part of the section are little altered except where locally fractured or vesiculated. Hydrothermal fluids have clearly been confined mainly to the subhorizontal interflow breccias and volcaniclastic layers.

T_h of fluid inclusions in quartz and calcite from the lower part of the USGS-N2 drill hole range between the present measured temperatures and about 367˚C with no evidence of boiling. However, mineral assemblages, textures, and isotopic data indicate that temperatures throughout the drill hole could not have been significantly hotter than at present for a long period of time. A probable explanation for the hotter T_h is that the system attained higher temperatures because of greater pressure of an overlying deep intracaldera lake at the time the fluid inclusions formed. Lacustrine sediments in the upper part of the drill hole attest to the presence of a past overlying lake. Differences in the chemistry of precaldera and postcaldera rocks at Newberry volcano also are attributed to the presence of an intracaldera lake overlying the magma chambers (Higgins, 1973).

According to models of the caldera hydrology, meteoric waters in the shallow porous caldera fill in the vicinity of the USGS-N2 drill hole have maintained cool temperatures except for the incursion of thermal fluids between 350- and 500-m depth (Sammel, Ingebritsen, and Mariner, 1988). These thermal fluids apparently spread laterally from an upflow zone such as the caldera ring fracture or a feeder dike. The fluids produced from the bottom 2 m of the USGS-N2 drill hole were probably a mixture of steam and CO_2, along with a significant amount of H_2S (Sammel, 1981). Isotope studies of the fluids produced from the bottom of the drill hole indicate that the liquid was a steam condensate (Carothers, Mariner, and Keith, 1987). The isotope studies, together with modeling studies of the fluids (Sammel, Ingebritsen, and Mariner, 1988), support the hypothesis that the fluid encountered at the bottom of the hole during drilling was largely steam and CO_2. If two-phase fluids existed in the flow breccia and vesicular basalt of the basal 2 m of the drill hole, such fluids probably were confined by the overlying impermeable lava flows. The flow breccia at 910-m depth appears to have contained similar two-phase fluids. Hydrothermal mineralogy studies indicate that hydrothermal fluids at the bottom of the USGS-N2 drill hole are evolving to a more oxidizing state.

Comparison of chemically analyzed rocks from the USGS-N2 drill hole with published analyses of unaltered surface rocks (Higgins, 1973; MacLeod and others, 1995) show an insignificant to moderate decrease in SiO_2, Na_2O, and K_2O, as well as possible slightly increased total Fe, and CaO; MnO, and MgO appear to be unchanged, while considerable scatter of the data points on chemical variation diagrams of Al_2O_3 and P_2O_5 may indicate both loss and gain of these elements. H_2O, CO_2, and S contents of some of the USGS-N2 drill-hole analyses range to significantly greater values than the unaltered surface rocks. Some of the trends observed on chemical variation diagrams for major elements apparently result from differences between precaldera and postcaldera lavas as explained by Higgins (1973). Conversely, Higgins (1973) found that trace-element analyses for basaltic and rhyolitic rocks plotted in distinctly separate fields. Trace-element analyses for rocks of intermediate composition from the geothermal drill holes appear to complete the differentiation trend.

The age of the hydrothermal system penetrated by the USGS-N2 drill hole is unknown. The latest caldera collapse occurred more than 10,000 years ago (MacLeod and Sammel, 1982). Local intracaldera volcanic activity since that time

indicates ongoing although probably intermittent thermal injections into the caldera fill; the hydrothermal system below 697-m depth could have developed prior to the latest caldera collapse. Petrologic and mineralogic studies of the USGS-N2 geothermal system shows that it is a young evolving system associated with the evolution of Newberry volcano. The 1.35-ka age of the youngest dated silicic lava and the numerous small volcanic features of post-Mazama age within the caldera (MacLeod, Sherrod, and Chitwood, 1982) indicate an active volcanic system. The youth, large volume of both silicic and basaltic volcanic rocks, and the thermal springs of Newberry volcano provide a favorable setting for a significant geothermal system (MacLeod, Walker, and McKee, 1975). Except for much deeper (3,000 m), slightly hotter (270˚C) temperatures at Meager Mountain in British Columbia, Canada (Souther, 1985), the 265˚C temperature at 930-m depth at the USGS-N2 drill hole is as yet the highest temperature reported in a Cascades geothermal system. The volume of geothermal fluids may be restricted, however, because of localization within narrow interflow zones.

REFERENCES CITED

Achauer, U., Evans, J.R., and Stauber, D.A., 1988, High-resolution seismic tomography of compressional wave velocity structure at Newberry volcano, Oregon Cascade Range: Journal of Geophysical Research, v. 93, no. B9, p. 10,135-10,147.

Arestad, J.F., Potter, R.W., II, and Stewart, G.E., 1988, Stratigraphic test drilling in the Newberry crater KGRA, Oregon: Geothermal Resources Council Bulletin, v. 17, no. 10, p. 3-8.

Arnold, R.G., 1966, Mixtures of hexagonal and monoclinic pyrrhotite and the measurement of the metal content of pyrrhotite by X-ray diffraction: American Mineralogist, v. 51, p. 1,221-1,227.

Bacon, C.R., 1983, Eruptive history of Mount Mazama and Crater Lake caldera, Cascade Range, U.S.A.: Journal of Volcanology and Geothermal Research, v. 18, p. 57-115.

Baedecker, P.A., ed., 1987, Methods for geochemical analysis: U.S. Geological Survey Bulletin 1770, 156 p.

Bailey, S.W., 1982, Nomenclature for regular interstratifications: American Mineralogist, v. 67, p. 394-398.

Bargar, K.E., 1980, Lithologic log of drill cuttings for Northwest Geothermal Corporation drill hole at Lost Creek near Mount Hood, Oregon: U.S. Geological Survey Open-File Report 80-1166, 19 p.

——1990, Hydrothermal alteration in geothermal drill hole CTGH-1, High Cascade Range, Oregon: Oregon Geology, v. 52, no. 4, p. 75-81.

Bargar, K.E., and Beeson, M.H., 1981, Hydrothermal alteration in research drillhole Y-2, Lower Geyser Basin, Yellowstone National Park, Wyoming: American Mineralogist, v. 66, p. 473-490.

——1984, Hydrothermal alteration in research drill hole Y-6, Upper Firehole River, Yellowstone National Park, Wyoming: U.S. Geological Survey Professional Paper 1054- B, 24 p.

——1985, Hydrothermal alteration in research drill hole Y-3, Lower Geyser Basin, Yellowstone National Park, Wyoming: U.S. Geological Survey Professional Paper 1054-C, 23 p.

Bargar, K.E., Beeson, M.H., and Keith, T.E.C., 1981, Zeolites in Yellowstone National Park: The Mineralological Record, v. 12, p. 29-38.

Bargar, K.E., Erd, R.C., Keith, T.E.C., and Beeson, M.H., 1987, Dachiardite from Yellowstone National Park, Wyoming: Canadian Mineralogist, v. 25, p. 475-483.

Bargar, K.E., and Fournier, R.O., 1988, Effects of glacial ice on subsurface temperatures of hydrothermal systems in Yellowstone National Park, Wyoming: Fluid-inclusion evidence: Geology, v. 16, p. 1077-1080.

Bargar, K.E., and Keith, T.E.C., 1984, Hydrothermal alteration mineralogy in Newberry 2 drill core, Newberry volcano, Oregon: U.S. Geological Survey Open-File Report 84-92, 62 p.

——1986, Hydrothermal mineralization in GEO N-1 drill hole, Newberry volcano, Oregon: U.S. Geological Survey Open-File Report 86-440, 12 p.

Bargar, K.E., Keith, T.E.C., and Beeson, M.H., 1993, Hydrothermal alteration in the Mount Hood area, Oregon: U.S. Geological Survey Bulletin 2054, 70 p.

Bargar, K.E., Keith, T.E.C., Swanberg, C.A., and Walkey, W.C., 1990, Hydrothermal alteration in cores from geothermal drill holes on the flanks of Newberry volcano, Oregon [abs.]: Eos, Transactions, American Geophysical Union, v. 71, no. 43, p. 1691.

Bird, D.K., Schiffman, P., Elders, W.A., Williams, A.E., and McDowell, S.D., 1984, Calc-silicate mineralization in active geothermal systems: Economic Geology, v. 79, p. 671-695.

Black, G.L., 1983, Newberry hydrology, in Priest, G.R., Vogt, B.F., and Black, G.L., eds., Survey of potential geothermal exploration sites at Newberry volcano, Deschutes County, Oregon: Oregon Department of Geology and Mineral Industries Open-File Report O-83-3, p. 28-36.

Black, G.L., Priest, G.R., and Woller, N.M., 1984, Temperature data and drilling history of the Sandia National Laboratories well at Newberry caldera: Oregon Geology, v. 46, no. 1, p. 7-9.

Blackwell, D.D., Black, G.L., and Priest, G.R., 1981, Geothermal gradient data (1978): Oregon Department of Geology and Mineral Industries Open-File Report O-81-3A, 63 p.

Blackwell, D.D., Hull, D.A., Bowen, R.G., and Steele, J.L., 1978, Heat flow of Oregon: Oregon Department of Geology and Mineral Industries Special Paper 4, 42 p.

Bodnar, R.J., Reynolds, T.J., and Kuehn, C.A., 1985, Fluid-inclusion systematics in epithermal systems, *in* Berger, B.R., and Bethke, P.M., eds., Geology and geochemistry of epithermal systems: Society of Economic Geologists Reviews in Economic Geology, v. 2, p. 73-97.

Bodnar, R.J., and Sterner, S.M., 1984, Synthetic fluid inclusions in natural quartz: I. Compositional types synthesized and applications to experimental geochemistry: Geochimica et Cosmochimica Acta, v. 48, p. 2,659-2,668.

Browne, P.R.L., 1969, Sulfide mineralization in a Broadlands geothermal drill hole, Taupo Volcanic Zone, New Zealand: Economic Geology, v. 64, p. 156-159.

——1970, Hydrothermal alteration as an aid in investigating geothermal fields, *in* United Nations Symposium on the development and utilization of geothermal resources, Pisa, Italy, September 22-October 1, 1970, Proceedings: Pisa, Italy, Istituto Internazionale per le Ricerche Geotermiche, Geothermics, Special Issue 2, p. 564-570.

——1978, Hydrothermal alteration in active geothermal fields: Annual Reviews in Earth and Planetary Sciences, v.6, p. 229-250.

Browne, P.R.L., and Ellis, A.J., 1970, The Ohaki-Broadlands hy-

drothermal area, New Zealand, mineralogy and related geochemistry, American Journal of Science, v. 269, p. 97-131.

Browne, P.R.L., and Lovering, J.F., 1973, Composition of sphalerites from the Broadlands Geothermal Field and their significance to sphalerite geothermometry and geobarometry: Economic Geology, v. 68, p. 381-387.

Carothers, W.W., Mariner, R.H., and Keith, T.E.C., 1987, Isotope geochemistry of minerals and fluids from Newberry volcano, Oregon: Journal of Volcanology and Geothermal Research, v. 31, p. 47-63.

Catchings, R.D., and Mooney, W.D., 1988, Crustal structure of east central Oregon: relation between Newberry volcano and regional crustal structure: Journal of Geophysical Research, v. 93, no. B9, 10,081-10,094.

Cavarretta, G., Gianelli, G., and Puxeddu, M., 1980, Hydrothermal metamorphism in theLarderello Geothermal Field:Geothermics, v. 9, p. 297-314.

Collins, S.D., 1991, Newberry National Volcanic Monument making a consensus process work: Geothermal Resources Council Transactions, v. 15, p. 417-424.

Coombs, D.S., 1955, X-ray observations on wairakite and non-cubic analcime: Mineralogical Magazine, v. 30, p. 699-708.

Craig, J.R., and Scott, S.D., 1974, Sulfide phase equilibria, *in* Ribbe, P.H., ed., Sulfide mineralogy: Mineralogical Society of America Short Course Notes, v.1, p. CS1-CS110.

Deer, W.A., Howie, R.A., and Zussman, J., 1966, An introduction to the rock-forming minerals: London, Longman, 528 p.

Donnelly-Nolan, J.M., 1988, A magmatic model of Medicine Lake volcano, California: Journal of Geophysical Research, v. 93, no. B5, p. 4,412-4,420.

Drummond, S.E., and Ohmoto, H., 1985, Chemical evolution and mineral deposition in boiling hydrothermal systems: Economic Geology, v. 80, p. 126-147.

Dunn,P.J.,Rouse, R.C., and Norberg, J.A., 1978, Hydroxyapophyllite, a new mineral, and a redefinition of the apophyllite group: I. Description, occurrences, and nomenclature: American Mineralogist, v. 63, p. 196-202.

Earth Science Laboratory, 1986, Announcement of open file data release: University of Utah Research Institute, Salt Lake City, Utah, Cascades Newsletter, no. 2, 2 p.

——1987, Announcement of open file data release: University of Utah Research Institute, Salt Lake City, Utah, Cascades Newsletter, no. 3, 3 p.

Ellis, A.J., 1970, Quantitative interpretation of chemical characteristics of hydrothermal systems, *in* United Nations Symposium on the Development Utilization of Geothermal Resources, Pisa, Italy, September 22-October 1, 1970, Proceedings: Pisa, Italy, Istituto Internazionale per le Ricerche Geotermiche, Geothermics,Special Issue2,p.516-528.

Finlow-Bates, T., and Stumpfl, E.F., 1981, The behavior of so-called immobile elements in hydrothermally altered rocks associated with volcanogenic submarine-exhalative ore deposits: Mineralium Deposita, v. 16, p. 319-328.

Fitterman, D.V., Stanley, W.D., and Bisdorf, R.J., 1988, Electrical structure of Newberry volcano, Oregon: Journal of Geophysical Research, v. 93, no. B9, p. 10,119-10,134.

Friedman, Irving, 1977, Hydration dating of volcanism at Newberry crater, Oregon: U.S. Geological Survey Journal of Research, v. 5, no. 3, p. 337-342.

Frondel, C., and Bauer, L.H., 1955, Kutnahorite: a manganese dolomite, $CaMn(CO_3)_2$: American Mineralogist, v. 40, p. 748-760.

Gabrielson, O., and Sundius, N., 1965, Ca-rich kutnahorite from Langban, Sweden: Arkiv för Mineralogi och Geologi, v. 4, p. 287-289.

Gettings, M.E., and Griscom, Andrew, 1988, Gravity model studies of Newberry volcano, Oregon: Journal of Geophysical Research, v. 93, no. B9, p. 10,109-10,118.

Gottardi, G., and Galli, E., 1985, Natural zeolites: Berlin, Springer-Verlag, 409 p.

Grim, R.E., 1968, Clay mineralogy: San Francisco, McGraw-Hill Book Co., 596 p.

Griscom, Andrew, and Roberts, C.W., 1983, Gravity and magnetic interpretation of Newberry volcano, Oregon, *in* Priest, G.R., Vogt, B.F., and Black, G.L., eds., Survey of potential geothermal exploration sites at Newberry volcano, Deschutes County, Oregon, Oregon Department of Geology and Mineral Industries Open-File Report O-83-3, p. 68-81.

Hedenquist, J.W., and Henley, R.W., 1985, The importance of CO_2 on freezing point measurements of fluid inclusions: evidence from active geothermal systems and implications for epithermal ore deposition: Economic Geology, v. 80, p. 1379-1406.

Heller, L., and Taylor, H.F.W., 1956, Crystallographic data for the calcium silicates: London, Her Majesty's Stationery Office, 79 p.

Hemley, J.J., Hostetler, P.B., Gude, A.J., and Mountjoy, W.T., 1969, Some stability relations of alunite: Economic Geology, v. 64, p. 599-612.

Hey, M.H., 1954, A new review of the chlorites: Mineralogical Magazine, v. 30, p. 277-292.

Higgins, M.W., 1973, Petrology of Newberry volcano, central Oregon: Geological Society of America Bulletin, v. 84, no. 2, p. 455-488.

Honda, S., and Muffler, L.J.P., 1970, Hydrothermal alteration in core from research drill hole Y-1, Upper Geyser Basin, Yellowstone National Park, Wyoming: American Mineralogist, v. 55, p. 1714-1737.

Horton, D.G., 1985, Mixed-layer illite/smectite as a paleotemperature indicator in the Amethyst vein system, Creede district, Colorado, USA: Contributions to Mineralogy and Petrology, v. 91, p. 171-179.

Hower, J., 1981, X-ray diffraction identification of mixed-layer clay minerals, *in* Longstaffe, F.J., ed., Short course in clays and the research geologist: Toronto, Mineralogical Association of Canada, Short course handbook 7, p. 39-59.

Hurlbut, C.S., Jr., 1971, Dana's manual of mineralogy (18th ed.): New York, John Wiley & Sons, Inc., 579 p.

Ingebritsen, S.E., Carothers, W.W., Mariner, R.H., Gudmundsson, J.S., and Sammel, E.A., 1986, Flow testing of the Newberry 2 research drill hole, Newberry volcano, Oregon: U.S. Geological Survey Water Resources Investigations Report 86-4133, 23 p.

Jakobsson S.P., and Moore, J.G., 1986, Hydrothermal minerals and alteration rates at Surtsey volcano, Iceland: Geological Society of America Bulletin, v. 97, p. 648-659.

Keith, T.E.C., and Bargar, K.E., 1988, Petrology and hydrothermal mineralogy of U.S. Geological Survey Newberry 2 drill core from Newberry Caldera, Oregon: Journal of Geophysical Research, v. 93, no. B9, p. 10,174-10,190.

Keith, T.E.C., Bargar, K.E., Howe, S.S., Carothers, W.W., and Barnes, Ivan, 1984a, Mineralogical studies of the hydrothermal system in Newberry Volcano drill hole 2, Oregon: Geothermal Resources Council, Transactions, v. 8, p. 125-128.

Keith, T.E.C., and Boden, J.R., 1981, Volcanic stratigraphy and alteration mineralogy of drill cuttings from EWEB 1 drill hole, Linn County, Oregon: U.S. Geological Survey Open-File Report 81-250, 11 p.

Keith, T.E.C., Gannett, M.W., Eichelberger, J.C., and Waibel, A.F., 1986, Lithology and hydrothermal alteration of drill hole RDO-1, Newberry caldera, Oregon: Oregon Geology, v. 48, no. 9, p. 103-107, 110.

Keith, T.E.C., Mariner, R.H., Bargar, K.E., Evans, W.C., and Presser, T.S., 1984b, Hydrothermal alteration in Oregon's Newberry volcano No. 2, fluid chemistry and secondary mineral distribution: Geothermal Resources Council Bulletin, v. 13, no. 4, p. 9-17.

Keith, T.E.C., and Muffler, L.J.P., 1978, Minerals produced during cooling and hydrothermal alteration of ash-flow tuff from Yellowstone drill hole Y-5: Journal of Volcanology and Geothermal Research, v. 3, p. 373-402.

Keith, T.E.C., White, D.E., and Beeson, M.H., 1978, Hydrothermal alteration and self-sealing in Y-7 and Y-8 drill holes in northern part of Upper Geyser Basin, Yellowstone National Park, Wyoming: U.S. Geological Survey Professional Paper 1054-A, 26 p.

Kissin, S.A., and Scott, S.D., 1982, Phase relations involving pyrrhotite below 350°C: Economic Geology, v. 77, p. 1739-1754.

Kreiger, P., 1930, Notes on an X-ray diffraction study of the series calcite-rhodochrosite: American Mineralogist, v. 15, p. 23-29.

Kristmannsdóttir, H., 1976, Types of clay minerals in hydrothermally altered basaltic rocks, Reykjanes, Iceland: Jökull, v. 26, p. 30-39.

——1983, Chemical evidence from Icelandic geothermal systems as compared to submarine geothermal systems, *in* Rona, P.A., Bostrom, K., Laubier, L., and Smith, K.L., Jr., eds., Hydrothermal processes at seafloor spreading centers: New York, NATO Conference Series IV, Marine Sciences, 12, Plenum Press, p. 291-320.

Kristmannsdóttir, H., and Tómasson, J., 1978, Zeolite zones in geothermal areas of Iceland, *in* Sand, L.B., and Mumpton, F.A., eds., Natural zeolites-occurrence, properties, use: New York, Pergamon Press, p. 277-284.

Krupp, R.E., and Seward, T.M., 1987, The Rotokawa geothermal system, New Zealand: An active epithermal gold-depositing environment: Economic Geology, v. 82, p. 1109-1129.

Kusakabe, H., Minato, H., Utada, M., and Yamanaka, T., 1981, Phase relations of clinoptilolite, mordenite, analcime and albite with increasing pH, sodium ion concentration and temperature: Tokyo, University of Tokyo, Scientific Papers of the College of General Education, v. 31, p. 39-59.

MacLeod, N.S., and Sammel, E.A., 1982, Newberry volcano, Oregon, A Cascade Range geothermal prospect: Oregon Geology, v. 44, no. 11, p. 123-131; published simultaneously in California Geology, v. 35, no. 11, p. 235-244.

MacLeod, N.S., and Sherrod, D.R., 1988, Geologic evidence for a magma chamber beneath Newberry volcano, Oregon: Journal of Geophysical Research, v. 93, no. B9, p. 10,067-10,079.

MacLeod, N.S., Sherrod, D.R., and Chitwood, L.A., 1982, Geologic map of Newberry volcano, Deschutes, Klamath, and Lake Counties, Oregon: U.S. Geological Survey Open-File Report 82-847, scale 1:62,500.

MacLeod, N.S., Sherrod, D.R., Chitwood, L.A., and Jensen, R.A., 1995, Geologic map of Newberry volcano, Deschutes, Klamath, and Lake Counties, Oregon: U.S. Geological Survey Miscellaneous Geologic Investigations Map I-2455, scales 1:62,500 and 1:24,000.

MacLeod, N.S., Sherrod, D.R., Chitwood, L.A., and McKee, E.H., 1981, Newberry volcano, Oregon, *in* Johnston, D.A., and Donnelly-Nolan, Julie, eds., Guides to some volcanic terranes in Washington, Idaho, Oregon, and northern California: U.S. Geological Survey Circular 838, p. 85-103.

MacLeod, N.S., Walker, G.W., and McKee, E.H., 1976, Geothermal significance of eastward increase in age of upper Cenozoic rhyolitic domes in southeast Oregon, *in* Second United Nations Symposium on the Development and Use of Geothermal Resources, San Francisco, Calif., 1975, Proceedings: Washington, D.C., U.S. Government Printing Office, v. 1, p. 465-474.

Mariner, R.H., Swanson, J.R., Orris, G.J., Presser, T.S., and Evans, W.C., 1980, Chemical and isotopic data for water from thermal springs and wells of Oregon: U.S. Geological Survey Open-File Report 80-737, 50 p.

McCulloh, T.H., Frizzell, V.A. Jr., Stewart, R.J., and Barnes, Ivan, 1981, Precipitation of laumontite with quartz, thenardite, and gypsum at Sespe Hot Springs, Western Transverse Ranges, California: Clays and Clay Minerals, v. 29, no. 5, p. 353-364.

McDowell, S.D., and Paces, J.B., 1985, Carbonate alteration minerals in the Salton Sea geothermal system, California, USA: Mineralogical Magazine, v. 49, p. 469-479.

McKibben, M.A., 1979, Ore minerals in the Salton Sea geothermal system, Imperial Valley, California, U.S.A.: Riverside, University of California, M.S. thesis, 90 p.

McKibben, M.A., and Elders, W.A., 1985, Fe-Zn-Cu-Pb mineralization in the Salton Sea geothermal system, Imperial Valley, California: Economic Geology, v. 80, no. 3, p. 539-559.

Merlino, Stefano, 1988, Gyrolite: its crystal structure and crystal chemistry: Mineralogical Magazine, v. 52, p. 377-387.

Muffler, L.J.P., Bacon, C.R., and Duffield, W.A., 1982, Geothermal systems of the Cascades, *in* Pacific Geothermal Conference, Auckland, New Zealand, November 8-12, 1982, Proceedings: Auckland, New Zealand, University of Auckland Geothermal Institute, Part 2, p. 337-343.

Muffler, L.J.P., and White, D.E., 1969, Active metamorphism of Upper Cenozoic sediments in the Salton Sea geothermal field and the Salton Trough, southeastern California: Geological Society of America Bulletin, v. 80, p. 157-182.

Mumpton, F.A., 1960, Clinoptilolite redefined: American Mineralogist, v. 45, p. 351-369.

Muramatsu, Y., 1984, Fluid inclusion study in the Takinoue geothermal field, Iwate Prefecture, Japan: an application to the estimate of the present underground temperature, *in* New Zealand Geothermal Workshop, 6th, Auckland, New Zealand, 1984, Proceedings: Auckland, New Zealand, University of Auckland Geothermal Institute, p. 21-25.

Murata, K.J., and Larson, R.R., 1975, Diagenesis of Miocene siliceous shales, Temblor Range, California: U.S. Geological Survey Journal of Research, v. 3, p. 553-566.

Nelson, C.H., Carlson, P.R., and Bacon, C.R., 1988, The Mount Mazama climactic eruption (~6900 yr B.P.) and resulting convulsive sedimentation on the Crater Lake caldera floor, continent, and ocean basin, *in* Clifton, H.E., ed., Sedimentologic consequences of convulsive geologic events: Geological Society of America Special Paper 229, p. 37-57.

Ogihara, S., and Iijima, A., 1990, Exceptionally K-rich clinoptilolite-heulandite group zeolites from three offshore boreholes of north-

ern Japan: European Journal of Mineralogy, v. 2, p. 819-826.

Olmstead, D.L., and Wermiel, D.E., 1988, Newberry Crater geothermal resource area, Deschutes County, Oregon: Oregon Department of Geology and Mineral Industries Open-File Report O-88-3, scale 1: 24,000.

Passaglia, E., 1970, The crystal chemistry of chabazites: American Mineralogist, v. 55, p. 1,278-1,301.

Passaglia, E., and Rinaldi, R., 1984, Katoite, a new member of the $Ca_3Al_2(SiO_4)_3$-$Ca_3Al_2(OH)_{12}$ series and a new nomenclature for the hydrogrossular group of minerals: Bulletin de Mineralogie, v. 107, p. 605-618.

Peterson, N.V., and Groh, E.A., 1969, The ages of some Holocene volcanic eruptions in the Newberry volcano area, Oregon: Ore Bin, v. 31, no. 4, p. 73-87.

Phillips, W.R., and Griffen, D.T., 1981, Optical mineralogy: the nonopaque minerals: San Francisco, W.H. Freeman and Company, 677 p.

Potter, R.W., II, Clynne, M.A., and Brown, D.L., 1978, Freezing point depression of aqueous sodium chloride solutions: Economic Geology, v. 73, p. 284-285.

Priest, G.R., Hadden, R.M., Woller, N.M., and Brand, C.B., 1983, Preliminary soil-mercury survey of Newberry volcano, Deschutes County, Oregon, *in* Priest, G.R., Vogt, B.F., and Black, G.L., eds., Survey of potential geothermal exploration sites at Newberry volcano, Deschutes County, Oregon: Oregon Department of Geology and Mineral Industries Open-File Report O-83-3, p. 45-67.

Roedder, E., 1962, Studies of fluid inclusions: I. Low temperature application of a dual-purpose freezing and heating stage: Economic Geology, v. 57, p. 1045-1061.

——1984, Fluid inclusions: Mineralogical Society of America Reviews in Mineralogy, v. 12, 644 p.

Rosenberg, P.E., 1963, Subsolidus relations in the system $CaCO_3$-$FeCO_3$: American Journal of Science, v. 261, p. 683-690.

Sammel, E.A., 1981, Results of test drilling at Newberry volcano, Oregon—and some implications for geothermal prospects in the Cascades: Geothermal Resources Council Bulletin, v. 10, no. 11, p. 3-8.

——1983, The shallow hydrothermal system at Newberry volcano, Oregon: a conceptual model: Geothermal Resources Council Transactions, v. 7, p. 325-330.

Sammel, E.A., and Craig, R.W., 1983, Hydrology of the Newberry volcano caldera, Oregon: U.S. Geological Survey Water Resources Investigations Report 83-4091, 52 p.

Sammel, E.A., Ingebritsen, S.E., and Mariner, R.H., 1988, The hydrothermal system at Newberry volcano, Oregon: Journal of Geophysical Research, v. 93, no., B9, p. 10,149-10,162.

Seki, Y., 1972, Lower grade stability limit of epidote in the light of natural occurrences: Geological Society of Japan Journal, v. 78, p. 405-413.

Sherrod, D.R., and Smith, J.G., 1990, Quaternary extrusion rates of the Cascade Range, northwestern United States and southern British Columbia: Journal of Geophysical Research, v. 95, no. B12, p. 19,465-19,474.

Sigvaldson, G.E., and White, D.E., 1962, Hydrothermal alteration in drill holes GS-5 and GS-7, Steamboat Springs, Nevada: U.S. Geological Survey Professional Paper 450-D, p. D113-D117.

Souther, J.G., 1985, Geothermal potential of the Garibaldi Belt, Mount Meager and Mount Cayley, British Columbia, *in* Guffanti, M., and Muffler, L.J.P., eds., Proceedings of the Workshop on Geothermal Resources of the Cascade Range, May 22-23, 1985, Menlo Park, Calif.: U.S. Geological Survey Open-File Report 85-521, p. 51-52.

Starkey, H.C., Blackmon, P.D., and Hauff, P.L., 1984, The routine mineralogical analysis of clay-bearing samples: U.S. Geological Survey Bulletin 1563, 32 p.

Stauber, D.A., Green, S.M., and Iyer, H.M., 1988, Three-dimensional *P* velocity structure of the crust below Newberry volcano, Oregon: Journal of Geophysical Research, v. 93, no. B9, p. 10,095-10,107.

Steiner, A., 1977, The Wairakei geothermal area, North Island, New Zealand, its subsurface geology and hydrothermal rock alteration: New Zealand Geological Survey Bulletin 90, 136 p.

Steinthórsson, S., and Sveinsbjörnsdóttir, A.E., 1981, Opaque minerals in geothermal well no. 7, Krafla, northern Iceland: Journal of Volcanology and Geothermal Research, v. 10, p. 245-261.

Stonecipher, S.A., 1978, Chemistry of deep-sea phillipsite, clinoptilolite, and host sediments, *in* Sand, L.B., and Mumpton, F.A., eds., Natural zeolites–occurrence, properties, use: New York, Pergammon Press, p. 221-234.

Swanberg, C.A., and Combs, Jim, 1986, Geothermal drilling in the Cascade Range, preliminary results from a 1387-m core hole, Newberry volcano, Oregon: Eos, Transactions, American Geophysical Union, v. 67, no. 29, p. 578-580.

Swanberg, C.A., Walkey, W.C., and Combs, Jim, 1988, Core hole drilling and the "rain curtain" phenomenon at Newberry volcano, Oregon: Journal of Geophysical Research, v. 93, no. B9, p. 10,163-10,173.

Taguchi, S., and Hayashi, M., 1982, Application of the fluid inclusion thermometer to some geothermal fields in Japan: Geothermal Resources Council Transactions, v. 6, p. 59-62.

Taguchi, S., Hayashi, M., Mimura, T., Kinoshita, Y., Gokou, K., and Abe, I., 1984, Fluid inclusion temperature of hydrothermal minerals from the Kirishima geothermal area, Kyushu, Japan: Japan Geothermal Energy Association Journal, v. 21, no. 2, p. 119-129.

Tsusue, A., 1967, Magnesian kutnahorite from Ryujima mine: American Mineralogist, v. 52, p. 1,751-1,761.

Tulloch, A.J., 1982, Mineralogical observations on carbonate scaling in geothermal wells at Kawerau and Broadlands, *in* Pacific Geothermal Conference, Auckland, New Zealand, November 8-12, 1982, Proceedings: Auckland, New Zealand, University of Auckland Geothermal Institute, Part 1, p. 131-134.

Walker, G.W., 1974, Some implications of late Cenozoic volcanism to geothermal potential in the High Lava Plains of south-central Oregon: Ore Bin, v. 36, no. 7, p. 109-119.

Walkey, W.C., and Swanberg, C.A., 1990, Newberry volcano, Oregon: new data supports conceptual hydrologic model: Geothermal Resources Council Transactions, v. 14, pt. 1, p. 743-748.

Williams, Howell, 1935, Newberry volcano of central Oregon: Geological Society of America Bulletin, v. 46, p. 253-304.

Wright, P.M., and Nielson, D.L., 1986, Electrical resistivity anomalies at Newberry volcano, Oregon; comparison with alteration mineralogy in GEO corehole N-1: Geothermal Resources Council Transactions, v. 10, p. 247-252.

Zabinski, W., 1966, Hydrogarnets: Polska Akademia Nauk, Komisja Nauk Mineralogicznych, Prace Mineralogiczne, v. 3, p. 1-61.

Zucca, J.J., and Evans, J.R., 1992, Active high-resolution compressional wave attenuation tomography at Newberry volcano, central Cascade Range: Journal of Geophysical Research, v. 97, no. B7, p. 11,047-11,055.

APPENDIX 1.

LITHOLOGIC DESCRIPTION OF DRILL CORE USGS-N2 FROM WITHIN THE CALDERA OF NEWBERRY VOLCANO

Depth (m)	*Description of drill core*
0-42	Unconsolidated rhyolitic pumiceous ash and lapili.
42-98	Obsidian flow.
98-320	Predominantly light- to medium-gray lapilli tuff, tuff breccia, and subaqueous volcaniclastic beds in shades of gray, green, brown, and black. Volcanic fragments are mostly hydrated basaltic glass, but locally the fragments are finely crystal line with some phenocrysts of plagioclase and olivine, as well as sporadic clinopyroxene, magnetite, quartz, and cristobalite. Lower part of unit grades downward within a few millimeters into glassy basaltic sandstone and grit from 290 to 301 m and into siltstone and mudstone from 301 to 320 m. Hydrothermal minerals identified near base of interval include aragonite, calcite, siderite, analcime, chabazite, faujasite, erionite, gyrolite, apophyllite, garnet?, apatite, chlorite, and smectite.
302.8	Light-greenish-gray, fine-grained, crudely bedded lacustrine siltstone with parallel and irregularly oriented fractures filled by calcite and siderite. Composed predominantly of unaltered glass shards with a few small plagioclase laths.
313.3	Orange-brown, well-indurated, lacustrine siltstone with about 1 cm thick layer of pumice-rich coarse sand grains. XRD analysis of a whole-rock sample shows plagioclase, faujasite, analcime, and chabazite. In thin section, rock consists primarily of glass pervasively altered to zeolite; however, grain size is small and individual minerals were indiscernable. Orange-brown color appears to result from glass altered to amorphous clay.
320-360	Nearly all of dominantly rhyolitic pumiceous sand and gravel composing this unit appears to have been water sorted or reworked and was probably deposited in an intracaldera lake. Lithic material consists of multicolored, angular to subangular, aphanitic or porphyritic volcanic fragments. Local layers contain mixed lithic and pumice clasts in a finer grained glassy or ashy groundmass. Minor calcite and magnesite were identified by XRD analysis in a few samples; siderite and smectite are somewhat more abundant.
357.8	Light-gray lithic-rich pumiceous tuff with a mostly unaltered glassy groundmass containing crystals of plagioclase, clinopyroxene, and magnetite. Very slight alteration of pumiceous groundmass to brownish smectite; small rounded to irregular-shaped blebs of siderite also formed in groundmass. Some lithic fragments contain slight to moderate smectite alteration; a few magnetite crystals are partly altered to hematite. Quartz, olivine(?), and cristobalite identified in XRD analysis of this and other samples in this interval probably are associated with lithic fragments.
360-460	Predominantly rhyolitic pumiceous lithic tuff and local pumice-lapilli tuff with abundant lithic fragments. Pumice and lithic fragments are mixed in an ashy or sandy pumiceous groundmass. Although proportion of pumice to lithic clasts is variable throughout unit, more pumice is found in upper and lower parts, where clast size is small, and more lithic clasts are found in middle part, where clast size is large. Most XRD analyses of samples from upper part of interval show that amorphous glass is prevalent. Other minerals identified are K-feldspar, plagioclase, clinopyroxene, magnetite, quartz, devitrification cristobalite, and vapor-phase tridymite. Hydrothermal minerals are predominantly siderite and smectite; however, near base of interval the alteration assemblage (analcime, clinoptilolite, dachiardite, mordenite, ankerite-dolomite, calcite, magnesite, chlorite, quartz, pyrrhotite, marcasite, and pyrite) becomes more abundant and varied due to injection of an underlying rhyolite sill.
408.7	Light-gray coarse-grained sandstone with abundant fragments of pumice and lava along with crystals of plagioclase, clinopyroxene, and magnetite. Glassy matrix and pumiceous lithic fragments are mostly unaltered. Small cubic pyrite crystals and minor brown patches of smectite occur throughout; diverse shapes of siderite crystal aggregates line vesicles and are superimposed on pumice fragments and glassy matrix.
442.3	Olive-green crystal-lithic tuff with pumice and lava-flow lithic fragments,plagioclase, K-feld spar, minor magnetite (some hematite alteration), and altered pyroxene(?) crystals. Matrix is extensively altered to greenish smectite with patches of calcite. XRD analyses also show clinoptilolite and devitrification cristobalite.
454.2	Light-green crystal-lithic tuff with abundant plagioclase and a few magnetite crystals. Matrix glass and pumice fragments are altered to green chlorite and later fibrous mordenite; XRD analysis also shows devitrification cristobalite. Some red-orange patches consist of calcite partly replaced by later siderite.
460-470	Moderately fractured, light- to medium-gray rhyodacite sill that is massive, dense, and locally flow banded in its central part. Sill may have been a hot intrusion into water-saturated pumiceous-lithic tuff. Glassy top and brecciated base were chilled and subsequently devitrified with concentric hydration cracks in cryptocrystalline matrix. Sill contains a few small plagioclase phenocrysts and small plagioclase-rich mafic xenoliths. Hydrothermal alteration minerals consist of smectite, siderite, quartz, mordenite, pyrite, marcasite, and pyrrhotite. Some core samples contain pyrrhotite that is partly oxidized, forming lepidocrosite, goethite, and sulfur.

[1]Lithologic dcscriptions of Newberry drill cores are based on binocular microscope observations of core samples and petrographic studies of thin sections. For some intervals, a summary of the thin-section data is provided without regard to specific sample depths.

468.5 White, leached, fine-grained rhyodacite with light-gray banding. Contains a few plagioclase phenocrysts in groundmass of tiny plagioclase laths. Devitrification cristobalite and K-feldspar are present in XRD analyses. Siderite occurs as vein-fillings and irregular patches; some murky patches are probably smectite.

469.1 Dark-gray, glassy to devitrified rhyodacite. A few plagioclase phenocrysts and pyrite grains occur in glassy groundmass that is partly devitrified to cristobalite. Perlitic cracks are filled with siderite, mordenite, and smectite.

470-501.4 White, gray, tan, and light-green, pumiceous-lithic tuff with local pumice-lapilli tuff similar to that overlying the rhyodacite sill. Two thin (less than 1-m thick) glassy dikes intersect tuff at 471 and 479 m. Multicolored lithic fragments are mostly dark aphanitic volcanic rocks, although some fragments contain plagioclase phenocrysts and magnetite crystals. K-feldspar, devitrification cristobalite, and unaltered glass are identified in XRD analyses. Predominant hydrothermal minerals in this interval are siderite, smectite, and pyrite; calcite, chlorite, and mordenite are locally abundant.

496.2 Light- to medium-gray crystal-lithic tuff. Crystals are mostly plagioclase with a few magnetite grains; K-feldspar and devitrification cristobalite were noted in XRD analysis but were not observed in thin section. Some lithic fragments have quartz veining thought to be unrelated to the present hydrothermal system. Obsidian and pumice fragments are completely altered to grayish smectite and fibrous mordenite which also are prevalent in the altered groundmass. Cubic and pyritohedral pyrite crystals, associated with rims of lithic fragments, vein fillings, and open-space deposits in altered glass fragments, are partly oxidized to iron-oxide stains and are closely associated with brownish siderite.

501.4-552 Massive to flow-banded, dense rhyodacite lava flow, brecciated at its top and in its basal 5 m. Fractures throughout, some coated by hydrothermal minerals, are oriented both parallel to and across flow banding; local unfilled vapor-phase partings are parallel to flow banding in massive part of flow. Groundmass of lava flow is cryptocrystalline to aphanitic and contains approximately 15 percent plagioclase and clinopyroxene phenocrysts ranging up to about 1.5 cm in length; clinopyroxene content increases near base of flow. XRD analyses show minor quartz and K-feldspar, as well as vapor-phase tridymite and devitrification cristobalite. Hydrothermal minerals deposited on numerous fractures and vesicles consist of orange, reddish-brown, or pale-yellow siderite mostly deposited in disk-shaped crystal aggregates, smectite, and hexagonal bladed marcasite that is partly altered to pyrite.

515.7 Light-gray rhyodacite flow with plagioclase phenocrysts and a few associated subhedral magnetite crystals. Fractures in a few plagioclase crystals are filled with siderite and pyrite. Groundmass consists of small plagioclase laths and minute magnetite grains. Scattered pyrite crystals and crystal clusters are partly oxidized and have orange halos. Irregular orange-stained patches and siderite deposits are scattered throughout groundmass.

548.2 Dark-gray rhyodacite flow containing glomeroporphyritic clots of plagioclase, clinopyroxene, and magnetite phenocrysts in fine-grained groundmass of tiny plagioclase laths and magnetite crystals. Siderite with earlier tridymite fills vapor-phase cavities and veins that cut through both plagioclase and clinopyroxene crystals. Most clinopyroxene phenocrysts have brown-black rims and fracture fillings of iron oxide. K-feldspar and devitrification cristobalite were detected in XRD analysis.

552-552.5 Thin interlayer of pervasively altered bedded ash and pumice lapilli. XRD analyses show plagioclase and hydrothermal alteration minerals: siderite, smectite, and pyrite.

552.5-600 Light-gray to black dacite lava flows with brecciated tops and local intra- or interflow breccias less than 0.5 m thick. Flows have local zones of vapor-phase colorless tridymite crystals associated with needle-like crystals of a brown amphibole that formed in open spaces along partings parallel to flow banding. Dacite groundmass is cryptocrystalline with as much as 10 percent plagioclase and less than 3 percent clinopyroxene and magnetite phenocrysts. Hydrothermal minerals deposited on fractures and in cavities consist predominantly of orange to pale-yellow siderite, buff, gray, or green smectite, and tiny cubic pyrite crystals. Some amorphous opal, chalcedony, cristobalite, calcite, marcasite, and hematite were identified by XRD.

600-603 Orangish, nonsorted, lithic-rich tuff with ashy groundmass. Partly oxidized, angular lithic fragments are composed of plagioclase and devitrification cristobalite. Oxidation to hematite and presence of natrojarosite indicate this zone may have been exposed to surface weathering for a substantial period of time or that it might have been an aquifer for late-meteoric thermal water. Other secondary minerals are siderite, smectite, and pyrite.

603-607 Large brecciated fragments of black dacite in a buff to white ashy matrix. Plagioclase and devitrification cristobalite were identified in XRD analyses of both dacite fragments and the matrix material. Hydrothermal minerals are siderite,pyrite, and smectite.

607-656.5 Light-gray to black, dense, massive, locally fractured dacite lava flows. Groundmass of dacite is cryptocrystalline to aphanitic with thin plagioclase laths and specks of magnetite; locally hydration cracks are apparent. Dacitic lavas contain about 15 percent plagioclase phenocrysts (many of which are zoned or partly resorbed), 5 percent clinopyroxene and magnetite phenocrysts, and 1 percent glomeroporphyritic clots of plagioclase and clinopyroxene. Most whole-rock XRD analyses show devitrification cristobalite. Drill core from this interval usually contains siderite, pyrite, and smectite; marcasite occurs in several samples, but amorphous opal was found in only two fracture fillings.

631.9 Dark-gray dacite flow with fine-grained groundmass consisting of plagioclase laths, tiny magnetite crystals, and rare clinopyroxene grains. Mostly euhedral phenocrysts consist of plagioclase, magnetite, and clinopyroxene that locally form glomeroporphyritic clots. Thin fracture filling consists of colorless, rhombic(?) siderite crystals. Fine-grained siderite and brownish smectite form alternating bands or concentric layers of a sphere.

656.2 Dark-gray, vesicular, dacite flow. Fine-grained groundmass consists of plagioclase laths and tiny magnetite crystals. Mostly euhedral phenocrysts of plagioclase, clinopyroxene, and magnetite frequently form glomeroporphyritic clots. Some vesicles are partly filled by colorless, disk-shaped clusters of rhombic siderite crystals. Tiny cubic pyrite crystals were deposited in a few vesicles and are associated with reddish-brown to opaque crystals (in transmitted light) that are grayish in reflected light and may be leucoxene resulting from alteration of magnetite.

656.5-697 Light-gray to black dacite breccia with large fragments. Breccia fragments contain plagioclase, clinopyroxene, and magnetite phenocrysts in fine-grained groundmass of plagioclase laths and magnetite crystals. Most, but not all, magnetite phenocrysts appear to be altered to leucoxene(?) with veins of pyrite. Devitrification cristobalite was identified in several samples by XRD.Green, buff, or gray smectite and yellow to orange siderite crystals formed in cavities between breccia fragments. Some disk-shaped crystals of siderite in cross sections appear to have formed as concentric layers around a neucleus of brown clay(?). Fractures at base of interval contain bronze-colored hexagonal pyrrhotite platelets; white rhombic crystals of ankerite-dolomite were identified in matrix of three samples.

659.9 Light-gray dacite breccia fragments have fine-grained groundmass of plagioclase laths and magnetite crystals. Phenocrysts of plagioclase and clinopyroxene form some glomeroporphyritic clots with magnetite that has altered to leucoxene(?) and pyrite. Green smectite and colorless siderite crystal clusters were deposited in open spaces between breccia fragments.

697-743.5 Two dark-gray, massive dense andesitic lava flows and associated breccias. A flow-top breccia from 697 to 702.6 m and a massive flow with few fractures from 702.6 to 707.4 m are relatively unaltered. Conversely, highly fractured, leached, interflow breccia between 707.4 and 715 m is intensely altered. A second massive, dense but fractured andesitic flow occurs from 715 to 735 m; brecciated, fractured, altered, leached basal part of this flow continues from 735 to 743.5 m.Conspicuous flow banding occurs in upper flow unit, but otherwise flows are petrographically very similar. Both flows have dark-brown fine-grained groundmass (74 percent) with tiny plagioclase laths (An_{59}). XRD analyses of most whole-rock samples contain cristobalite. Phenocrysts consist of about 20 percent subhedral to euhedral, locally zoned plagioclase (An_{61}), 5 percent subhedral to euhedral clinopyroxene, and 1 percent magnetite. Glomeroporphyritic clots of plagioclase and clinopyroxene make up about 1 percent of rock. Hydrothermal alteration becomes more abundant and varied in lower part of unit. Radiating fibrous mordenite crystals line cavities in a few samples. Calcite is late-fracture and vesicle filling; siderite gradually diminishes in abundance and finally ceases to form below about 715-m depth. Smectite is sporadically abundant throughout interval, whereas chlorite becomes more plentiful in lower part of andesitic lavas and breccias. Mixed-layer chlorite-smectite was detected in XRD analysis of one sample. Fracture fillings and open spaces between breccia fragments are lined by colorless colloform cristobalite, locally in association with colorless to white chalcedony, and colorless quartz crystals and massive deposits. Pyrrhotite is disseminated in groundmass of some andesite flows and was deposited on many fractures. Pyrite occurs in most samples and may have formed, at least in part, from alteration of pyrrhotite.

743.5-757.5 Light-green andesitic crystal- and crystal-lithic tuffs. Plagioclase crystals are unaltered in upper part of interval but are partly altered to calcite in samples near base. Calcite also fills vesicles and fractures along with earlier tiny quartz grains. Small quartz grains also fill open space in altered pumice fragments. Groundmass of most samples has altered to green chlorite; however, some white smectite occurs in upper part of unit and illite was identified on XRD analyses from lower part. A few bronze-colored hexagonal pyrrhotite crystals and cubic pyrite crystals were observed.

757.5-932 Massive, dense, locally vesicular but sparsely fractured, subhorizontal basaltic-andesite to basalt lava flows and interflow breccias make up lower part of USGS-N2 drill core. Petrographically, flows have different groundmass characteristics (grain size and textures), proportions of phenocrysts, and SiO2 contents. Rounded clinopyroxenite xenoliths occur in lower basalt flows. Flow tops and basalt breccias at 792.8 to 795.5,809.2 to 810.8 m, 850.4 to 852.8 m, 910.4 to 911.1 m, and 930 to 930.5 m are altered and bleached but are not extensively fractured. Interval between 930-932 m, at bottom of drill hole, is extensively altered and bleached distinctively different from overlying lava flows.

757.5-761.7 Light-greenish-gray basaltic breccia. A few breccia fragments have unaltered(?) tiny groundmass plagioclase laths and abundant tiny opaque grains (leucoxene?) that are light gray in reflected light. Phenocrysts are notably absent, but sporadic rectangular calcite deposits suggest that plagioclase has been completely replaced. Vesicles, matrix material between breccia fragments, and most lithic fragments are completely altered primarily to quartz crystals and calcite along with green chlorite. Tiny cubic pyrite crystals are disseminated throughout one sample; smectite and illite were identified in XRD analyses of some samples.

761.7-792.8 Medium-gray to greenish-black basalt or basaltic andesite lava flow with trachytic to felty texture con-

sisting of approximately 2 percent plagioclase and less than 1 percent clinopyroxene phenocrysts. Groundmass contains plagioclase laths and tiny clinopyroxene and magnetite crystals. Hydrothermal alteration is more intense in upper and lower parts of flows. Fractures and vugs are coated by colorless quartz crystals as long as 7 mm, white to colorless rhombic and bladed calcite crystals as much as 1 cm across, bronze-colored pyrrhotite platelets, and some cubic pyrite crystals. Green clay deposits on fractures and in groundmass of a few samples consist of smectite, mixed-layer chlorite-smectite, chlorite, and illite in decreasing order of abundance. A few samples have calcite or patches of brownish iron-oxide(?) groundmass stains.

795.5-809.2 Light-greenish-gray to black basalt lava flow has holocrystalline groundmass composed of plagioclase laths and anhedral clinopyroxene and magnetite; it is porphyritic with about 5 percent plagioclase phenocrysts, some of which are zoned, about 5 percent clinopyroxene phenocrysts, and 1 percent glomeroporphyritic clots of clinopyroxene and plagioclase. Hydrothermal alteration is more intense in upper part of flow where plagioclase crystals are altered to calcite and white illite-smectite mixed-layer clay. Clinopyroxene crystals appear to be completely altered to green chlorite. Patches of calcite and gray clay and crystals of tiny cubic pyrite are disseminated in groundmass of several samples. Fractures and vesicles generally are filled by quartz, calcite, and either chlorite, smectite, or mixed-layer chlorite-smectite.

810.8-850.4 Thick dark-greenish-gray to black basalt flow is highly vesicular (locally as much as 40 percent vesicles between 822.4 and 844.3 m). Groundmass is holocrystalline with plagioclase laths, clinopyroxene, and magnetite. Locally zoned and partly resorbed plagioclase phenocrysts make up 10 percent of rock near top of flow and about 50 percent at base. Clinopyroxene phenocrysts make up about 3 percent of rock in upper part of flow and increase slightly in abundance toward base; olivine phenocrysts altered to iddingsite are present at base of flow. Glomeroporphyritic clots of clinopyroxene and plagioclase make up less than 1 percent of rock. Colorless and white calcite is a late fracture and vug filling and partly replaces plagioclase crystals. Smectite was identified by XRD analyses in a few green clay samples from fractures and vugs, but most of these clays consist of chlorite or mixed-layer chlorite-smectite. Bluish colloform chalcedony was deposited on a few fractures. Colorless euhedral quartz crystals are early open-space fillings in most samples but formed later than chlorite in some samples. In a few samples more than one generation of quartz crystals occur and late quartz replaces calcite. Cubic pyrite crystals are plentiful in a few samples. Reddish hematite partly replaces magnetite in lower half of interval.

852.8-910.4 Dark greenish-black basalt flow similar to flow above but is coarser grained with more abundant phenocrysts. Intergranular groundmass is composed of anhedral clinopyroxene and magnetite and subhedral plagioclase laths. Flow consists of about 30 to 60 percent zoned plagioclase, about 3 percent clinopyroxene phenocrysts, and 5 percent olivine phenocrysts that are altered to iddingsite (mostly brown-green chlorite and hematite, but one sample also contains calcite). Minor vesicles occur at top and base of flow. White, pink, or orange calcite fills vesicles and fractures and partly replaces plagioclase phenocrysts in a few samples. One sample contains white hexagonal prisms of apatite in cavities. Minor illite was detected in XRD analyses of two whole-rock samples. Chlorite and mixed-layer chlorite-smectite occur as open-space fillings and groundmass alteration throughout the basalt flow. Bluish colloform chalcedony and colorless massive to crystalline quartz were deposited in many fractures and vesicles. Cubic pyrite crystals occur in several samples, but bronze, hexagonal, tabular, pyrrhotite crystals coat cavities and are disseminated in one sample from lava flow. Hematite replaces spherical magnetite deposits in one fracture filling.

911.1-930 Medium-gray to greenish-black basalt flow is texturally similar to flow above but has about 40 percent vesicles at its top with vesicularity decreasing rapidly to massive basalt within about 3.5 m. Flow includes about 25 percent plagioclase phenocrysts that are partly zoned and slightly to extensively resorbed, 5 percent olivine phenocrysts altered to iddingsite, 3 percent clinopyroxene phenocrysts, and <1 percent rounded xenocrystic clots of anhedral clinopyroxene. Calcite partly replaces plagioclase phenocrysts, and colorless euhedral rhombic calcite crystals are deposited in vesicles and fractures. XRD analysis of one whole-rock sample shows smectite. XRD analyses also show chlorite or mixed-layer chlorite-smectite deposited in vesicles, fractures, and groundmass of most samples. Colorless euhedral quartz crystals or massive quartz are formed in vesicles and fractures. Bronze-colored platy pyrrhotite crystals are in one sample. Pyrite fracture fillings and disseminated crystals occur in a few samples. Euhedral yellow-green epidote crystals are deposited in vesicles and, with calcite, replace plagioclase phenocrysts. Colorless euhedral anhydrite crystals were deposited in open spaces of one sample. Red rim is present around a clinopyroxene phenocryst in one sample.

930.5-932 Light- to medium-gray leached vesicular lava flow at bottom of drill hole is pervasively altered and distinctively different from overlying lava flows. Plagioclase phenocrysts and holocrystalline groundmass are partly altered to calcite. Bladed or blocky calcite crystals also were deposited in vesicles. Olivine is altered to green clay; both chlorite and illite were identified in whole-rock XRD analysis. Green fibrous chlorite lines vesicles and was earliest deposit. Some small euhedral quartz crystals were deposited later. Pyrite is disseminated throughout bottom sample, and pyrrhotite was deposited on a fracture surface.

APPENDIX 2.

LITHOLOGIC DESCRIPTION OF DRILL CORE GEO-N1 FROM THE SOUTH FLANK OF NEWBERRY VOLCANO

Depth (m)	*Description of drill core*
0-148.4	No core recovery.
148.4-357.2	Several, light-, medium-, and dark-gray, basalt to andesite lava flows; flow breccias, cinder layers, and thin (<1m) tuff beds occur between lava flows.
180.7	Fine-grained holocrystalline basaltic andesite lava flow; groundmass consists of plagioclase laths and anhedral clinopyroxene and magnetite grains. Clinopyroxene phenocrysts are scarce; some plagioclase phenocrysts are zoned. Rare olivine phenocrysts were observed in several other samples from this interval (Earth Science Laboratory, 1986). Deuteric iron oxide stains much of the breccias. Except for one occurrence of calcite and a few white (amorphous silica?) fracture and vesicle coatings, core samples are unaltered.
357.2-362.1	Horizontally bedded, light-brown to bright-orange, soft friable dacitic-rhyodacitic tuff interval with fiamme. XRD analysis shows mostly plagioclase with minor devitrification cristobalite and hematite.
362.1-658.9	Medium- to dark-gray andesitic to basaltic lava flows that are usually dense, although highly fractured with some vesicular or flow-banded intervals. Between lava flows are flow breccias or green, brown, and orange lithic-tuff beds. Interval is cut by seven thin (<1 m to 2.5 m thick) dark-gray to black aphanitic dikes that commonly have glassy chill margins. Some dikes display minor vesiculation, and at least one contains inclusions of light-gray volcanic fragments. Whole-rock XRD analyses show plagioclase, clinopyroxene, and minor devitrification cristobalite. Sparse olivine was noted in published description (Earth Science Laboratory, 1986) for some core samples. Flow breccias and many fractures have dark-red to orange deuteric to hydrothermal(?) iron-oxide staining; XRD analyses show that iron oxides range from amorphous to well-crystallized hematite. Some fractures and open spaces of vesicles or between breccia fragments contain white, yellow, or orange smectite. Lithic-tuff interval just above dike at about 572 m contains mixed-layer illite-smectite. White blocky calcite and yellowish botryoidal chalcedony were identified by XRD analysis in open spaces of two flow breccias.
658.9-664.2	Pink rhyodacitic ash-flow tuff. XRD analysis shows minor hematite alteration, primary plagioclase and magnetite, devitrification cristobalite, and vapor-phase tridymite.
664.2-1,132.0	Series of thin basaltic lava flows (includes a few basaltic andesite and andesitic flows) with intervening flow breccias, ash and cinder beds, lithic tuff, tuff breccia, lapilli tuff, and ash-flow tuff. Core from this interval is cut by several basaltic dikes (<1 m to ~12 m thick). Brief hand-specimen and thin-section descriptions of some chemically analyzed samples are included below.
703.3	Dark-gray holocrystalline basalt dike with glassy chill margins and vertical flow banding marked by trains of tiny unfilled vesicles. Groundmass consists of euhedral plagioclase laths and anhedral clinopyroxene and magnetite crystals. A few plagioclase phenocrysts are slightly larger than groundmass crystals. Minor devitrification cristobalite and fracture coatings of hydrothermal smectite were identified by XRD analysis.
744.3	Dark-gray to black medium-grained vesicular basalt lava flow with ophitic texture. Groundmass plagioclase laths and subhedral magnetite crystals are enclosed by large, optically continuous clinopyroxene phenocrysts. Larger plagioclase and olivine phenocrysts are scarce. Devitrification cristobalite was identified by XRD analysis. Colorless calcite and green smectite line one sampled fracture from this flow; a vesicle-filling sample contains tiny colorless phillipsite crystals.
789.0	Dark-gray vesicular basalt flow with plagioclase laths ranging from groundmass to phenocryst size. Elongate clinopyroxenes enclose plagioclase laths (ophitic texture) and are partly altered to green (iron-rich?) smectite and exsolved subhedral magnetite; magnetite is partly altered to red iron oxide, possibly hematite. Partly altered olivine phenocrysts form several percent of rock. Vesicles, many having horizontal elongation, are lined with orange or green stubby fibrous smectite, sometimes forming boytryoids, and later botryoidal, massive, or acicular carbonates (ankerite-dolomite, calcite, and kutnohorite in XRD analyses).
843.4	Light-gray, medium- to fine-grained basalt flow. Groundmass consists of plagioclase laths and abundant anhedral clinopyroxene and anhedral to subhedral magnetite crystals partly altered to hematite. Centers of some large euhedral zoned plagioclase phenocrysts have a sieve texture. A few plagioclase crystals are extensively fragmented. Large subhedral olivine phenocrysts with reddish rims (magnetite altered to hematite) form glomeroporphyritic clots with plagioclase. XRD analysis of this sample also shows devitrification cristobalite. Fractures and vesicles contain green clay and colorless needles or massive deposits of aragonite and calcite.
859.4	Medium-gray basalt flow near base of above lava flow. Groundmass consists of small anhedral magnetite grains and plagioclase laths within large, distinctively separated anhedral clinopyroxene crystals (ophitic texture). Sieve-textured plagioclase phenocrysts occur as at 843.4 m. Occasional large olivine crystals, partly altered to green smectite, are glomeroporphyritic with plagioclase. Colorless calcite and radiating needles of aragonite coat a steep fracture. Calcite and okenite were identified in XRD analyses of other samples from this basalt flow.
932.7	Dark-gray medium-grained porphyritic basalt flow with ophitic texture. Groundmass contains plagioclase laths enclosed by anhedral clinopyroxene, subhedral blocky magnetite partly altered to hematite, and dark-brown interstitial glass altered to al-

tered to iddingsite. Various sizes of plagioclase phenocrysts display zoning, twinning, or albitized edges, or are extensively shattered. Sample is cut by a near-vertical fracture lined by tiny white crystal aggregates of kutnohorite and later dark-green clay. Fracture fillings in other samples from this lava flow also contain calcite and ankerite-dolomite in addition to kutnohorite.

939.7 Medium-gray vesicular basalt flow with palagonitized and devitrified glass (cristobalite identified by XRD analyses). Groundmass has small scattered plagioclase laths and very dark devitrified glass with vesicles partly to completely filled with yellow-brown palagonite(?) or smectite. A few phenocrysts of fresh plagioclase and clinopyroxene and one glomeroporphyritic clot of clinopyroxene, plagioclase, and magnetite occur. Other samples from this lava flow contain fracture and vesicle fillings of kutnohorite, siderite, smectite, and aragonite. A few tiny pyrite crystals coat flow partings of one sample along with smectite and later siderite.

953.0 Dark-gray to black, medium- to fine-grained microvesicular basalt dike (~2 m thick). Groundmass consists of large needle-like plagioclase laths in dark glassy matrix that appears to be partly altered to clay, although smectite was not identified in whole-rock XRD analysis. Sample has a few small plagioclase phenocrysts. Numerous small vesicles occur in steeply dipping trains; many vesicles are partly to completely filled by botryoidal siderite. Siderite may have brownish iron oxide(?) or clayey(?) core with concentric layering or radial structure that has a very thin brownish boundary between growth layers. Some vesicles are coated by colorless botryoidal isometric opal. A few vesicles contain both siderite and opal; relations between these two secondary minerals are unclear, but siderite may be later.

1,015.0 Dark-gray to black aphanitic basalt or basaltic andesite flow. Groundmass of tiny anhedral magnetite grains, some with reddish hematite alteration, and plagioclase laths in dark glassy matrix. Anhedral to subhedral clinopyroxene phenocrysts are partly in glomeroporphyritic association with rounded, elongate to stubby and twinned plagioclase crystals. Vesicles are filled or coated with fibrous brown to green smectite; a few vesicles contain carbonate (kutnohorite?) fillings.

1,033.6 Medium-gray microporphyritic andesite flow. Groundmass of small plagioclase laths, anhedral clinopyroxene crystals, and anhedral magnetite grains (minor hematite alteration). Clinopyroxene phenocrysts are small. Many anhedral to subhedral plagioclase phenocrysts are sieve textured; others are twinned or zoned, and a few have overgrowths of later plagioclase. A few vesicles are filled by brown fibrous smectite or siderite. Light-caramel-colored siderite and pale-green smectite coat a vertical fracture. Colorless aragonite also coats fractures in other samples from this lava flow.

1,068.3 Light-gray, medium- to fine-grained vesicular basalt or basaltic andesite. Groundmass contains plagioclase laths and abundant small anhedral clinopyroxene crystals and euhedral to anhedral magnetite grains (some hematite alteration). Plagioclase phenocrysts are elongate. Vesicles are mostly unfilled, but siderite (radial structure) associated with opaque iron oxide (magnetite?) coats a few vesicle walls and occurs between successive siderite layers. Fracture fillings in other samples from this lava flow contain deuteric(?) botryoidal magnetite (some altered to hematite) with later pyrite, siderite, and calcite.

1,114.8 Medium-gray basaltic andesite flow with pilotaxitic texture. Groundmass consists largely of equigranular plagioclase laths oriented parallel to flow direction; interstices between plagioclase crystals are filled by small anhedral clinopyroxene crystals and magnetite grains. A few plagioclase phenocrysts are present. Scarce vesicles are filled by reddish-brown, botryoidal iron oxide (hematite?), later radial carbonate minerals (aragonite, ankerite-dolomite, and calcite in XRD analysis) in concentric growth rings, and later green smectite.

1,132.0-1,386.8 Lowest part of drill hole contains a few, dark-gray, dense, basaltic lava flows, but most samples consist of medium-gray dacitic to rhyolitic lava flows lithologically variable, including porphyritic, vesicular, vitrophyric, and flow-banded zones. Between some lava flows are medium-gray to brick-red lithic tuffs, black glassy tuffs with perlitic, pumiceous, or scoriaceous textures, or brecciated zones containing a few black glassy clasts or consisting entirely of obsidian fragments. Thin-section notes are given below for two chemically analyzed samples from this drill-core interval.

1,150.8 Medium-gray, porphyritic rhyodacite with very fine grained groundmass containing tiny plagioclase laths and short linear trains of opaque magnetite grains. Phenocrysts of large plagioclase crystals, partly altered olivine, and clinopyroxene that usually forms glomeroporphyritic clots with plagioclase and magnetite phenocrysts. Magnetite only very slightly altered to reddish iron oxide. Light-caramel-colored hemispherical crystal clusters of siderite and later deposits of calcite or kutnohorite(?) and gray smectite were deposited on vapor-phase partings.

1191.5 Medium-gray, porphyritic rhyodacite with buff to green mottling around irregular vapor-phase cavities. Groundmass is cryptocrystalline with small plagioclase laths and stringers of magnetite grains; XRD analysis also shows cristobalite, K-feldspar, tridymite, and quartz(?). Plagioclase phenocrysts are abundant, and a few zoned or twinned euhedral to subhedral crystals form glomeroporphyritic clots with subhedral magnetite and a mafic mineral (olivine?) that is mostly altered to brownish and greenish smectite and a carbonate mineral (siderite or calcite?). Vapor-phase cavities contain brownish or greenish smectite and siderite filling spaces between tridymite crystals.